Direct Measurements of Polyelectrolyte Brush Responses using Atomic Force and Optical Microscopy

Dissertation

Von der Universität Bayreuth
zur Erlangung des akademischen Grades eines
Doktors der Naturwissenschaften (Dr. rer. nat.)
genehmigte Abhandlung

Fakultät für Biologie, Chemie und Geowissenschaften
Lehrstuhl Physikalische Chemie II

von

Johann Erath

Diplom-Physiker

geboren in Wasserlos, Alzenau

Erstgutachter: Prof. Dr. Andreas Fery
Zweitgutachter: Prof. Dr. Georg Papastavrou

Dissertation eingereicht: 02.07.2013
Wissenschaftliches Kolloquium: 11.11.2013

Die vorliegende Arbeit wurde in der Zeit von Juli 2009 bis Juli 2013 am Lehrstuhl Physikalische Chemie II unter der Betreuung von Prof. Dr. Andreas Fery an der Universität Bayreuth angefertigt.

Vollständiger Abdruck der von der Fakultät für Biologie, Chemie und Geowissenschaften der Universität Bayreuth genehmigten Dissertation zur Erlangung des akademischen Grades eines Doktors der Naturwissenschaften (Dr. rer. nat.).

Dissertation eingereicht: 02.07.2013
Zulassung durch die Prüfungskommission: 10.07.2013
Wissenschaftliches Kolloquium: 11.11.2013

Amtierender Dekan: Prof. Dr. Rhett Kempe

Prüfungsausschuss:
Prof. Dr. Andreas Fery (Erstgutachter)
Prof. Dr. Georg Papastavrou (Zweitgutachter)
Prof. Dr. Josef Breu (Vorsitz)
Prof. Dr. Andreas Greiner

Contents

List of Figures

Abbreviations and Symbols

The most important and recurrent abbreviations and symbols of this thesis are listed in the following. Abbreviations and symboles that are not listed are explained in the main text.

Abbreviations

AdG Alexander and de Gennes

AFM Atomic Force Microscope

ATRP Atom Transfer Radical Polymerization

CF Carboxyfluorescein

Ch Chapter

CLSM Confocal Laser Scanning Microscopy

CP Colloidal Probe

DH Debey-Hückel

DMT Derjaguin, Muller and Toporov

Eq Equation

IPEC Interpolyelectrolyte complexes

InvOLS Inverted Optical Lever Sensitivity

JKR Johnson, Kendall and Roberts

LBL Layer By Layer

μCP Micro Contact Printing

MWC Milner, Witen, and Cates

NB Neutral Brush

OsB Osmotic Brush

PB Poisson-Boltzmann

PDMS Polydimethylsiloxane

PE Polyelectrolyte

PIMP Photoinitiated Mediated Polymerization

QMB Quartz crystal Micro Balance

RICM Reflection Interference Contrast Microscopy

SB Salted Brush

SCP Soft Colloidal Probe

SFA Surface Force Apparatus

SPB Spherical Polyelectrolye Brush

UV Ulraviolet

vdW van der Waals

Symbols

pK_a Acidity constant

θ Angle

l_B Bjerrum length

K_b Boltzman constant

H Brush height

c Concentration

a Contact radius

λ_D Debye length

δ Deformation, deflection

α Degree of ionization

ρ Density

D Seperation distance

r Distance

e Elementary charge

S Entropie

v_2 Excluded volume

F Force

f Free energy

σ^{-1} Grafting density

Λ Guoy-Chapman length

γ Interfacial energy

I Ionic strength

a Kuhn length

M Molecular weight

N Number of monomeres

NA Numerical aperture

ϵ Permittivity

L_p Persistence lenth

ν Poisson ratio

U Potential

P Pressure

R Radius, reduced radius

K Reduced modulus

n Refractive index

f_{res} Resonance frequency

k Spring constant

ϵ_i Strain in i direction

σ_i Stress in i direction

σ_S Surface charge density

μ_T Tabor parameter

T Temperature

w Work of adhesion

E Young's modulus

List of Publications

1. *Characterization of Adhesion Phenomena and Contact of Surfaces by Soft Colloidal Probe AFM.*
   Erath, J., Schmidt, S., and Fery, A., Soft Matter, 2010. 6(7): p. 1432-1437.

2. *Direct Correlation between Local Pressure and Fluorescence Output in Mechanoresponsive Polyelectrolyte Brushes.*
   Bunsow, J., **Erath, J.**, Biesheuvel, P. M., Fery, A., Huck, W. T. S., Angewandte Chemie-International Edition, 2011. 50(41): p. 9629-9632.

3. *Sensitive as Human Skin: Polymer Surfaces with High Precision Pressure Detection.*
   Fery, A. and **Erath, J.**, International Journal of Materials Research, 2011. 102(12): p. 1524-1525.

4. *Tuning of the Elastic Modulus of Polyelectrolyte Multilayer Films built up from Polyanions Mixture.*
   Trenkenschuh, K., **Erath, J.**, Kuznetsov, V., Gensel, J., Boulmedais, F., Schaaf, P., Papastavrou, G., Fery, A., Macromolecules, 2011. 44(22): p. 8954-8961.

5. *Adsorption of Spherical Polyelectrolyte Brushes: from Interactions to Surface Patterning.*
   Hanske, C., **Erath, J.**, Kuehr, C. , Trebbin, M., Schneider, C., Wittemann, A., Fery, A., Zeitschrift Für Physikalische Chemie - International Journal of Research in Physical Chemistry and Chemical Physics, 2012. 226(7-8): p. 569-584.

6. *Reversible Swelling Transitions in Stimuli-Responsive Layer-by-Layer Films containing Block Copolymer Micelles.*
   Gensel, J., Dewald, I., **Erath, J.**,Betthausen, E., Mueller, A. H. E., Fery, A., Chemical Science, 2013. 4(1): p. 325-334.

7. *Clay-Based Nanocomposite Coating for Flexible Optoelectronics Applying Commercial Polymers.*
   Kunz, D.A., Schmid, J., Feicht, P., **Erath, J.**, Fery, A., Breu J., ACS Nano, 2013. 7(5): p. 4275-80.

8. *In-plane Modulus of Singular 2:1-Clay Lamellae Applying a Simple Wrinkling Technique.*
   Kunz, D., **Erath, J.**, Kluge, D., Thurn, H.; Putz, B.; Fery, A., Breu, J., ACS Applied Materials and Interfaces, 2013. 5: p. 5851-5855

9. *Phototunable Surface Interactions.*
   Erath, J., Cui, J., Schmid, J., Kappl, M., del Campo, A., Fery, A., Langmuir, 2013. 29: p. 12138-12144

Achievements

- **Best lecture award:** *Soft colloidal probe AFM: A new method for the investigation of adhesion and contact of soft surfaces*, ACS Spring Meeting 2010 (Biofunctional Architectures Symposium), San Francisco, USA, March 21-15, 2010

- **Best poster award:** *Correlation of Local Pressure and Optical Response of Mechanoresponsive Polyelectrolyte Brushes*, International Conference on Scanning Probe Microscopy on Soft Polymeric Materials: SPM on SPM 2012, Kerkrade, The Netherlands, September 23-26, 2012

- **Highlighted Publication:** *Direct Correlation between Local Pressure and Fluorescence Output in Mechanoresponsive Polyelectrolyte Brushes*, published in Angewandte Chemie international Edition, 2011 was highlighted in: Nature Materials, 10, 724, 2011

1

Overview

1.1 Outline

This thesis addresses direct measurements of the response from polyelectrolyte (PE) layers, composed of polyelectrolyte brushes. In particular, systems that are studied are polyelectrolyte brushes on hard substrates and layers that are built up of colloidal building blocks, i.e. spherical polyelectrolyte brushes and PE micelles composed of double-end-tethered annealed polyelectrolyte brushes. For the investigation of these so-called "smart" coatings, coatings that can switch their properties in response to external stimuli (or *vice versa*), atomic force (AFM) and optical microscopy was used. New techniques by means of combination of AFM and optical microscopy were developed. Also, established physico-chemical techniques were used to explore and characterize properties of the polymer brush systems.

Smart coatings are an interdisciplinary research field and everyone has something to bring to the table[1]: A chemist is for example interested in developing new synthetic methodologies or in studying polymerization in the confined dimensions of a thin film; an engineer is interested in understanding transport phenomena and barrier properties of new coatings and to design new devices; a biologist is interested in biomimetic systems that enable the replication of *in-vivo* conditions and cellular interactions; a nanotechnology oriented scientist thinks about the unique nanoscale dimension by which structure-property relationships can be derived; and a physicist is interested in interfacial phenomena, in particular the understanding of conformational changes and the resulting response.

We, me and my cooperation partners, addressed all of these points. By combining the capabilities of the involved groups in polymer synthesis, chemical characterization, atomic force- and optical microscopy, and micro-mechanical modeling, we developed new polymer brush systems that show unique properties, characterized these systems, emerged an understanding of the observed response and related this to possible applications. Examples are the rational design of sensors, actuators, and reversible adhesives.

1.2 Content of the Individual Chapters

After an introduction **Chapter 2** gives a review of the status of research on PE layers and of their theoretical treatment. In particular the most important aspects of PEs, functionalization of surfaces with PEs, and properties of polymer brushes are discussed. Furthermore the experimental techniques, i.e. AFM and optical microscopy

[1] The following passage is adapted from Ref. [1].

and fundamentals of interaction forces and contact mechanics that are relevant to the experiments presented in this thesis are introduced.
The thesis consist of five individual chapters that present issued publications in **Chapters five to nine** and work in progress that is presented as drafts in **further perspectives (Chapter 8)**.
The first paper (**Chapter 3**) presents a novel method that can be used to study adhesion and contact phenomena of surfaces based on a soft colloidal probe (SCP), attached to an AFM cantilever using the Johnson, Kendall, and Roberts (JKR) approach. In the second part (**Chapter 4**), a novel method is established to map contact stresses with unprecedented precision using mechanosensitive polymer brush layers. This system is calibrated using the SCP probe technique, introduced in Ch. 3.
Further, polymer brushes can be used for the design of responsive layer systems and to tune surface properties, such as wettability, adhesion, and friction. **Chapter 5** presents an approach for gradual tuning of surface interactions based on photo-responsive polymer brushes.
Also, responsive layers can be built from colloidal building blocks. Interaction properties of spherical polymer brushes (SPBs) with multilayers as a function of ionic strength are studied in **Chapter 6**. The measurement results can be used to explain and to regulate the absorption behavior of SPBs and to design functional layer systems.
Further, highly sensitive coatings are designed, based on block copolymer micelles. These coatings are investigated with respect to their swelling behavior which depends on pH and ionic strength (**Chapter 7**). Also the resulting changes in their porosity and mechanical properties are studied.
In **Chapter 8** further perspectives for mechanoresponsive systems are adressed. After discussions about further possibilities for direct measurements of contact stresses of soft materials (**Ch.8.1**), mechanoresponsive polymer brush systems are used in **Ch. 8.2** to study contact and adhesion of biomimetic adhesives. **Ch. 8.3** shows possibilities to enhance the sensitivity and resolution of the mechanoresponsive polymer brushes by rational design of the brush layers.

Soft Colloidal Probe AFM

Chapter 3: ”Soft Colloidal Probe AFM” [2] introduces a novel technique to characterize adhesion and contact on the micron scale.
Such phenomena are important for all kinds of soft matter interactions. Current issues of research are interface phenomena in biological systems, as cell migration or cellular

differentiation. Understanding the adhesive properties of cells to the substrate will help to control such behavior. Another important research field is miniaturization of components. The performance of nano and micronscale components is determined by their interfacial properties. Such, for materials selection, device design, and performance accurate determination of the interfacial properties is necessary. Also of growing interest are interfacial properties of complex synthetic systems, e.g. polymer brushes, multilayers and patterned surfaces, since such smart coatings can tailor surface properties like wettability, adhesion, permeability or optical features.

Requirements for the characterization of adhesion and contact phenomena are that information on the micron-sized contact zone and on dynamics of contact formation is accessible. Here, we introduce a novel approach for the investigation of such phenomena of soft matter surfaces that combines advantages of a macro scale method, the so-called "JKR apparatus" and a micro-scale method, namely colloidal probe (CP) atomic force microscopy (AFM).

In this soft colloidal probe (SCP) AFM technique an elastomeric colloidal probe, made of polydimethylsiloxane (PDMS) is attached to an AFM cantilever, rendering the contact area between probe and sample much larger as compared to standard CPs (e.g. composed of silicon or glass). This allows to determine the contact behavior of the probe, i.e. the contact area, via interferometry as a function of applied load (Figure 1.1A). The load can be controlled with subnanonewton precision using the AFM feedback loop. We could show that the contact situation can be described using a contact mechanics model developed by Johnson, Kendall, and Roberts (JKR).

In order to establish the technique, we developed a protocol for the SCP preparation and solved the problem of optical lever sensitivity determination for cantilevers functionalized with soft probes. SCPs made of PDMS with a diameter in the order of $10\,\mu$m and a Young's modulus in the order of 1 MPa were prepared via suspension polymerization of the precursor polymer in tenside solution. SCPs where attached to the cantilever in order to ensure an adequate (large enough) contact area between the particle and the cantilever.

In order to measure adhesion energies, we pressed the SCP against the substrate of choice and recorded the contact area by micro interferometry (i.e. reflection interference contrast microscopy: RICM) *in situ*. Fitting the data with the JKR theory yields the adhesion energy: the contact area (a) can be described as a function of applied load (P), elastic properties (K) and work of adhesion (w), $a = f(P, K, w)$, and all parameters except the work of adhesion are known (Figure 1.1B). We tested this method at ambient conditions as well as in aqueous media on well-known surface chemistries

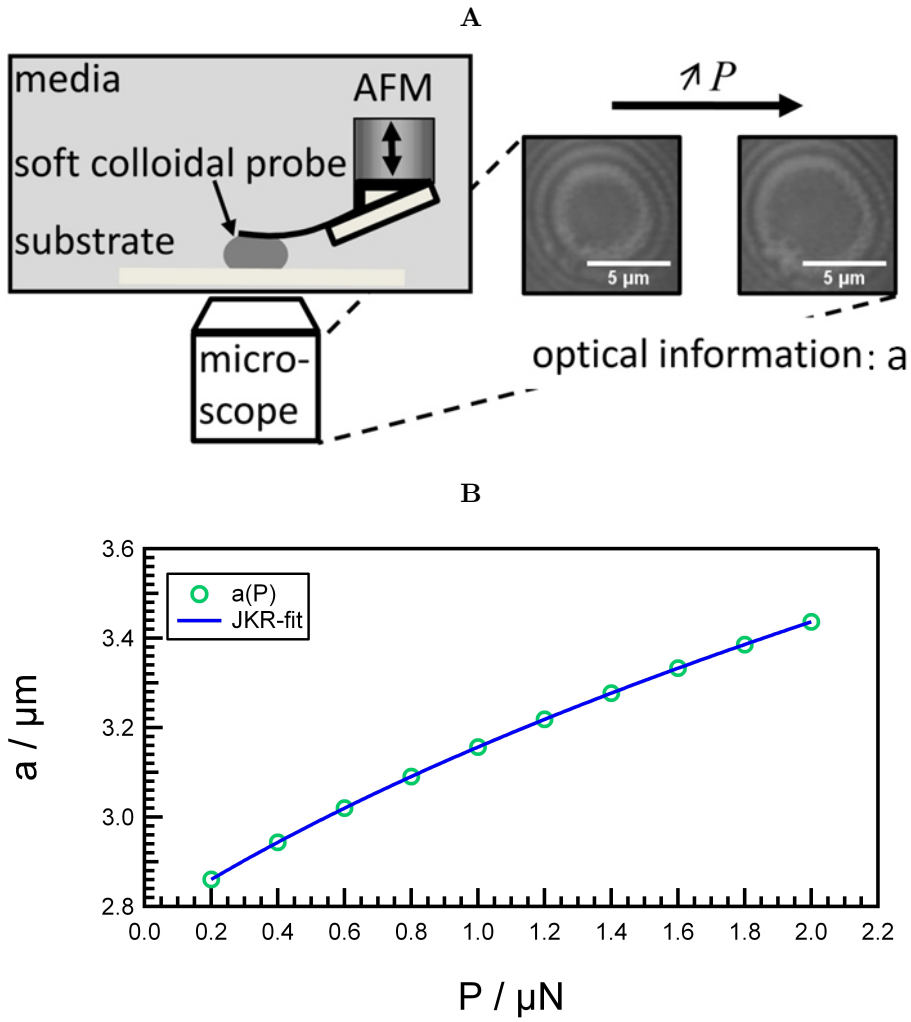

Figure 1.1: The soft colloidal probe technique: 1.1A Experimental setup, 1.1B Analysis of the thermodynamic work of adhesion

and can clearly separate the contributions of capillary forces in air, hydration forces, and hydrophobic interactions in water.
Full ensemble of data (for every load w can be determined) and the large contact area make the SCP approach an outstanding method for adhesion measurements with an enhanced sensitivity. Additionally it is possible to study soft matter contact situations at controlled conditions on the micron scale. This fact can be exploited to investigate stress sensitive systems, because the local stress can be determined from JKR theory for an adjusted applied load. In the contact zone the sample under investigation is exposed to various pressures and its response can be analyzed.

Mechanoresponsive Polyelectrolyte Brushes

Chapter 4: "Mechanoresponsive Polyelectrolyte Brushes" [3] introduces a promising technique for local detection of stress distributions with outstanding resolution. Therefore stress is translated by a mechanoresponsive polyelectrolyte brush into an optical output.
Accurate knowledge of stress distribution in the contact area is crucial for understanding soft matter contact situations. The key challenge in the experimental studies of stress distributions in soft matter contacts is the demand of combining high stress sensitivity (on the order of kPa) with high lateral resolution (below micrometer). Classical solutions, such as stress sensors (often called pressure sensors) using the deflection of mechanical elements like membranes as a means for quantifying stresses are reaching fundamental limits in terms of the lateral dimensions. Even most sophisticated microelectromechanical system approaches (MEMS) have so far only reached the pressure sensitivity for lateral dimensions of $>> 10\,\mu$m. Mechanoresponsive materials even in their early stages of developments, overcome these fundamental limitations. In these systems, a mechanical stimulus directly affects the electrical, chemical or optical property of a material sensor. For these material based approaches, the limiting factor in terms of lateral resolution is how locally the material responds to external pressure and how accurately these changes can be read out.
Polymer brushes are particularly interesting in this respect, since they consist of individual, surface grafted, but not laterally crosslinked polymers. The weak lateral coupling, indeed, is a necessary condition for high lateral resolution. At the same time, polymer brushes are themselves soft matter systems and thus match the typical range of elastic properties and deformability, allowing for suitable sensitivity. The key challenge however is to modify the polymer brushes such that their compression state can

be read out in a simple fashion with high lateral resolution.
We developed promising mechanical addressable surfaces, that report stress fields by translating a mechanical stimulus (stress) into an optically detectable response in aqueous solution (Figure 1.2A). These surfaces were realized on the basis of cationic, fluorescently labeled polyelectrolyte brushes: Poly[2-(Methacryloyloxy)Ethyl] Trimethyl Ammonium Chloride (PMETAC) copolymer brushes labeled with carboxyfluorescein dye (CF). The dye molecules are covalently immobilized on the brush. Such surfaces report stress by a change in fluorescence due to dye quenching. Polymer brush compression leads to an association of CF with the quaternary ammonium groups of METAC, while local stretching of the chains causes a decrease in quenching. Quantitative characterization of the mechanoresponsive properties of polyelectrolyte brushes were performed using soft colloidal probe AFM introduced in Ch. 3.
Pressure was applied to the brushes using an atomic force microscope (AFM) equipped with a cantilever functionalized with an elastomeric probe made of PDMS. Due to mechanical deformation of the soft colloidal probe, the contact area of the system is large enough to be monitored with a confocal laser scanning microscope (CLSM) *in situ*. Upon contact of the SCP with the surface, a dark spot surrounded by a bright rim occurs (Figure 1.2A). In order to understand the behavior of the observed response, the contact situation underneath the PDMS bead is modeled using the contact mechanics theory of Johnson, Kendall, and Roberts (JKR). The JKR model describes the contact as interplay between elastic deformation and adhesion (Figure 1.2B). The resulting stress distribution underneath the bead remains compressive at the center, while stresses are tensile at the edge of the contact area. We can assign the decrease in fluorescence intensity (as compared to the background intensity) to areas of compression and the slight increase at the rim of fluorescence to areas of tension. With this observation, a response function $I(p)$ which correlates local fluorescence intensity (I) to local (calculated) stress (p) was established (Figure 1.2C) . We demonstrated that stress distributions could be translated into local fluorescence signals with a lateral resolution limited by the optical read-out (1 micron) and a stress sensitivity of at least 10 kPa.
Also, the response of the sensor stabilized well before the acquisition time ($1-2$ s) and it is constant over several minutes and completely reversible.
Further, brush compression and quenching can be induced by the addition of salts. We could show that the dependency of the relative intensity on p is only weakly changing with salt concetration of the solution.

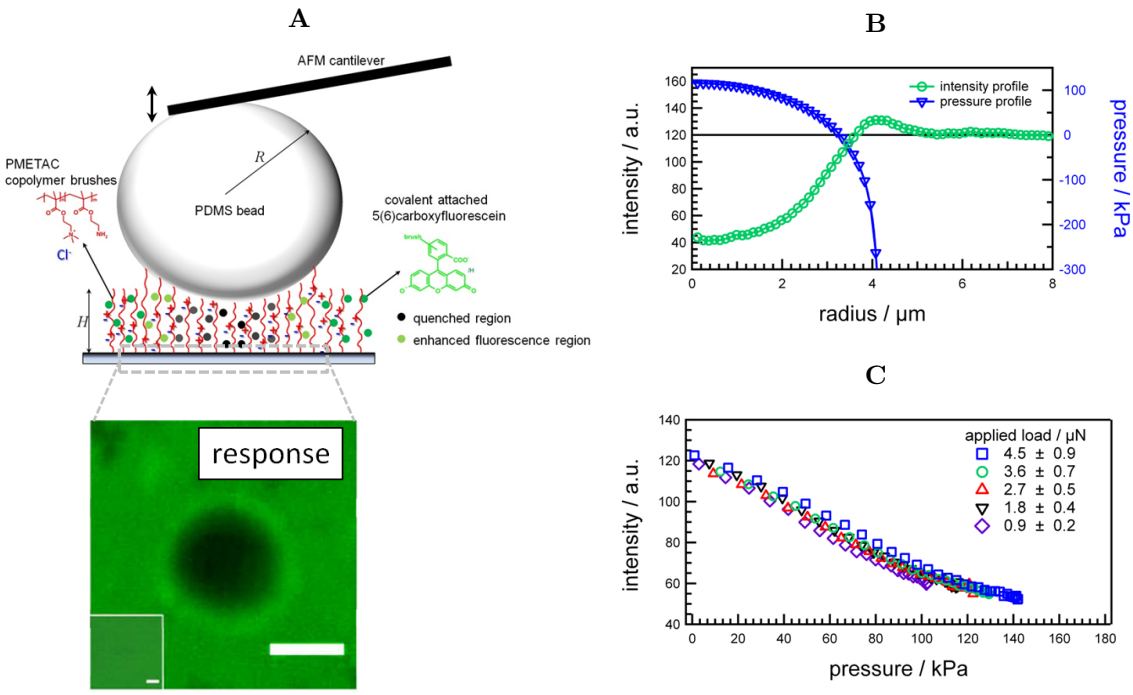

Figure 1.2: Mechanoresponsive surfaces: 1.2A Experimental design to measure the fluorescence-based readout. PMETAC copolymer brush with covalently immobilized CF (brush height $H \approx 100\,\text{nm}$) compressed with a SCP (Radius $R \approx 15\,\mu\text{m}$) and observed fluorescence signal, 1.2B Detected intensity and calculated stress profile, 1.2C Determined response function

Phototunable Surface Interactions

Chapter 5: "Phototunable Surface Interactions" [4] reports on a novel approach to tune surface interactions gradually with light.
Gradual tuning of surface properties, in particular wettability , adhesion, and friction is important for a large number of applications and allows matching of surface properties for the desired application. For example surface gradients can be used for manipulation of the motion of liquids or to prepare water harvesting surfaces. Another application is controlled attachment or detachment of chemical compounds. This can be used for instance in drug delivery systems or lab on the chip devices.
Instead of tuning the surface properties by variation of the synthesis protocol (as varying the molecular architecture) this chapter inserts a simple alternative to tune surface properties via light. Light responsive polymer brushes were obtained by surface initiated atom transfer radical polymerization (ATRP) of a methacrylate monomer containing ionizable -COOH side groups caged with photo-removable 4,5-dimethoxy-2-nitrobenzyl (NVOC) (Figure 1.3A). Photo-response was possible using photo labile caged compounds. The neutral polymer brush (PNVOCMA) transforms to a charged, hydrophilic poly(metacrylic acid) polymer (PMAA) brush upon exposure with ultraviolet light ($\lambda = 365\,\mathrm{nm}$) due to removal of the o-nitrobenzyl groups. The light-dependent compositional change can be controlled by exposure time, intensity and allows to define intermediate interfacial states (instead of variation of brush length or grafting density). As a consequence the surface properties change. We show how the physical properties, in particular wettability, hydrophobicity, adhesion, and lubrication of the brush can be gradually tuned with the exposure dose using quarz micro balance technique, condensation microscopy, atomic force microscopy (AFM), force mapping and friction force spectroscopy. For this purpose patterned brush substrates were prepared by irradiated through a structured quartz mask. In this way an internal standard was conserved in the experiment that allowes comparison between different samples and to create an internal reference for the surface properties.
We obtained a relationship between photoconversion and irradiation dose and followed the light-modulated generation of hydrophilic COOH groups using quartz crystal micro balance technique. Here the water uptake of the hydrophilic polymer brush was detected that increases as a function of time (Figure 1.3B). Visualization of the wettability differences between the PNVOCMA and the PMAA polymer brushes was also possible by condensation microscopy. Water condensed primarily on the exposed regions, i.e. PMAA-rich areas that are more hydrophilic than areas covered by unexposed

PNVOCMA. This can be for example exploit for selective adsorbtion of particles and therefore for the design of hirachical structures from colloidal building blocks. Further, using imaging AFM, we could identify a topographic contrast of around 3 nm between 0% und 100% conversion that can be asigned to the release of NVOC groups.
As a consequence of photoconversion, interfacial surface forces change as well. To analyze the physical properties of the defined intermediate chemical states we used force spectroscopy and friction measurements. Therefore, we determined the interfacial properties between the polymer brush and the cantilever probe (SiO_2 tip). By force spectroscopy and quantitative imaging (every pixel of a detected image contains information on adhesion and repulsion) we demonstrated that adhesion forces on irradiated areas decreased and repulsive forces increased due to electrostatic repulsion. Above 75% conversion, a clear contrast between irradiated and no irradiated areas could be observed, which was not detectable below 50%. Also, solvent forces and steric interactions contribute to this behavior. In case of friction measurements we could observe a continuous increase of friction force contrast between PNVOCMA and PMAA areas (Figure 1.3C).

Interactions of Spherical Polyelectrolyte Brushes

Chapter 6: "Interactions of Spherical Polyelectrolyte Brushes" [5] covers, how surface properties, in particular interaction forces, can be tailored to adjust the adsorption behavior of spherical polyelectrolyte brushes for hierarchical particle organization.
Alternative to functionalize surfaces with PE molecules such as for example using polymer brushes (as shown in Ch. 5), surface modification is also possible using colloidal building blocks. This offers interesting possibilities since the colloids can carry various functionalities. Additionally, the size of colloidal particles increases the adsorption energy as compared to single (macro-) molecules while ensuring that interfacial interactions are dominant over inertia or other forces for the macro-scale.
Understanding the underlying interactions between the colloidal building block and the substrate of interest is fundamental for surface modification and further applications. Examples are the design of hierarchical structures of metal colloids out of suspension that allows surface enhanced raman spectoscopy due to plasmon coupling between adjacent particles.
In this work, we investigated the interaction of the colloidal building blocks, i.e. anionic spherical polyelectrolyte brushes (SPB: Polystyrene (PS) core and attached polystyrene sulfonate (PSS) chains) and substrates functionalized with polyelectrolyte multilayers

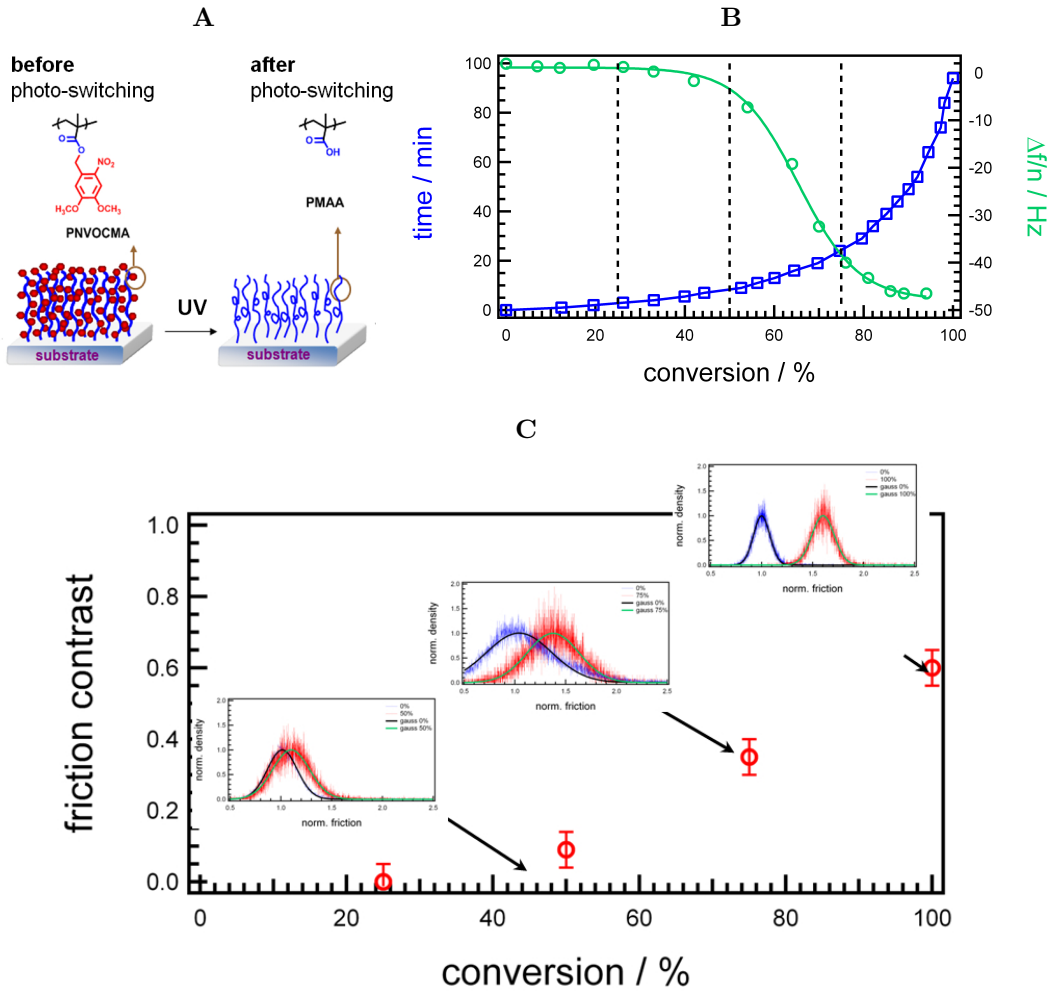

Figure 1.3: Phototunable surface interactions: 1.3A Photo-responsive system 1.3B time and water uptake vs. photo conversion and 1.3C friction contrast vs. photo conversion.

consisting of polystyrene sulfonate (PSS) and poly-(diallyl dimethyl ammonium chloride) (PDA) (Figure 1.4A). For this purpose, we established a protocol for the preparation of micrometer-sized polystyrene particles (orders of 10 μm) decorated with PSS chains as model system for SPBs nanoparticles. Using centrifugal sedimentation and zeta potential measurements we could prove successful functionalization.
The particles were glued to an AFM cantilever and interactions between the particles and polyelectrolyte multilayers were measured using force spectroscopy. Comparison of the interactions between SPBs that were used as CPs, with oppositely charged, amino-functionalized substrates, and uncoated PS cores with amino-functionalized substrates confirm the fuctionalization of the PS particles with PSS chains. Using these probes and measure the interactions between these "micron SPBs" and PDA and PSS terminated multilayers we could show that the adhesive properties of the SPBs can be controlled by the ionic strength and the charge of the substrate (Figure 1.4B).
In addition, we studied the adsorption behavior of SPBs as a function of the ionic strength and the influence of the substrate charge (Figure 1.4C). For this purpose, we used nanosized SPBs (order of 100 nm) consisting of a PS core grafted with PSS chains. Covering a wide range of ionic strengths we have found a clear dependence of the surface coverage of SPBs on the substrate on the NaCl concentration and the substrate charge.
With increasing ionic strength, the coverage increased for oppositely charged surfaces up to an ionic strength of 10 mM. No SPB adsorption occurs on equally charged surfaces. Further increase of the ionic strength of the solution results in a gradual loss of the substrate selectivity. This can be explained by the transition of the polymer brush from the osmotic to the salted brush regime. In the osmotic brush regime the release of counterions and electrostatic repulsion of SPBs and charged substrates determine adsorption respectively. In the salted brush regime that can be assigned to ionic strengths > 10 mM, attractive secondary interactions become dominant.
We utilize this behavior for the design of hierarchical surface patterns. Therefore we prepared charge patterned substrates using micro contact printing for selective SPB adsorption.

Swelling Behavior of Block Copolymer Micelles

Chapter 7: "Swelling Behavior of Block Copolymer Micelles" [6] deals with highly responsive coatings based on block copolymer micelles.
Smart coatings, which can reversibly switch their physico-chemical properties in re-

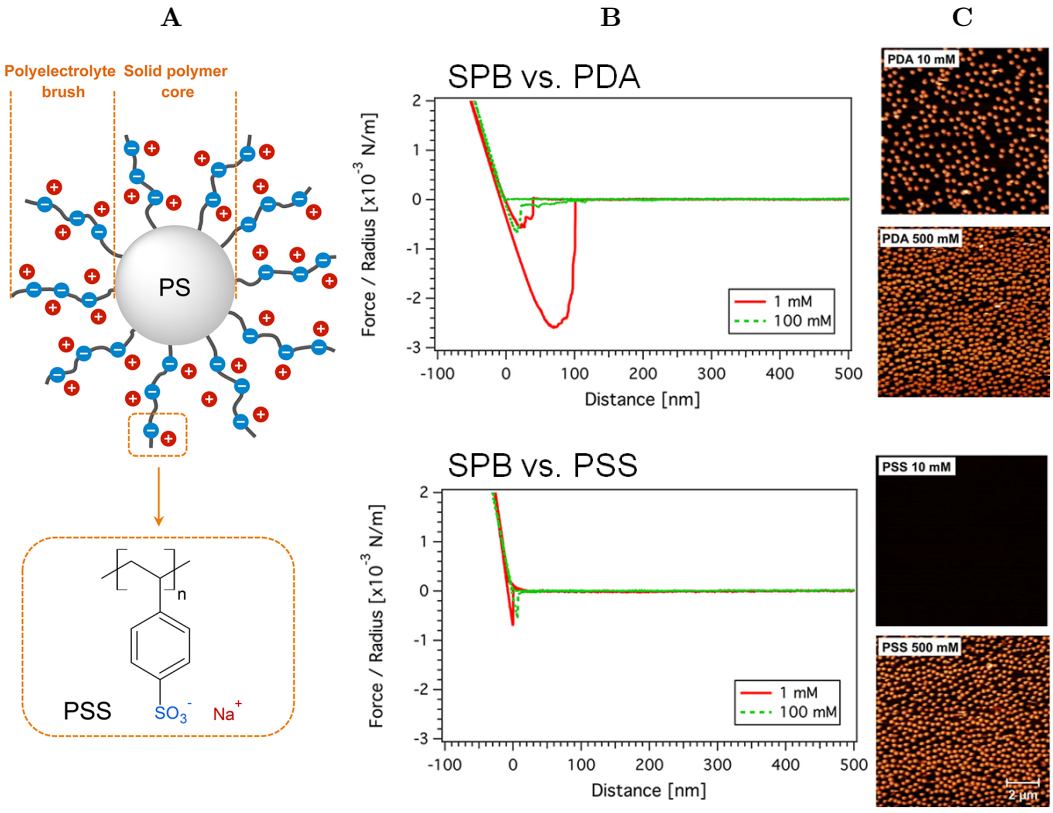

Figure 1.4: Interactions of Spherical Polyelectrolyte Brushes: 1.4A Design of the SPBs, 1.4B Interactions of SPB with PE functionalized substrates, 1.4C Adsorption behavior of SPBs depending on the salt concentration.

action to external stimuli are a very attractive research field regarding its potential applications (as shown above). Examples are drug delivery, microfluidic systems, cell tissue engineering, as well as sensing, or actuation.
Our goal was to create highly responsive and stable coatings. Therefore we used micells that are composed of a hydrophobic polybutadiene core, an annealed anionic poly(methacrylic acid) polymer brush shell and a quenched cationic corona of quaternized poly(2-(dimethylamino)ethyl methacrylate) as building block. These micelles were assembled from solution (pH 4 buffer, where the shell is uncharged) with a quenched polyanion (anionic poly(sodium 4-styrenesulfonate: PSS) into multilayers as scatched in Figure 1.5A using the layer-by-layer (LBL) approach. This system combines the advantages of the highly responsive annealed polymer brushes, the functionality and internal hierarchy of colloidal building blocks and the simple preparation procedure of LBL films.
These multilayer are studied with respect to morphology, porosity swelling degree and the corresponding mechanical properties dependent on the composition of the film and the surrounding medium. Using ellipsometry, AFM imaging and force spectroscopy we followed the pH triggered reversible swelling and contraction of the multilayer films and the resulting mechanical properties. Also, the dependence on the number of deposition steps was investigated.
We could show that morphology and porosity strongly depend on the number of deposition steps. The porosity can be tuned between 0% and 50% for 20 or 1 deposition steps, respectively. The porosity has a big influence on the water uptake and the corresponding swelling behavior. We could vary water uptake by around two orders of magnitude and the swelling degree by more than three orders of magnitude. The swelling decreases with increasing film thickness.
Pore opening and closing and the resulting degree of swelling can be regulated by the solution pH (between pH 4 and pH 12). We observed a 6-fold increase in film thickness. This could be associated to an increase in Young's modulus from a few kPa to hundreds of kPa (Figure 1.5B).

Further Perspectives

Chapter 8: "Further Perspectives" addresses new aspects of the mechanoresponsive systems based on cationic polymer brushes (Ch. 4). Understanding the nature and the distribution of stresses at the contacts of deformable solids is fundamental to the fields of soft mechanics and adhesion. The results of mechanoresponsive systems based on

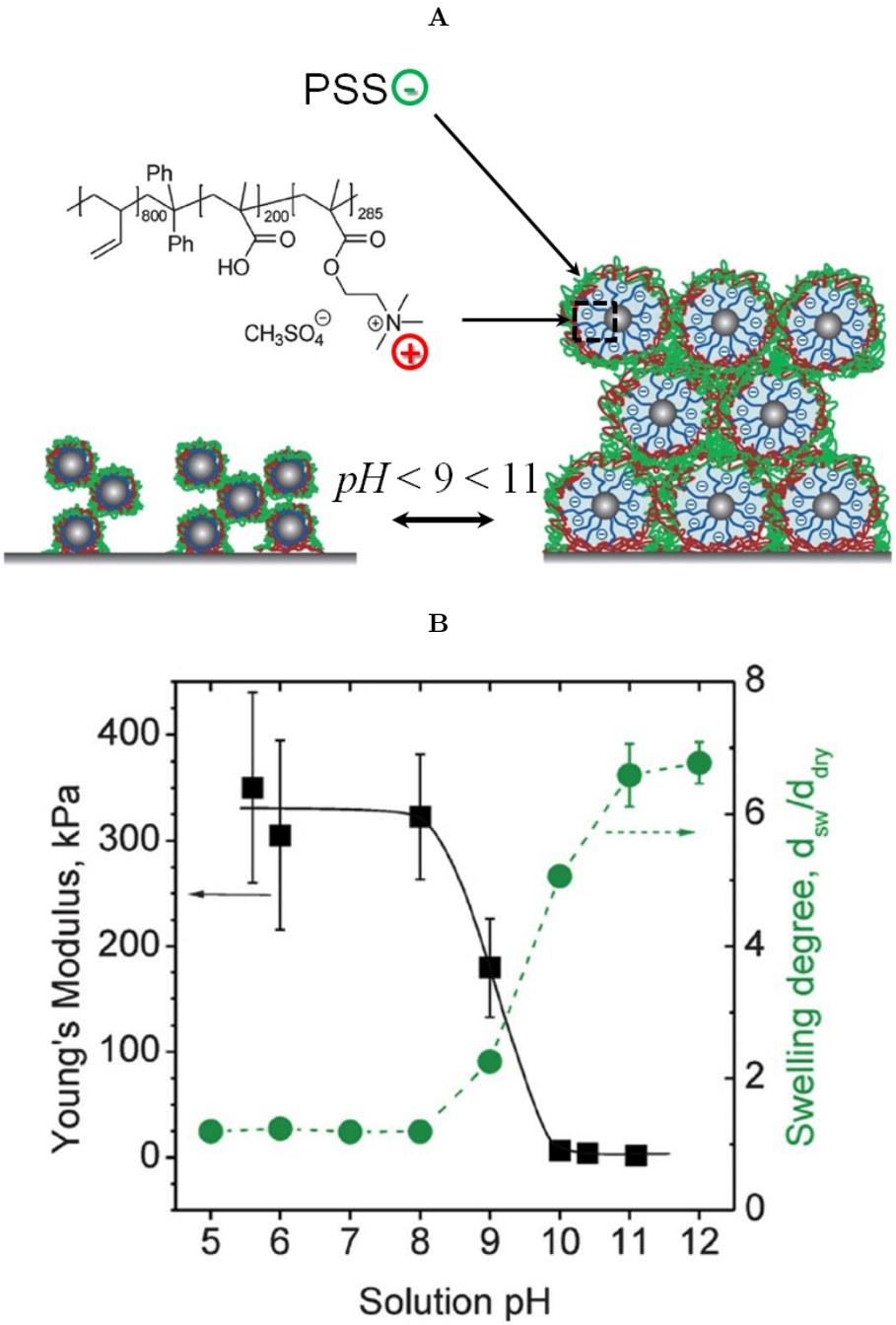

Figure 1.5: Swelling of Block Copolymer Micelles: 1.5A Micelles are composed of a hydrophobic polybutadiene core, an annealed anionic poly(methacrylic acid) polymer brush shell and a quenched cationic corona of quaternized poly(2-(dimethylamino)ethyl methacrylate). These micelles are assembled in layer-by-layer films using PSS. 1.5B Response of block copolymer micelles to pH.

cationic polymer brushes are very promising, and several fundamental aspects can be addressed to fully unfold the potential of this detection scheme (Ch.8.1).
Also, such surfaces are of particular interest for the understanding of bioinspired reversible adhesives as will be discussed in Ch.8.2. Further, possible enhancement of the sensitivity and resolution of the mechanoresponse by rational design of brush layers is discussed in Ch.8.3.

1.3 Individual Contributions

This work is the outcome of close collaborations and knowledge transfer between different groups and individual contributions of diverse persons besides the author.

Soft Colloidal Probe AFM

- I developed the method, performed and analyzed all experiments, and wrote the manuscript.
- S. Schmidt helped to develop the method and corrected the manuscript.
- A. Fery analyzed the results, helped with discussions, and correcting the manuscript.

Mechanoresponsive Polyelectrolyte Brushes

- I developed the method for stress detection, performed and analyzed all experiments for stress detection, wrote parts of the manuscript and corrected the manuscript.
- J. Bünsow developed the synthesis protocol for the mechanoresponsive polymer brushes, characterized the polymer brushes, helped to develop the method and with the experiments for stress detection, wrote parts of the manuscript, and corrected the manuscript.
- P. M. Biesheuvel helped to analyze and discuss the results.
- A. Fery analyzed the results, helped with discussions, and corrected the manuscript.
- W.T.S. Huck analyzed the results and finalized the manuscript.

Photo-Tunable Surface Interactions

- I performed and analyzed all experiments for the characterization of surface properties of the polymer brush, and wrote the manuscript.
- J. Cui synthesized and characterized the brushes substrates, and corrected the manuscript.
- J. Schmid helped with force spectroscopy measurements and the development of the condensation microscopy technique.

- M. Kappl helped with the AFM measurements, participated in discussions, and corrected the manuscript.
- A. del Campo analyzed the results, helped with discussions, and corrected the manuscript.
- A. Fery analyzed the results, helped with discussions, and corrected the manuscript.

Interactions of Spherical Polyelectrolyte Brushes

- I performed the AFM interaction measurements, analyzed these experiments, was involved in scientific discussions, wrote parts of the manuscript, and corrected the manuscript.
- C. Hanske performed adsorption experiments, the micro contact printing, analyzed these experiments, was involved in scientific discussions, and wrote the manuscript.
- C. Kühr and C. Schneider synthesized and characterized the SPBs and the microparticles.
- M. Trebbin produced a special designed stamp for micro contact printing using soft lithography.
- A. Wittemann developed the synthesis protocol for the SPBs, was involved in scientific discussions, wrote parts of the manuscript, and helped correcting the manuscript.
- A. Fery analyzed the results, helped with discussions, and corrected the manuscript.

Swelling of Block Copolymer Micelles

- I performed colloidal probe AFM measurements, was involved in scientific discussion, wrote parts of the manuscript, and corrected the manuscript.
- J. Gensel and I. Dewald performed most of the experiments, and analyzed these experiments. J. Gensel wrote the manuscript.
- E. Betthausen conducted the synthesis and characterization of the polymer used, was involved in scientific discussions, and corrected the manuscript.

- A. H. E. Müller helped with discussions, and corrected the manuscript.
- A. Fery analyzed the results, helped with discussions, and corrected the manuscript.

Further perspectives

Direct measurements of contact stresses of soft materials for rational design of reversible adhesives

- I wrote the manuscript.
- M. Chaudurhi helped with discussions.
- A. del Campo helped with discussions.
- A. Fery helped with discussions.

Contact and Adhesion of Biomimetic Patterned Adhesives

- I developed the method to study stress distributions of biomimetic contacts, performed and analyzed the experiments and wrote the manuscript.
- D. Drotlef produced masters for the biomimetic substrates and performed the adhesion and the SEM measurements.
- I. Dewald synthesized and characterized the mechanoresponsive brush substrates.
- J. Bünsow helped to develop the method to study stress distributions of biomimetic contacts, developed the synthesis protocol for the mechanoresponsive brush substrates, and corrected the manuscript.
- M. Chaudurhi helped with discussions.
- A. del Campo analyzed the results, helped with discussions, and corrected the manuscript.
- A. Fery analyzed the results, helped with discussions, and corrected the manuscript.

Tuning the response of mechanoresponsive brushes

- I performed and analyzed all experiments, developed the theoretical models, and wrote the manuscript.
- J. Neubauer and I. Dewald synthesized the brush substrates. J. Neubauer helped with force spectroscopy experiments and the analysis of the data.
- S. Block helped to analyze the experiments, and developed the theoretical model.
- J. Bünsow helped with discussions.
- S. Carregal and W. Parak developed the synthesis protocol for attachment of SNARF molecules.
- A. del Campo helped with discussions.
- A. Fery helped with discussions.

1.4 References

[1] Knoll. *Functional Polymer Films*. Vol. 1. Wiley-VCH. Weinheim, Germany, 2011.

[2] J. Erath, S. Schmidt, and A. Fery. "Characterization of adhesion phenomena and contact of surfaces by soft colloidal probe AFM". In: *Soft Matter* 6.7 (2010), pp. 1432–1437.

[3] J. Bunsow et al. "Direct Correlation between Local Pressure and Fluorescence Output in Mechanoresponsive Polyelectrolyte Brushes". In: *Angewandte Chemie-International Edition* 50.41 (2011), pp. 9629–9632.

[4] J. Erath et al. "Phototunable surface interactions". In: *Langmuir* 29.39 (2013), pp. 12138–44.

[5] C. Hanske et al. "Adsorption of Spherical Polyelectrolyte Brushes: from Interactions to Surface Patterning". In: *Zeitschrift Fur Physikalische Chemie-International Journal of Research in Physical Chemistry and Chemical Physics* 226.7-8 (2012), pp. 569–584.

[6] J. Gensel et al. "Reversible swelling transitions in stimuli-responsive layer-by-layer films containing block copolymer micelles". In: *Chemical Science* 4.1 (2013), pp. 325–334.

2

Theory and Status of the Field

2.1 Introduction

Thin polymer films[1] on hard substrates have attracted interest over the last decades due to their importance in understanding material properties and their potential applications [1]. Examples are protective coatings or microelectronics. Often these films have interesting surface properties like defined wettability, adhesion, permeability, or optical properties just to name a few. Although the importance of such functional polymer films is undisputed, most interest has been paid to coatings that switch their properties in response to external stimuli or vice versa [1, 2, 3, 4, 5] (Figure 2.1). Such stimuli-responsive polymer films on hard substrates are named smart, intelligent or sensitive coatings. Stimuli can be physical (temperature, electric or magnetic fields, and pressure) or chemical (changes of the environment as pH and ionic strength, or specific reactions), see Tab. 2.1.

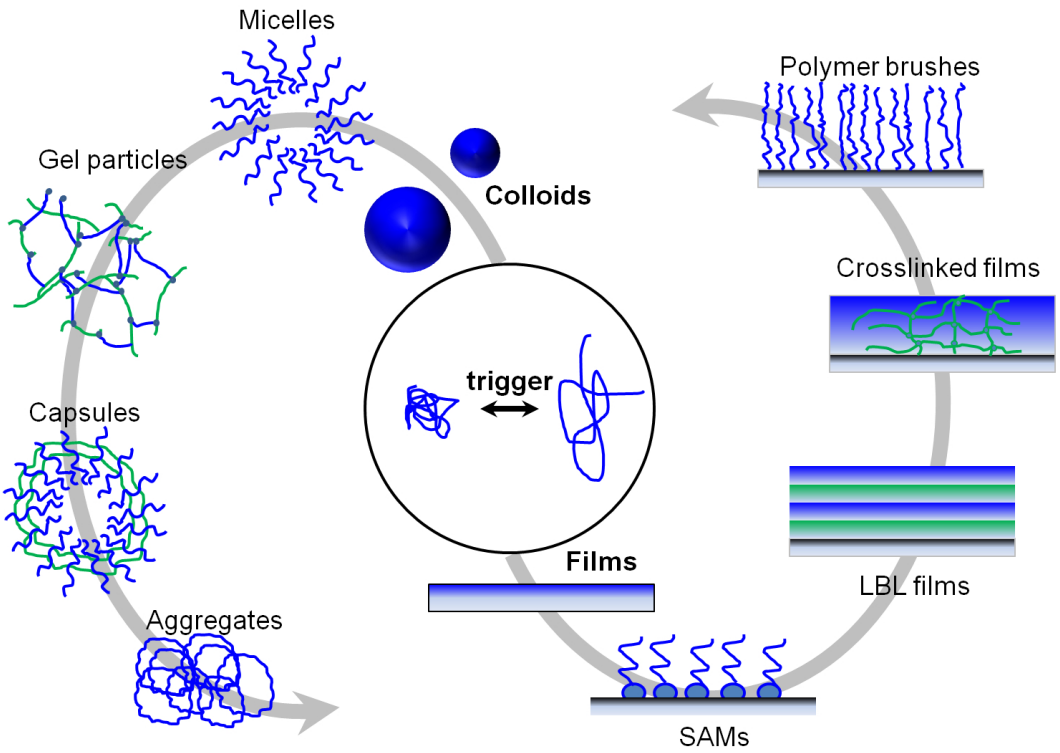

Figure 2.1: Examples for responsive systems (adapted from [5] ©Nature Publishing Group)

Even more exciting are coatings with reversible response, where by switching off the external stimuli the output state is re-established. The development of stimuli-responsive

[1]Thin films refers in this thesis to coatings with thicknesses in the submicron range ($< 1\,\mu$m)

Table 2.1: Typical external triggers of responsive surfaces

chemical	physical
pH	temperature
ionic strength	electric or magnetic fields
specific reactions	pressure
	light

systems has emerged as a major research topic both in fundamental and applied research. The latter addressing issues such as tissue engineering, drug delivery, reactive surfaces, sensors or actuators, separation systems, as pointed out in the reviews Ref. [5, 4, 6, 7, 8, 9, 10, 11, 12, 13, 14].

In general the change in the physical properties of smart coatings is caused by a change in the conformation of polymers attached to the surface. Formation of such polymer coatings can be realized by self-assembly from solution, adsorption on surfaces (formation of thin film networks), built-up of multilayer films, or covalent grafting to a surface. In particular endgrafted polymers form a so called "polymer brush", if the grafting density is high and the polymers are stretched due to steric or electric interactions [5, 13].

Polymer brushes, especially polyelectrolyte polymer brushes, are an attractive building block for stimuli responsive films, because they are very flexible with respect to their molecular design and it is possible to tune their conformation and chemical state and therefore their physical properties by changing the environment [9, 15]. The benefits of polyelectrolyte polymer brushes (compared to neutral polymer brushes) are their charges. Due to the charge, resulting interactions and conformation changes are more pronounced. By incorporation of addressable functional groups, the surface can be triggered by external fields.

Details and specific examples of several functional smart coatings, in particular polymer brushes are shown in the following sections (see Ch. 2.2).

2.2 From Polymers to Polyelectrolyte Brushes

The present chapter gives a review on the literature available, points out the main parameters, and summarizes status of the field. Particular emphasis is laid on the interpretation of experiments presented in this thesis. The introduction is oriented on monographics [1, 16, 17] and the cited literature.

2.2.1 Neutral Polymers

Macromolecules that are built of a large number of repeating covalently bond units (monomers) are known as polymers. These molecules have a lot of interesting physical properties and these days many applications. For a more detailed overview the reader is referred to Ref. [18, 19]. An ideal neutral polymer chain with no inter-chain interactions can be described by a Gaussian chain (rather a freely jointed chain or wormlike chain) (Figure 2.2A). This Gaussian chain model for neutral polymers assumes a chain where the effective bond length a (Kuhn length: including the stiffness of the polymer) is Gaussian distributed and r is the distance from the initial monomer. The conformation distribution is given by

$$\psi(\vec{r_j}) = \left(\frac{3}{2\pi a^2}\right)^{3N/2} \exp\left(-\sum_{j=1}^{N} \frac{3\vec{r_j}^2}{2a^2}\right) \tag{2.1}$$

The resulting mean square end-to-end vector[2] that scales as

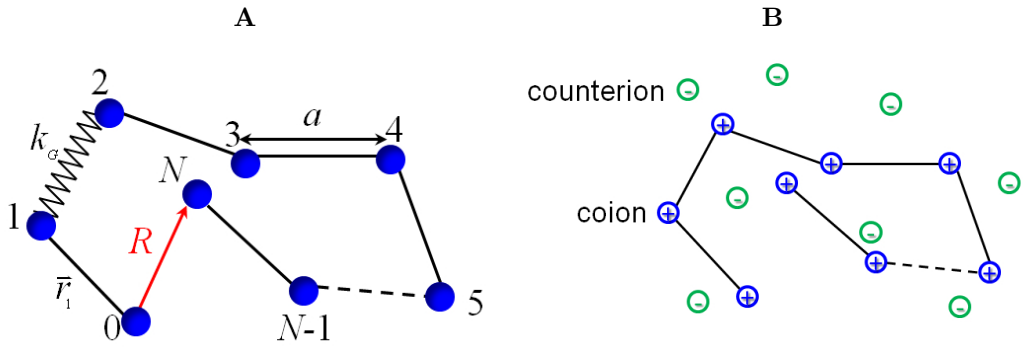

Figure 2.2: Possible polymer systems: Neutral polymer 2.2A, Charged polymer: e.g. polycation, 2.2B

$$\left\langle \vec{R}^2 \right\rangle \equiv R^2 = Na^2 \tag{2.2}$$

$$\Rightarrow R \propto N^{1/2} \tag{2.3}$$

defines the size of such a freely jointed Gaussian chain. The potential of the Gaussian chain $U(\vec{r_j})$, with an end-to-end vector $\vec{R}$ is often modeled by bodies connected by

[2] the average end-to-end vector $\vec{R}$ is zero

harmonic springs that can be described by Hook's law

$$U(\vec{r_j}) = \sum_{j=1}^{N} \frac{3K_bT}{2a^2} \vec{r_j}^2, \tag{2.4}$$

where K_b is the Boltzman constant and T the absolute temperature. The spring constant $k_G = \frac{3K_bT}{Na^2}$ of the polymer relates to the entropic stretching force required to maintain the end-to-end vector $\vec{R}$ of the chain.
So far, no interactions with other monomers and solvent molecules are considered. In a real polymer chain, segments interact with each other if they come close. Additionally, if the polymer is dissolved, the interactions with the surrounding environment come into play. As a result each chain segment requires its own finite volume. Statistically, this can be described by a self-avoiding random walk. The excluded volume v_2 is defined by

$$v_2 \equiv \int d\vec{r} \left[1 - \exp\left(\frac{-u(\vec{r})}{K_bT} \right) \right], \tag{2.5}$$

where $u(\vec{r})$ is the interaction potential between the chain segments (e.g. the Lenard Jones potential). The Boltzmann factor accounts for the relative probability to find a second monomer at temperature T at a distance r [16].
The free energy of the chain

$$f(\vec{R}, N) = U(\vec{R}, N) - TS(\vec{R}, N), \tag{2.6}$$

with U the inner energy and S the entropy can be modeled by a virial expansion with respect to the local concentration $c(\vec{r})$ where many-body interactions are considered [16]:

$$\frac{f}{K_BT} = \int d\vec{r} \left(\frac{1}{2} v_2 c(\vec{r})^2 + \frac{1}{6} v_3 c(\vec{r})^3 + O(c(\vec{r})^4) \right) \approx v_2 \frac{N^2}{R^3} + v_3 \frac{N^3}{R^6} + O(v_4), \tag{2.7}$$

The excluded volume v_2 characterizes two-body interactions. The component v_3 accounts for three-body interactions, and so forth. The surrounding liquid of the polymer determines which term dominates. If $v_2 \neq 0$, the two-body interaction dominates and determines the size of the polymer. If $v_2 > 0$ the polymer swells due to excluded volume repulsion and if $v_2 < 0$ the polymer collapses into a globule according to the three-body term. In the cases where $v_2 = 0$ the tree-body interaction is the dominant contribution and the polymer behaves approximately like an ideal polymer with no interactions. By minimization of f with respect to R, the size of the polymer can be

approximated in consideration of the solvent

$$R \propto aN^{\nu} \text{ with } \nu = \begin{cases} 3/5, & \text{for } v_2 > 0: \text{ good solvent} \\ 1/3, & \text{for } v_2 < 0: \text{ bad solvent} \\ 1/2, & \text{for } v_2 = 0: \ \theta \text{ solvent} \end{cases} \tag{2.8}$$

The excluded volume has an increasing influence on the size of a polymer with increasing N. These results are in good agreement with modern many-body theory approaches.

If polymers adsorb onto an interface, i.e. a surface, the chains get confined which is associated with an increase in the free energy (see Eq. 2.6). Consequently, for a stable conformation there must be an attractive interaction that leads to a decrease of the free energy. If entropic restrictions dominate, no adsorption will take place. The adsorbed polymer can either be in equilibrium with the surrounding solution or it can be in a restricted equilibrium.

2.2.2 Polyelectrolytes

Polyelectrolytes (PEs) are water soluble polymers that carry ionized or ionizable groups (charges) [16, 20] (Figure 2.2B).

PEs are an interdisciplinary research field covering many areas from life science in the form of nucleic acids, proteins and peptides to supramolecular chemistry, just to mention a few [16, 17]. In addition PEs have found extensive use in many applications. Examples are films and textile industry, chemical industry uses them as flocculating and coagulating agents, petrol, and cosmetic industry as additives in conditioners [21], and many others [17]. The synthesis and formation of PEs is described elsewhere, e.g. Ref. [16].

Charged groups can be cationic or anionic. The geometric position of the charged groups (on side chaines or along the polymer backbone) is relevant for the physical properties of the PE, e.g. in complex formation. If number and position of charges are fixed inside the polymer, the system is referred to as quenched PE. If the charges are mobile inside the polymer and the degree of charging α is not constant, the polymer is referred to as annealed PE. An example for quenched PEs is poly(sodium 4-styrene sulfonate) (PSS), and for annealed PEs poly(acrylic acid) (PAA).

Besides the number of monomer units (equals to the molecular weight), the charge density and the charge distribution of the anionic or cationic charges along the polymer

chain are parameters to characterize PEs [16]. The bulk concentration C_j of species j leads to an ionic strength I (in mol/l) of

$$I = \frac{1}{2}\sum_j z_j^2 C_j(\vec{r}), \tag{2.9}$$

and the local charge density $\rho(\vec{r})$ is related to the local ion concentration c_j by

$$\rho(\vec{r}) = e\sum_j z_j c_j(\vec{r}), \tag{2.10}$$

where e is the elementary charge, c_j local ion concentration, and z_j the valency of species j.

For PEs, the excluded volume (monomer-monomer repulsion) is much larger compared to neutral polymers due to the electrostatic Coulomb potential that determines the conformation and interactions of the polymer.

The Coulomb potential $u(\vec{r})$ is determined by the Poisson equation for electrostatics

$$\nabla^2 u(\vec{r}) = \frac{-\rho(\vec{r})}{\epsilon}, \tag{2.11}$$

where ϵ[3] is the dielectric permeability. Dissolving the PE in aqueous (salt) solution (electrolyte solution) leads to immobilized counter-charges, i.e. counterions that maintain electric neutrality and are attracted by the charged units of the PE. Attraction leads to screening of the Coulomb interactions. The distribution of the mobile counterions is governed by the electric field around the PE and the balance of electrostatic energy and entropic contributions ($S \propto k_B T \ln(r)$) [22].

The Coloumb potential of the PE is determined by the Poisson equation Eq. 2.11 and depends on its geometry

$$u(\vec{r}) \propto \begin{cases} 1/r \text{ for a point like system} \\ r \text{ for a planar system} \\ \ln(r) \text{ for a line like system.} \end{cases} \tag{2.12}$$

For a point like system, the entropic contribution of the energy is larger compared to the electrostatic energy and counterions are unbound. For a planar system most counterions are bound to the surface and form the so called Gouy-Chapman layer (Eq.

[3] $\epsilon \cdot \epsilon_0 \equiv \epsilon$

2.28). In case of a line like charge the balance depends on the charge density (both contributions $\propto \ln r$).
If the PE system (i.e. a charged surface) is in thermodynamic equilibrium the resulting charge density of the ions at position $\vec{r}$ follows a Boltzmann-like behavior

$$\rho_j(\vec{r}) = C_j \exp(\frac{-u_{ij}(\vec{r})}{k_B T}). \tag{2.13}$$

The many-body interactions u_{ij} can be averaged and approximated by a mean field potential for low molecular weight and weakly charged PEs. Following the theory of Debye Hückel (DH) the mean field potential can be expressed as

$$u_{\text{mean}} = z_j e \left\langle \phi(\vec{r}) \right\rangle \tag{2.14}$$

where inter-particle correlations are neglected and $\langle \phi(\vec{r}) \rangle$ is a time-averaged potential (each counterion interacts with a diffuse cloud of the other counterions). Additionally, electro neutrality can be assumed

$$\sum_j \frac{z_j e C_j}{\epsilon} = 0. \tag{2.15}$$

Insertion into Eq. 2.11 yields the Poisson Boltzmann equation (PB equation), connecting the electrostatic potential to the charge density of the ions

$$\nabla^2 u_{\text{mean}} = \sum_j \frac{z_j e}{\epsilon} C_j \exp(-\frac{u_{\text{mean}}}{k_B T}). \tag{2.16}$$

For weak potentials $u_{\text{mean}} << k_B T / z_j r$, this equation can be expanded using a Taylor series and then linearized. This results in the Debye Hückel equation [23]:

$$\nabla^2 u_{\text{mean}} = \frac{1}{\lambda_D^2} u_{\text{mean}}, \tag{2.17}$$

with the so called "Debye length" λ_D

$$\lambda_D = \sqrt{\frac{\epsilon K_b T}{\sum_j (z_j^2 C_j(\vec{r})) e^2}} = \sqrt{\frac{\epsilon K_b T}{2 I e^2}}. \tag{2.18}$$

The Debye Hückel equation (2.17) can be solved (PE on a surface) using

$$u_{\text{mean}}(\vec{r}) = u_0 \exp(-\frac{r}{\lambda_D}). \tag{2.19}$$

This (2.19) shows that the Debye length can be interpreted as a screening length of the Coloumb potential (Figure 2.3). Assuming an n:n salt solution ($A_nB_n \rightarrow A^{n+} + B^{n-}$) the Debye length is $\lambda_D = \frac{0.304\,\text{nm}}{n\sqrt{I}}$. For $r << \lambda_D$ the electrostatic interactions are purely Coulomb and for $r >> \lambda_D$, the electrostatic interactions are screened completely and the behavior of the PE converges to a neutral polymer. If the electrolyte solution screens the electrostatic repulsion, the PE starts to coil.
Two boundary conditions have to be fulfilled. The first condition demands that the total charge (surface charge plus the charge of the mobile ions) must be zero [24]. The surface charge density σ and the distribution of the ions ρ are related in the Graham equation, what can be deducted from electro neutrality conditions of the system

$$\sigma = -\int_0^\infty \rho dr = \sqrt{8c\epsilon K_B T}\sinh\left(\frac{eu_{\text{mean}}}{2K_BT}\right) \approx \frac{\epsilon u_{\text{mean}}}{\lambda_D}. \tag{2.20}$$

Furthermore the potential has to vanish for large distances.
For nonlinear PB theory one can show that

$$u(\vec{r}) = 2\frac{K_BT}{ze}\ln\left[\frac{1+\xi\exp(-\frac{r}{\lambda_D}}{1-\xi\exp(-\frac{r}{\lambda_D}}\right] \tag{2.21}$$

$$\approx \frac{4K_BT}{ze}\xi\exp(-\frac{r}{\lambda_D}) \text{ for } r >> \lambda_D, \tag{2.22}$$

with $\xi = \tanh(zeu_o)/(4K_BT)$ [24]. In summary the potential of a PE decays with the debye length. The prefactor depends on the geometry of the object and the boundary conditions (see Ch. 2.3 for more details on the interactions of two charged surfaces).

However, these approximations fail in case of strong charged PEs where counterions condense to reduce the electrostatic potential. That meanes the counterions become trapped by the PE in order to balance the electrostatic energy by a decrease in entropy. That effect is called "counterion condensation" [25, 26]. Depending on the corresponding parameters, Coulomb interactions or the loss of entropy dominate and determine the counterion-distribution [16]. If the electrostatic energy (Eq. 2.12) is small compared to entropic contributions, counterions cannot be stabilized and no counterion condensation occurs. That is the case if the number of charges per unit length (Γ)

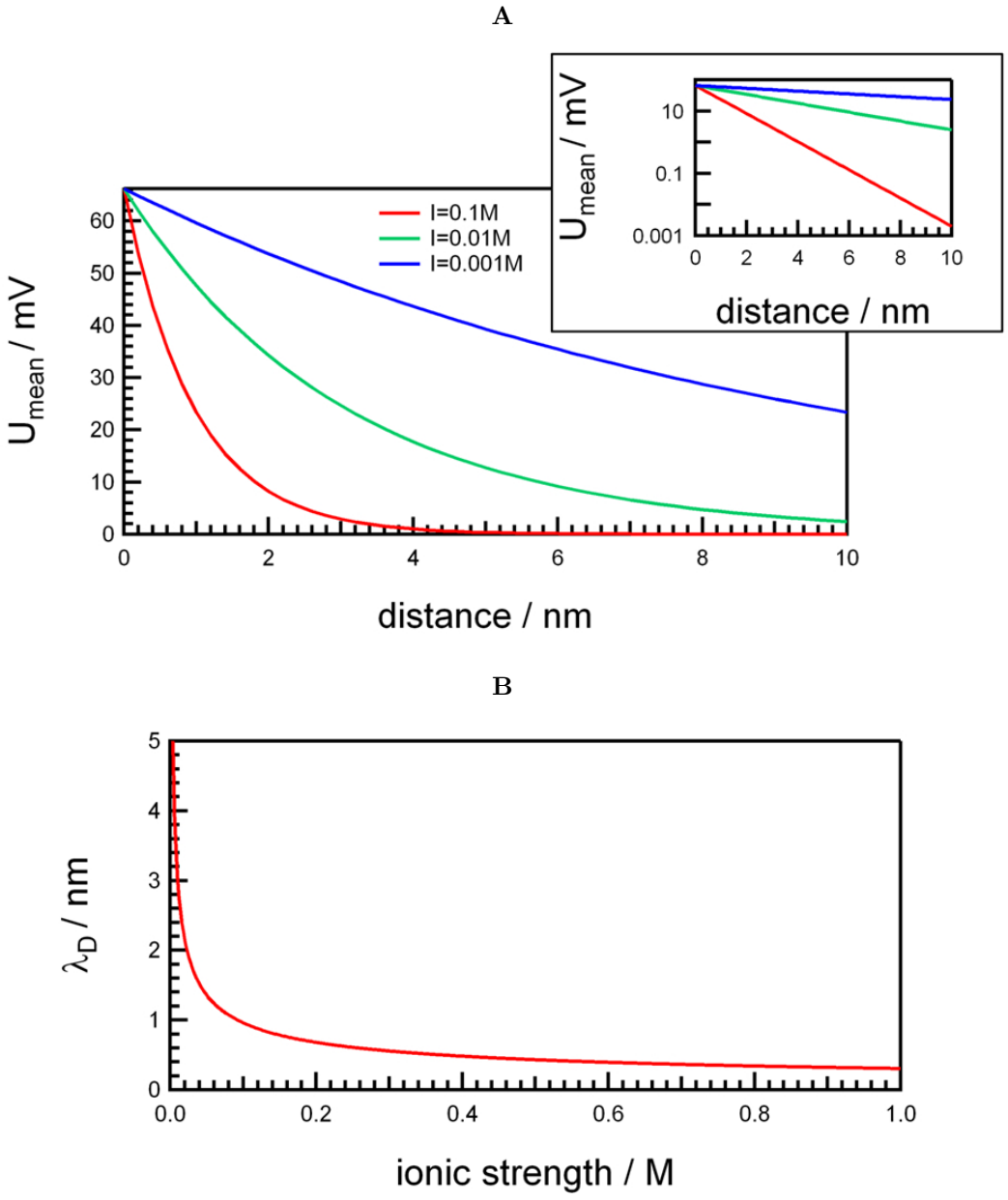

Figure 2.3: 2.3A Potential of a PE: $U_{\text{mean}}(r)$ for ($U_0 = 66\,\text{mV}$, $T = 293.15\,\text{K}$ and ionic strength $I = 0.1 - 0.001\,\text{M}$). Inset displays a log plot for these potentials. 2.3B Debye length λ_D for a 1:1 salt as a function of the ionic strength I.

is smaller than one charge per Bjerrum length $\Gamma < 1/l_B$. The Bjerrum length l_B is defined as the length at which two electron charges have an interaction energy in the magnitude of the thermal energy

$$l_B = \frac{e^2}{4\pi K_b T \epsilon}. \tag{2.23}$$

In pure water at standard lab pressure and temperature $l_B \approx 0.7\,\mathrm{nm}$. If the electrostatic energy is large compared to entropic contributions (if the number of charges per unit length is higher than one charge per Bjerrum length $\Gamma > 1/l_B$), counterion condensation to the PE occurs to reduce the charge density until a maximum of one charge per Bjerrum length $\rho_{\max} = e/l_b$ is reached. Uncompensated counterions can be described using the DH approach. The effect of counterion condensation can be described using the model proposed by Oosawar [4][27].
Due to electrostatic effects, PEs are quite stiff. This stiffnes effect can be described using an electrostatic persistence length, "Odijk length" L_p. One can show that the persistence length L_p of the PE, describing its stiffness, is proportional to the Debye length λ_D^2 for flexible poyelectrolytes [28, 29, 30]. If the PE is diluted in an electrolyte solution of low salt concentration, the polymer is strongly stretched ($L = L_{max}/(\Gamma/l_B)$, with L the length of the stretched PE, L_{max} the maximal length aligning the monomer units of the polymer, and Γ the number of charges per unit length (vice versa for high concentrated electrolyte solutions).
The excluded volume for PEs results in an increased excluded volume compared to neutral polymers due to the electrostatic interactions ($v_2 \propto L_p \lambda_D$).

In case of annealed PEs, both the ionic strength and the pH of the solution strongly affect the properties of the polymer. The pH determines the degree of dissociation and thus the actual charge density. This dependence makes such systems interesting for many applications [31]. The chemical equilibrium of annealed PEs is described by a modified version of the Henderson-Hasselbalch equation [16] which relates the pH of the solution and the fraction of charged groups. For molecular acids this results in:

$$pK_{a(app)} = pH + log\frac{1-\alpha}{\alpha} \tag{2.24}$$

[4]The PE is locally stiffen and can be approximated as a cylinder, that traps all countions inside a cylindric cell [27]

where α describes the actual degree of dissociation and the pK_a is defined by the law of mass. Overbeek showed that the experimentally observed apparent $pK_{a(app)}$ (Eq. 2.24) of an annealed PEs, depends on the intrinsic value pK_a^0

$$pK_{a(app)} = pK_a^0 + \frac{1}{\ln(10)RT}\frac{dG}{d\alpha} \tag{2.25}$$

with the term $dG/d\alpha$ describing the work necessary to carry charges against the electrostatic attraction from a PE to infinite distance [32]. In other words, the second term represents the shift in the dissociation constant due to changes in the electrostatic free energy of a PE upon variation of the number of charged groups [1].

In contrast to neutral polymers (Ch. 2.2.1), the structural properties of adsorbed PEs are mostly dominated by electrostatic interactions. A charged surface can be neutralized by a oppositely charged PE, which is entropically favorable and therefore promotes PE adsorption [20, 33, 34, 35, 36]. Several theoretical approaches like self-consistent field theory (SCF), Monte-Carlo simulations, or scaling approaches have been applied to describe the adsorption behavior. Possible conformations depending on the adsorption energy are so called trains (all PEs are in contact with the substrate), loops (parts of the PE are not in contact with the substrate), and tails (non-adsorbed ends of the PE) as sketched in Figure 2.4A [37, 38]. One adsorbed layer of PEs has a thickness in the order of the chain diameter ($\approx 1\,\mathrm{nm}$).
The adsorption is accomplished by a confinement of the PE, which involves an increase in free energy. For compensation of this increase an additional attractive interaction must stabilize the adsorption. The driving forces of adsorption are the gain of entropy by complexation with oppositely charged surfaces and release of counterions as well as the release of solvent molecules, on the fulfillment of electro neutrality. However, often more PEs are adsorbed than necessary for electroneutrality, which is called "charge overcompensation". This can lead to a charge reversal of the surface.
Since electrostatic interactions are dominant, parameters like surface charge, ionic strength, pH and the architecture of the PE govern the adsorption. It depends on the balance between electrostatic and non-electrostatic interactions whether an increase in salt concentration leads to an increase or decrease in adsorption [39]. Two regimes were proposed to describe this effect. In the so called "screening reduced" adsorption regime (high surface charge, low charge density of the PE, weak non-electrostatic contribution), Coulomb interactions between segments and the surface dominate. If the attraction between polyelectrolyte and surface is purely electrostatic only this regime

is valid. Several adsorbed layers of PE are possible, due to the long range nature of the Coulomb interactions. The adsorbed amount decreases with an increase in ionic strength due to screening effects. The PE can be released from the surface when a critical salt concentration is reached. In the regime of "screening enhanced" adsorption (generally quenched PEs) non-electrostatic interactions (short range interactions) between the segments and the surface are dominant. The adsorption increases with ionic strength because salt screens the repulsion between the equally charged groups on the polymer. In the intermediate case, when both forces are of roughly equal importance, changing the salt concentration will hardly affect the adsorption [39]. The different adsorption regimes are shown in Figure 2.4B

The adsorbed layer thickness can be calculated by minimizing the free energy [40, 41]. Assuming that the Debye length λ_D is larger than the adsorbed layer thickness d (valid for not too high ionic strength, see 2.18), two regimes can be obtained for the layer thickness: one for relatively large salt concentrations (or rather stiff polymers) and small layer thickness and one where the layer thickness is larger than the persistence length but smaller than the screening length

$$d \propto \begin{cases} \left(\frac{\ln(l_B \sigma_S \Gamma L_P^2}{l_B \sigma_S \Gamma L_P^{1/3}}\right)^{3/5} & \text{for } d < \lambda_D < L_p \\ \left(\frac{L_P}{l_B \sigma_S \Gamma}\right)^{1/3} & \text{for } L_p < d < \lambda_D \end{cases} \tag{2.26}$$

with σ_S the charge density of the surface, Γ the charge density of the chain, and L_p the effective persistence length [41].

2.2.3 Self Assembly of Polyelectrolytes

If PEs are dissolved in aqueous solution with suitable counterparts that are oppositely charged, they form aggregates due to electrostatic interactions (other intermolecular forces are possible as well) [42]. These aggregates can build up interpolyelectrolyte complexes (IPECs), which form a new class of macromolecules [43, 44]. The complexation is driven by the release of counterions which leads to an increase in entropy. Several theories and studies exist to describe the features and physical properties of the resulting IPECs [45]. IPECs can consist of a PE with a second oppositely charged PE, with low molecular counterions, ionic surfactants, colloidal particles, and others (Figure 2.5A). These IPECS are interesting for numerous applications. Examples are the build up of polyelectrolyte multilayers, where many oppositely charged PEs are adsorbed in layers in altering order [46].

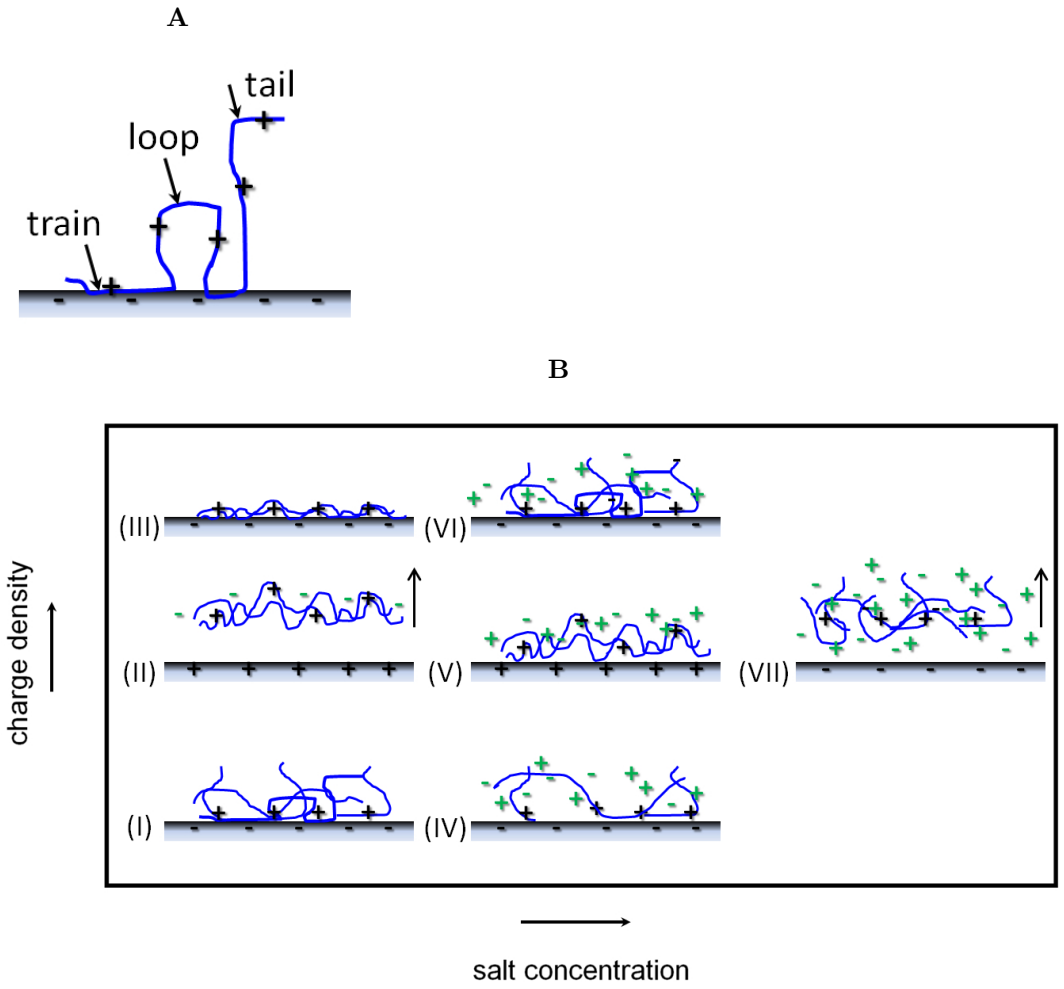

Figure 2.4: Adsorption of PEs: 2.4A Adsorbed polyelectrolyte chain form trains, loops and tails. 2.4B Different Adsorption regimes of PEs depending on charge density and salt concentration: (I) low charge density, low salt concentration: formation of loops and tails, high adsorbed amount; (II) PE has the same charge as the substrate, low salt concentration: PE releases from the surface; (III) strong charge density, low salt concentration: PE lies flat and stable on the surface, weaker adsorption as in (I); (IV) low charge density, high salt concentration: screening of electrostatic interactions, adsorption amount can increase or decrease; (V) PE has the same charge as the substrate, high salt concentration: electrostatic repulsion is screened, adsorption is possible; (VI) high charge density, high salt concentration: similar to (I) due to screening of electrostatic interactions; (VII) above a critical salt concentration all PEs release from the surface.

If the polymer consists of two or more blocks, that are distinguishable by the chemical and physical properties and linked by covalent bonds, the system phase separates and can self-assemble to complex structures like spheres, cylinders, or lamellae. These different architectures result in a big number of functionalities, as reported in Ref. [47]. The geometry and the physical properties of these complex systems are tunable by parameters like block length, number of blocks, solvent quality, ionic strength, and -in case of annealed PEs- pH. The complexity of the structures and the number of different morphologies increase drastically with the number of blocks, as for example described for ABC triblock terpolymers in Ref. [48]. When a block copolymer is dissolved at a concentration exceeding the critical micellar concentration (cmc) and if one of the blocks is soluble whereas the other is not they form micellar structures with a solvophobic core and corona pointing into the solution (Figure 2.5B)[49].

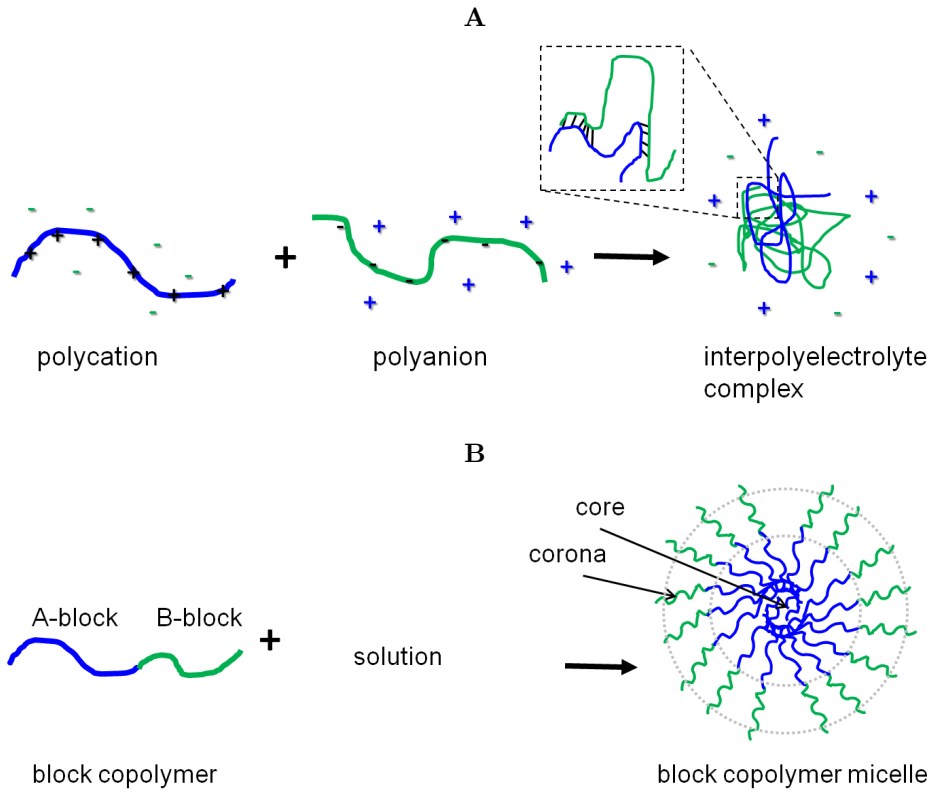

Figure 2.5: Self assembly of polyelectrolytes: 2.5A Formation of an interpolyelectrolyte complexes (reproduced from [44] ©RSC). 2.5B Formation of a block copolymers micelle.

2.2.4 Functionalization of Surfaces with Polyelectrolytes

There are many possibilities to functionalize surfaces with PEs (Figure 2.6). It is beyond the scope of this work to explain all possible techniques in detail. Here an overview over several techniques is given, following the scope made in Ref. [1].
Two ways of surface functionalizations can be distinguished: physical or chemical functionalization. In case of physical functionalization the molecules are coupled to the substrate via physical interactions, while chemical functionalization involves covalent attachement of molecules [50].
Often the Langmuir Blodgett technique was extensively used for functionalization of surfaces with polymers [51] (Figure 2.6A). After equilibration of polymer monolayers at an air-liquid interface the PEs were transferred to a substrate of choice by dipping the substrate into the liquid. Using several dipping steps, multilayers can be realized. However, this technique has some limitations with respect to type, topography, and size of the substrate and requires special equipment. Another approach to produce smart surfaces is based on self-assembly of monolayers (SAM) due to chemical adsorption (Figure 2.6B) [52, 53, 54, 55]. Multilayers can be obtained by targeted molecular design of the monolayers. However, these films are limited to certain classes of covalent or coordinative chemistry.
An elegant approach for the formation of functional surfaces, is the layer-by-layer deposition technique (LBL) (Figure 2.6C). Here oppositely charged PEs (or other molecules) are deposited as films via dipping, spin, or spray coating in altering order onto the sample substrate. This process is driven by electrostatic interactions and the gain of entropy by release of counterions and solvent molecules and complex formation (see Ch. 2.2.3) [56]. The technique was established by Decher [57][5] and has nowadays a lot of applications, particularly in the development of responsive coatings [59, 60]. This is due to advantages like easy handling, low cost equipment, and no restrictions with respect to topography, geometry, chemistry, and size of the substrates. In addition, the thickness of the film and the resulting charge of the sample can be adjusted by the number of deposition steps (1 up to around 1000), the PE used (e.g. molecular weight [61]), and the properties of the solution (concentration, ionic strength, pH [62, 63] and dipping time) [64, 62]. For example LBLs are used for biomedical applications and cell substrates [65, 66], for coatings (walls) of microcapsules that can be used for e.g. drug delivery [67, 68], controling surface wettability [69], for the design of optical sensors [70], for the preperation of light emmiting diodes [71], or fuel cell membranes [72]. The

[5] already first reported by Iler [58]

LBL technique also allows incorporation of objects like nanoparticles [70], micelles [73, 74], and others.
Chemical functionalization is possible by grafting of polymers by direct growth from/to initiators on the surface (Figure 2.6D). If the distance between initiator molecules is low (high density of initiators), and the distance between the polymers is smaller than typical coil dimensions in solution, the polymers stretch away from the surface and form a so called "polymer brush" [50]. Parameters like molecular architecture, grafting density, and the chain length can be easily controlled by the synthesis protocols. The physical properties of the polymer brush can be tuned by changing the environment or by external fields. Also it is possible to design multifunctional surfaces by combination of different functional molecules.
In this thesis polymer brushes are mainly used for the formation of responsive layers. Theoretical basics as well as applications are discussed in Ch. 2.2.5.
It is straight forward to introduce micro-patterns to the above discussed approaches, using micro contact printing (μCP) and soft lithography methods as introduced by Whitesides and co-workers [75, 76].

2.2.5 Polymer Brushes

A polymer brush is formed when polymers are grafted onto a surface and the interaction potential of the polymers overlap[6] [78, 50, 79, 80]. As a result the polymers stretch away from the surface. These polymers can be both, neutral or charged. In case of charged polymers, polyelectrolyte brushes are obtained. Polymer brushes represent an effective approach to create smart coatings. In particular PE brushes are capable of responding to a wide range of external stimuli, such as ionic strength, pH, chemical compounds, temperature, light etc. [81]. Brushes can be grafted onto planar substrates, onto curved ones, e.g. colloidal particles (spherical brushes) [82], or on long chain molecules, which are named "bottle-brush" [50, 83] (Figure 2.7). The steric repulsion between the chains, the electrostatic interactions, and the osmotic pressure of the counterions result in new interesting physical properties, which will be explained further (see below) [14]. It is possible to achieve different polymer brush architectures by modification of the synthesis protocol and by combination of different functional molecules. Examples are block copolymer brushes, mixed polymer brush and brushes

[6]It should be noticed that a full description of all physical (theoretical), chemical (synthesis) properties and applications is beyond the scope of this work. For further information see [1, 77].

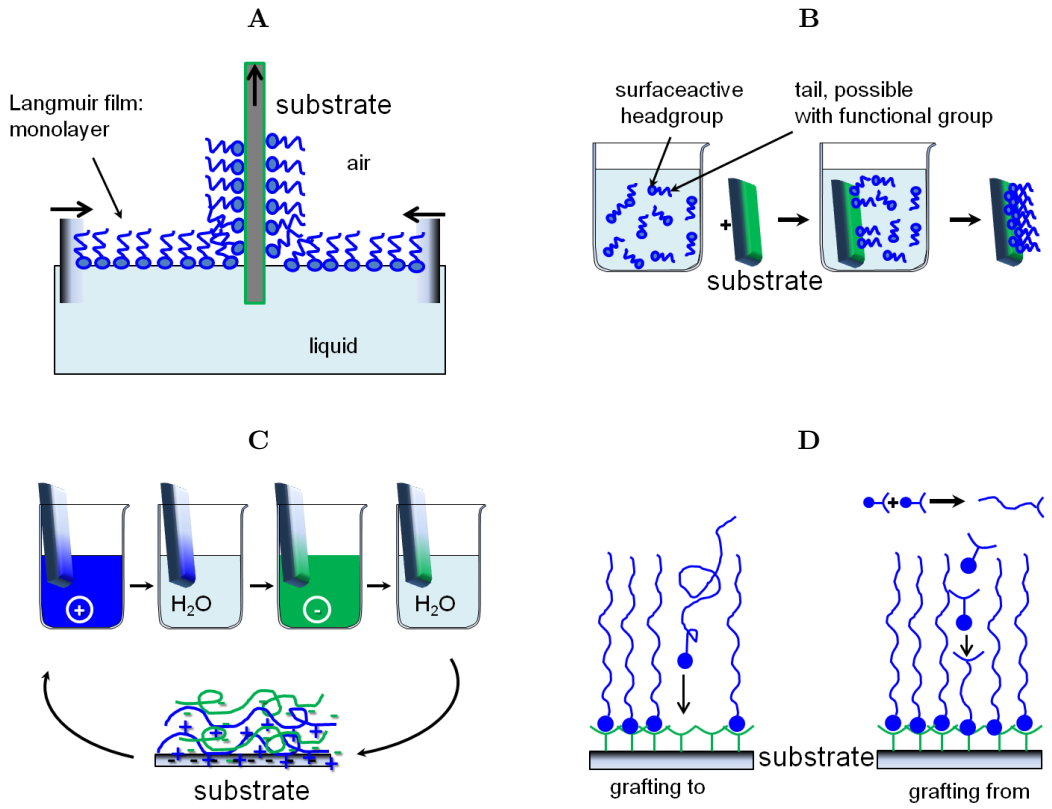

Figure 2.6: Functionalization of surfaces with polyelectrolytes (adapted from [1]): 2.6A Langmuir Blodgett technique, 2.6B Self assembly of monolayers, 2.6C Layer by layer deposition technique, 2.6D Formation of a polymer brush via garfting to or grafting from technique.

with an internal gradient [84, 85]. Polymer brushes allow for tailoring surface properties, e.g. adjustable wettability [86, 87, 3, 88], friction reduction [89, 90], and can serve for example as protection layers for preventing colloidal aggregation and flocculation [91], as separation system for liquids [92], as actuators [93, 94], or mechanoresposive sensors [9], as chemical reactors [95], or for immobilization of proteins [96, 97] and can be applied in biotechnology [98].

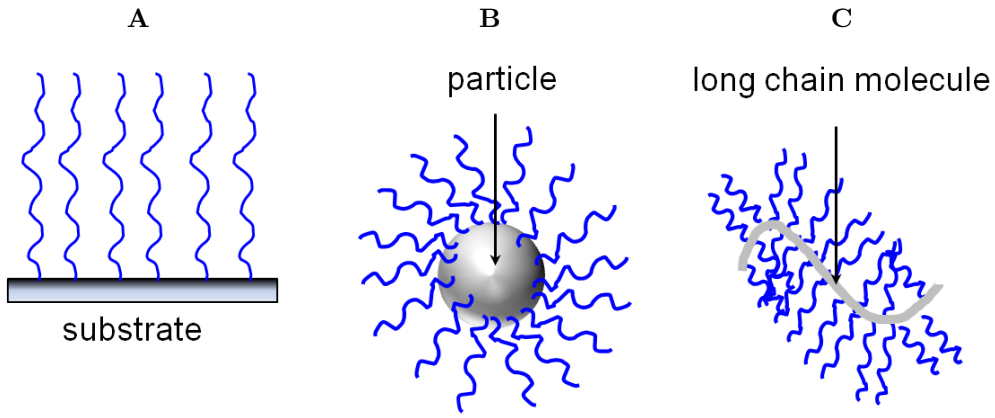

Figure 2.7: Different types of polymer brushes: 2.7A Polymer brush on planar substrate, 2.7B Spherical polymer brush, 2.7C Bottle-brush

Preparation of Polymer Brushes

As described above (Ch. 2.2.4), the grafting of polymers onto a substrate to form a polymer brush can be achieved using the "grafting-to" or the "grafting-from" technique (Figure 2.6D). The "grafting-to" method is almost an extension of the SAM technique using larger molecules and is working on the basis of physiorption or bond formation between chemical groups on the substrate and the polymer chain. This approach is limited since diffusion of the macromolecules is slow and already grafted molecules hinder other molecules to attach. The "grafting-from" technique, also used in this thesis, overcomes these limitations of the grafting-to approach. In "grafting-from" methods the polymer chain grows from surface anchored initiators. Any existing polymerization technique can be used in "grafting-from", as long as the required initiator can be attached to the surface. The most common technique is surface initiated controlled radical polymerization [84, 99] which allows to insert a wide range of functionalities into the brush. In these techniques, a dynamic equilibrium between active radicals and inactive chains exists, as sketched in Figure 2.8. In the presented work Surface-Initiated

Atom Transfer Radical Polymerization (SI-ATRP) and photoinitiated polymerization (PIMP) was used. The ATRP approach was first reported by Huang et al. [100] and was extensively studied over the last years [101, 102]. The reaction is based on a reversible redox activation of a dormant alkyl halide-terminated polymer chain by halogen transfer to a transition metal (Figure 2.8B. This reaction is chemical versatile and compatible with many media. Changing reaction parameters like Cu(II) to Cu(I) ratio, type of ligand, counterion, solvent, or the initiator allows to control the reaction and thus the emerging polymer chain [84, 103]. In case of photo initiated polymerization, the initiator is activated by irradiation with light (e.g. UV light). Upon exposure of light ($h\nu$, with frequency ν), the photoinitiator splits into radicales as sketched in Figure 2.8C. In the presence of water-soluble monomers as for example acrylic acid polymerization leads to PE chains grafted onto the surface. Switching off the light stops the polymerization and allows for control over the polymerization. The polymer length increases linearly with illumination time and intensity [84, 104]. For more details the reader is referred to [84, 99].

Theory of Polymer Brushes

If a polymer is grafted to a surface, the polymer chain can be adsorbed in two different ways and can form a so-called "pancake" or "mushroom", depending on the tendency to adsorb and on the solvent (2.9A). In case of the mushroom regime, the density profile is Gaussian and the size of the grafted polymer can be approximated using Eq. 2.8, whereas the polymer in the pancake regime is concentrated to the surface (see Figure 2.9A, 2.9C)[105].

When the polymer chains are densely grafted to a surface and the interaction potentials overlap, they become stretched by segment-segment interactions in equilibrium with the elastic free energy (related to the conformation entropy) and form a "polymer brush" (Figure 2.9B). This happens if the grafting density $1/\sigma$ (chains per area σ) exceeds the crossover grafting density $1/\sigma_{co}$. In case of a good solvent the crossover grafting density is given by

$$\frac{1}{\sigma_{co}} \propto R^{-2} \propto a^{-2}N^{-6/5}, \tag{2.27}$$

where a is the Kuhn length and N the number of monomers. The density profile of such a polymer brush can be described by a box or parabolic profile, see Figure 2.9C (more details see below).

If the substrate is curved and the curvature is small (smaller than the brush height), the curvature strongly influences the physical properties of the brush. In that case

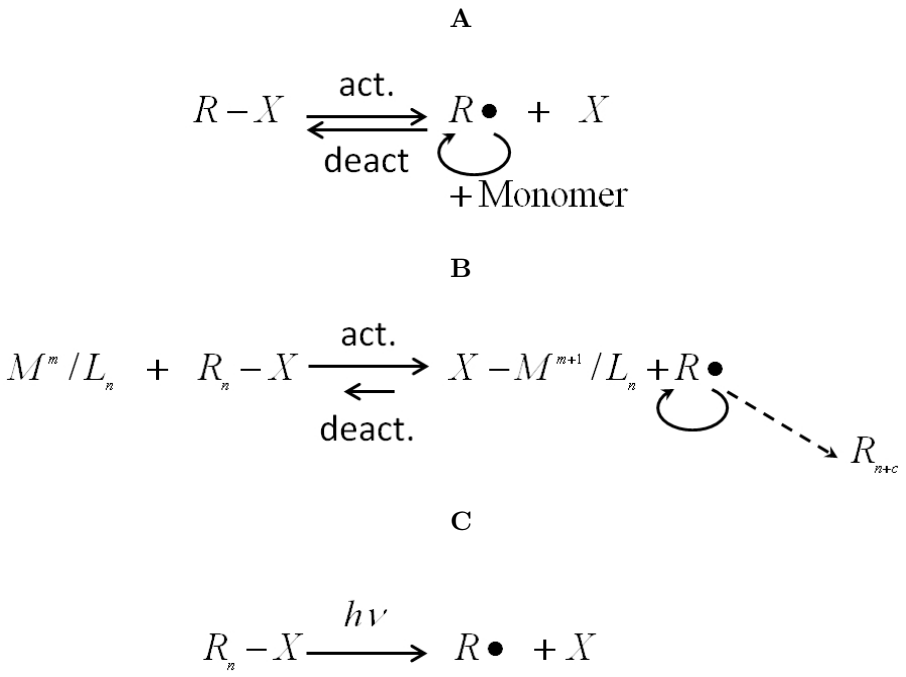

Figure 2.8: Preparation of polymer brushes (adapted from [102] ©American Chemical Society): 2.8A General concept of radical polymerization (with capped dormant species $R-X$, active free radical $R\bullet$, and stable deactivated species X), 2.8B Transition-Metal-Catalyzed atom transfer radical polymerization (with transition metal M^m e.g. CU(I), complexing ligand L_n, polymer chain R, termination R_{n+c} and x = Br or Cl), 2.8C Photo initiated polymerization

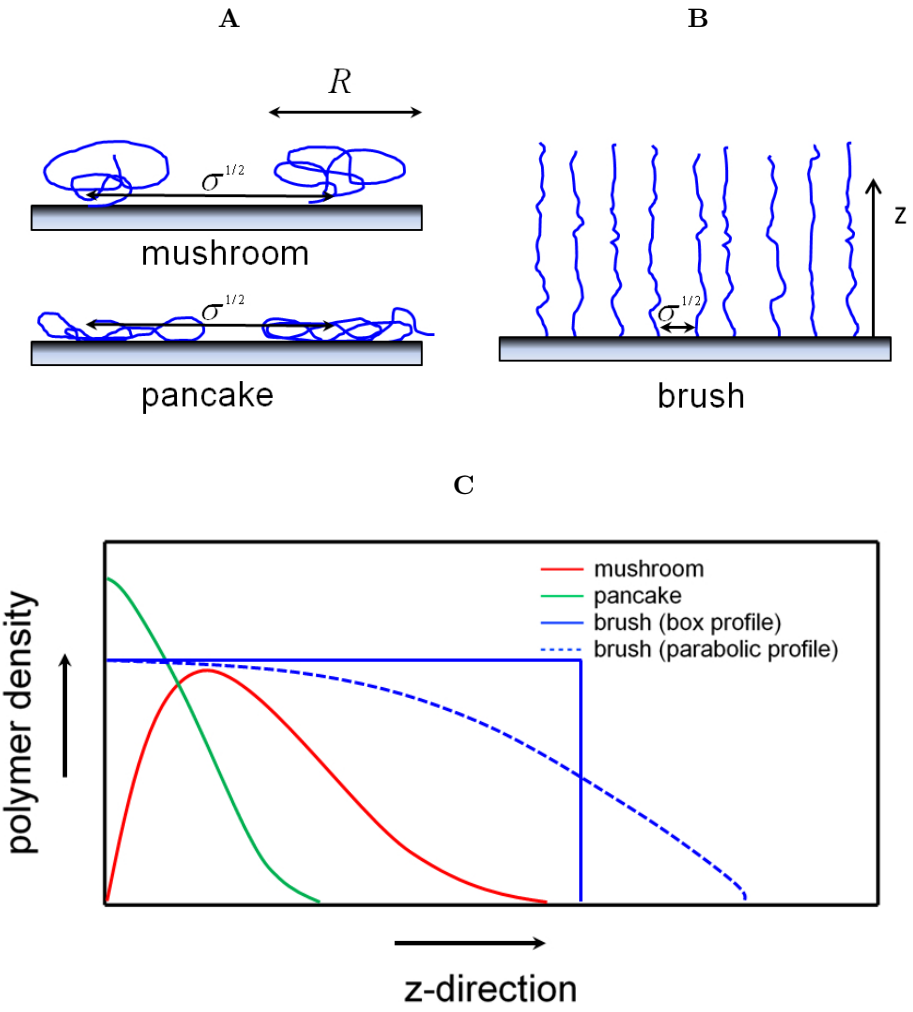

Figure 2.9: Grafted polymer chains: 2.9A mushroom and pancake, 2.9B High grafting density results in a crossover to a polymer brush, 2.9C Normalized polymer density of grafted polymer chains as a function of z-direction

the polymer brush properties are functions of the distance from the surface. For more details, the reader is referred to [82].

The discussion so far was for neutral polymers. If the monomer units are charged and the grafting density is high, a PE polymer brush is formed. For system neutrality, counterions that lead to an osmotic pressure are present in the brush (see Ch. 2.2.2). The polymer chains are stretched by segment-segment interactions and electrostatic (Coulomb) interactions in equilibrium with the elastic free energy gained by the entropic restoring force of the chain (see Ch. 2.2.1). These PE brushes can be either quenched (charges are fixed inside the brush), or annealed (charges are mobile in the brush).

The charge can be accounted for the degree of ionization α. The main important parameters for PE brushes $1/\sigma$ and α are combined in the so called "Gouy-Chapman" length

$$\Lambda = \frac{\sigma}{l_B N \alpha} \tag{2.28}$$

that defines the characteristic thickness of the counterion cloud (Figure 2.10). If the

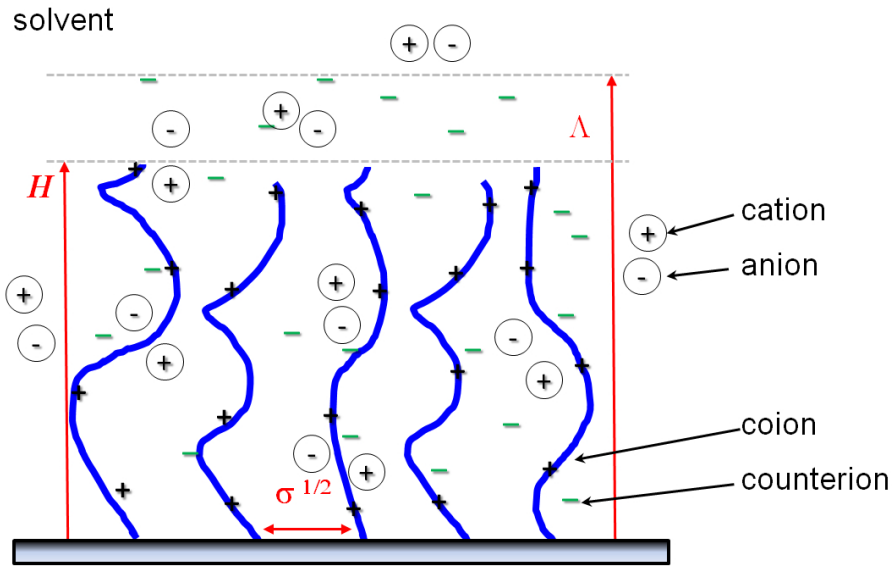

Figure 2.10: Parameters of a cationic polymer brush in salt solution

chains are densly packed (σ small) and strongly charged (large α) the Gouy-Chapman length is small and can be smaller than the brush height H ($\Lambda < H$). In that case the counterions are trapped inside the brush and compensate the immobilized charges of the polyions. If the grafting is relative spare and the degree of ionization is low, the Guoy-Chapman length becomes larger than the brush height H ($\Lambda > H$). In that case, the counterions spread into the solution beyond the edge of the brush.

The analytic expression for the charge and counterion distributions and the structure of the PE brush can be calculated using self-consistent field theory (SCF) [106, 107, 108, 109].
If the solution is salted, an additional screening of the Coulomb interactions between chain segments is provided by coions and counterions of the salt. This screening can be described by the Debye screening length λ_D (see Eq. 2.18).
For an understanding of the physical behavior and the internal structure of polymer brushes different models and approaches can be used. The first time, the influence of confinement on endgrafted polymer chains was studied by Alexander [110] and de Gennes [111] (AdG model). Using scaling arguments and describing the brush segments as so called "blobs"[7] they could show that the density of the brush reaches a homogenous plateau for $\sigma < z < H$ and drops down quickly for $z > H$, where z is the distance from the surface. This behavior can be described by a step profile (see Figure 2.9C)

$$\rho \propto \frac{N}{H\sigma} \tag{2.29}$$

for $0 < z < H$ and zero elswhere. This corresponds to a brush height of

$$H \propto N\sigma^{-1/3}. \tag{2.30}$$

The brush height scales linearly with the length of the attached polymer.
To describe the physics of polymer brushes, models based on these ideas and new approaches like SCF theories or numerical methods were applied. Also, the curvature of the substrate, polydispersity, changes in the environment, and other aspects were taken into account. To describe all of this is much beyond of the scope of this work and the reader is referred for example to Ref. [77]. In the following, just some aspects will be discussed following the conclusions of [107, 108, 109] (for details see Appendix A).
Different models are valid for different limits of behavior. In case of local compensation of immobilized charges by mobile ions, the "Local Electron neutrality Approximation" (LEA) can be used [107]. This approximation is applicable if Coulomb interactions in the polymer brush are screened by trapped counterions or by added salt on a scale smaller than the brush thickness. On the contrary, if the system is unable to retain counterions inside the brush, the system can be approximated by a capacitor model [112]. In general (most of the experimental systems), just a partial charge neutralization

[7] one blob contains a polymer segment that behaves like an ideal polymer

takes place and a fraction of mobile ions spreads beyond the edge of the brush. In that case, Self Consistent Field (SCF) is the theory of choice [106, 107, 108, 109].
The LEA assumes that the charge and the force is locally balanced inside the brush (see Appendix A for more details). In case of a neutral polymer brush it is sufficient to balance between the steric excluded volume interactions F_{conc} and the restoring force associated with the loss in entropy of the polymer chain upon stretching F_{conf} (also often called as elastic energy). Solving this balance results in a scaling law for the brush height, depending on the solvent quality. In case of a good solvent, the brush height H scales as follows [107]:

$$H \propto N\sigma^{-1/3}, \tag{2.31}$$

which is the same as the result of AdG (eq. 2.30). In case of PE brushes, the short range interactions are weak compared to electrostatic forces. Here electrostatic interactions F_{ion} are balanced by F_{conf}. Additional balance of the charges leads to two different scaling regimes for PE brushes in a salt solution where the brush height scales linearly with the polymer contour length [107]:

$$H \propto Na\alpha^{1/2} \quad , \quad \text{for } c_S < c_{CI} \tag{2.32}$$

$$H \propto N(a^2\alpha^2\sigma^{-1}C_S^{-1})^{1/3} \quad , \quad \text{for } c_S > c_{CI}, \tag{2.33}$$

where C_S is the salt concentration and C_{CI} the concentration of the counterions.
PE brushes that can be described by eq. 2.32 are called "osmotic brush" (OsB). This is the case if the salt concentration of the solution is low and the concentration of counterions inside the brush is equal to that of the immobilized charge. An important feature of the OsB is that the average thickness is independent of the grafting density (Eq. 2.32). Above a certain salt concentration, salt ions dominate over the immobilized charges inside the brush (Eq. 2.33) and a so called "salted brush" (SB) is formed. Here, the brush height decreases continuously with increaseing salt concentration and grafting density due to screening effects. Only free counterions contribute to the osmotic pressure. The transition from the OSB regime to the SB regime occurs when the bulk salt concentration equals the concentration of the free mobile counterions.
Equations 2.32 and 2.33 are quite general and apply to both quenched and annealed PE brushes [107]. For quenched brushes this is the final result. For the annealed case, the situation is more complex. The dissociation degree and the apparent pKa of the PE brush depend on its local electric field (environment), in particular on the solution

pH, the ionic strength, and on the grafting density. In case of weak polyacid brushes, the pKa shifts to higher values compared to the pKa of the polymer in bulk solution (or vice versa for basic brushes). Adding salt to the solution shifts the apparent pKa to lower values (close to pKa in bulk solution).
The degree of dissociation within the brush is close to zero at low salt concentrations. It increases in the OsB regime and reaches the bulk level (α_B of an individual polyacid molecule immersed in the solution [113]) in the salted brush regime.
Also, the brush height is affected by the ionic strength. Using scaling models or SCF one can show that the brush height (of an annealed polymer brush) passes a maximum that is located at the OsB/SB transition [107, 113, 114, 115, 116] (Figure 2.11). In addition, for annealed PE brushes the brush height is a function of the solution pH. The height increases for basic PEs with increasing pH and decreases under acidic conditions (or vice versa for acidic PEs).
In addition to the OsB and the SB regime, four other brush regimes can be distinguished which are seperated by the grafting density and the degree of ionization. Figure 2.12 summarizes these behaviors in phase diagrams for the salt-free and the salted case [107].

- Low grafting density (small $1/\sigma$); electrostatic interactions weak (small α) compared to the volume interactions ($F_{ion} << F_{conc}$) lead to grafted individual neutral coils (NC: mushroom regime $H \propto aN^{3/5}\nu_2^{1/5}$) or isolated charged chains in salted water (SC), respectively.

- Low grafting density (small $1/\sigma$), high electrostatic interactions (big α) lead to isolated grafted polyions stretched due to intramolecular Coulomb repulsion (IS: $H \propto aN\alpha^{2/3}$).

- High grafting density, weak electrostatic interactions (small α) compared to volume interactions ($F_{ion} << F_{conc}$) lead to a quasineutral regime, meaning that the brush behaves like a neutral brush where the brush height is balanced by the equlibrium of entropic stretching and steric interactions (NB: $H \propto N\sigma^{-1/3}$).

- Intermediate regime (charged Pincus brush (PB): $H \propto a^2N^3\alpha\sigma^{-1}$): mobile ions are distributed in the space above the grafting surface ($\Lambda > H$). This regime appears just in salt free solutions.

The above described LEA donot provide information on the intrinsic structure of free and confined brushes as a function of the brush parameters (grafting density, molecular

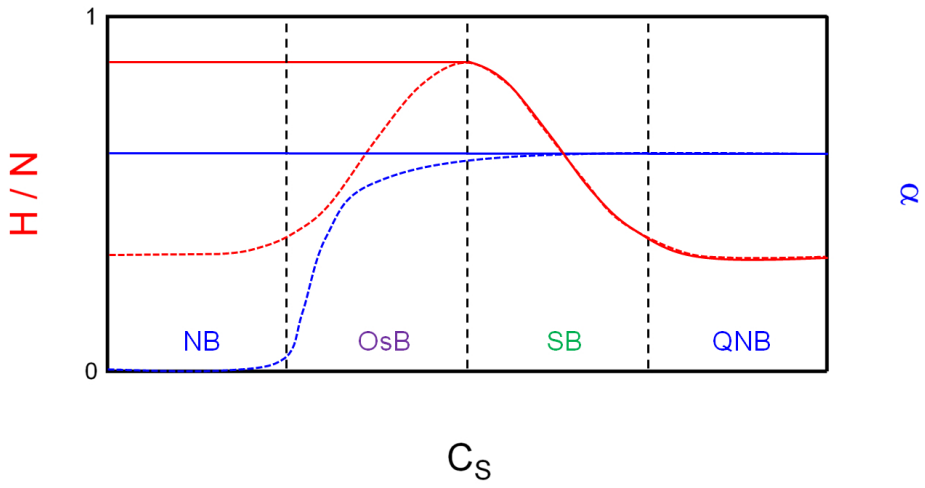

Figure 2.11: Brush properties as a function of salt concentration: Brushheight H for quenched (solid line) and annealed (dotted line) brushes and degree of dissociation within the brush α for quenched (solid line) and annealed (dotted line) brushes (adapted from ([113] ©American Chemical Society)

weight, degree of ionization, solution properties). To fulfill these requirements a theory is needed wich works without a priori assumptions and that give analytic expressions for the density profile of the monomers, the equilibrium distribution for the mobile ions inside and outside the brush, and the average thickness. An ansatz to solve this problem can be the self-consistent field theory (SCF [108, 109, 116]). Here, the intrinsic structure is obtained by minimization of the total free energy f_{tot}. The total free energy has three repulsive contributions: 1) The conformation free energy which describes the steric repulsion between chain segments (f_{conc}), 2) the free energy associated to the entropy S_{ion} confining counterions to a layer of thickness H: $-K_bTS_{ion}$, and 3) the direct electrostatic contribution f_{ion} if the PE brush is not locally electro neutral throughout the system. The attractive contribution to the total free energy f_{tot} is the entropic free energy loss f_{conf} [108].

$$f_{tot} = f_{conf} + f_{conc} + f_{ion} - K_bTS_{ion}. \tag{2.34}$$

Minimization (of this functional) and full expressions of the individual terms lead to functions of the polymer density profile inside the brush (parabolic form as scatched in Figure 2.9C, of the brush height, and of the charge density inside and outside the brush and thus the specific electrostatic potentials. For details see Ref. [108, 109, 116]. Also, the surface pressure, the conformation and the behavior of PE brushes in confinement can be obtained.

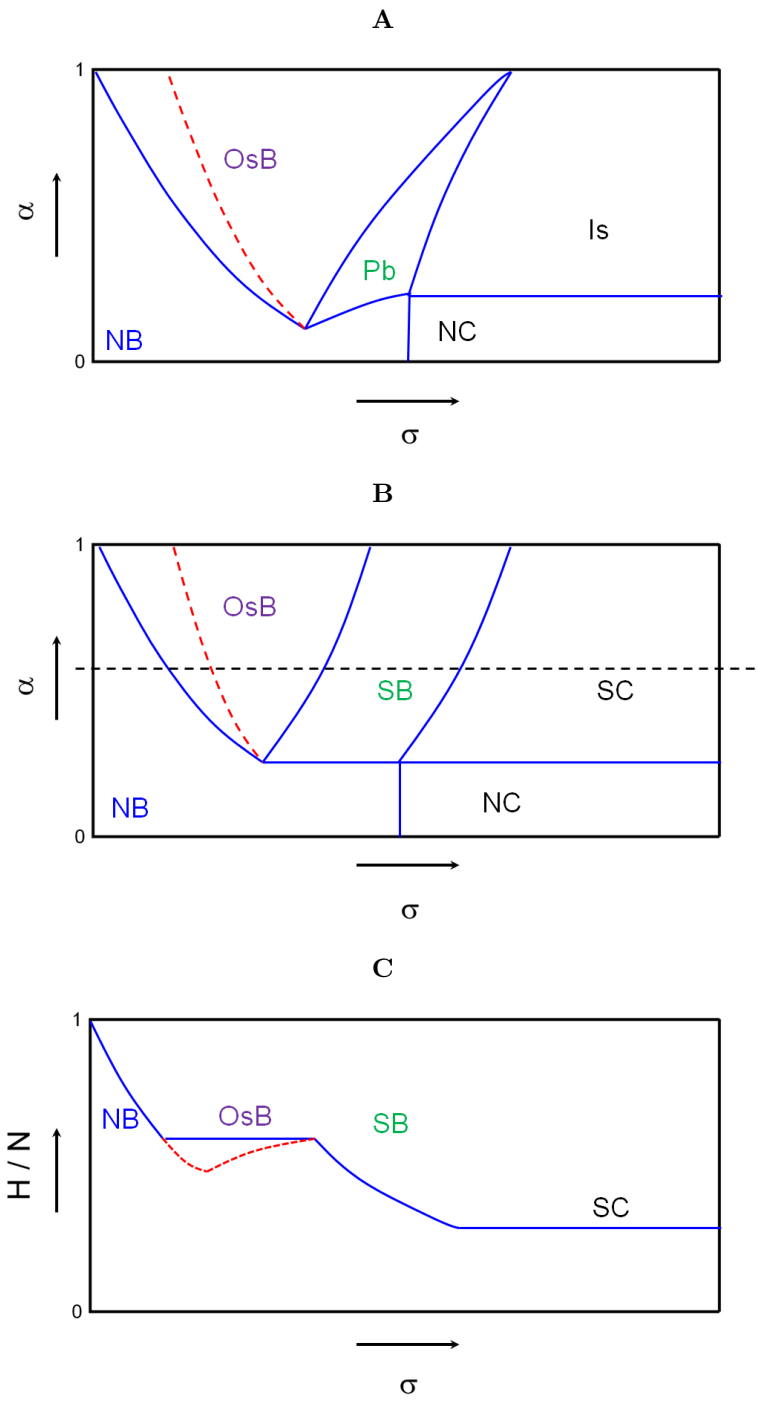

Figure 2.12: Phase diagram of polymer brushes (reproduced from [107] ©American Chemical Society): Type of polymer brush depending on the grafting density σ^{-1} and degree of dissociation α for the salt free case 2.12A and the salted case 2.12B. 2.12C Height as a function of the grafting density σ^{-1} along the black dotted line of 2.12B. (Quenched polymer brush: solid lines, annealed polymer brush: dotted line)

Also, PE brushes can be modeled using numerical methods, for example molecular dynamics (MD) simulations [117]. Results from SCF and MD simulations show the same behavior for polymer brush parameters.

2.3 Surface and Interfacial Forces

Interactions and adhesion play a major roles in natural science since they control surface properties and are crucial for many applications especially for objects or effects on the colloidal scale (order of microns). Examples are coatings of surfaces with polymers for surface protection [118], composites [119], paintings and adhesives (or nonsticking surfaces). Examples in nature are cell adhesion [120, 121], receptor-ligand interactions [122], and the effect of contact shape of animal pads on their sticking behavior [123]. Details on theoretical aspects are explained elsewhere [33, 124, 125, 24, 126, 127]. Here, just an overview is given with emphasis explaining the observed systems and the used techniques that are presented in the individual chapters. The presentation is oriented on [33, 124, 125, 24, 126, 127] and the cited literature.
Surface and interfacial forces are e.g. ionic, metallic, or covalent bonds, van der Waals forces, electrostatic or magnetic interactions as well as solvent forces like hydrophobic and hydrophilic interactions, hydrogen bonding and capillary forces. The type of interaction force depends on the type of the interacting material, its environment and the distance (long range $1 - 100\,\mathrm{nm}$ or short range $< 1\,\mathrm{nm}$).
When two bodies are brought into contact, the interaction forces lead to adhesion and the bodies can deform. The adhesion is characterized by the stress and the work needed to separate the interfaces, plus aspects like mechanical interlocking and interpenetration [126]. The total adhesion force (force needed to separate two bodies) is the superposition of all repulsive and attractive forces. The adhesion energy (also called Duprés work of adhesion) is the sum of the surface energies γ of the contacting surfaces i and j (in medium m) lowered by the interfacial energy γ_{ij} [24, 126]

$$w_{\mathrm{adh}} = \gamma_{im} + \gamma_{jm} - \gamma_{ij}. \tag{2.35}$$

If w_{adh} is positive the bodies attract each other. If w_{adh} is negative they repel each other. Measured results are in general lower than this theoretical value due to surface heterogeneities, roughness and wetting effects.

2.3.1 The Derjaguin Approximation

Interaction forces $F(D)$ of two bodies of any shape can be related to the interaction energy per unit area $w(D)$ between two planar plates as a function of the separation distance D and the material properties using the Derjaguin approximation[8] [128, 129]. For two interacting spheres with radii R_i and R_j it can be shown that

$$F(D) \approx \int_D^\infty 2\pi R P(D^*) dD^* = 2\pi R w(D), \tag{2.36}$$

where $R = R_i R_j/(R_i + R_j)$ is the reduced radius and $P(D)$ is the normal force per unit area acting between two planar surfaces (Figure 2.13). This approximation is valid for any type of interaction if the curvature of the probes is large compared to the separation distance and the conformation of the interacting system is independent of the distance from the surface (e.g. not valid for SPBs).

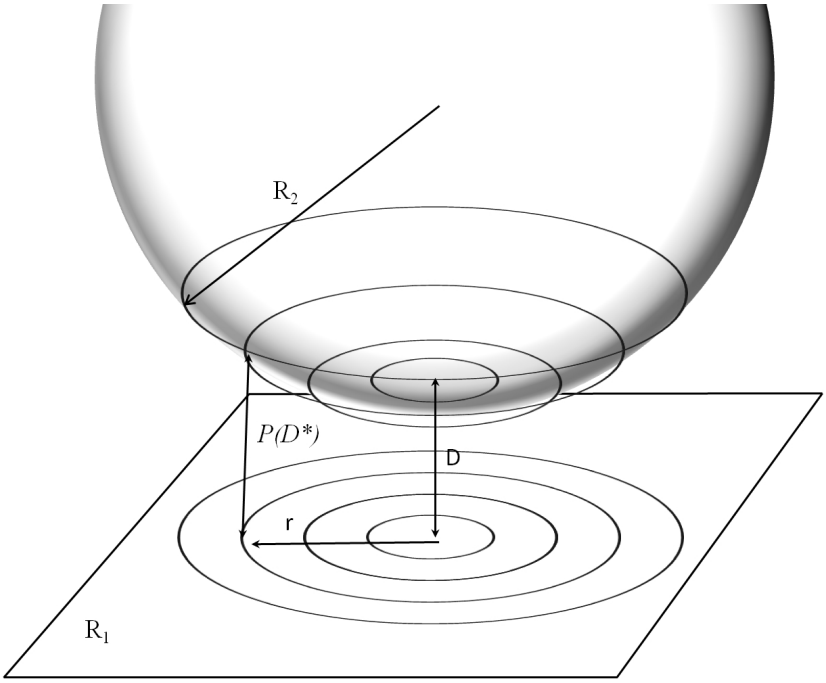

Figure 2.13: The Derjaguin approximation: Two interacting spheres with radii R_1 and $R_2 << R_1$ at separation distance D (adapted from [128] ©Elsevier).

[8]This is helpful as in many cases it is much easier to model the interactions for the planar case and measure forces between spheres or cylinders.

2.3.2 Van der Waals Interactions

Van der Waals (vdW) forces are of universal importance since they exist between any combination of molecules and surfaces independent of the charge, the material, or the surrounding medium [24, 126]. They are the sum of diverse dipole-dipole interactions, i.e. Keesom, Debye and London interactions. Keesom interactions describe the interplay between constant dipoles of the molecules dependent on the orientation and on the absolute temperature. Debye interactions take into account dipole induced interactions with a constant charge dependent on the orientation. London dispersion interactions act between all molecules and have quantum mechanical origin. They can be described by fluctuation induced dipoles. All potentials describing these interactions have a $1/r^6$ dependence, where r is the distance of the interacting molecules:

$$U_{\mathrm{vdW}}(r) = -\frac{C_D + C_K + C_L}{r^6} = -\frac{C_{\mathrm{VdW}}}{r^6} \tag{2.37}$$

and C_D, C_K, C_L are proportionality constants considering the Debye (D), Keesom (K) and London (L) contribution. They account the charge, the polarity, and the optical properties of the molecules or atoms, and the surrounding medium.
In case of macroscopic bodies, the force depends on the local distance of the bodies (determined by the geometry). The interactions can be approximated using the Hammaker approach (or more complex approaches like the Lifschitz theory or spectral methods). For example, for the interaction of two spherical objects with radii R_i and R_j at distance D the VdW potential and the resulting vdW force between two spheres can be approximated with

$$\begin{aligned} U_{\mathrm{vdW}}(D) &= -\frac{AR}{6D}, \\ \Rightarrow F(D) &= \frac{AR}{6D^2} \end{aligned} \tag{2.38}$$

where $A = \pi^2 C_{\mathrm{VdW}} \rho_i \rho_j$ is the Hammakar constant (with ρ the molecular density of the material) and $R = R_i R_j/(R_i + R_j)$ is the reduced radius of the system. In more extended theories, A is a complex function of the temperature, the dielectric properties, and the absorption frequencies of the material. Typical values of the Hamaker constant of condensed phases in vacuum are about 10^{-19} J.

2.3.3 Interactions of Charged Systems

If the bodies are charged, long range Coulomb interactions play a dominant role. The potential is determined by the Poisson equation (Eq. 2.11). For two point charges, the interaction potential is given by a $1/r$ dependency which can either be attractive or repulsive depending on the signs of the charges (Eq. 2.12). For macroscopic bodies the potential results, depending on the geometry, in diverse proportionalities of the distance r (eq. 2.12).
In solvent, most surfaces are charged, since it is energetically favorable to charge the surface with respecrt to the thermal energy K_BT [33]. This occurs by dissociation of ionizable groups or by the adsorption of charged species (Ch.2.2.2). For electro-neutrality, oppositely charged counterions are immobilized. This charging results in an electric double layer consisting of the so called inner "Stern" or "Helmholtz" layer where counterions are bound close to the surface and the diffuse Gouy-Chapman layer consisting of a diffuse counterion atmosphere [126] (Figure 2.14). In electrolyte solutions the potential in the diffuse layer decays exponentially (far away from the surface). This behavior is described quantitavely by the Debye screening length and is determined by the PB equation ($U \propto e^{-D\lambda_D^{-1}}$, see Eq. 2.16). The PB equation relates the ion distribution to the surface potential, by using the electro-neutrality condition.
If two charged surfaces are brought near to each other, the ion distribution overlap. Therefore an increase of the osmotic pressure due to the increase of mixing entropy of the ion clouds occures and the electrostatic double layer force arise (Figure 2.14A). One can show that it is enough to consider the counterion distribution at the midplane of both surfaces and the surface charge density σ_S (contact value theorem [9]). In addition to electro-neutrality, the surface charge density σ_S of the interacting objects influences the potential. That leads to additional boundary conditions. Three types can be identified: 1) Constant charge (cc: the surface charge density is constant. Solving the PB equation results in a distance dependence between $\sigma_{S,0}$ [24]), 2) the constant potential U_0 (cp): the surface potential is independent of the distance, and 3) the constant regulation approximation (cr: the surface charge depends on the charge density and on the distance).
Taking into account these conditions, the electrostatic double layer force between two

[9] general and also valid for other interactions

flat surfaces results in [128]

$$\frac{F(D)_{\mathrm{cc}}}{2\pi R} = \frac{\epsilon}{\lambda_D}\left(2U_{0,1}U_{0,2}e^{-D/\lambda_D} - \left(U_{0,1}^2 + U_{0,2}^2\right)e^{-2D/\lambda_D}\right) \text{ for cc} \quad (2.39)$$

$$\frac{F(D)_{\mathrm{cp}}}{2\pi R} = \frac{\lambda_D}{\epsilon}\left(2\sigma_{S0,1}\sigma_{S0,2}e^{-D/\lambda_D} + \left(\sigma_{S0,1}^2 + \sigma_{S0,2}^2\right)e^{-2D/\lambda_D}\right) \text{ for cp} \quad (2.40)$$

It should be noted that the presented approximations using continuum theory and are just valid for $D \geq \lambda_D$ and small surface potentials ($zeU_0 < K_BT$). For separations larger than the Debye length ($D >> \lambda_D$) and small surface potentials ($zeU_0 << K_BT$) the double layer interaction between two surfaces decays exponentially with the separation distance and can be approximated by

$$\frac{F(D)_{\mathrm{approx}}}{2\pi R} \approx \frac{2\epsilon U_{0,1}U_{0,2}}{\lambda_D}e^{-D/\lambda_D} = \frac{2\lambda_D\sigma_{S0,1}\sigma_{S0,2}}{\epsilon}e^{-D/\lambda_D} \quad (2.41)$$

$$\approx 64K_BT\rho\lambda_D\tanh^2\left(\frac{zeU_0}{4K_BT}\right)e^{-D/\lambda_D} \quad (2.42)$$

Figure 2.14A shows the electrostatic double layer force for cc and cp conditions, adapted from Ref. [128]. Examples for analytic and numeric expressions, of solutions of the full PB equation, and fitting to experimental data can be found in Ref. [33, 126, 130, 131, 132]. The above discussed solutions of the PB equation neglect aspects like surface heterogeneities, roughness, and the discrete character of ions.

The DLVO theory developed by Derjaguin, Landau, Verwey and Overbek combines the electrostatic repulsion at intermediate distances and the short ranged VdW forces to describe the interactions between charged surfaces in electrolyte solutions [126].

For short separation distances, additional attractive hydrophobic interactions between hydrophobic surfaces and hydration repulsion between hydrophilic surfaces have to be taken into account. The origin of these interactions is still under debate and no theory is available to explain the effects. Hydrophobic attraction between two surfaces can be stronger than VdW interactions and can be attributed to solution effects and cavitation bubbles. For the hydration force, it is assumed that water-water interactions cause repulsion. Experimental results show that these interactions can be described by an exponential decay function [128, 24].

2.3.4 Capillary Interactions

If a substrate is stored in air under standard lab conditions, a thin water films adsorbs on the surface. When two bodies are brought close to each other, a meniscus formes

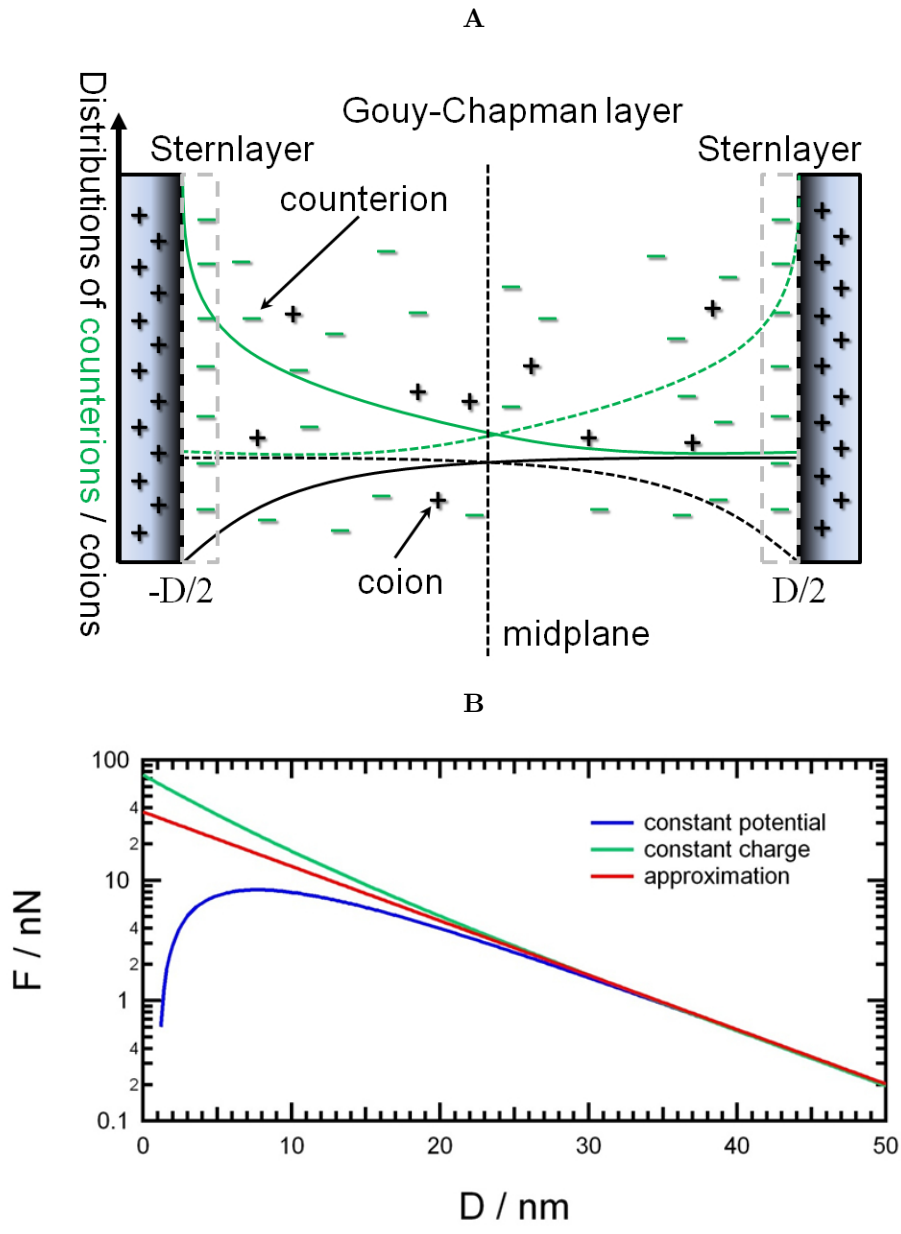

Figure 2.14: Interactions of charged Surfaces: 2.14A Distributions of counterions and coions of two interacting equal charged surfaces at distance D and schematic of the corresponding Stern- and Gouy-Chapman layer. 2.14B Electrostatic double layer force: Solutions of the PB equation for constant charge and constant potential conditions for a charged sphere with radius $R = 10\,\mu$m interacting with a charged surface in 0.1 M NaCL solution. Surface potentials for cp are $U_{0,1} = 80\,$mV and $U_{0,2} = 50\,$mV. Surface charge densities for cc are $\sigma_{S0,1} = 0.0058\,\mathrm{C/m^2}$ and $\sigma_{S0,2} = 0.0036\,\mathrm{C/m^2}$. The surface charge was adjusted by $\sigma_{S0,(1,2)} = \epsilon U_{0,(1,2)}/\lambda_D$ so that the potential at large separations D is identical. (Adapted from Ref. [128] ©Elsevier)

by condensation of water which causes the so-called "capillary" forces (such forces can also appear in liquid environment under certain conditions, e.g. caused by capillary bridges). These forces have a hysteresis character since they only occur when a condesation neck forms.
Using the equations of Young, Laplace, and Kelvin it is possible to characterize these forces. For two spheres with radii R_i and R_j with a liquid film of the thickness h, and the surface energy γ, the capillary force can be expressed by

$$F_{\text{cap}}(D) = -\frac{2\pi R\gamma(\cos\theta_i + \cos\theta_j)}{1 + D/h}, \tag{2.43}$$

where R is the reduced radius, θ is the contact angle of surface i and j, and D is the separation distance [24, 133].

2.3.5 Steric Interactions

At a certain small distance, all bodies repel each other due to steric interactions. For blank bodies, they have their origin in the Pauli principle and can be described using a hard wall potential.
If the body is covered with molecules, e.g. PEs, further aspects play a role [134]. Upon approach of PE-covered surfaces compression of PEs leads to an increase in the concentration of the polymer (increase in entropy) as well as the osmotic pressure and therefore in the restoring force. This force is dependent on the solvent quality, the resulting ion distribution, and on the grafting density (Ch. 2.2.5). Details about the interactions of polymer brushes are discussed below.

Interactions of Polymer Brushes

Now, consider two surface coverd with the same polymer brushes interacting with each other. Force balance of entropic forces (elastic repulsion), steric (volume) interactions, osmotic pressure, and in case of charged polymer brushes electrostatic contributions (Ch. 2.2.5) result in a repulsive pressure ($P(D)$: force per unit area) between the interacting bodies [115].
This force can be converted into the interaction energy per unit area ($w(D)$) between two parallel plates separated by distance D, using the Derjaguin approximation $w(D) = F(D)/2\pi R = -\int_{2h}^{D} P(D^*)dD^*$ (Eq. 2.36). Neutral brushes can be approximated using the de Gennes approach [135, 136, 137], which results in an interaction energy per unit

area $w(D)$ of

$$w(D)_{\mathrm{AdG}} = \frac{8k_BTH}{35\sigma^{3/2}}\left[7\left(\frac{D}{2H}\right)^{-5/4} + 5\left(\frac{D}{2H}\right)^{7/4} - 12\right] \text{ for } D < 2H, \tag{2.44}$$

where the apparent brush height depends on the regime the brush is in. For neutral brushes $H \propto N\sigma^{-1/3}$. Using mean field approaches and a box profile for the density, the interaction energy profile is given by [128, 138]

$$w(D)_{\mathrm{MF}} = \frac{6k_BTH^2}{Na^2\sigma}\left[2\left(\frac{D}{2H}\right)^{-1} + \left(\frac{D}{2H}\right)^{2} - 3\right] \text{ for } D < 2H. \tag{2.45}$$

Taking into account a parabolic monomer profile, which is more realistic than a box-profile, $w(D)$ results in the so called MWC dependence (Milner, Witten, Cates) [139, 140, 141]

$$w(D)_{\mathrm{MF,MWC}} = \frac{\pi^2 k_BTH^2}{8Na^2\sigma}\left[\left(\frac{D}{2H}\right)^{-1} + \left(\frac{D}{2H}\right)^{2} - \frac{1}{5}\left(\frac{D}{2H}\right)^{5} - \frac{9}{5}\right] \text{ for } D < 2H, \tag{2.46}$$

The scaling behavior is the same as for Eq. 2.45 minus a correction term accounting a less steep increase of repulsive interactions.

Obviosely the same approache, as derived for neutral brushes can be used for charged brushes, where screening by salt achieves electro neutrality. Also, in case of PE brushes in the salted brush regime it can be shown that the same approache, as derived for neutral brushes (Eq. 2.45), can be used. For this purpose the excuded volume must be extended with electrostatic contributions ($v_2 = v_0 + v_{el}$) [33][115]. This results in an appararent brush height h (Ch. 2.2.5) of

$$h = N\left(\frac{a^2}{6\sigma}\right)^{1/3}\left(v_0 + \frac{f^2}{2c_S}\right)^{1/3} \tag{2.47}$$

and finaly in

$$w(D)_{\mathrm{SB}} = \frac{k_BTN^2}{h\sigma^2}\left(v_0 + \frac{f^2}{2c_S}\right)\left[2\left(\frac{D}{2h}\right)^{-1} + \left(\frac{D}{2h}\right)^{2} - 3\right] \text{ for } D < 2h.$$

for quenched, salted PE brushes. Here v_0 is the non extended exluded volume, c_S the salt concentration and f the fraction of charged monomers. Equation 2.48 shows the same scaling behavior as 2.45. In case of osmotic brushes the scaling behavior of $w(D)$

differs compared to neutral polymer brushes [115, 139].

$$w(D)_{\mathrm{OsB}} = \frac{2k_BT}{\sigma}\left[\frac{3}{2}\frac{h^2}{Na^2}\left(\left(\frac{D}{2h}\right)^2-1\right)+\frac{N^2v_o}{2\sigma h}\left(\left(\frac{D}{2h}\right)^{-1}-1\right)-fN\ln\left(\frac{D}{2h}\right)\right] \quad \text{for } D<2h, \tag{2.48}$$

Figure 2.15 shows that the scaling laws for the interaction energy per unit area follow the same trend, in particular for strong deformations. For $0.2 > D/2H > 0.9$ equations 2.44, 2.45 and 2.46 can be approximated with an exponential decay (Figure 2.15) [126]:

$$w(D)_{\mathrm{approx}} \approx \frac{100k_BTH}{\pi\sigma^{3/2}}e^{-\pi D/H} \text{ for } 0.2 > D/2H > 0.9. \tag{2.49}$$

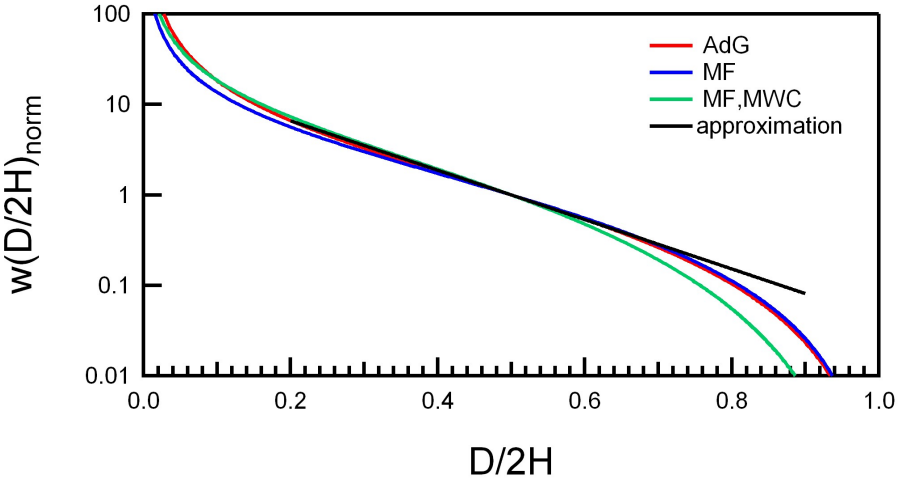

Figure 2.15: Interactions of polymer brushes: AdG-profile, MW-profile, MWC-profile and approximation. $w(D/2H)_{\mathrm{norm}} = w(D/2H)/w(0.5)$ (adapted from Ref. [33])

These discussed equations can be extended for annealed brushes. If just one of the surfaces is covered by a brush the force is reduced by a factor of four.

A complete diagram of different compression states for quenched and annealed PE brushes as a function of polymer and salt concentration was derived by Zhulina et al. [142]. Counter intuitively, the restoring force for neutral brushes depends stronger on deformation than in quenched PE brushes and even stronger than for annealed PE brushes. This is due to recombination of charged groups with counterions which reduce the osmotic pressure inside the brush. Adding salt leads to an increase in the restoring force.

2.3.6 Contact Mechanics

If two bodies contact each other, they deform and a contact area is created under the influence of an external applied force and surface interactions. Accurate knowledge on contact parameters like contact area a and deformation δ as a function of the applied force as well as on the resulting stress distribution is a crucial requirement to understand effects in nature and for applications. Examples are reversible adhesives in both biological and non-biological systems.
Several theories exist that describe the contact situation and connect molecular interactions and continuum models. The most important theories of contact mechanics for linear elastic bodies are introduced without derivations in the following, oriented on reviews [124, 24, 127, 128].

Material Parameter

First, several material parameters must be introduced. The stress acting on a material is defined as the force per cross sectional area A. For normal loads in z direction this is

$$\sigma_z = F_z/A. \tag{2.50}$$

The resulting relative elongation of the body is quantified by the strain ϵ

$$\epsilon_z = \frac{\Delta L_z}{L_z}, \tag{2.51}$$

with the total length in z-direction L_z and the length change ΔL_z. The elastic deformation of the body can be related to its Young's modulus E which is defined for an isotropic elastic material[10] as the proportionality factor between the applied strain and the resulting stress

$$\sigma_z = E\epsilon_z. \tag{2.52}$$

Typical values for E are in the range of tens of kPa (e.g. gels), some MPa (e.g. rubbers), up to some GPa (e.g. metals) [24]. When a material is stretched in one direction, it will normally contract perpendicular to this direction. This effect is considered by the Poisson ratio ν

$$\nu = \frac{\epsilon_{x,y}}{\epsilon_z} \tag{2.53}$$

for a material stretched in z direction. The Poisson ratio ν is in the range of 0 up to 0.5 (0.5 for perfectly incompressible materials). Rubbers reach values close to the upper

[10] In general this have to be defined using tensor analysis

limit of 0.5 [24], whereas glass has a Poisson ratio of around 0.1 for example.

Contact Mechanic Models

The first model to describe the contact between two non- adhering, isotropic, linear elastic spheres was given by H. Hertz in 1881[143]. H. Hertz calculated the deformation δ and contact area a as a function of applied load F, geometrical terms ($R = R_i R_j/(R_i + R_j)$), and material parameters as accounted for the reduced modulus K

$$K = \frac{4}{3}\left(\frac{1-\nu_i^2}{E_i} + \frac{1-\nu_j^2}{E_j}\right)^{-1}. \tag{2.54}$$

The resulting contact parameters as well as the stress distribution $\sigma(r)$ in the contact zone (as a function of distance from the axial center r) are summarized in Figure 2.17 and Tab. 2.2 [127, 128]. Applying some simple conversions, the force to achieve a certain deformation δ can be obtained by

$$F^{\text{Hertz}}(\delta) = K R^{1/2} \delta^{3/2}. \tag{2.55}$$

Taking adhesion in the contact area into account, Johnson, Kendall and Roberts (JKR)

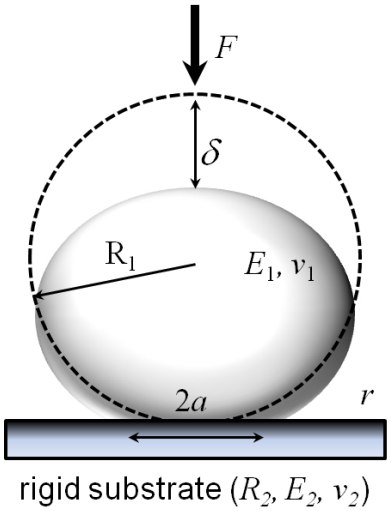

Figure 2.16: Contact parameters of a sphere pressed against a flat substrate

developed a more realistic model for soft contacts [144]. By balancing surface energies and the elastic potential, they calculated the contact area and the deformation as a function of applied load and surface energy per unit area w, as well as the resulting stress distribution (Figure 2.17 and Tab. 2.2). The JKR theory is valid for soft samples

with a large reduced radius and large adhesion forces. In case of zero external load, finite contact radius, deformation, and stress are observed due to adhesion [127]

$$a_0{}^{\mathrm{JKR}} = \left(\frac{6\pi w R^2}{K}\right)^{1/3}, \tag{2.56}$$

at a deformation of

$$\delta_0^{\mathrm{JKR}} = \frac{a_0^2}{R} - \frac{2}{3}\sqrt{\frac{6\pi w a_0}{K}}. \tag{2.57}$$

Due to the strength of adhesion, the interacting bodies still adhere while pulling (negative loads) until a critical force F_{adh} is reached (see Tab. 2.2). It should be noted that the expression for the adhesion force is independent of the elastic properties of the material. Furthermore, the aspect of experimentally observed adhesion hysteresis can be explained using the JKR theory. The contact area is larger when unloading than in the loading case until rupture at a critical contact radius of $a_c = 0.63a_0$ and a (negative) deformation of $\delta_c = -(\pi w^2 R/12K)^{1/3}$.

At the same time Derjaguin, Muller, und Toporov (DMT) developed an alternative model where adhesion is present around the contact zone [145]. The DMT model assumes that the surface profile is the same as for Hertzian contacts. Adhesion is included by an additional load caused by the surface forces around the contact area. The DMT theory can be applied to contacts of stiff samples with small radii and small adhesion. In case of zero external load, finite contact radius, deformation, and stress occur

$$a_0^{\mathrm{DMT}} = \left(\frac{2\pi w R^2}{K}\right)^{1/3}, \tag{2.58}$$

at a deformation of

$$\delta_0^{\mathrm{DMT}} = \frac{a_0^2}{R}. \tag{2.59}$$

Due to adhesion, the interacting bodies adhere while pulling (negative loads) until a critical force is reached. The deformation parameters are summarized in Figure 2.17 and Tab. 2.2.

If the interaction energy is negligible or for very high loads ($F > 10^3\pi w R$), the results of JKR and DMT models reduce to the equations given by the Hertz model.

As mentioned above, both the JKR and the DMT model are valid for different limits of material parameters. For quantification of the validity of the particular model, Tabor introduced "the Tabor parameter" which is defined by the ratio between neck height

Table 2.2: Expressions for contact parameters of different contact mechanic models. Adapted from Ref. [128].

	Hertz	JKR	DMT
a^3	$\frac{FR}{K}$	$\frac{R}{K}\left(F+3\pi Rw+\sqrt{6\pi RwF+(3\pi Rw)^2}\right)$	$\frac{FR}{K}+\frac{2\pi wR^2}{K}$
δ	$\frac{a^2}{R}=\left(\frac{F^2}{K^2R}\right)^{1/3}$	$\frac{a^2}{R}-\sqrt{\frac{8\pi aw}{3K}}$	$\frac{a^2}{R}=\left(\frac{(F+2\pi Rw)^2}{K^2R}\right)^{1/3}$
σ	$\frac{3Ka}{2\pi R}\sqrt{1-r^2/a^2}$	$\frac{3Ka}{2\pi R}\sqrt{1-r^2/a^2}-\sqrt{\frac{3Kw}{2\pi a}}\frac{1}{\sqrt{1-r^2/a^2}}$	$\frac{3Ka}{2\pi R}\sqrt{1-r^2/a^2}$
F_{adh}	0	$-\frac{3}{2}\pi wR$	$-2\pi wR$

at critical deformation due to adhesion and the range of surface forces z_0 [146]

$$\mu_T=\left(\frac{16Rw^2}{9K^2z_0^3}\right)^{1/3}. \tag{2.60}$$

For $\mu_T << 1$, the DMT model is valid and for $\mu_T >> 1$ JKR theory applies.
Maugis introduced a more general theory, which describes the transition range between the JKR and the DMT model and applies to all materials from large hard spheres with high surface energy to small soft bodies with low surface energies. The Maugis theory describes interactions by a Dugdale model and results in expressions for the contact parameters as a function of the so-called "Maugis parameter" ($\mu_M \approx 1.16\mu_T$). For analytic expressions of the contact parameters, the reader is referred to Ref. [127, 147]. Figure 2.18 shows an overview for the availability of the presented contact mechanic models.
A general expression for the contact parameters of two axisymmetric elastic bodies (i.e. sphere, parabola, or cone) was given by Sneddon's solution [127]. The reader should notice that the contact radius must be known for these expressions. Also, one can show for any punch that the load displacement can be written in the form

$$F(\delta)=\alpha\delta^n, \tag{2.61}$$

with α including material parameters and n dependent on the geometry ($n = 1$ for flat cylinders, $n = 2$ for cones, $n = 1.5$ for paraboloids i.e. spheres) [128].
The expressions of the stress distributions presented above (see Tab. 2.2) have limitations in their phyical meanings, since the stresses in the descriptions are infinite at the edge of contact. This unphysical situation can be resolved using additional parameters. One can show that the peak stress can only be in the order of the elastic modulus for

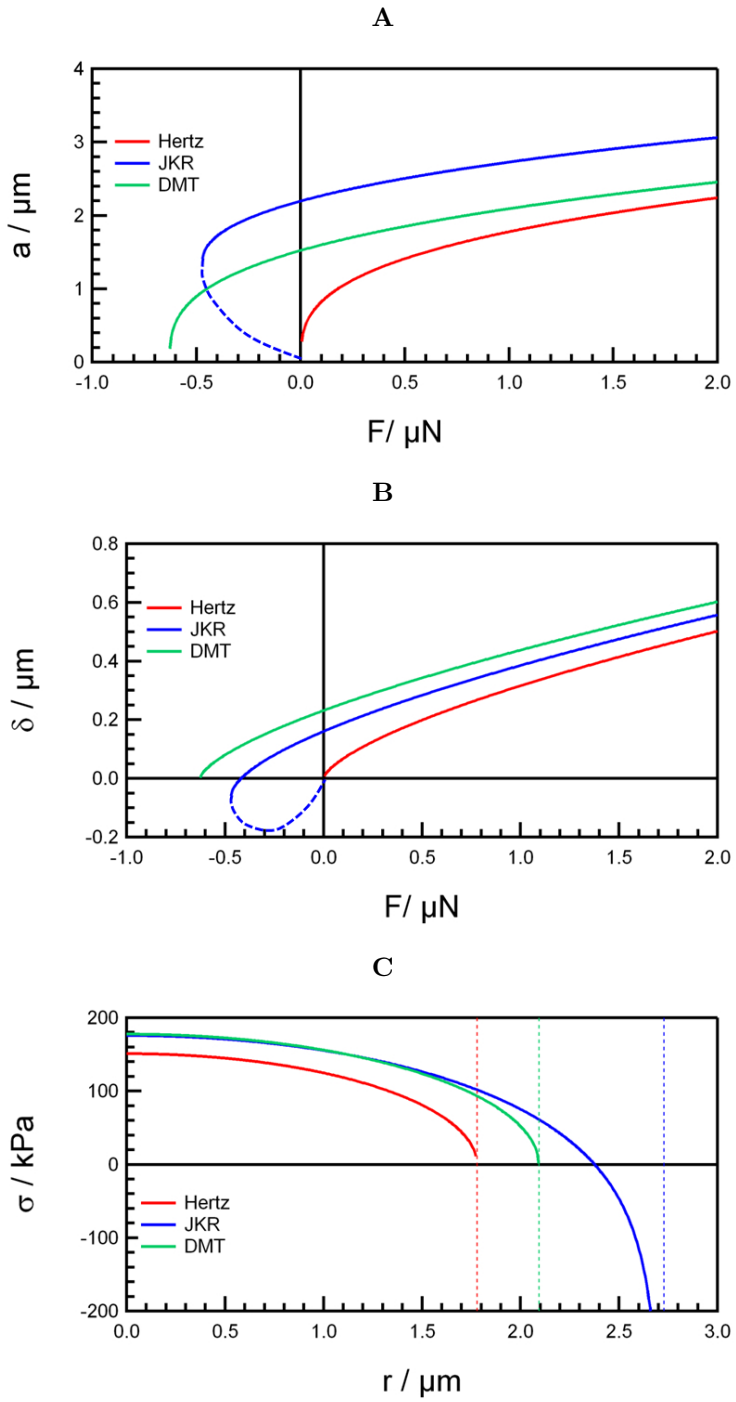

Figure 2.17: Contact mechanics of elastic bodies: 2.17A Contact radius as a function of applied load, 2.17B Deformation as a function of applied load for a soft sphere ($R = 10\,\mu$m, $E = 1\,$MPa, $w = 10\,$mJ/m^2) pressed against a hard substrate (dotted lines show the hysteresis character of the JKR theory). 2.17C Stress in the contact zone of a soft sphere for an applied load of $F = 1\,\mu$N (dotted lines show the contact radius).

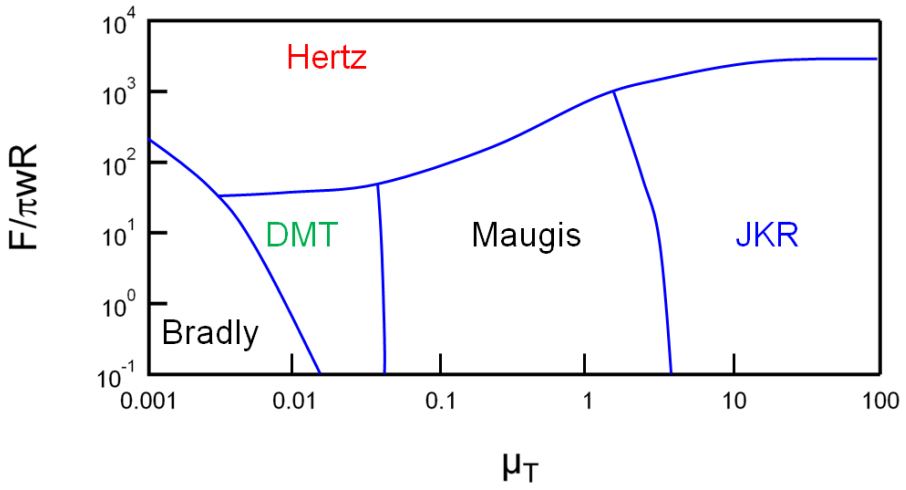

Figure 2.18: Availability of contact mechanic models (reproduced from [148] ©Elsevier)

soft materials or the predicted VdW stress of the interface.

Above, only total linear elastic deformations were treated. For indentations where plastic deformation or viscoelastic phenomena occur the situation is even more complex due to nonlinear behavior. Approaches to model these contact problems were developed for example by Oliver and Pharr [149]. Also, heterogeneities and roughness are neglected in the continuum elastic theories described above and should be taken into account for a full realistic description [150, 151].

Table 2.3: Experimental methods to study responsive layers, FTIR: Fourier transform infrared spectroscopy, QMB: Quartz crystal micro balance, SFA: Surface force apparatus, AFM: Atomic force microscope, JKR: JKR apparatus

properties	methods
chemical structure	FTIR, QMB, spectroscopy
thickness and density	scattering techniques, ellipsometry, reflectometry spectroscopy, microscopy, SFA, AFM
surface interactions and mechanics	SFA, AFM, JKR, microscopy

2.4 Experimental Methods: Atomic Force and Optical Microscopy

For characterization and understanding of responsive surfaces experimental techniques are necessary. Novel scanning probe microscopy approaches and optical methods can give insights into the behavior of surfaces and interfaces [125]. Exemplary experimental approaches to study the chemical structure, the thickness and density of responsive PE surface, as well as surface interactions and mechanical properties are summarized in Table 2.3 [1, 17]. These methods are accomplished by new theoretical approaches and modeling techniques. This section focus on the used techniques in this thesis, in particular atomic force and optical microscopy. The discussion is oriented on [124, 125, 24, 126] and the cited literature.

2.4.1 Atomic Force Microscopy (AFM)

Several characterization methods are known to study the response of smart coatings (Table 2.3). In this thesis, the focus is set on changes of interactions and mechanical properties of such systems on the colloidal scale. One of the most suitable techniques for surface characterization in this regime is atomic force microscopy (AFM) [152]. Complementary methods can be e.g. the surface force apparatus [153, 154], the JRK apparatus [155], or optical or magnetic tweezers [156].
The AFM was invented by Binnig et al. in the 1980s [157] on the basis of the scanning tunneling microscope. Nowadays, the AFM has many fields of applications [158]. Besides the original intention of imaging surface topographies, the AFM allows for detecting surface and interfacial forces, molecular interactions and characterization of the mechanical and the electrical properties of the surface of the studied material, just to name a few.

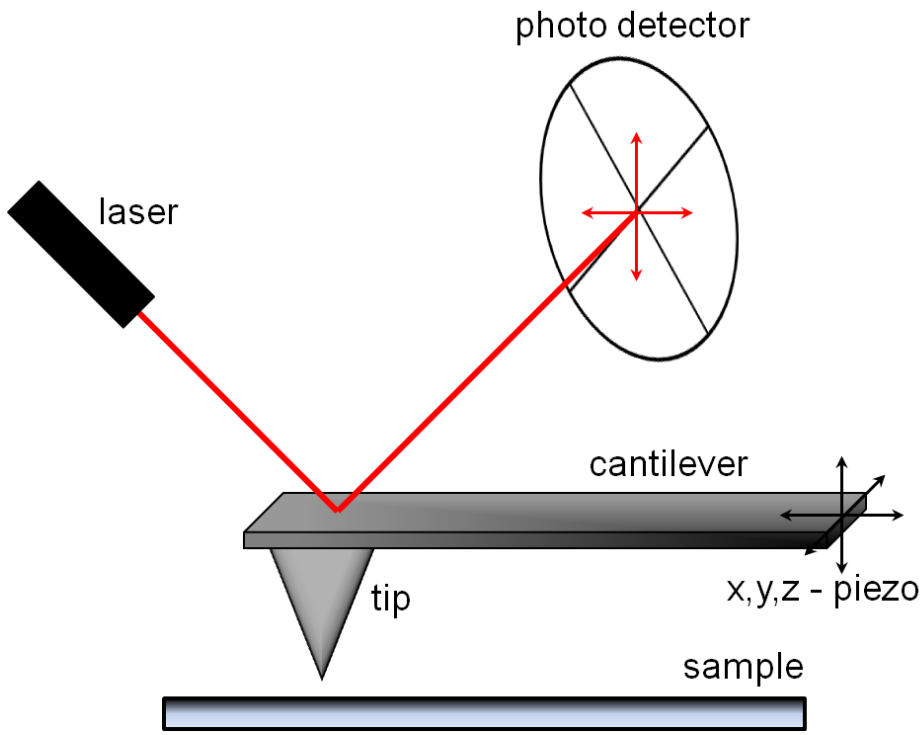

Figure 2.19: Working principle of an AFM

The working principle of an AFM is based on interactions between the sample and a probe as a function of their distance. The probe is commonly a cantilever which deflects towards or away from the surface depending on attractive or repulsive forces. The deflection can be detected at high precision using several methods. The most common detection method is the optical lever approach where a laser beam is focused on the backside of the cantilever and is reflected to a position-sensitive photodiode (Figure 2.19). The position-sensitivity is achieved by subdivision of the detector (typically quarterized), which results in different intensities on the individual areas and finaly in a current signal. The current can be transformed into the required information, in particular height changes (these can be further converted to interaction forces, hardness, and roughness.)
The acting force can be calculated from the deflection of the cantilever by Hooks law

$$F(\delta_c) = k_c \delta_c, \tag{2.62}$$

where k_c is the spring constant and δ_c the deflection of the cantilever.
The relative position of cantilever and sample is controlled by piezoelectric elements with a precession of 0.1 nm in x-, y-, and z- direction. Typical cantilevers are made from

silicon or silicon nitrid and have a spring constant in the order of $(0.001 - 100)\,\mathrm{N/m}$. For enhancement of the reflectivity of the cantilever, the backside of the cantilever can be coated with a metal.
The advantages of an AFM are its high spatial resolution on the nm scale (determined by the convolution of the tip and the sample), high sensitivity towards forces in the range from pN up to some μN, and a resolution for deformations smaller than 1 nm (determined by the spring constant of the cantilever). These pros and the ability to study nearly any kind of solid (or liquid) interface in various environments in a big temperature range have made the AFM one of the most popular tools in surface science. Also, other surface properties can bes studied, as for example electrical properties by controling an electric potential applied to the cantilever. For instance lateral electric properties are important in the semiconductor and hard disc industry [159].
Drawbacks of the AFM are that the technique is relatively slow and limited to surface (rather than bulk) properties. Additionally, the operating distances are limited by the used piezos (typically in the range of $10\,\mu$m for z-, and $100\,\mu$m in x- and y- direction).

Imaging AFM

For imaging, (typically) sharp tip cantilevers are scanned in x- and y- direction over the sample substrate. Three main operation modes can be distinguished: 1) the contact mode, 2) the noncontact mode, and 3) the tapping mode. In contact mode, interaction forces are detected while the cantilever tip remains in contact with the sample during scanning. The resulting deflection (constant height) or the applied force to keep the deflection constant (constat force), are used as the signal. Using a feedback loop the signal can be directly converted into a topographic image. The noncontact and the tapping mode are dynamic modes. Here the cantilever is oscillated near its resonance frequency and shifts of amplitude and frequency are detected. In case of the noncontact mode, shifts of the resonance frequency are detected while moving the cantilever above the surface (no contact). The tapping mode combines benefits of both, the contact and non-contact mode, by oscillating the cantilever near its resonance frequency, while allowing for small impacts of the cantilever tip into the sample.
The resulting image of these modes is mathematically a convolution of the sample and the probe. As a result the spatial resolution is limited by the geometry of cantilever tip[11]. An overview of the different imaging modes is given in Ref. [158, 160, 161].

[11] Additional factors are external and internal vibrations and the damping quality of the cantilever.

Force Spectroscopy

Besides imaging, the AFM can be used for direct force measurements [128, 152]. For this, the cantilever is driven in z- direction towards or away from the surface. The cantilever deflection δ_c is recorded as a function of the piezo hub Z. This outcome can be transformed into a force versus distance (FD) curve (often named force-separation or force-indentation curve, depending on the experiment). For that purpose the voltage of the photodiode must be related to the force acting on the cantilever. If no artifacts occurs (e.g. due to very large cantilever deflections), the deflection of the cantilever is linear proportional to the voltage of the photodiode V

$$\delta_c = SV, \tag{2.63}$$

where S is the so-called "inverted optical lever sensitivity" (InvOLS). If the spring constant of the cantilever k_c is known precisely[12] (from calibration measurements, see below), the deflection can be transformed into the acting force using Hooks law (eq. 2.62)

$$F(Z) = k_c SV. \tag{2.64}$$

The separation of a cantilever from the surface D is related to the movement of the z-piezo Z as

$$D = Z - (\delta_C + \delta_S), \tag{2.65}$$

where δ_c is the cantilever deflection and δ_S the deformation of the sample surface. FD curves reflect the contributions of surface interactions and Hooks law of the cantilever. A schematic example of a FD curve is shown in Figure 2.20.

When the cantilever is far away from the surface, no interactions occure and cantilever deflection is zero. This part of the FD curve is called "baseline".

If the cantilever comes close to the surface, the cantilever will start to bend due to surface forces. In case of attractive forces, the cantilever will bend towards the surface and jump into contact (jtc) when the gradient of the attractive forces overcomes the spring constant of the cantilever. When the surface forces are repulsive (e.g. due to electrostatic diffuse layer froces, Ch. 2.3.3) the cantilever starts to bend away from the surface which results in an increase of the detected force.

If the cantilever movement is sustained, the cantilever will deflect as described by Eq. 2.62 in combination with the deformation of the sample (Tab. 2.2). In case of a hard substrate (stiffness of the cantilever is much smaller than the stiffness of the substrate),

[12] Manufacture values are typically not realible, see below for several calibration methods

this results in the constant compliant region, where probe and sample surface move in parallel. At a certain point, the piezo movement is turned back and the cantilever retracts. Trace and retrace in contact are named as contact part, contain information on the mechanics of the sample. They can be described by contact mechanical models (Ch. 2.3.6).
In case of attractive forces (adhesion between the sample and the probe), the cantilever will stay in contact until the restoring force of the cantilever overcomes the adhesion force F_{adh} and the cantilever jumps out of contact (joc) (For expressions of F_{adh} see Tab. 2.2). The included area between trace and retrace of the FD curve contains information on the work of adhesion (adhesion hysteresis).

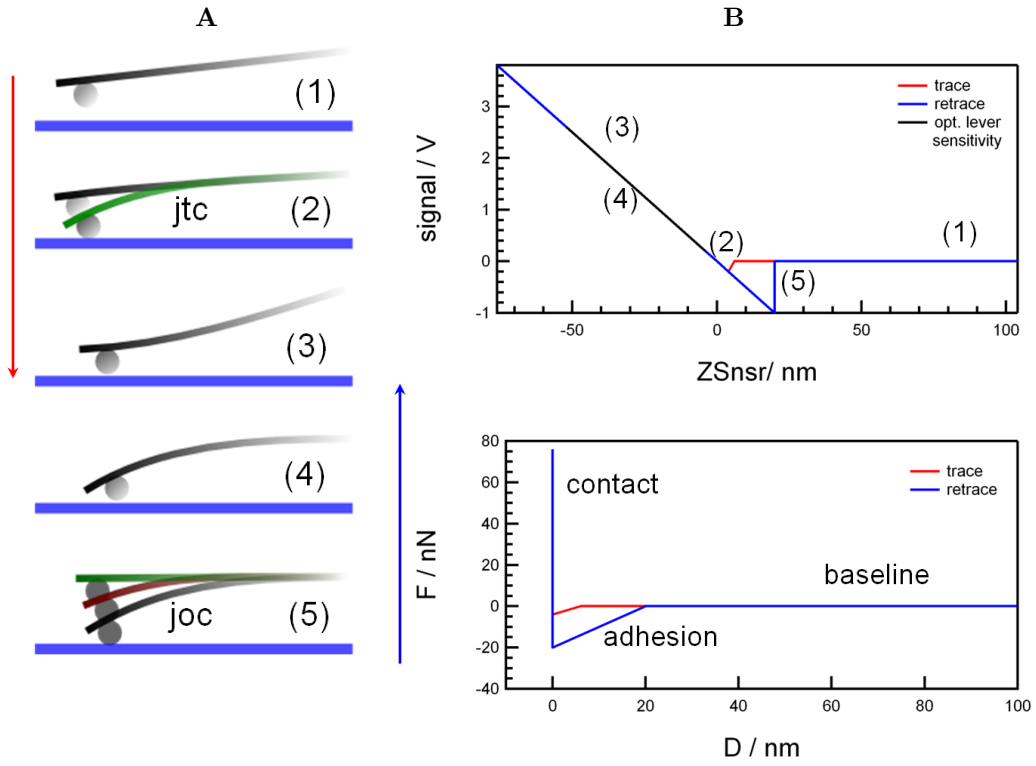

Figure 2.20: Force distance curve: 2.20A Cantilever movement, 2.20B Detected raw data, top (schematic of hard tip interacting with a hard substrate) converted to a force distance curve, bottom.

The presented FD curve (Figure 2.20) is just a simplified example. For complete interpretation of the experimentally detected FD curves, including all surface and molecular interactions, mechanical properties (as introduced in Ch. 2.3) and hydrodynamic effects of the sample, the reader is referred to Ref. [128, 152]. In these reviews also many

applications, related to force spectroscopy, are discussed.
Acquiring FD curves on several mashes of a digital grid results in a so called FD map (force volume).
Until now, vertical deflections of the cantilever were discussed only. Lateral deflections can be also help to learn about surface properties, e.g. friction and lateral restoring forces as a function of the surface topography and sample geometry. Calibration of the lateral spring constant and interpretation of data needs special effort and the reader is referred to Ref. [162].

The Colloidal Probe Technique

In general, AFM probes are sharp tips (tip diameter in the range of 5-20 nm) in the front of the AFM cantilever(Figure 2.21A). While these tips allow to establish very small contacts, the contact geometry is rather ill defined because the shape of AFM tips cannot be controlled accurately in the manufacturing process and during measurement. However, for quantitative measurements of surface interactions, it is often useful to measure with defined contact (or interaction) geometries [163]. A major step to overcome this problem was the introduction of the colloidal probe (CP) technique by Ducker (Figure 2.21B) [164]. For the CP technique, colloidal particles (mostly spherical) of several microns in diameter (typically $1-50\,\mu$m) and with a surface roughness of only a few nanometres are attached to the AFM cantilever[13]. The radius can be measured e.g. during preparation using an optical microscope. A CP can be attached to the cantilever using micromanipulation under optical control with a light microscope. Most common attachment protocols use epoxy glue or sintering [165, 166]. The CP can be adapted to the experiment by choice of the material or by additional functionalization.
Full knowledge about the surface geometry, i.e. the CP radius allows for usage of the Derjaguin approximation (Eq. 2.36) and thus normalization of the data to a unit area. In this way, it is possible to compare different interaction measurements.
Since its introduction, the CP technique has found many applications in interaction measurements [165].

[13]In principle, any kind of material that can be glued to the cantilever can be used.

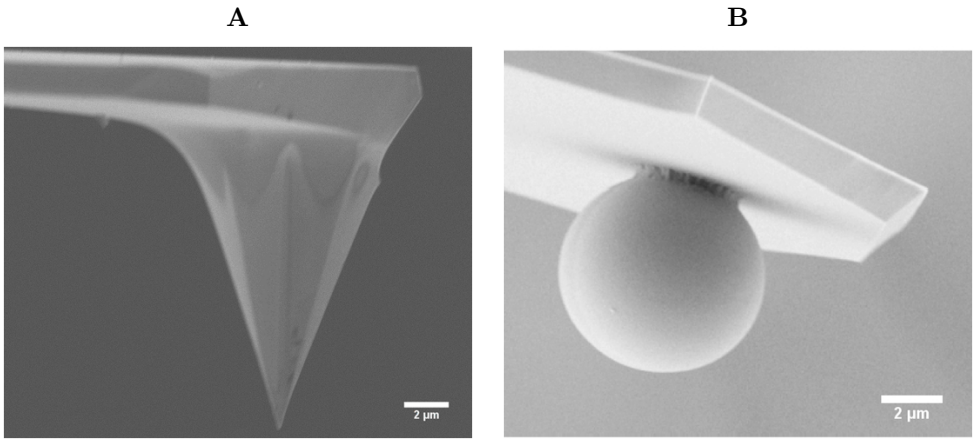

Figure 2.21: AFM cantilever probes: 2.21A Sharp tip, 2.21B Colloidal probe (Ref. [167])

Calibration of the Spring Constant of AFM Cantilevers

For the transformation of the voltage signal of the photodiode into a force, accurate knowledge about the mechanical properties of the cantilever, as quantified by the spring constant and the resonance frequency are necessary. These parameters can be determined by several techniques, namely dimensional, static, and dynamic methods [24]. The dimensional methods are based on the dimensions and the material properties of the cantilever. For rectangular cantilevers the force constant is given by

$$K_c = \frac{Ebd^3}{2L^3}, \tag{2.66}$$

where E is the Youngs modulus of the cantilever material, and b, d and L its dimensions in width, thickness and length.
In static methods, a known force is applied to the cantilever and the resulting deflection is measured. Both methods have problems such as unknown material parameters, exact determination of the cantilever thickness or experimental effort.
Dynamic methods based on the detection of the resonance frequency of the cantilever overcome these problems. Dynamic methods determine the spring constant of the cantilever with an uncertainty of about 10%. The thermal noise method developed by Hutter and Bechhoefer [168] uses the thermal fluctuations of the cantilever that are detected far away from the surface and computed back to the spring constant using

equipartition theorem

$$k_c = \frac{k_B T}{\langle \delta_c^2 \rangle} \tag{2.67}$$

The power spectrum $P(f)$ of the recorded signal is calculated which is a function of δ_c^2 versus the frequency f (Wiener-Kinchin theorem). Integration of the power spectrum over all frequencies results in $\langle \delta_c^2 \rangle$. Typically, just the first resonance peak where most of the energy is stored is fitted by the thermal response function of a harmonic spring/oscillator

$$k_c = \frac{k_B T}{\int P(f) df} \approx \frac{2 k_B T}{\pi A f_{res} Q}, \tag{2.68}$$

with the resonance frequency f_{res} of the spring, the amplitude A, and the quality factor of the first resonance peak Q ($Q = f_{res}/\Delta_f$, Δ_f: full width at half maximum).
The Sader method is based on hydrodynamics [169, 170]. From knowledge about f_{res}, Q, and the planar geometry of the cantilever L and b, the spring constant can be calculated

$$k_c = 0.1906 \rho b^2 L Q f_{res}^2 \Sigma_i(Re), \tag{2.69}$$

where ρ is the density of fluid surrounding the cantilever and $\Sigma_i(Re)$ is the imaginary part of the hydrodynamic function depending on the Reynolds number Re of the fluid. Cleveland et al. introduced another method based on the resonance shift to f_M when adding an additional mass M to the cantilever [171].

$$k_c = \frac{M}{1/f_M^2 - 1/f_{res}^2}. \tag{2.70}$$

2.4.2 Optical Techniques

Direct visualization of the response of PE layer systems can be achieved by several optical techniques, e.g. optical microscopy. The thickness and thickness changes can be accurately measured, e.g. by ellipsometry [172]. This section should give a short introduction into the techniques used in this thesis, i.e. bright field microscopy, micro interferometry and confocal microscopy. For more details, the reader is referred to Ref. [172].

Optical Microscopy

Optical microscopy has been known for over 1000 years and still is a frequently used and important tool in surface science.
Typical light microscopes are configured in the so-called "Köhler illumination" (Figure

2.22A). Irradiated light from the light source is focused by a condenser lens onto the sample. The light passes through or gets reflected by the sample into the objective and generates a picture in the focus plane of the ocular or the detector. Scattering of light can be reduced, and the contrast (e.g. phase contrast [173]) and the depth of field can be adjusted using additional apertures. Instead of using the alterations of light, also fluorescence microscopy is possible. For details the reader is referred to Ref. [172, 174]. The total magnification m_{tot} of a specimen is the product of the magnifications of the objective m_{obj} and the ocular m_{oc}

$$m_{tot} = m_{obj} m_{oc}. \tag{2.71}$$

For the adjustment of the total magnification the objective is typically changed while the ocular is held constant. For measurements, resolution r is usually more important than magnification. The resolution is defined as the minimal distance between two objects that can be distinguished (distance between the central maximum and the first minimum in the Airy disk [175]). The resolution is determined by the optical components and the wavelength λ of the light. Using optical theory (the Rayleigh criterion), it can be shown that r is proportional to the ratio of the wavelength and the numerical aperture NA.

$$r = 0.61 \frac{\lambda}{NA}. \tag{2.72}$$

NA is set by the deflection at the aperture

$$NA = n_i sin\phi, \tag{2.73}$$

having values from around 0.05 to 1.5. n_i is the refractive index of the surrounding medium of the objective (air $n_i = 1$ or immersions media, e.g. oil $n_i = 1.5$) and ϕ is half of the opening angle of the objective.

Confocal Microscopy

Confocal laser scanning microscopy (CLSM) has become an important tool for many investigations [172, 175]. Samples studied with this technique must be labeled with an emitting fluorescent dye (e.g. fluorophore, quantum dot) [174].
The CLSM presents a special kind of optical microscope with regard to illumination, detection, and image formation (Figure 2.22B). Coherent light is emitted by a laser system onto the sample. The light passes through a pinhole aperture that is situated

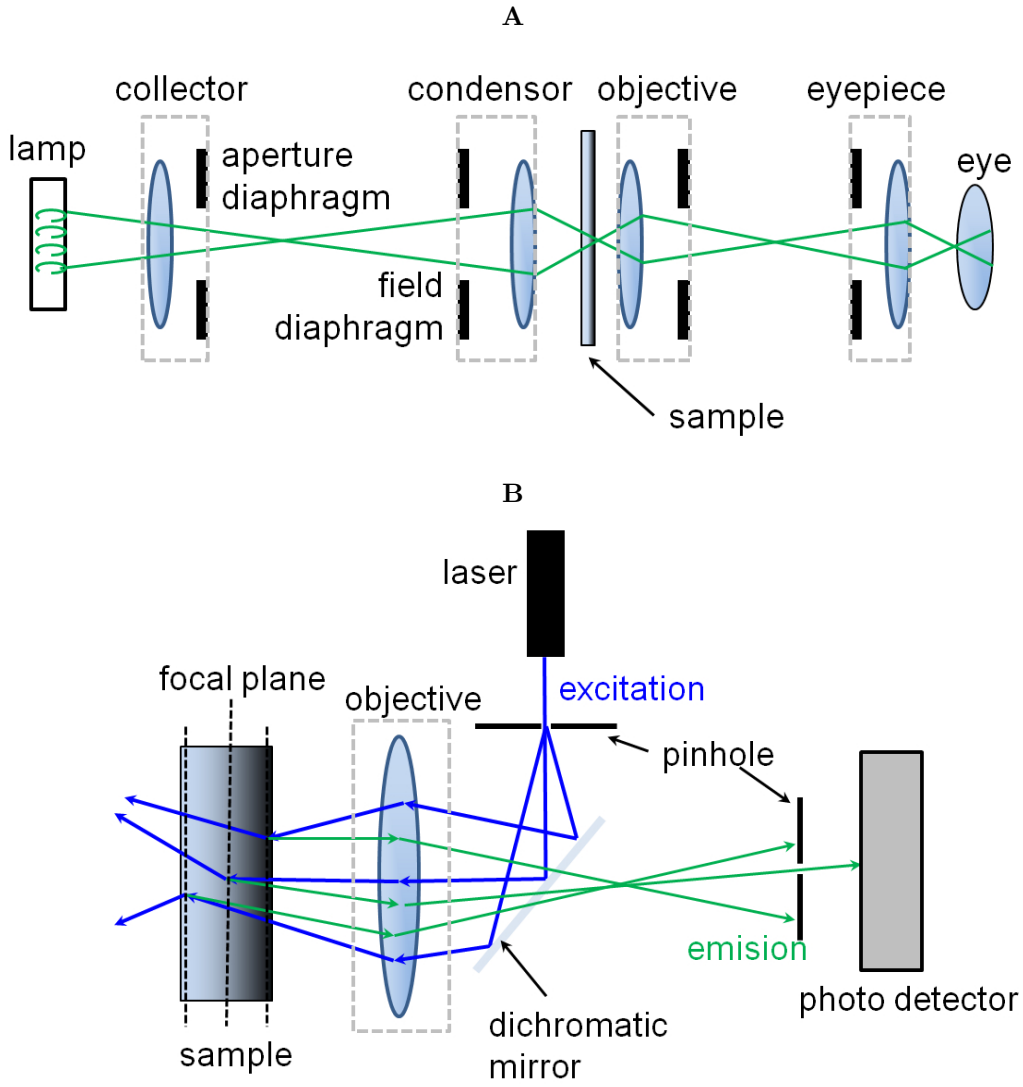

Figure 2.22: Optical microscopy: 2.22A Schematic of a light microscope in transmission mode adjusted for Koehler illumination. 2.22B Schematic of a confocal microscope. Just light from the focal plane can reach the detector.

in the conjugate plane (confocal) with a scanning point on the sample [175]. The laser light excites the dye. The re-emitted light (red shifted compared to the excitation) is detected by a photo multiplier [174]. The light path is specified by the experimental setup. For example, the reemitted light can pass a beam splitter and be focused onto a second pinhole aperture positioned in front of the detector. The pinhole has a diameter that can be adjusted to a size less than the airy diameter. By this approach, only light from the focal plane is detected. Nearly all defocused light is blocked by the pinhole. The depth of the focal plane is approx 1.5 times the spatial resolution. Scanning the so-called confocal volume in x- and y- direction over the sample allows for reconstructing two dimensional pictures with a defined "optical thickness". Additional scanning in z-direction allows for reconstruction of three dimensional objects.
Modern CLSMs consist of multiple laser excitation sources which permit multifluorescence imaging. Also, emission spectroscopy is possible with a CLSM.
More information concerning the theory of image formation, facilities, and applications can be found in Ref. [172, 175].

Microinterferometry

A possibility to achieve contrast is micro interferometry. Here optical path length differences or phase shifts produce interference patterns and contrast enhancement, repectively. The combination of the high depth resolution, in the order of 10 nm, and a lateral resolution of 0.2 μm makes these microinterferometry techniques to interesting tools to measure contact geometries on the colloidal scale.
In this thesis the reflection interference contrast microscopy (RICM) was used which is based on interference of reflected light from the sample due to path length differences and phase shifts from reflections on different media (Figure 2.23). Using apertures and an array of polarization filters allows to block perturbations due to stray light. Information, applications and the theory of image formation can be found in reviews, e.g. Ref. [176, 177, 178, 179, 180].
The sample is irradiated with monochromatic light with a wavelength λ and intensity I_0. Reflected light from the sample interfers constructively and destructively on the detector (as in case of Newton rings). Assuming perpendicular incidence of light and neglecting the curvature of the object, the interference pattern is given by

$$I = I_1 + I_2 + 2\sqrt{I_1 I_2}\cos(2kh(x) + \delta), \tag{2.74}$$

with I_1 and I_2 the intensities of the reflected light of the substrate and the sample, $h(x)$ the local height of the specimen, $k = 2\pi n/\lambda$ the wave number of the light and δ accounting for possible phase shifts.
Reconstruction of the specimen is possible by the use of an arccos-trafo of Eq. 2.74 that can be adopted stepwise to the interference pattern. For that purpose, a rough knowledge of the sample geometry is needed, in order to consider the right curvature of the object. For absolute distance measurements, a certain reference point must be known. Without this knowledge, the absolute distance perpendicular to the surface can onloy be measured with two-color RICM [179].

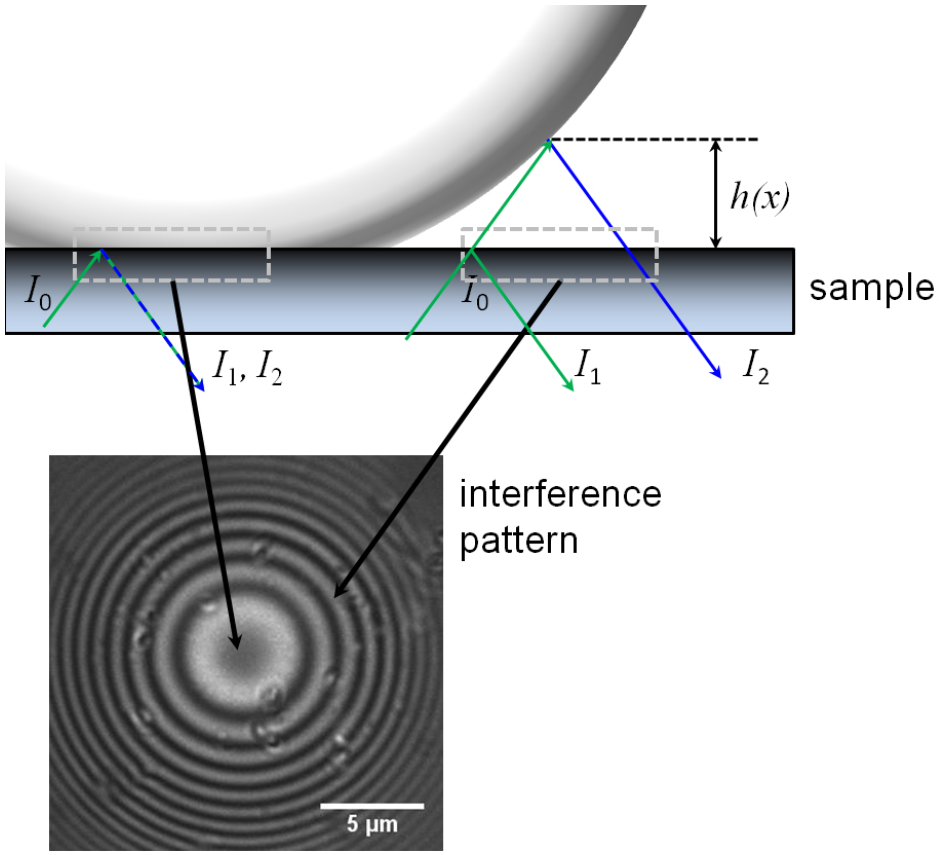

Figure 2.23: Principle of reflection interference contrast microscopy (RICM): I_0 incident light, I_1 reflected light from the substrate, I_2 reflected light from the sample and interference pattern (of a glass sphere) on the detector.

2.5 References

[1] Knoll. *Functional Polymer Films*. Vol. 1. Wiley-VCH. Weinheim, Germany, 2011.

[2] T. P. Russell. "Surface-responsive materials". In: *Science* 297.5583 (2002), pp. 964–967.

[3] A. Sidorenko et al. "Switching of polymer brushes". In: *Langmuir* 15.24 (1999), pp. 8349–8355.

[4] K. Glinel et al. "Responsive polyelectrolyte multilayers". In: *Colloids and Surfaces a-Physicochemical and Engineering Aspects* 303.1-2 (2007), pp. 3–13.

[5] M. A. C. Stuart et al. "Emerging applications of stimuli-responsive polymer materials". In: *Nature Materials* 9.2 (2010), pp. 101–113.

[6] C. D. H. Alarcon, S. Pennadam, and C. Alexander. "Stimuli responsive polymers for biomedical applications". In: *Chemical Society Reviews* 34.3 (2005), pp. 276–285.

[7] A. L. Black, J. M. Lenhardt, and S. L. Craig. "From molecular mechanochemistry to stress-responsive materials". In: *Journal of Materials Chemistry* 21.6 (2011), pp. 1655–1663.

[8] E. Cabane et al. "Stimuli-Responsive Polymers and Their Applications in Nanomedicine". In: *Biointerphases* 7.1-4 (2012), pp. 1–27.

[9] J. Bunsow, T. S. Kelby, and W. T. S. Huck. "Polymer Brushes: Routes toward Mechanosensitive Surfaces". In: *Accounts of Chemical Research* 43.3 (2010), pp. 466–474.

[10] A. Kumar, H. A. Biebuyck, and G. M. Whitesides. "Patterning Self-Assembled Monolayers - Applications in Materials Science". In: *Langmuir* 10.5 (1994), pp. 1498–1511.

[11] Y. Liu et al. "Controlled switchable surface". In: *Chemistry-a European Journal* 11.9 (2005), pp. 2622–2631.

[12] G. Pasparakis and M. Vamvakaki. "Multiresponsive polymers: nano-sized assemblies, stimuli-sensitive gels and smart surfaces". In: *Polymer Chemistry* 2.6 (2011), pp. 1234–1248.

[13] I. Tokarev, M. Motornov, and S. Minko. "Molecular-engineered stimuli-responsive thin polymer film: a platform for the development of integrated multifunctional intelligent materials". In: *Journal of Materials Chemistry* 19.38 (2009), pp. 6932–6948.

[14] F. Zhou and W. T. S. Huck. "Surface grafted polymer brushes as ideal building blocks for "smart" surfaces". In: *Physical Chemistry Chemical Physics* 8.33 (2006), pp. 3815–3823.

[15] Omar Azzaroni. "Polymer brushes here, there, and everywhere: Recent advances in their practical applications and emerging opportunities in multiple research fields". In: *Journal of Polymer Science Part a-Polymer Chemistry* 50.16 (2012), pp. 3225–3258.

[16] H. Dautzenberg. *Polyelectrolyts*. Hanser. Munich, Germany, 1994.

[17] H.S. Nalwa. *Handbook of Polyelectrolytes and Their Applications*. American Scientific Publishers. USA, 2002.

[18] M. Rubinstein and R. H. Collby. *Polymer Physics*. Vol. 1. Oxford University Press. NY, USA, 2003.

[19] G. Strobel. *The Physics of Polymers: Concepts for Understanding Their Structures and Behavior*. Springer. Heidelberg, Germany, 2007.

[20] A. V. Dobrynin and M. Rubinstein. "Theory of polyelectrolytes in solutions and at surfaces". In: *Progress in Polymer Science* 30.11 (2005), pp. 1049–1118.

[21] C. Wood et al. "From conditioning shampoo to nanomechanics and haptics of human hair". In: *Journal of cosmetic science* 62.2 (2011), pp. 259–64.

[22] M. Gueron and G. Weisbuch. "Poly-Electrolyte Theory .1. Counterion Accumulation, Site-Binding, and Their Insensitivity to Poly-Electrolyte Shape in Solutions Containing Finite Salt Concentrations". In: *Biopolymers* 19.2 (1980), pp. 353–382.

[23] P. Debye and E. Hueckel. In: *Physikalische Zeitschrift* (1923).

[24] H. J. Butt and M. Kappl. *Surface and Interfacial Forces*. Weinheim, Germany: Wiley-VCH, 2010.

[25] G. S. Manning. "Limiting Laws and Counterion Condensation in Polyelectrolyte Solutions .I. Colligative Properties". In: *Journal of Chemical Physics* 51.3 (1969), pp. 924–.

[26] G. S. Manning and B. H. Zimm. "Cluster Theory of Polyelectrolyte Solutions .I. Activity Coefficients of Mobile Ions". In: *Journal of Chemical Physics* 43.12 (1965), pp. 4250–.

[27] A. Deshkovski, S. Obukhov, and M. Rubinstein. "Counterion phase transitions in dilute polyelectrolyte solutions". In: *Physical Review Letters* 86.11 (2001), pp. 2341–2344.

[28] B. Y. Ha and D. Thirumalai. "Electrostatic Persistence Length of a Polyelectrolyte Chain". In: *Macromolecules* 28.2 (1995), pp. 577–581.

[29] T. Odijk. "Polyelectrolytes near the Rod Limit". In: *Journal of Polymer Science Part B-Polymer Physics* 15.3 (1977), pp. 477–483.

[30] T. Odijk and A. C. Houwaart. "Theory of Excluded-Volume Effect of a Polyelectrolyte in a 1-1 Electrolyte Solution". In: *Journal of Polymer Science Part B-Polymer Physics* 16.4 (1978), pp. 627–639.

[31] E. Raphael and J. F. Joanny. "Annealed and Quenched Polyelectrolytes". In: *Europhysics Letters* 13.7 (1990), pp. 623–628.

[32] J. T. G. Overbeek. "The Dissociation and Titration Constants of Polybasic Acids". In: *Bulletin Des Societes Chimiques Belges* 57.5-6 (1948), pp. 252–261.

[33] S. Block. *On surface forces and morphology of linear polyelectrolytes physisorbed onto oppositely charged surfaces*. Greifswald, Germany, 2010.

[34] G. J. Fleer. *Polymers at interfaes*. Springer. Berlin, Germany, 1993.

[35] G. J. Fleer, J. Scheutjens, and M. A. C. Stuart. "Theoretical Progress in Polymer Adsorption, Steric Stabilization and Flocculation". In: *Colloids and Surfaces* 31 (1988), pp. 1–29.

[36] M. A. C. Stuart. "Poly-Electrolyte Adsorption". In: *Journal De Physique* 49.6 (1988), pp. 1001–1008.

[37] J. M. H. M. Scheutjens and G. J. Fleer. "Statistical-Theory of the Adsorption of Interacting Chain Molecules .1. Partition-Function, Segment Density Distribution, and Adsorption-Isotherms". In: *Journal of Physical Chemistry* 83.12 (1979), pp. 1619–1635.

[38] J.M.H.M. Scheutjens and G. J. Fleer. "Statistical-Theory of the Adsorption of Interacting Chain Molecules .2. Train, Loop, and Tail Size Distribution". In: *Journal of Physical Chemistry* 84.2 (1980), pp. 178–190.

[39] H. G. M. Vandesteeg et al. "Polyelectrolyte Adsorption - a Subtle Balance of Forces". In: *Langmuir* 8.10 (1992), pp. 2538–2546.

[40] R. R. Netz and D. Andelman. "Neutral and charged polymers at interfaces". In: *Physics Reports-Review Section of Physics Letters* 380.1-2 (2003), pp. 1–95.

[41] R. R. Netz and J. F. Joanny. "Adsorption of semiflexible polyelectrolytes on charged planar surfaces: Charge compensation, charge reversal, and multilayer formation". In: *Macromolecules* 32.26 (1999), pp. 9013–9025.

[42] J. Kotz, S. Kosmella, and T. Beitz. "Self-assembled polyelectrolyte systems". In: *Progress in Polymer Science* 26.8 (2001), pp. 1199–1232.

[43] V. A. Kabanov and A. B. Zezin. "Soluble Interpolymeric Complexes as a New Class of Synthetic Poly-Electrolytes". In: *Pure and Applied Chemistry* 56.3 (1984), pp. 343–354.

[44] Dmitry V. Pergushov, Axel H. E. Mueller, and Felix H. Schacher. "Micellar interpolyelectrolyte complexes". In: *Chemical Society Reviews* 41.21 (2012), pp. 6888–6901.

[45] V. A. Kabanov. "Polyelectrolyte complexes in solution and in the condensed phase". In: *Uspekhi Khimii* 74.1 (2005), pp. 5–23.

[46] S. A. Sukhishvili, E. Kharlampieva, and V. Izumrudov. "Where polyelectrolyte multilayers and polyelectrolyte complexes meet". In: *Macromolecules* 39.26 (2006), pp. 8873–8881.

[47] F. H. Schacher, P. A. Rupar, and I. Manners. "Functional Block Copolymers: Nanostructured Materials with Emerging Applications". In: *Angewandte Chemie-International Edition* 51.32 (2012), pp. 7898–7921.

[48] C. A. Fustin, V. Abetz, and J. F. Gohy. "Triblock terpolymer micelles: A personal outlook". In: *European Physical Journal E* 16.3 (2005), pp. 291–302.

[49] G. Riess. "Micellization of block copolymers". In: *Progress in Polymer Science* 28.7 (2003), pp. 1107–1170.

[50] J. Ruhe et al. "Polyelectrolyte brushes". In: *Polyelectrolytes with Defined Molecular Architecture I.* Vol. 165. Advances in Polymer Science. Berlin, Germany: Springer-Verlag, 2004.

[51] A. Ulman. *An Introduction to Ultrathin Organic Films from Langmuir-Blodgett to Self Assembly.* Academic Press. San Diego, USA, 1991.

[52] J. C. Love et al. "Self-assembled monolayers of thiolates on metals as a form of nanotechnology". In: *Chemical Reviews* 105.4 (2005), pp. 1103–1169.

[53] F. Schreiber. "Structure and growth of self-assembling monolayers". In: *Progress in Surface Science* 65.5-8 (2000), pp. 151–256.

[54] A. Ulman. "Formation and structure of self-assembled monolayers". In: *Chemical Reviews* 96.4 (1996), pp. 1533–1554.

[55] G. M. Whitesides and B. Grzybowski. "Self-assembly at all scales". In: *Science* 295.5564 (2002), pp. 2418–2421.

[56] G. Decher. "Multilayer Thin Films". In: (2012).

[57] G. Decher. "Fuzzy nanoassemblies: Toward layered polymeric multicomposites". In: *Science* 277.5330 (1997), pp. 1232–1237.

[58] R. K. Iler. "Multilayers of Colloidal Particles". In: *Journal of Colloid and Interface Science* 21.6 (1966), pp. 569–.

[59] K. Ariga, J. P. Hill, and Q. Ji. "Layer-by-layer assembly as a versatile bottom-up nanofabrication technique for exploratory research and realistic application". In: *Physical Chemistry Chemical Physics* 9.19 (2007), pp. 2319–2340.

[60] P. T. Hammond. "Form and function in multilayer assembly: New applications at the nanoscale". In: *Advanced Materials* 16.15 (2004), pp. 1271–1293.

[61] Z. J. Sui, D. Salloum, and J. B. Schlenoff. "Effect of molecular weight on the construction of polyelectrolyte multilayers: Stripping versus sticking". In: *Langmuir* 19.6 (2003), pp. 2491–2495.

[62] S. T. Dubas and J. B. Schlenoff. "Swelling and smoothing of polyelectrolyte multilayers by salt". In: *Langmuir* 17.25 (2001), pp. 7725–7727.

[63] S. S. Shiratori and M. F. Rubner. "pH-dependent thickness behavior of sequentially adsorbed layers of weak polyelectrolytes". In: *Macromolecules* 33.11 (2000), pp. 4213–4219.

[64] S. T. Dubas and J. B. Schlenoff. "Factors controlling the growth of polyelectrolyte multilayers". In: *Macromolecules* 32.24 (1999), pp. 8153–8160.

[65] T. Boudou et al. "Multiple Functionalities of Polyelectrolyte Multilayer Films: New Biomedical Applications". In: *Advanced Materials* 22.4 (2010), pp. 441–467.

[66] L. Richert et al. "Layer by layer buildup of polysaccharide films: Physical chemistry and cellular adhesion aspects". In: *Langmuir* 20.2 (2004), pp. 448–458.

[67] L. L. del Mercato et al. "LbL multilayer capsules: recent progress and future outlook for their use in life sciences". In: *Nanoscale* 2.4 (2010), pp. 458–467.

[68] G. Sukhorukov, A. Fery, and H. Mohwald. "Intelligent micro- and nanocapsules". In: *Progress in Polymer Science* 30.8-9 (2005), pp. 885–897.

[69] L. Zhai et al. "Stable superhydrophobic coatings from polyelectrolyte multilayers". In: *Nano Letters* 4.7 (2004), pp. 1349–1353.

[70] S. Srivastava and N. A. Kotov. "Composite Layer-by-Layer (LBL) Assembly with Inorganic Nanoparticles and Nanowires". In: *Accounts of Chemical Research* 41.12 (2008), pp. 1831–1841.

[71] A. C. Fou et al. "Fabrication and properties of light-emitting diodes based on self-assembled multilayers of poly(phenylene vinylene)". In: *Journal of Applied Physics* 79.10 (1996), pp. 7501–7509.

[72] J. L. Lutkenhaus and P. T. Hammond. "Electrochemically enabled polyelectrolyte multilayer devices: from fuel cells to sensors". In: *Soft Matter* 3.7 (2007), pp. 804–816.

[73] J. Cho et al. "Nanoporous block copolymer micelle/micelle multilayer films with dual optical properties". In: *Journal of the American Chemical Society* 128.30 (2006), pp. 9935–9942.

[74] N. Ma et al. "Polymer micelles as building blocks for layer-by-layer assembly: An approach for incorporation and controlled release of water-insoluble dyes". In: *Chemistry of Materials* 17.20 (2005), pp. 5065–5069.

[75] B. D. Gates et al. "New approaches to nanofabrication: Molding, printing, and other techniques". In: *Chemical Reviews* 105.4 (2005), pp. 1171–1196.

[76] Y. N. Xia and G. M. Whitesides. "Soft lithography". In: *Angewandte Chemie-International Edition* 37.5 (1998), pp. 551–575.

[77] R Advincula et al. *Polymer brushes*. Wiley-VCH. Weinheim, Germany, 2004.

[78] S. T. Milner. "Polymer Brushes". In: *Science* 251.4996 (1991), pp. 905–914.

[79] W. J. Brittain and S. Minko. "A structural definition of polymer brushes". In: *Journal of Polymer Science Part a-Polymer Chemistry* 45.16 (2007), pp. 3505–3512.

[80] B. Zhao and W. J. Brittain. "Polymer brushes: surface-immobilized macromolecules". In: *Progress in Polymer Science* 25.5 (2000), pp. 677–710.

[81] X. Dai et al. “Direct Visualization of Reversible Switching of Micropatterned Polyelectrolyte Brushes on Gold Surfaces Using Laser Scanning Confocal Microscopy”. In: *Langmuir* 24.22 (2008), pp. 13182–13185.

[82] M. Ballauff. “Spherical polyelectrolyte brushes”. In: *Progress in Polymer Science* 32.10 (2007), pp. 1135–1151.

[83] M. Ballauff and O. Borisov. “Polyelectrolyte brushes”. In: *Current Opinion in Colloid and Interface Science* 11.6 (2006), pp. 316–323.

[84] R. Barbey et al. “Polymer Brushes via Surface-Initiated Controlled Radical Polymerization: Synthesis, Characterization, Properties, and Applications”. In: *Chemical Reviews* 109.11 (2009), pp. 5437–5527.

[85] L. Ionov et al. “Gradient mixed brushes: "Grafting to" approach”. In: *Macromolecules* 37.19 (2004), pp. 7421–7423.

[86] O. Azzaroni et al. “Switching the properties of polyelectrolyte brushes via "Hydrophobic collapse"”. In: *Macromolecules* 38.24 (2005), pp. 10192–10199.

[87] G. Reiter, P. Auroy, and L. Auvray. “Instabilities of thin polymer films on layers of chemically identical grafted molecules”. In: *Macromolecules* 29.6 (1996), pp. 2150–2157.

[88] F. Xia et al. “Dual-responsive surfaces that switch superhydrophilicity and superhydrophobicity”. In: *Advanced Materials* 18.4 (2006), pp. 432–+.

[89] J. Klein et al. “Reduction of Frictional Forces between Solid-Surfaces Bearing Polymer Brushes”. In: *Nature* 370.6491 (1994), pp. 634–636.

[90] U. Raviv et al. “Lubrication by charged polymers”. In: *Nature* 425.6954 (2003), pp. 163–165.

[91] P. Pincus. “Colloid Stabilization with Grafted Polyelectrolytes”. In: *Macromolecules* 24.10 (1991), pp. 2912–2919.

[92] L. Sun, G. L. Baker, and M. L. Bruening. “Polymer brush membranes for pervaporation of organic solvents from water”. In: *Macromolecules* 38.6 (2005), pp. 2307–2314.

[93] S. Moya et al. “Locking and unlocking of polyelectrolyte brushes: toward the fabrication of chemically controlled nanoactuators”. In: *Angewandte Chemie-International Edition* 44.29 (2005), pp. 4578–4581.

[94] S. Santer and J. Ruhe. “Motion of nano-objects on polymer brushes”. In: *Polymer* 45.25 (2004), pp. 8279–8297.

[95] Y. Mei et al. "High catalytic activity of platinum nanoparticles immobilized on spherical polyelectrolyte brushes". In: *Langmuir* 21.26 (2005), pp. 12229–12234.

[96] R. Iwata et al. "Control of nanobiointerfaces generated from well-defined biomimetic polymer brushes for protein and cell manipulations". In: *Biomacromolecules* 5.6 (2004), pp. 2308–2314.

[97] A. Wittemann and M. Ballauff. "Interaction of proteins with linear polyelectrolytes and spherical polyelectrolyte brushes in aqueous solution". In: *Physical Chemistry Chemical Physics* 8.45 (2006), pp. 5269–5275.

[98] W. Senaratne, L. Andruzzi, and C. K. Ober. "Self-assembled monolayers and polymer brushes in biotechnology: Current applications and future perspectives". In: *Biomacromolecules* 6.5 (2005), pp. 2427–2448.

[99] S. Edmondson, V. L. Osborne, and W. T. S. Huck. "Polymer brushes via surface-initiated polymerizations". In: *Chemical Society Reviews* 33.1 (2004), pp. 14–22.

[100] X. Y. Huang and M. J. Wirth. "Surface-initiated radical polymerization on porous silica". In: *Analytical Chemistry* 69.22 (1997), pp. 4577–4580.

[101] V. Coessens, T. Pintauer, and K. Matyjaszewski. "Functional polymers by atom transfer radical polymerization". In: *Progress in Polymer Science* 26.3 (2001), pp. 337–377.

[102] K. Matyjaszewski and J. H. Xia. "Atom transfer radical polymerization". In: *Chemical Reviews* 101.9 (2001), pp. 2921–2990.

[103] N. Cheng et al. "The effect of [Cu-I]/[Cu-II] ratio on the kinetics and conformation of polyelectrolyte brushes by atom transfer radical polymerization". In: *Macromolecular Rapid Communications* 27.19 (2006), pp. 1632–1636.

[104] X. Guo and M. Ballauff. "Spatial dimensions of colloidal polyelectrolyte brushes as determined by dynamic light scattering". In: *Langmuir* 16.23 (2000), pp. 8719–8726.

[105] P.G. de Gennes. *Scaling Concepts in Polymer Physics*. Vol. 1. Cornell University Press. NY, USA, 1979.

[106] R. Israels et al. "Charged Polymeric Brushes - Structure and Scaling Relations". In: *Macromolecules* 27.12 (1994), pp. 3249–3261.

[107] E. B. Zhulina, T. M. Birshtein, and O. V. Borisov. "Theory of Ionizable Polymer Brushes". In: *Macromolecules* 28.5 (1995), pp. 1491–1499.

[108] E. B. Zhulina and O. V. Borisov. "Structure and interaction of weakly charged polyelectrolyte brushes: Self-consistent field theory". In: *Journal of Chemical Physics* 107.15 (1997), pp. 5952–5967.

[109] E. B. Zhulina, J. K. Wolterink, and O. V. Borisov. "Screening effects in a polyelectrolyte brush: Self-consistent-field theory". In: *Macromolecules* 33.13 (2000), pp. 4945–4953.

[110] S. Alexander. "Adsorption of Chain Molecules with a Polar Head a-Scaling Description". In: *Journal De Physique* 38.8 (1977), pp. 983–987.

[111] P. G. de Gennes. "Conformations of Polymers Attached to an Interface". In: *Macromolecules* 13.5 (1980), pp. 1069–1075.

[112] O. V. Borisov and E. B. Zhulina. "Structure of weakly charged polyelectrolyte brushes: Monomer density profiles". In: *Journal De Physique Ii* 7.3 (1997), pp. 449–458.

[113] R. Israels, F. A. M. Leermakers, and G. J. Fleer. "On the Theory of Grafted Weak Polyacids". In: *Macromolecules* 27.11 (1994), pp. 3087–3093.

[114] M. Biesalski, D. Johannsmann, and J. Ruhe. "Synthesis and swelling behavior of a weak polyacid brush". In: *Journal of Chemical Physics* 117.10 (2002), pp. 4988–4994.

[115] P. M. Biesheuvel. "Ionizable polyelectrolyte brushes: brush height and electrosteric interaction". In: *Journal of Colloid and Interface Science* 275.1 (2004), pp. 97–106.

[116] E. B. Zhulina and O. V. Borisov. "Poisson-Boltzmann Theory of pH-Sensitive (Annealing) Polyelectrolyte Brush". In: *Langmuir : the ACS journal of surfaces and colloids* 27.17 (2012), pp. 10615–33.

[117] A. Kumar. *Molecular dynamics simulations of polyelectrolyte brushes*. Golm, Germany, 2006.

[118] W. Funke. "Problems and progress in organic coatings science and technology". In: *Progress in Organic Coatings* 31.1-2 (1997), pp. 5–9.

[119] L. T. Drzal and M. Madhukar. "Fiber Matrix Adhesion and Its Relationship to Composite Mechanical-Properties". In: *Journal of Materials Science* 28.3 (1993), pp. 569–610.

[120] S. Schmidt et al. "Adhesion and Mechanical Properties of PNIPAM Microgel Films and Their Potential Use as Switchable Cell Culture Substrates". In: *Advanced Functional Materials* 20.19 (2010), pp. 3235–3243.

[121] L. Zhang and T. J. Webster. "Nanotechnology and nanomaterials: Promises for improved tissue regeneration". In: *Nano Today* 4.1 (2009), pp. 66–80.

[122] C. Zhu et al. "Measuring receptor/ligand interaction at the single-bond level: Experimental and interpretative issues". In: *Annals of Biomedical Engineering* 30.3 (2002), pp. 305–314.

[123] C. Greiner, A. del Campo, and E. Arzt. "Adhesion of bioinspired micropatterned surfaces: Effects of pillar radius, aspect ratio, and preload". In: *Langmuir* 23.7 (2007), pp. 3495–3502.

[124] J. Erath. *Kolloidale-Kraft-Spektroskopie mit weichen Partikeln*. University Bayreuth, Germany, 2009.

[125] H. J. Butt, K. Graf, and M Kappl. *Physics and Chemistry of Interfaces*. Weinheim, Germany: Wiley-VCH, 2004.

[126] Israelachvili J.N. *Intermolecular and Surface Forces*. 2nd ed. Amsterdam, The Netherlands: Academic Press, 2007.

[127] D. Maugis. *Contact, Adhesion and Rupture of Elastic Solids*. Heidelberg, Germany: Springer, 2000.

[128] H. J. Butt, B. Cappella, and M. Kappl. "Force measurements with the atomic force microscope: Technique, interpretation and applications". In: *Surface Science Reports* 59.1-6 (2005), pp. 1–152.

[129] Derjaguin. In: *Kolloid Z* (1934).

[130] S. H. Behrens and M. Borkovec. "Electrostatic interaction of colloidal surfaces with variable charge". In: *Journal of Physical Chemistry B* 103.15 (1999), pp. 2918–2928.

[131] S. H. Behrens and M. Borkovec. "Exact Poisson-Boltzmann solution for the interaction of dissimilar charge-regulating surfaces". In: *Physical Review E* 60.6 (1999), pp. 7040–7048.

[132] R. Pericet-Camara et al. "Interaction between charged surfaces on the Poisson-Boltzmann level: The constant regulation approximation". In: *Journal of Physical Chemistry B* 108.50 (2004), pp. 19467–19475.

[133] F. M. Orr, L. E. Scriven, and A. P. Rivas. "Pendular Rings between Solids - Meniscus Properties and Capillary Force". In: *Journal of Fluid Mechanics* 67.4 (1975), pp. 723–742.

[134] H. J. Butt et al. "Steric forces measured with the atomic force microscope at various temperatures". In: *Langmuir* 15.7 (1999), pp. 2559–2565.

[135] S. Block and C. A. Helm. "Measurement of long-ranged steric forces between polyelectrolyte layers physisorbed from 1 M NaCl". In: *Physical Review E* 76.3 (2007).

[136] S. Block and C. A. Helm. "Conformation of poly(styrene sulfonate) layers physisorbed from high salt solution studied by force measurements on two different length scales". In: *Journal of Physical Chemistry B* 112.31 (2008), pp. 9318–9327.

[137] P. G. de Gennes. "Polymers at an Interface - a Simplified View". In: *Advances in Colloid and Interface Science* 27.3-4 (1987), pp. 189–209.

[138] J. U. Kim and M. W. Matsen. "Compression of Polymer Brushes: Quantitative Comparison of Self-Consistent Field Theory with Experiment". In: *Macromolecules* 42.9 (2009), pp. 3430–3432.

[139] M. Balastre et al. "A study of polyelectrolyte brushes formed from adsorption of amphiphilic diblock copolymers using the surface forces apparatus". In: *Macromolecules* 35.25 (2002), pp. 9480–9486.

[140] S. T. Milner, T. A. Witten, and M. E. Cates. "A Parabolic Density Profile for Grafted Polymers". In: *Europhysics Letters* 5.5 (1988), pp. 413–418.

[141] S. T. Milner, T. A. Witten, and M. E. Cates. "Theory of the Grafted Polymer Brush". In: *Macromolecules* 21.8 (1988), pp. 2610–2619.

[142] E. B. Zhulina, O. V. Borisov, and T. M. Birshtein. "Static forces in confined polyelectrolyte layers". In: *Macromolecules* 33.9 (2000), pp. 3488–3491.

[143] H. Hertz. "Ueber die Beruehrung fester elastischer Koerper". In: *Journal fuer die reine und angewandte Mathematik* 92 (1881).

[144] K. L. Johnson, K. Kendall, and A. D. Roberts. "Surface Energy and Contact of Elastic Solids". In: *Proceedings of the Royal Society of London Series a-Mathematical and Physical Sciences* 324.1558 (1971), pp. 301–.

[145] B. V. Derjaguin, V. M. Muller, and Y. P. Toporov. "Effect of Contact Deformations on Adhesion of Particles". In: *Journal of Colloid and Interface Science* 53.2 (1975), pp. 314–326.

[146] D. Tabor. "Surface Forces and Surface Interactions". In: *Journal of Colloid and Interface Science* 58.1 (1977), pp. 2–13.

[147] D. Maugis. "Adhesion of Spheres - the JKR-DMT Transition Using a Dugdale Model". In: *Journal of Colloid and Interface Science* 150.1 (1992), pp. 243–269.

[148] K. L. Johnson and J. A. Greenwood. "An adhesion map for the contact of elastic spheres". In: *Journal of Colloid and Interface Science* 192.2 (1997), pp. 326–333.

[149] W. C. Oliver and G. M. Pharr. "Measurement of hardness and elastic modulus by instrumented indentation: Advances in understanding and refinements to methodology". In: *Journal of Materials Research* 19.1 (2004), pp. 3–20.

[150] Y. I. Rabinovich et al. "Adhesion between nanoscale rough surfaces - I. Role of asperity geometry". In: *Journal of Colloid and Interface Science* 232.1 (2000), pp. 10–16.

[151] Y. I. Rabinovich et al. "Adhesion between nanoscale rough surfaces - II. Measurement and comparison with theory". In: *Journal of Colloid and Interface Science* 232.1 (2000), pp. 17–24.

[152] B. Cappella and G. Dietler. "Force-distance curves by atomic force microscopy". In: *Surface Science Reports* 34.1-3 (1999), pp. 1–+.

[153] P. M. Claesson et al. "Techniques for measuring surface forces". In: *Advances in Colloid and Interface Science* 67 (1996), pp. 119–183.

[154] J. N. Israelachvili, D. J. Mitchell, and B. W. Ninham. "Theory of Self-Assembly of Hydrocarbon Amphiphiles into Micelles and Bilayers". In: *Journal of the Chemical Society-Faraday Transactions II* 72 (1976), pp. 1525–1568.

[155] M. K. Chaudhury and G. M. Whitesides. "Direct Measurement of Interfacial Interactions between Semispherical Lenses and Flat Sheets of Poly(Dimethylsiloxane) and Their Chemical Derivatives". In: *Langmuir* 7.5 (1991), pp. 1013–1025.

[156] K. C. Neuman and A. Nagy. "Single-molecule force spectroscopy: optical tweezers, magnetic tweezers and atomic force microscopy". In: *Nature Methods* 5.6 (2008), pp. 491–505.

[157] G. Binnig, C. F. Quate, and C. Gerber. "Atomic Force Microscope". In: *Physical Review Letters* 56.9 (1986), pp. 930–933.

[158] V. V. Tsukruk and S. Singamaneni. *Scanning Probe Microscopy of Soft Matter*. Weinheim, Germany: Wiley-VCH, 2012.

[159] R. Berger et al. "Electrical Modes in Scanning Probe Microscopy". In: *Macromolecular Rapid Communications* 30.14 (2009), pp. 1167–1178.

[160] R. Garcia and R. Perez. "Dynamic atomic force microscopy methods". In: *Surface Science Reports* 47.6-8 (2002), pp. 197–301.

[161] C.-W. Yang et al. "Imaging of soft matter with tapping-mode atomic force microscopy and non-contact-mode atomic force microscopy". In: *Nanotechnology* 18.8 (2007).

[162] B. Bhushan. "Nanotribology, nanomechanics and nanomaterials characterization". In: *Philosophical Transactions of the Royal Society a-Mathematical Physical and Engineering Sciences* 366.1869 (2008), pp. 1351–1381.

[163] H. J. Butt. "Measuring Electrostatic, Vanderwaals, and Hydration Forces in Electrolyte-Solutions with an Atomic Force Microscope". In: *Biophysical Journal* 60.6 (1991), pp. 1438–1444.

[164] W. A. Ducker, T. J. Senden, and R. M. Pashley. "Direct Measurement of Colloidal Forces Using an Atomic Force Microscope". In: *Nature* 353.6341 (1991), pp. 239–241.

[165] M. Kappl and H. J. Butt. "The colloidal probe technique and its application to adhesion force measurements". In: *Particle and Particle Systems Characterization* 19.3 (2002), pp. 129–143.

[166] V. Kuznetsov and G. Papastavrou. "Note: Mechanically and chemically stable colloidal probes from silica particles for atomic force microscopy". In: *Review of Scientific Instruments* 83.11 (2012).

[167] V. Bosio. *Interactions of multilayer coated surfaces studied by collodial probe atomic force microscopy*. Potsdam, Germany, 2003.

[168] J. L. Hutter and J. Bechhoefer. "Calibration of Atomic-Force Microscope Tips". In: *Review of Scientific Instruments* 64.7 (1993), pp. 1868–1873.

[169] J. E. Sader, J. W. M. Chon, and P. Mulvaney. "Calibration of rectangular atomic force microscope cantilevers". In: *Review of Scientific Instruments* 70.10 (1999), pp. 3967–3969.

[170] J. E. Sader et al. "Method for the Calibration of Atomic-Force Microscope Cantilevers". In: *Review of Scientific Instruments* 66.7 (1995), pp. 3789–3798.

[171] J. P. Cleveland et al. "A Nondestructive Method for Determining the Spring Constant of Cantilevers for Scanning Force Microscopy". In: *Review of Scientific Instruments* 64.2 (1993), pp. 403–405.

[172] H. Gross. *Handbook of Optical Systems*. Vol. 1-4. Wiley-VCH. Weinheim, Germany, 2008.

[173] F. Zernike. "How I Discovered Phase Contrast". In: *Science* 121.3141 (1955), pp. 345–349.

[174] J. R. Lakowicz. *Principles of Fluorescence Spectroscopy*. Vol. 3. Berlin, Germany: Springer, 2006.

[175] N. S. Claxton, T. S. Fellers, and Davidson M. W. *Laser scanning confocal microscopy*. 13.04.2013. URL: `http://trans.ucc.ie/website2012/en/anatomy/research/bsic/confocalimagingsystems/fv1000/Laser-Scanning-Confocal-Microscopy-Introduction.pdf`.

[176] D. Gingell and I. Todd. "Interference Reflection Microscopy - Quantitative Theory for Image Interpretation and Its Application to Cell-Substratum Separation Measurement". In: *Biophysical Journal* 26.3 (1979), pp. 507–526.

[177] J. Ploem. "Reflection contrast microscopy as a tool for investigation of the attachment of living cells to a glass surface". In: *Mononuclear Phagocytes in Immunity, Infection, and Pathology, Blackwell scientific publications.* (1975).

[178] J. Radler and E. Sackmann. "Imaging Optical Thicknesses and Separation Distances of Phospholipid-Vesicles at Solid-Surfaces". In: *Journal De Physique II* 3.5 (1993), pp. 727–748.

[179] J. Schilling et al. "Absolute interfacial distance measurements by dual-wavelength reflection interference contrast microscopy". In: *Physical Review E* 69.2 (2004).

[180] G. Wiegand, K. R. Neumaier, and E. Sackmann. "Microinterferometry: three-dimensional reconstruction of surface microtopography for thin-film and wetting studies by reflection interference contrast microscopy (RICM)". In: *Applied Optics* 37.29 (1998), pp. 6892–6905.

3

Characterization of adhesion phenomena and contact of surfaces by soft colloidal probe AFM

Erath, J., S. Schmidt, and A. Fery, Characterization of adhesion phenomena and contact of surfaces by soft colloidal probe AFM. Soft Matter, 2010. 6(7): p. 1432-1437.

Abstract

We present a method based on colloidal probe atomic force microscopy (AFM) to measure adhesion energies and to study other contact phenomena of surfaces. The method employs an elastomeric colloidal probe, rendering the contact area between probe and sample much larger as compared to standard atomic force microscopy techniques. The technique allows us to determine the contact area via microinterferometry and measure the applied forces at the same time. The adhesion properties can then be accessed by using the Johnson-Kendall-Roberts (JKR) approach, i.e. measuring (a) the contact area as a function of applied load, and (b) the elastic parameters and the thermodynamic work of adhesion. We test this method in ambient conditions as well as in aqueous media on well-known surface chemistries, and can clearly characterize the contributions of capillary in air, hydration forces and hydrophobic interactions in water. This novel method provides a means to study the contact behavior of soft colloids and enhanced sensitivity for adhesion measurements.

3.1 Introduction

Adhesion and contact phenomena are important in many branches of nature and technology. Two centuries of research have proven their significance in fields such as nano(bio)technology [1, 2, 3] and biophysics [4, 5]. For example, adhesion forces determine cell differentiation [6] and allow lizards to climb sheer walls [7, 8]. Adhesion technology is vital in coatings, composite materials [9, 10] or adhesives [11]. There are still many open questions on adhesion and contact phenomena of soft matter systems. Current research focuses on the behavior of (bio)polymers in water [12, 13, 14], biosystems that make use of various adhesion strategies on multiple length scales [4] or dynamic phenomena like rearrangement of polymers inside the contact area [15, 16] or switchable polymer brushes that change their adhesion properties by changing their environmental conditions [17]. To tackle such challenges several methods suitable for different length scales were developed [18, 19, 20]. With regard to the size of contact areas that are accessible, existing methods can be grouped into macro- and microscalecontact methods. Therefore, developments in adhesion measurement methods allowed the study of macro- and microscale-contact phenomena: macro-scale contacts are characterized using Peel and torsion tests [20, 21, 22] and wetting methods like contact-angle measurements [23, 24]. For ultra-thin films, the surface force apparatus (SFA) [25, 26, 27] provides an unparalleled sensitivity and vertical resolution on the

nanometre-scale for macro-scale contacts. The so-called JKR apparatus takes advantage of the fact that the contact area for large elastomeric lenses can be modeled using the Johnson-Kendall-Roberts theory [28]. Here, adhesion energies are derived using the dependence of contact area on the applied load. This method has been successfully applied through the last years, for example as described in Ref. [20] and [29, 30, 31, 32].

The advantage of macro-scale methods is the well-defined contact area. However, these methods are limited to smooth and chemically homogenous samples over a few hundred μm^2. On the micro- and nanoscale the resolution of an atomic force microscope (AFM) [33] is required in order to study surface interactions. [18] Here, surface interactions are measured by force-distance measurements, [34] where a sharp AFM tip (typical radius of curvature in the range of $5 - 20\,nm$) is brought into contact with the sample. In this mode usually the pull-off force of the AFM probe from the sample surface is used as a measure of the surface-probe interactions. While this technique allows access to extremely small contact areas, the contact area is rather illdefined and cannot be independently determined. The reason is that the shape of AFM tips cannot be accurately controlled in the manufacturing process or even during measurement and therefore, AFM tips do not satisfy the demand for a well-defined contact geometry. A major step towards solving this problem was the introduction of the colloidal probe-AFM technique [35] by Ducker et al. [36] and Butt [37] in the 1990s. Colloidal particles of several micrometres in size are attached to AFM cantilevers. Typically silica spheres or plastic beads with a diameter in the range of $1 - 50\,mm$ and with surface roughnesses of only a few nanometres are used [18, 35]. While the probe geometry is well defined as compared to standard AFM tips, the contact radii with hard substrates are still in the order of $100\,nm$ and thus hard to determine in situ. Because of that major drawback, one still has to rely on assumptions rather than direct measurement of the contact area which is problematic for determining the work of adhesion. In the last years the colloidal probe technique was extended to measure interaction forces or to describe the contact behavior between other kinds of probes, for example segments of hairs [38] or soft probes like droplets [39, 40, 41, 42] or bubbles [43].

In this paper we describe a novel technique combining the advantages of the JKR method with the colloidal probe AFM approach. We modify the colloidal probe technique to obtain a larger contact area between probe and sample by using soft colloidal particles, made of cross-linked polydimethylsiloxane (PDMS). The elastic properties, the size of the probe and thus the size of the contact area can be controlled by varying the preparation methodology of the soft probes. Under suitable conditions the contact

areas are sufficiently large to allow in situ measurement using microinterferometry [44, 45]. Consequently, the adhesion properties of the system can be accessed by using the JKR approach.

3.2 Experimental

Materials and methods

The instrumental setup relies on a combination of interference microscopy and AFM as sketched in Figure 3.1 and the use of novel probe particles. In the following, we summarize the probe preparation and mounting procedure, cantilever calibration, as well as technical details of the setup.

Fabrication and characterization of soft colloidal probes (SCPs)

The soft probes were prepared via cross-linking droplets of the precursor polymer in solution. PDMS (Sylgard 184 kit) was purchased from Dow Corning, USA. First the prepolymer was mixed with the curing agent using a 10 : 3 ratio. Then, a Milli-Q water dispersion containing 5 wt% PDMS precursor and 0.1 wt% sodium dodecyl sulfate (CAS number 151-21-3, Sigma-Aldrich, Germany) was prepared. After curing for three days at room temperature, the cross-linked PDMS droplets were extracted by freeze-drying. The resulting particles were characterized with an inverted optical microscope (Axiovert 200, Zeiss, Germany) to determine particle sizes. Using AFM force-distance measurements (Nanowizard I, JPK Instruments AG, Germany) the Young's modulus was determined as well. The mean diameter of the particles was in a range of 10 to 30 μm and the corresponding Young's modulus in the order of 1 MPa.

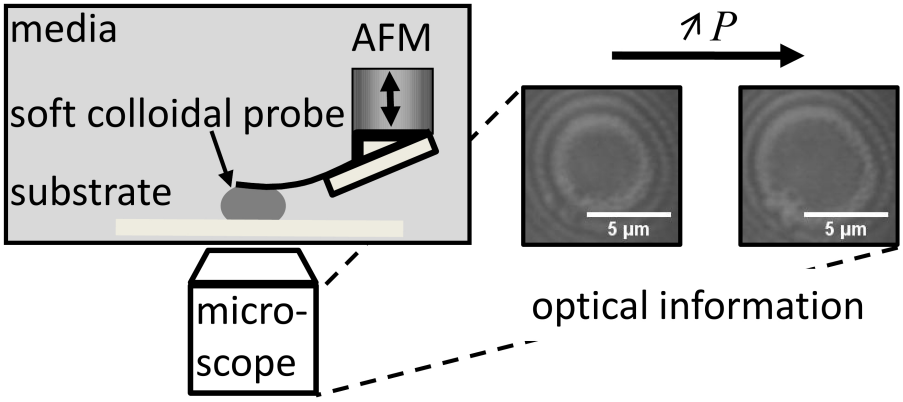

Figure 3.1: Schematic of the experimental setup: Combination of AFM and optics.

Mounting the probes and calibration

The colloidal particles were attached with epoxy resin (UHU schnellfest, Germany) on pre-calibrated AFM cantilevers ($7 - 28\,\mathrm{Nm}^1$, tipples NSC 12, Micromash, Estonia) using a micromanipulator (MP-285, Shutter Instrument, USA). The force constant was detected with the thermal noise method, introduced by Hutter and Bechhoefer [46]. A typical PDMS particle attached to a cantilever is shown in Figure 3.2. Deliberately, we established a large contact area between cantilever and particle, such that during measurement, the particle deformation took place mainly at the substrate-probe interface (see Figure 3.3A). After attachment, the SCP was washed in Milli-Q water and dried by a stream of nitrogen. Afterwards, the SCP was treated for 40 s in 1 mbar air plasma at 0.1 kW intensity (PDC-32 G plasma cleaner, Harrick, USA) in order to remove surface impurities and to provide a well-defined silica-like layer on the SCP surface. Under those conditions the thickness of the oxide layer is on the nanoscale [47]. Thus, the elastic properties of the probe are not significantly affected by this process.

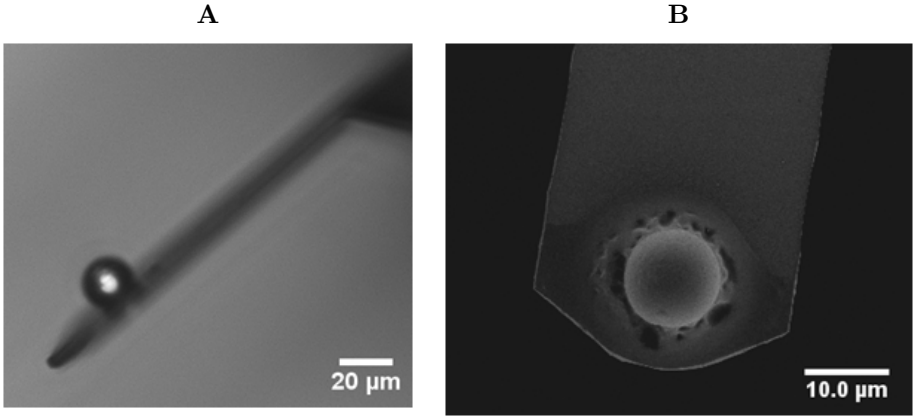

Figure 3.2: Attached PDMS particle on cantilever: 3.2A light microscopy image and 3.2B REM image.

Force spectroscopy

A commercial AFM (Nanowizard I, JPK Instruments AG, Germany) was used for all AFM measurements. SCPs were mounted into the AFM setup and the optical lever sensitivity was detected (see Results and discussion section: Boundary conditions, calibration and modeling of the SCP). The maximum applied force was between 1600 nN and 2500 nN. For the JKR approach, the load was changed stepwise in intervals of

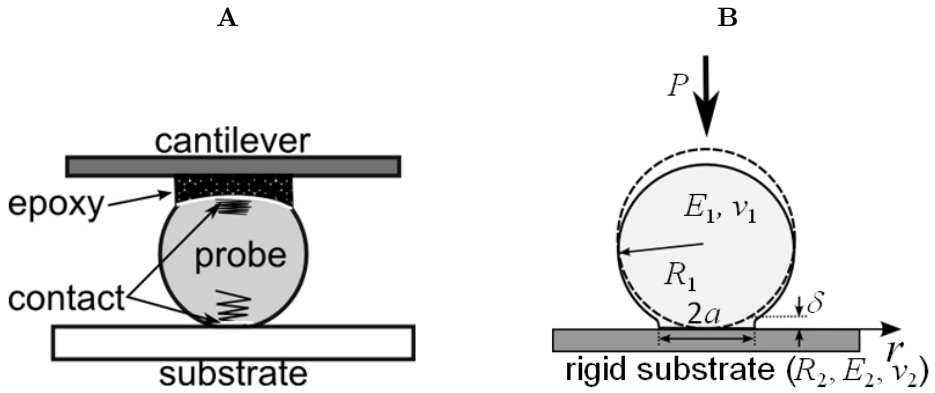

Figure 3.3: 3.3A Schematic of the contact behavior of the systems, probe-substrate and probe-cantilever; 3.3B sketch illustrating the contact parameters: the dotted line represents the undeformed probe, the solid line represents the deformed probe.

around 200 nN. The presented measurements show the mean value of four different detection positions of the probe on the substrate. The force-distance curves were recorded using the following parameters: the speed of the piezo actuator was set to $8\,\mu\mathrm{ms}^{-1}$. The force-distance curves were measured on different spots using the force-mapping mode of the AFM. Measurements were undertaken on at least 64 spots on a $100\,\mu\mathrm{m}^2$ grid on the substrate.

Reflection interference contrast microscopy

We used reflection interference contrast microscopy [48, 49] (RICM) to evaluate the contact area of the SCPs with a hard substrate (functionalized glass surface) *in situ*. During RICM, the sample was illuminated with monochromatic light in reflection geometry. Light was reflected by the substrate and the SCP interface. Due to phase shift and the path length difference between the reflected beams an interference pattern similar to Newton rings can be observed. This interference pattern provides information about the local distance between the SCP and the substrate, as well as the contact area. To enhance the interference pattern we used the antiflex technique introduced by Ploem [50]. For illumination we used a Hg-vapor lamp with two different monochromators (481 nm and 546 nm). A Zeiss Antiflex 63 X NO 1.25 oil-immersion objective, additional polarizers to avoid internal reflections and a Zeiss AxiocamHRm camera were used to image the RICM patterns. Details of the calibration of the RICM setup and the evaluation process of the contact area are summarized in Ch. 3.A and further

details of the setup are reported in Ref.[44, 45, 51] and [52].

Test surface preparation

To test the method, we studied samples with known surface chemistry. Here, symmetrically functionalized surfaces (SCP-substrate), i.e. hydrophilic-hydrophilic and hydrophobic-hydrophobic systems, were studied. The surfaces were modified via silanisation agents by gas phase deposition. Hydrophilic surfaces were prepared using [hydroxy(polyethyleneoxy)propyl]triethoxysilane (8-12EO), 50% ethanol (ABCR, Germany); hydrophobic surfaces were prepared using (heptadecafluoro-1,1,2,2-tetrahydrodecyl) dimethylchlorosilane (ABCR, Germany).

3.3 Results and Discussion

Boundary conditions, calibration and modeling of the SCP

The deformation of the SCP can only be observed at the side of the probe facing the substrate. Therefore, the main deformation of the soft probe should be located in the contact regime of probe and surface. This can be ensured by rendering the contact area of particle and cantilever much larger than the contact area of probe and surface (see Figure 3.3A). Hence we used SCPs where the contact between colloidal particle and cantilever was adequate (large enough) after the attachment. In order to perform AFM force-distance measurements the spring constant of the cantilever as well as its inverted optical lever sensitivity (InvOLS) are required. The InvOLS is the proportionality constant between photodiode signal and the cantilever deflection. Measuring both parameters allows calculation of the InvOLS. In the case of a SCP-modified cantilever this leads to some special challenges: Usually, the cantilever deflection is determined by pressing the cantilever on a hard, non-deformable substrate. In this case the piezo displacement is identical to the cantilever deflection and the InvOLS can be directly read from force-distance curves recorded on hard substrates. This is not possible with an SCP attached to the cantilever. Therefore, we developed two alternative approaches to determine InvOLS: for measurements in air, we used a noncontact approach to determine InvOLS [53]. We use cantilevers for which the spring constant has been determined ex situ and carry out a spring constant determination using the thermal noise method in situ. As this method requires the InvOLS as an input parameter, it can be used to derive it by adjusting the InvOLS until it matches the known spring constant (see Ch. 3.A). In liquid the thermal noise method cannot be used due to

high damping [18]. In this case, we detected the optical lever sensitivity by analysis of the slope of a force-distance curve in contact region, while pressing the apex of the cantilever against a sharp edge.

In order to derive adhesion energies the system has to be modelled using the proper contact-mechanic theory [54]. The first analytical description of contact between two isotropic, homogeneous, linear elastic bodies, but without adhesion contribution, was given by Hertz. [55] Regarding the adhesion contribution there are several theories which apply for certain limits of contact behavior. The respective limiting cases are described by the elastic and adhesive properties of the system [54]. Contact parameters like contact radius, deformation, pressure distribution, etc. are functions of load, elastic parameters of the system and the adhesion interaction. The two most common theories were developed by Johnson, Kendall and Roberts [28] (JKR theory) and Derjaguin, Muller and Toporov [56] (DMT theory). Tabor [57] showed that it is possible to separate (to quantify) the different limits of contact behavior with a parameter μ_T (respectively Maugis [58] $\lambda \propto \mu_T$) by comparing the elastic deformation caused by the surface interactions with the range of surface forces:

$$\mu_T = \left(\frac{16 R w^2}{9 K^2 z_0^3} \right)^{1/3} \tag{3.1}$$

where R is the effective radius of curvature, K is the effective elastic modulus of the system, w is the thermodynamic work of adhesion and z_0 is the equilibrium separation of the surfaces (interatomic equilibrium distance for solid-solid interactions in the Lennard-Jones potential, typically on the range of 0.3 to 0.5 nm). R and K are given by:

$$\frac{1}{R} = \frac{1}{R_1} + \frac{1}{R_2} \text{ and } \frac{1}{K} = \frac{3}{4} \left(\frac{1-\nu_1^2}{E_1} + \frac{1-\nu_2^2}{E_2} \right) \tag{3.2}$$

here R_1 and R_2 are the radii of curvature of the interacting surfaces, E_1 and E_2 are their Young's moduli, and ν_1 and ν_2 their Poisson ratios (Figure 3.3B. In the case of soft solids, large radius of curvature and large adhesion energy ($\mu_T > 5$), the JKR theory is valid. For stiff solids, small radius of curvature and weak energy of adhesion ($\mu_T < 5$) the DMT theory is valid [54].

To analyze our data we have to decide first of all which theory is suitable to describe our system. We are interested in flat, hard surfaces interacting with the soft probes. For an elastomeric sphere (R_1, E_1, $\nu_1 = 0.5$) touching such a surface ($R_2 \to \infty$, $E2 >> E1$), the effective radius of curvature R reduces to R_1 and the effective modulus of the system K equals $16/9E_1$ (see Eq. 3.2). With a probe radius in the range of $R_1 = 10\,\mu$m, a

Young's modulus on the order of $E_1 = 1\,\mathrm{MPa}$ and a typical thermodynamic work of adhesion in the range of $w = 10\,\mathrm{mJm^{-2}}$ the Tabor parameter (Eq. 3.1) lies in the range of $\mu_T > 50$. Therefore, we are in the limit of the JKR theory. Following the JKR theory the contact radius between two spheres pressed together by a load P is given by:

$$a^3 = \frac{R}{K}\left(P + 3\pi Rw + \sqrt{6\pi RwP + (3\pi Rw)^2}\right) \tag{3.3}$$

Adhesion measurements

JKR describe the contact area as a function of load P, elastic properties K, and the adhesion energy w: $a = f(P, K, w)$, see Eq. 3.3. In order to obtain the adhesion energy we press the SCP against the substrate of choice, which can be done with subnanonewton precision using the AFM feedback loop. Simultaneously, we record the adhesion area by microinterferometric imaging. The data are collected at discrete load-force intervals of $\Delta P > 100\,\mathrm{nN}$. Figure 3.4 shows a typical experiment of a hydrophilic functionalized SCP against a hydrophilic hard substrate in water. The JKR fit, as shown in Figure 3.4B, was computed using Eq. 3.3, yielding the adhesion energy and the Young's modulus as fit parameters. To crosscheck the Young's modulus we detected force-distance curves of SCPs on a hard substrate. The force-distance curves were transformed into force-deformation curves of the soft probe by subtracting the effect of the cantilever deflection. Then we fitted the contact region of the force deformation curves with the Hertz model [55]. Both moduli are in the same range (variation $< 25\%$). This is in agreement with findings reported in literature, e.g. Ref. [59] To test the method further, we investigated surfaces with known surface chemistry. Adhesion interaction of symmetrically functionalized surfaces, hydrophilic probe-hydrophilic substrate and hydrophobic probe-hydrophobic substrate, was investigated and compared to literature results.

Hydrophilic interactions

For the hydrophilic probe and the hydrophilic substrate in water we expect relatively small adhesion forces due to hydrophilic interactions [60]. The JKR approach leads to values of $w_{water} = 1.8 \pm 0.3\,\mathrm{mJm^{-2}}$ (Figure 3.5A) using a particle with a radius of $R = 10.9\,\mu\mathrm{m}$ contact with the hydrophilic surface. The Young's modulus of the particle detected by the JKR fit was $E = 0.7 \pm 0.1\,\mathrm{MPa}$. The value of $1.8\,\mathrm{mJm^{-2}}$ is at the detection limit of adhesion energies for the SCP method at this stage, but in a reasonable range considering that the hydrophilic surface might be slightly contaminated. Values

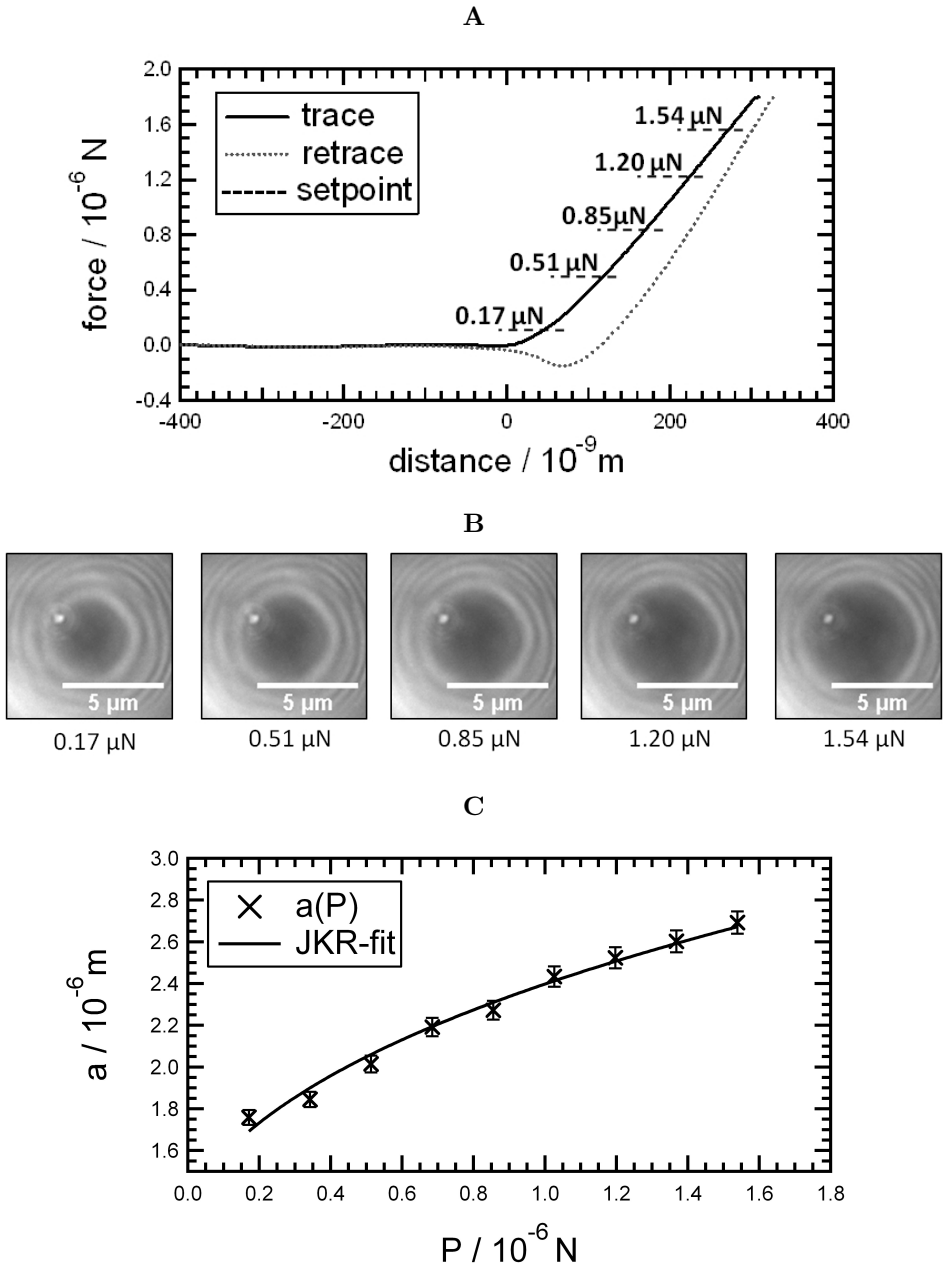

Figure 3.4: Analysis of the thermodynamic work of adhesion w by extraction of the contact radius a for varying loads P. 3.4A Force-distance curve of a hydrophilic soft colloidal probe against a hydrophilic surface (solid line represents approach cycle, dotted line represents the retraction cycle, and dashed lines show readings of the contact area as shown in 3.4B. 3.4B RICM images of the SCP allowed determination of the contact radius. 3.4C The plot of a against P follows the JKR predictions. The thermodynamic work w is extracted from the JKR fits (cross-makers, X, denote experimental data, black line denotes the JKR fit).

for the work of adhesion of hydrophilic surfaces with OH end groups in water reported in the literature, e.g. Ref. [61] and [62] lie in the same range ($\approx 1.5\,\mathrm{mJm^{-2}}$).

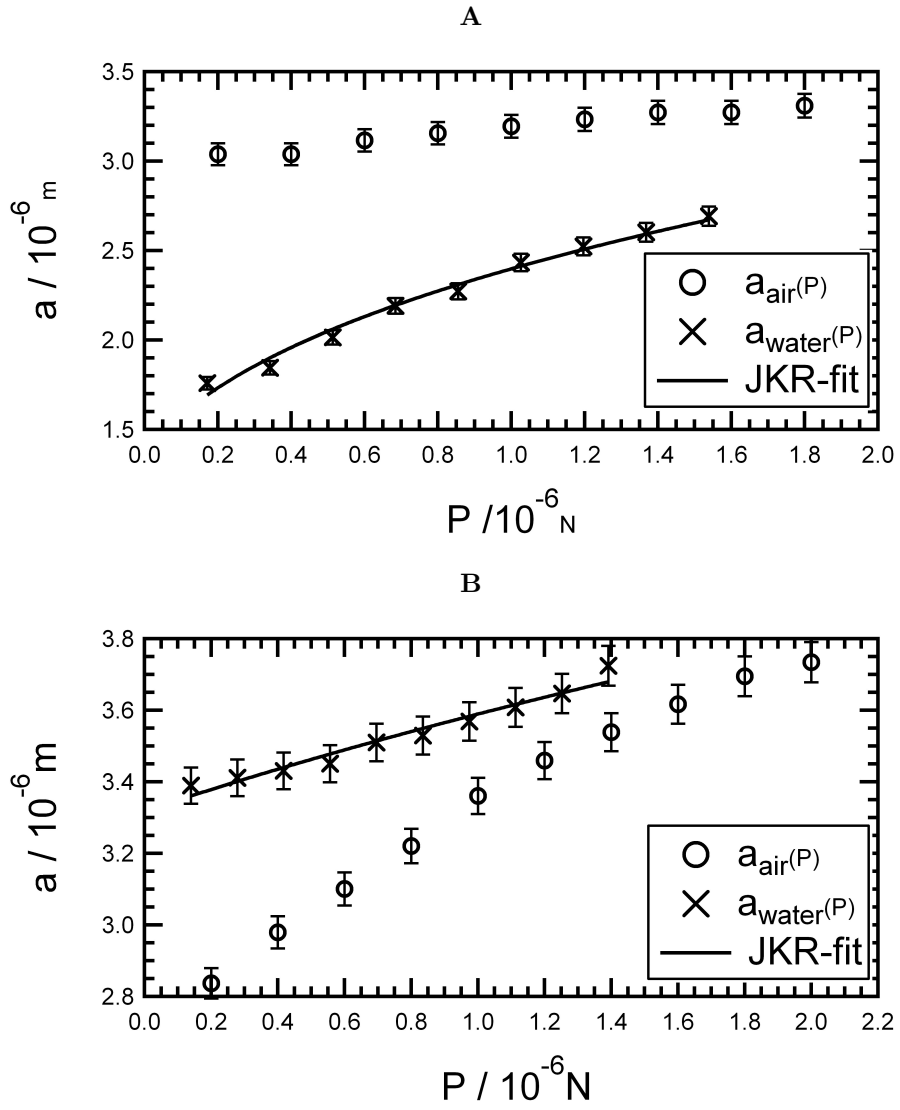

Figure 3.5: Contact radius as a function of applied load: 3.5A hydrophilic probe-hydrophilic substrate and 3.5B hydrophobic probe-hydrophobic substrate.

Hydrophobic interactions

Here much larger attractive hydrophobic interaction forces to the hydrophilic system can be expected [60]. The evaluation of the contact radii as functions of load with the JKR approach resulted in large adhesion interactions, $w_{\mathrm{water}} = 32 \pm 4\,\mathrm{mJm^{-2}}$ (Figure 3.5B). The Young's modulus of the particle with a radius of $R = 10.5\,\mu\mathrm{m}$ was

$E = 1.2 \pm 0.1\,\mathrm{MPa}$. The values for w_{water} of fluorocarbon reported in literature, e.g. Ref. [63] and [64], are higher but lie in the same range ($w_{\mathrm{water,CF}} \approx 50\,\mathrm{mJm^{-}2}$). The deviation could be explained by surface roughness of the hard substrate [65, 66, 67, 68] (the roughness of the soft probe is minimized by minimization of the energy during the preparation process). Furthermore, contact-angle measurements showed that the silanisation by gas phase deposition was not perfect (measured contact angle: $\approx 100°$ (Ref. [63]: $\approx 110°$)).

Influence of capillary forces in air

In ambient conditions, a water film is present on the surfaces. As a result, capillary forces control the adhesion interactions between probe and the surfaces. Indeed for hydrophilic surfaces the adhesion area in air is larger as compared to the measurements in water (Figure 3.5 a). This is the case over the whole range of applied loads, although the differences between adhesion in air and water become smaller for larger loads. That is because the capillary force is an additional load-contribution, becoming smaller relative to increasing applied loads. For the hydrophobic system the contact area in air is smaller as compared to the contact area in liquid (Figure 3.5 b) due to the absence of attractive hydrophobic interactions in air, in contrast to the water case. Capillary forces are also greatly diminished on a hydrophobic surface. The capillary force is a long-range force that also depends on the probe and substrate deformation [51]. This effect is not included in the JKR theory. Therefore, the JKR theory does not describe the measurements in air. At very high loads the additional force due to capillarity becomes negligible and the experiment in air also approaches the JKR prediction. The maximum load we apply with the AFM is around $P = 2000\,\mathrm{nN}$, which is not enough to conceal the effect of capillary forces.

3.4 Conclusion and Outlook

We have introduced a novel approach for AFM based adhesion measurements, which combines the advantages of the JKR apparatus with the advantages of AFM force spectroscopy. The use of soft colloidal probes (SCPs) allows for *in situ* determination of contact area as a function of applied load. Therefore, similar to the JKR apparatus, adhesion energies can be determined from a fit of a whole set of data on contact areas and load forces rather than from assumed contact areas and pull-off forces as it is common practice in AFM adhesion measurements (see Ch. 3.A). The dimensions of

contact areas and probe are orders of magnitude smaller than for the JKR apparatus. This allows for the determination of adhesion energies for heterogeneous (and micron-scale-patterned) samples and greatly reduces the amount of substances necessary for the measurement. In order to establish the technique, we introduce preparation protocols for SCPs and solve the problem of InvOLS determination which poses special problems due to the soft nature of the SCPs. We show that the SCP-substrate contact can still be described well by Johnson-Kendall-Roberts theory. Finally, we perform first test measurements on hydrophilic and hydrophobic contacts in air and water, which agree with expectations. The method works well to measure adhesion energies in liquid. In air, the results cannot be accounted for by JKR-type models since capillary forces are dominating under these conditions (while they are absent under liquid). Still, our method provides data for this (more complex) scenario as well, which might serve as experimental basis for investigation of capillary forces.

Beyond the basic examples discussed here, SCP is expected to provide advantages for a broader range of systems and for addressing scientific issues previously not accessible: The reduction of dimensions of the setup as compared to the JKR technique allows for increased measurement speed, since this speed is severely limited by drag forces and drainage of the contact area for macroscopic setups. These both scale with the typical dimension of the setup. Especially in soft matter systems, one expects that adhesion energies become time dependent due to the necessity of rearrangements of macromolecules and/or receptor-ligand types in the contact zone. These phenomena could be investigated using setups that allow for faster measurements, like the one introduced here. The setup can also be used to study adhesion hysteresis in soft matter systems [15, 69, 16]. As well, adhesion mediated by receptor-ligand type contacts as it is commonly found in biological or biomimetic systems [70, 71, 72] can result in complex pattern formation in the contact zone. Since the contact zone can in our case be monitored using optical techniques, these effects can be studied. Finally, with regard to adhesion measurements, the approach based on PDMS particles used here can be extended towards softer particles, which are especially of interest for the study of biological specimens. By varying the cross-link density [73] of PDMS elastomers, the elastic constants can be adjusted between several 10 s of kPa and the low MPa range. In this study, we have for the sake of simplicity of probe preparation focused on the upper limit representing the fully cross-linked case. For the lower limit, the probes would approach typical values for soft biological materials like cells and thus provide ”elasticity matched” partners for these materials for adhesion measurements. Beyond adhesion measurements like we have reported them here, the fact that the

contact-mechanical situation is wellknown in our case can be exploited for investigation of pressure-sensitive systems: The local pressure (distribution) in the contact area is precisely known from JKR theory. Thus at a given load force, the sample is exposed to various pressures in the contact area and it's reaction can be investigated.

Acknowledgements

J. Erath thanks the Deutsche Forschungsgemeinschaft (SFB 840, TP B5) for financial support. S. Schmidt gratefully acknowledges financial support by the Fraunhofer Society and the Max- Planck-Society in the network of excellence "Synthetic Bioactive Surfaces" and the Deutsche Forschungsgemeinschaft (Forschergrupp 608: TP: Fe 600/10-1).

3.5 References

[1] K. B. Lee et al. "Protein nanoarrays generated by dip-pen nanolithography". In: *Science* 295.5560 (2002), pp. 1702–1705.

[2] N. Sniadecki et al. "Nanotechnology for cell-substrate interactions". In: *Annals of Biomedical Engineering* 34.1 (2006), pp. 59–74.

[3] M. M. Stevens and J. H. George. "Exploring and engineering the cell surface interface". In: *Science* 310.5751 (2005), pp. 1135–1138.

[4] E. Arzt, S. Gorb, and R. Spolenak. "From micro to nano contacts in biological attachment devices". In: *Proceedings of the National Academy of Sciences of the United States of America* 100.19 (2003), pp. 10603–10606.

[5] B. Bhushan. "Biomimetics: lessons from nature - an overview". In: *Philosophical Transactions of the Royal Society a-Mathematical Physical and Engineering Sciences* 367.1893 (2009), pp. 1445–1486.

[6] L. Zhang and T. J. Webster. "Nanotechnology and nanomaterials: Promises for improved tissue regeneration". In: *Nano Today* 4.1 (2009), pp. 66–80.

[7] K. Autumn and A. M. Peattie. "Mechanisms of adhesion in geckos". In: *Integrative and Comparative Biology* 42.6 (2002), pp. 1081–1090.

[8] A. K. Geim et al. "Microfabricated adhesive mimicking gecko foot-hair". In: *Nature Materials* 2.7 (2003), pp. 461–463.

[9] L. T. Drzal and M. Madhukar. "Fiber Matrix Adhesion and Its Relationship to Composite Mechanical-Properties". In: *Journal of Materials Science* 28.3 (1993), pp. 569–610.

[10] D. J. Gardner et al. "Adhesion and surface issues in cellulose and nanocellulose". In: *Journal of Adhesion Science and Technology* 22.5-6 (2008), pp. 545–567.

[11] G. Mendonca et al. "Advancing dental implant surface technology - From micron-to nanotopography". In: *Biomaterials* 29.28 (2008), pp. 3822–3835.

[12] V. Grabovac, D. Guggi, and A. Bernkop-Schnurch. "Comparison of the mucoadhesive properties of various polymers". In: *Advanced Drug Delivery Reviews* 57.11 (2005), pp. 1713–1723.

[13] U. Hersel, C. Dahmen, and H. Kessler. "RGD modified polymers: biomaterials for stimulated cell adhesion and beyond". In: *Biomaterials* 24.24 (2003), pp. 4385–4415.

[14] H. Lee, N. F. Scherer, and P. B. Messersmith. "Single-molecule mechanics of mussel adhesion". In: *Proceedings of the National Academy of Sciences of the United States of America* 103.35 (2006), pp. 12999–13003.

[15] S. Perutz et al. "Investigation of adhesion hysteresis in poly(dimethylsiloxane) networks using the JKR technique". In: *Journal of Polymer Science Part B-Polymer Physics* 36.12 (1998), pp. 2129–2139.

[16] M. Tirrell. "Measurement of interfacial energy at solid polymer surfaces". In: *Langmuir* 12.19 (1996), pp. 4548–4551.

[17] E. S. Gil and S. M. Hudson. "Stimuli-reponsive polymers and their bioconjugates". In: *Progress in Polymer Science* 29.12 (2004), pp. 1173–1222.

[18] H. J. Butt, B. Cappella, and M. Kappl. "Force measurements with the atomic force microscope: Technique, interpretation and applications". In: *Surface Science Reports* 59.1-6 (2005), pp. 1–152.

[19] P. M. Claesson et al. "Techniques for measuring surface forces". In: *Advances in Colloid and Interface Science* 67 (1996), pp. 119–183.

[20] A. Olah and G. J. Vancso. "Characterization of adhesion at solid surfaces: Development of an adhesion-testing device". In: *European Polymer Journal* 41.12 (2005), pp. 2803–2823.

[21] D. E. Packham. *Handbook of Adhesion*. Wiley. Chichester, 2005.

[22] Y. Wei and J. W. Hutchinson. "Interface strength, work of adhesion and plasticity in the peel test". In: *International Journal of Fracture* 93.1-4 (1998), pp. 315–333.

[23] R. J. Good. "Contact-Angle, Wetting, and Adhesion - a Critical-Review". In: *Journal of Adhesion Science and Technology* 6.12 (1992), pp. 1269–1302.

[24] D. Y. Kwok and A. W. Neumann. "Contact angle measurement and contact angle interpretation". In: *Advances in Colloid and Interface Science* 81.3 (1999), pp. 167–249.

[25] C. A. Helm, J. N. Israelachvili, and P. M. McGuiggan. "Role of Hydrophobic Forces in Bilayer Adhesion and Fusion". In: *Biochemistry* 31.6 (1992), pp. 1794–1805.

[26] J. N. Israelachvili and G. E. Adams. "Measurement of Forces between 2 Mica Surfaces in Aqueous-Electrolyte Solutions in Range 0-100 Nm". In: *Journal of the Chemical Society-Faraday Transactions I* 74 (1978), pp. 975–.

[27] J. N. Israelachvili and P. M. McGuiggan. "Forces between Surfaces in Liquids". In: *Science* 241.4867 (1988), pp. 795–800.

[28] K. L. Johnson, K. Kendall, and A. D. Roberts. "Surface Energy and Contact of Elastic Solids". In: *Proceedings of the Royal Society of London Series a-Mathematical and Physical Sciences* 324.1558 (1971), pp. 301–.

[29] D. Ahn and K. R. Shull. "JKR studies of acrylic elastomer adhesion to glassy polymer substrates". In: *Macromolecules* 29.12 (1996), pp. 4381–4390.

[30] A. Falsafi et al. "Direct measurement of adhesion between viscoelastic polymers: A contact mechanical approach". In: *Journal of Rheology* 41.6 (1997), pp. 1349–1364.

[31] M. Rundlof et al. "Application of the JKR method to the measurement of adhesion to Langmuir-Blodgett cellulose surfaces". In: *Journal of Colloid and Interface Science* 230.2 (2000), pp. 441–447.

[32] M. Rundlof and L. Wagberg. "Formation of multilayers on silica surfaces of a cationic polyelectrolyte and dissolved and colloidal substances originating from mechanical wood pulp-Adsorption and influence on adhesion". In: *Colloids and Surfaces a-Physicochemical and Engineering Aspects* 237.1-3 (2004), pp. 33–47.

[33] G. Binnig, C. F. Quate, and C. Gerber. "Atomic Force Microscope". In: *Physical Review Letters* 56.9 (1986), pp. 930–933.

[34] B. Cappella and G. Dietler. "Force-distance curves by atomic force microscopy". In: *Surface Science Reports* 34.1-3 (1999), pp. 1–+.

[35] M. Kappl and H. J. Butt. "The colloidal probe technique and its application to adhesion force measurements". In: *Particle and Particle Systems Characterization* 19.3 (2002), pp. 129–143.

[36] W. A. Ducker, T. J. Senden, and R. M. Pashley. "Direct Measurement of Colloidal Forces Using an Atomic Force Microscope". In: *Nature* 353.6341 (1991), pp. 239–241.

[37] H. J. Butt. "Measuring Electrostatic, Vanderwaals, and Hydration Forces in Electrolyte-Solutions with an Atomic Force Microscope". In: *Biophysical Journal* 60.6 (1991), pp. 1438–1444.

[38] C. Wood et al. "AFM Based Single Hair Interaction Measurements". In: *SOFW* 11 (2009).

[39] R. R. Dagastine et al. "Forces between two oil drops in aqueous solution measured by AFM". In: *Journal of Colloid and Interface Science* 273.1 (2004), pp. 339–342.

[40] R. R. Dagastine et al. "Dynamic forces between two deformable oil droplets in water". In: *Science* 313.5784 (2006), pp. 210–213.

[41] R. Manica et al. "Dynamics of interactions involving deformable drops: Hydrodynamic dimpling under attractive and repulsive electrical double layer interactions". In: *Langmuir* 23.2 (2007), pp. 626–637.

[42] Grant B. Webber et al. "Measurements of dynamic forces between drops with the AFM: novel considerations in comparisons between experiment and theory". In: *Soft Matter* 4.6 (2008), pp. 1270–1278.

[43] I. U. Vakarelski et al. "Bubble colloidal AFM probes formed from ultrasonically generated bubbles". In: *Langmuir* 24.3 (2008), pp. 603–605.

[44] F. Dubreuil, N. Elsner, and A. Fery. "Elastic properties of polyelectrolyte capsules studied by atomic-force microscopy and RICM". In: *European Physical Journal E* 12.2 (2003), pp. 215–221.

[45] A. Fery and R. Weinkamer. "Mechanical properties of micro- and nanocapsules: Single-capsule measurements". In: *Polymer* 48.25 (2007), pp. 7221–7235.

[46] J. L. Hutter and J. Bechhoefer. "Calibration of Atomic-Force Microscope Tips". In: *Review of Scientific Instruments* 64.7 (1993), pp. 1868–1873.

[47] N. Bowden et al. "The controlled formation of ordered, sinusoidal structures by plasma oxidation of an elastomeric polymer". In: *Applied Physics Letters* 75.17 (1999), pp. 2557–2559.

[48] A. S. G. Curtis. "Mechanism of Adhesion of Cells to Glass - Study by Interference Reflection Microscopy". In: *Journal of Cell Biology* 20.2 (1964), pp. 199–215.

[49] M. Kuhner and E. Sackmann. "Ultrathin hydrated dextran films grafted on glass: Preparation and characterization of structural, viscous, and elastic properties by quantitative microinterferometry". In: *Langmuir* 12.20 (1996), pp. 4866–4876.

[50] J. Ploem. "Reflection contrast microscopy as a tool for investigation of the attachment of living cells to a glass surface". In: *Mononuclear Phagocytes in Immunity, Infection, and Pathology, Blackwell scientific publications.* (1975).

[51] S. Schmidt, M. Nolte, and A. Fery. "Single-colloidal-particle microcontact printing". In: *Physical Chemistry Chemical Physics* 9.36 (2007), pp. 4967–4969.

[52] J. K. Ferri et al. "Separating membrane and surface tension contributions in Pickering droplet deformation". In: *Soft Matter* 4.11 (2008), pp. 2259–2266.

[53] M. J. Higgins et al. "Noninvasive determination of optical lever sensitivity in atomic force microscopy". In: *Review of Scientific Instruments* 77.1 (2006).

[54] K. L. Johnson and J. A. Greenwood. "An adhesion map for the contact of elastic spheres". In: *Journal of Colloid and Interface Science* 192.2 (1997), pp. 326–333.

[55] H. Hertz. "Ueber die Beruehrung fester elastischer Koerper". In: *Journal fuer die reine und angewandte Mathematik* 92 (1881).

[56] B. V. Derjaguin, V. M. Muller, and Y. P. Toporov. "Effect of Contact Deformations on Adhesion of Particles". In: *Journal of Colloid and Interface Science* 53.2 (1975), pp. 314–326.

[57] D. Tabor. "Surface Forces and Surface Interactions". In: *Journal of Colloid and Interface Science* 58.1 (1977), pp. 2–13.

[58] D. Maugis. "Adhesion of Spheres - the JKR-DMT Transition Using a Dugdale Model". In: *Journal of Colloid and Interface Science* 150.1 (1992), pp. 243–269.

[59] S. A. Chizhik et al. "Micromechanical properties of elastic polymeric materials as probed by scanning force microscopy". In: *Langmuir* 14.10 (1998), pp. 2606–2609.

[60] Israelachvili J.N. *Intermolecular and Surface Forces*. 2nd ed. Amsterdam, The Netherlands: Academic Press, 2007.

[61] P. Warszynski et al. "Interpretation of adhesion force between self-assembled monolayers measured by chemical force microscopy". In: *Colloids and Surfaces a-Physicochemical and Engineering Aspects* 214.1-3 (2003), pp. 61–75.

[62] G. Papastavrou, S. Akari, and H. Mohwald. "Interactions between hydrophilic and hydrophobic surfaces on microscopic scale and the influence of air bubbles as observed by scanning force microscopy in aqueous and alcoholic mediums". In: *Europhysics Letters* 52.5 (2000), pp. 551–556.

[63] S. Ohnishi et al. "Characterization of fluorocarbon monolayer surfaces for direct force measurements". In: *Langmuir* 16.6 (2000), pp. 2722–2730.

[64] S. Ohnishi, V. V. Yaminsky, and H. K. Christenson. "Measurements of the force between fluorocarbon monolayer surfaces in air and water". In: *Langmuir* 16.22 (2000), pp. 8360–8367.

[65] E. R. Beach et al. "Pull-off force measurements between rough surfaces by atomic force microscopy". In: *Journal of Colloid and Interface Science* 247.1 (2002), pp. 84–99.

[66] S. Biggs and G. Spinks. "Atomic force microscopy investigation of the adhesion between a single polymer sphere and a flat surface". In: *Journal of Adhesion Science and Technology* 12.5 (1998), pp. 461–478.

[67] Y. I. Rabinovich et al. "Adhesion between nanoscale rough surfaces - II. Measurement and comparison with theory". In: *Journal of Colloid and Interface Science* 232.1 (2000), pp. 17–24.

[68] D. M. Schaefer et al. "Surface-Roughness and Its Influence on Particle Adhesion Using Atomic-Force Techniques". In: *Journal of Adhesion Science and Technology* 9.8 (1995), pp. 1049–1062.

[69] P. Silberzan et al. "Study of the Self-Adhesion Hysteresis of a Siloxane Elastomer Using the Jkr Method". In: *Langmuir* 10.7 (1994), pp. 2466–2470.

[70] A. K. Dillow and M. Tirrell. "Targeted cellular adhesion at biomaterial interfaces". In: *Current Opinion in Solid State and Materials Science* 3.3 (1998), pp. 252–259.

[71] E. L. Florin, V. T. Moy, and H. E. Gaub. "Adhesion Forces between Individual Ligand-Receptor Pairs". In: *Science* 264.5157 (1994), pp. 415–417.

[72] E. Sackmann. "Supported membranes: Scientific and practical applications". In: *Science* 271.5245 (1996), pp. 43–48.

[73] F. Carrillo et al. "Nanoindentation of polydimethylsiloxane elastomers: Effect of crosslinking, work of adhesion, and fluid environment on elastic modulus". In: *Journal of Materials Research* 20.10 (2005), pp. 2820–2830.

3.A Supporting Information

RICM

In order to reconstruct the height profile of the object from the RICM images, three different approaches are possible: The simple theory (considers light which enters the sample in direction normal to the plane of the substrate), the finite aperture theory (correction for finite aperture effects) and the non-local theory (correction for finite aperture effects and corrections due to curved interfaces) [49]. To get the intensity distribution over the distance r from raw data we take the average of intensity profiles over an angle φ, shown in Figure 3.6A. For analysis of the intensity distribution we used the simple theory with correction factors for finite aperture and geometry effects [52]. To obtain the correction factors, we imaged glass beads (Polysciences Inc., Warrington, PA) on a glass surface in RICM mode. We recorded 10 glass beads with a diameter in the range of $30 - 50\,\mu$m and extracted the intensity profile, see Figure 3.6B. Using the profiles, we reconstructed the shape of the beads and compared it to the calculated shapes (R by measuring their size with light microscope), and determined the correction factors corresponding to our experimental setup presented in Figure 3.6C.

Optical Lever Sensitivity

In order to accurately determine the force from cantilever deflection the optical lever sensitivity is required. However, since we attached soft probes on the cantilevers, we cannot use the standard procedure in order to measure the optical lever sensitivity, i.e. force-distance measurements on a hard substrate to obtain the cantilever deflection from the z-piezo displacement. Here we use the spring constant of the cantilever, which was measured before, in combination with the Thermal Noise Method to determine the optical lever sensitivity [53].

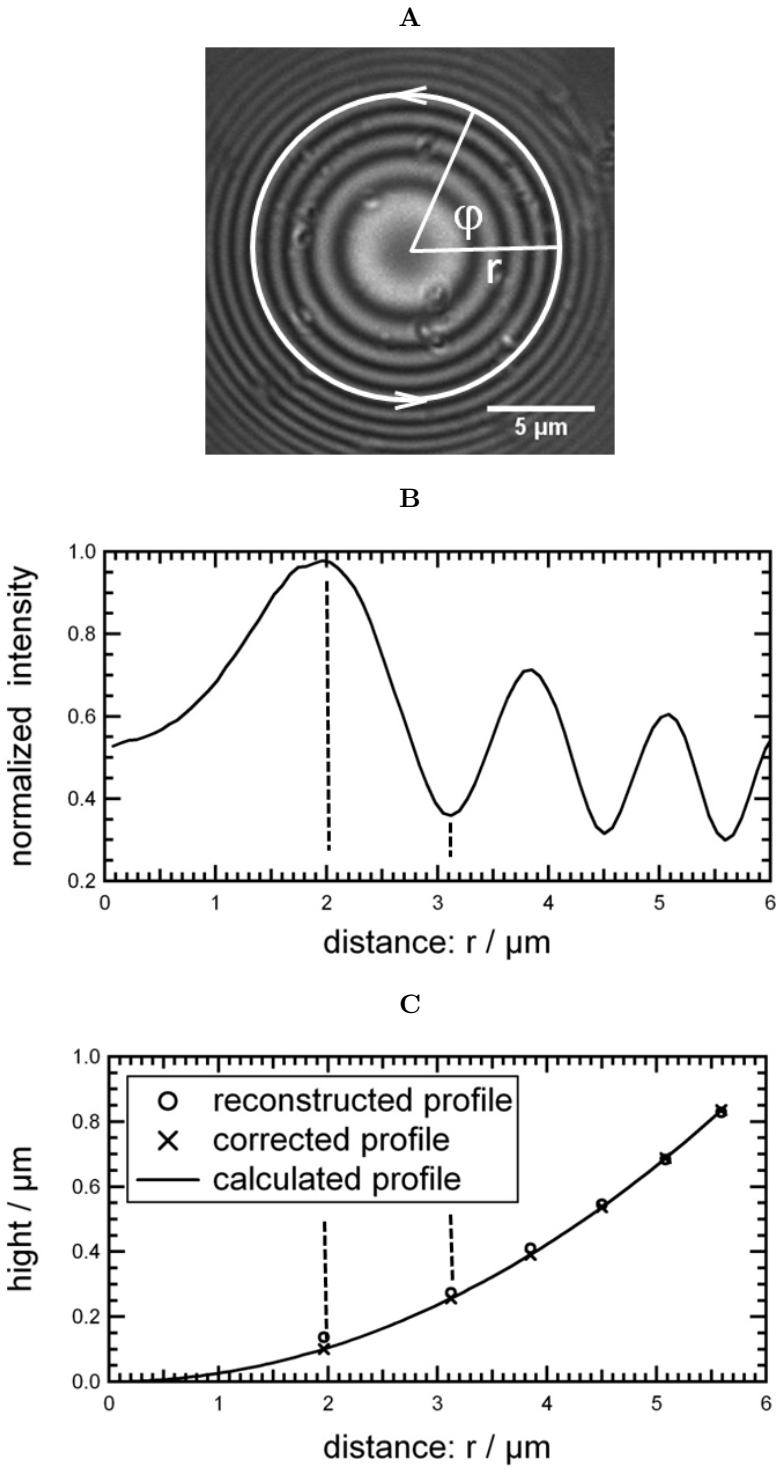

Figure 3.6: Evaluation of the RICM immages: 3.6A RICM image of a glass bead, 3.6B extracted intensity profile, 3.6C reconstruction of bead profile

The determination process is shown in the following flow chart:

1. Detection of spring constant of cantilever (without soft probe) $\Rightarrow k_c$
2. Detection of sensitivity of cantilever with soft probe onto a hard substrate $\Rightarrow S'$
3. Thermal Noise Method with soft probe on cantilever $\Rightarrow k_c'$
4. If $\Rightarrow k_c' \neq k_c$ change sensitivity and go back to 3.
   If $\Rightarrow k_c' = k_c$ sensitivity of the current setup.

In liquid the Thermal Noise Method cannot[1] be used due to high damping [18]. In this case, we detect the optical lever sensitivity by using the standard procedure, i.e. force-distance measurement on a hard substrate, but avoiding deformation of the colloidal probe. This can be done by approaching the very tip of the cantilever apex onto a sharp edge, not touching the soft colloidal probe. Any steep lithographic surface can be used as a sharp edge, here we use a cantilever chip (CSC38, Îij-mash, Estonia) glued onto a glass surface.

Force spectroscopy mode

In addition to the JKR approach shown in the main text, the soft colloidal probe setup also allows to obtain the adhesion from AFM force-distance curves. Form force-distance curves as shown in Figure 3.7 we determine the work of adhesion W_{adh} (area of the force curve under the baseline [34]). Simultaneously we measure the contact radius a of the adhesion area at maximum load via RICM. The adhesion energy per unit area w can then be calculated according to dividing W_{adh} by πa^2. For statistics, we detect the force-distance curves in mapping mode, defining a $100\,\mu\mathrm{m}^2$ grid on the substrate with at least 64 data points. Afterwards, the force-displacement measurements are done on each point of the grid. For the hydrophilic system in water we found $w_{\mathrm{water}} = (0.9 \pm 0.1)\,\mathrm{mJ/m^2}$, and in air $w_{\mathrm{air}} = (40 \pm 10)\,\mathrm{mJ/m^2}$. For the hydrophobic probes in water we obtained $w_{\mathrm{water}} = (45 \pm 10)\,\mathrm{mJ/m^2}$ and $w_{\mathrm{air}} = (11 \pm 5)\,\mathrm{mJ/m^2}$ in air. These values agree well with values reported in the literature. The capillary force is a line effect, so in air w in units $\mathrm{J/m^2}$ represents a reference value.

[1] can just approximately used (included after publication)

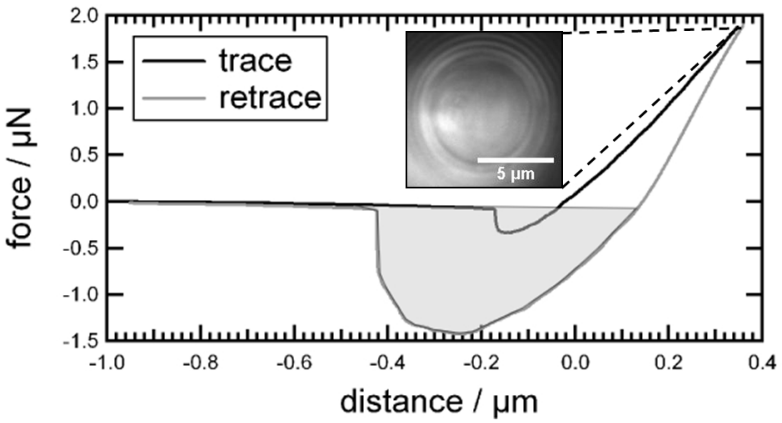

Figure 3.7: Analysis of the thermodynamic work of adhesion: Collect force distance curve, evaluating work of adhesion Wadh (gray area) and measuring simultaneously the particle-surface contact area at maximum load by micro interferometry (RICM).

4

Direct Correlation between Local Pressure and Fluorescence Output in Mechanoresponsive Polyelectrolyte Brushes

Bunsow, J., Erath, J., Biesheuvel, P. M., Fery, A., Huck, W. T. S., Direct Correlation between Local Pressure and Fluorescence Output in Mechanoresponsive Polyelectrolyte Brushes. Angewandte Chemie-International Edition, 2011. 50(41): p. 9629-9632.

4.1 Introduction

In recent years, there has been huge progress in the development of stimuli-responsive polymeric materials [1], and especially mechanoresponsive polymers, which convert mechanical stimuli into optical, electrical or chemical signals are a particularly attractive class of materials [2, 3, 4, 5]. An ultimate goal of such materials would be to emulate the unique responsiveness of human skin, which can detect gentle touches of around 1 kPa at a spatial resolution of about 40 μm [6].
Here, we introduce a new concept for optical force mapping based on mechanoresponsive polyelectrolyte brushes, which in addition to their response to force also respond to changes in the chemical environment [7]. Dense, strong polyelectrolyte brushes are hard to compress due to the increase of the osmotic pressure of the counter-ions and the excluded volume interactions between the individual chains [8, 9]. Thus, they are not mechanically responsive per se, and to generate an optical signal a "mechanophore" [10] needs to be introduced. Previously, we used a pH-sensitive dye to act as a mechanosensitive building block, where the dissociation constant of the dye was a function of brush compression [7]. However, the dye was only infiltrated into the brush and not a covalent part of it. Furthermore, only qualitative information on the correlation between pressure and optical response was obtained. The key advance in the present work is the quantitative characterization of the mechanoresponsive properties of polyelectrolyte brushes functionalized by covalent attachment of fluorescent dye molecules. We have determined a response function $I(p)$, which correlates local fluorescence intensity (I) to local pressure (p) and we have found an excellent pressure sensitivity in the order of 10 kPa and a lateral resolution better than 1 μm.

4.2 Experimental

Full experimental details on polymer brush formation and characterization and determination of fluorescent monomer loading in brushes as well as a detailed description of soft colloidal probe experiments and JKR analysis is available in the Supporting Information section 4.A.

4.3 Results and Discussion

Our experimental platform consists of cationic poly[2-(methacryloyloxy)ethyl]trimethyl ammoniumchloride (PMETAC) brushes with a covalently attached fluorescent dye, 5(6)carboxyfluorescein (CF) (Figure 4.1; see Supporting Information 4.A for details on synthesis). To these brushes a defined force was applied using soft colloidal probe

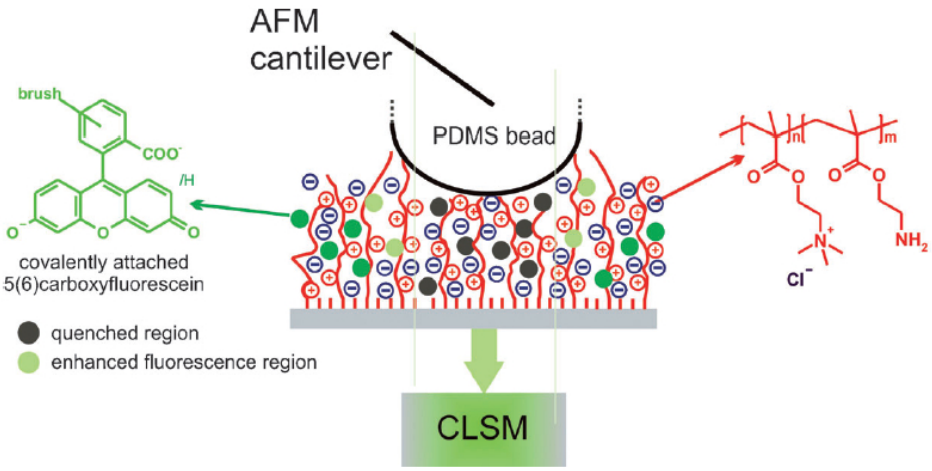

Figure 4.1: Experimental design to measure the fluorescence-based readout of the effect of mechanical compression of functionalized polyelectrolyte brushes using a soft colloidal probe.

atomic force microscopy (AFM) [11, 12], where an elastomeric particle is pressed against the substrate surface of interest with welldefined forces while the contact area between particle and substrate is monitored in situ with confocal laser scanning microscopy (CLSM) (Further information in Supporting Information 4.A).

A standard force experiment on PMETAC copolymer brushes with 10% fluorescently labeled monomers is shown in Figure 4.2. When approaching the bead to the surface (Figure 4.2A-4.2D), a dark area was observed where the bead was in contact with the brush. With increasing force, the contact area became larger due to elastic deformation of the polydimethylsiloxane (PDMS) bead. When retracting the bead from the brush (Figure 4.2E-4.2H), the radius of the dark contact area decreased with a significant hysteresis as a result of adhesion forces acting between the bead and the brush [13]. The most striking feature of the retract cycle was a bright "rim" surrounding the edge of the contact area. Control experiments on neutral brushes showed virtually no changes in fluorescence upon compression (see insets in Figure 4.2) while cationic brushes with different concentrations of dye showed qualitatively the same response as

shown in Figure 4.2. The rates of compression and release were chosen such that the deformation kinetics of the bead did not interfere with the brush response to changes in pressure, with the fluorescent signal stabilizing well before the acquisition time of $1 - 2\,\mathrm{s}$. The fluorescence output remained constant for at least several minutes and the response was completely reversible. When the bead was detached from the surface, the initial value of the fluorescence intensity was recovered. As demonstrated in Figure 4.3, force cycles could be repeated for at least four times without significant changes of the response.

Looking at the molecular nature of the polyelectrolyte brush, the question arises why

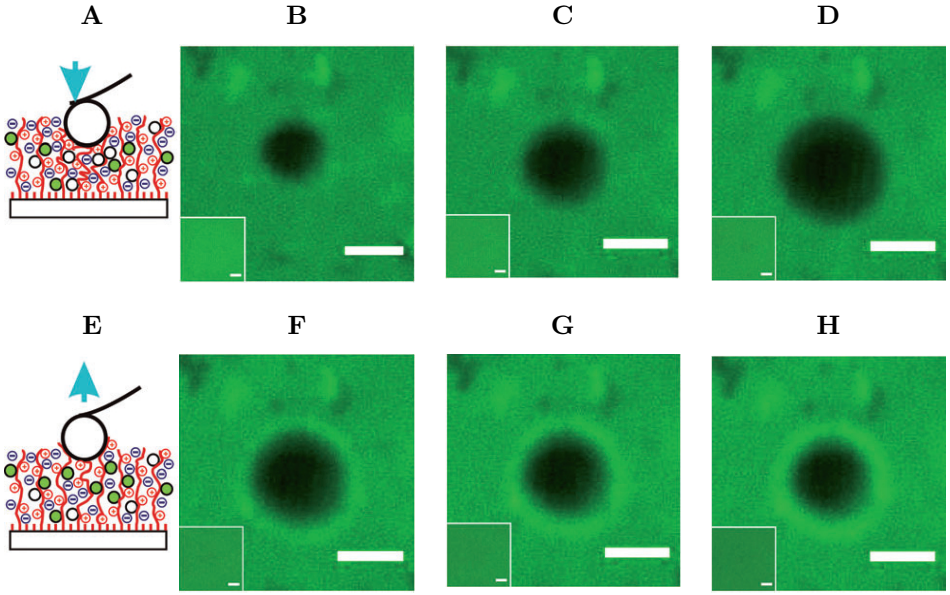

Figure 4.2: Representative compression experiment on fluorescently labeled PMETAC brushes in water. 4.2B-4.2D) Fluorescence images during approach 4.2A, using loads of 0.7, 2.8, and $5.6\,\mu$N. 4.2F-4.2H) Fluorescence images during retraction 4.2E, using loads of 2.8, 0.7, and $-1.4\,\mu$N. Scale bars represent a length of $5\,\mu$m. Insets show absence of any changes in fluorescence intensity during compression experiments on neutral brushes at loads of 0.3 4.2B, 1.3 4.2C, and $1.9\,\mu$N 4.2D during the approach and 1.3 4.2F, 0.8 4.2G, and $-0.5\,\mu$N 4.2H when retracting.

the fluorescence intensity of the brushes is a function of the applied force. Studies on CF encapsulated in liposomes at 0.2 M showed 97% fluorescence concentration quenching, with the residual fluorescence arising from dye molecules interacting with lipid [14]. Furthermore, CF forms non-fluorescent complexes with quaternary ammonium group containing polymers [15], which we also observed when METAC is added to a CF solution (see 4.A). Considering the high loading of dye in our brushes ($0.1 - 0.4\,\mathrm{M}$),

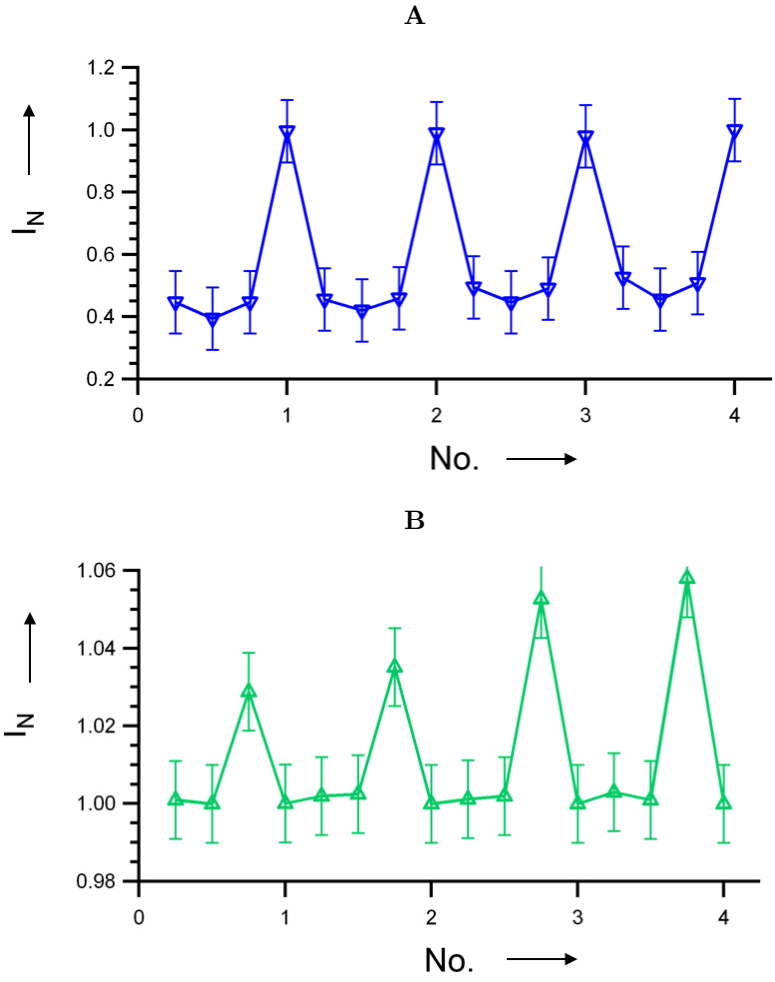

Figure 4.3: Reversibility of the response to compression and retraction of the bead measured in the 4.3A dark center and 4.3B bright edge, respectively. Values are the average of 3 measurements. One cycle shows the response I_N (normalized by the background intensity) to 0.6 μN and 2.9 μN loads during approach and a 0.6 μN load and completely withdrawn state during retraction.

and the possibility for the dye to complex with the cationic PMETAC brushes, we believe that the variations in fluorescence intensity are caused by reversible association of CF with the polymer brush. Compression leads to a higher local concentration of quaternary ammonium groups and an additional driving force for remaining free dye to form nonfluorescent complexes thereby extinguishing the remaining CF fluorescence. Conversely, the adhesion of the brushes to the beads leads to stretching of the chains and lowering of the local METAC concentration and hence a local higher concentration of dissociated dye molecules and a slightly brighter rim.

This molecular picture of the response of the dye-functionalized brushes to mechanical deformation can be quantified by modeling the contact situation underneath the PDMS bead with the theory developed by Johnson, Kendall and Roberts (JKR theory, see SI 4.A for a discussion of assumptions) [16, 17]. In a simplified approach, the PDMS bead is regarded as an elastic bead in contact with the polyelectrolyte brush as a hard adhesive substrate. In such a situation, JKR theory predicts that the pressure distribution underneath the bead is governed by the interplay between compression and adhesion. Analytically, the pressure profile underneath the bead can be described by Equations 4.1 and 4.2:

$$p(r) = p_0 \left(1 - \frac{r^2}{a^2}\right)^{1/2} + p_1 \left(1 - \frac{r^2}{a^2}\right)^{-1/2} \tag{4.1}$$

$$p_0 = \frac{3Ka}{2\pi R} \text{ and } p_1 = -\sqrt{\frac{2Kw}{2\pi a}} \tag{4.2}$$

where R is the effective radius of curvature, K is the effective elastic modulus of the system, w is the thermodynamic work of adhesion per unit area, $a(R, K, w, P)$ is the contact radius, and r is the distance from the axis of cylindrically symmetric systems. Elastic deformation of the bead on the surface leads to a positive contribution to the pressure and a zone of compressive stress underneath the bead [first part in Eq. 4.1]. At the edge of the contact area, adhesive contributions dominate, resulting in a region with negative pressure (tension) [second part in Eq. 4.1]. This tensile stress is very high at the edges.

We can now correlate the computed pressure profiles with extracted intensity profiles (obtained from data analysis with ImageJ). Figure 4.4A shows the calculated pressure profile for an adhesive contact using JKR theory (w, K and P measured by force spectroscopy, a calculated and measured, r measured by CLSM) and the experimentally obtained fluorescence intensity profiles. One finds a decrease in fluorescence intensity

(as compared to the background intensity) in areas of compression and a slight increase of fluorescence in areas of tension. These lateral variations of fluorescence intensity can be explained by the variations in local pressure in the contact area, as described by Equation 4.1: when a load is applied by the bead, the spherical bead shape results in a higher pressure in the center of the contact area, which decreases with increasing distance from the center. In our case additional adhesive interactions are present, leading to a transition to negative stresses at the edge of the contact. When the measured fluorescence intensity is correlated with the calculated lateral pressure variation, we obtain the response function $I(p)$, that is, the dependency of the local fluorescence intensity as a function of local pressure (Figure 4.4B). Figure 4.4B shows data for applied loads ranging from 0.9 to 4.5 μN while retracting, and clearly shows that all $I(p)$ data collapse onto one master curve, independent of the applied external load. Brush compression can also be induced by the addition of salts [18, 19], and Figure 4.4C shows that the response function drastically alters as the NaCl concentration is increased from 0.1 M to 1 M, with fluorescence intensity dropping strongly at high salt concentrations. Importantly, the dependency of the relative intensity I_N (absolute intensity divided by the background intensity) on p is only weakly changing with salt concentration (Figure 4.4D). Thus normalization provides a means to eliminate the effects of salt concentration on fluorescence over a broad range (zero up to greater than 1 M NaCl). The fluorescence output and responsiveness of the brushes can be switched off by the addition of 0.1 M $NaClO_4$, which leads to hydrophobic collapse and dehydration of the brushes [20].

4.4 Conclusion and Outlook

In summary, we have demonstrated mechanoresponsive polyelectrolyte brushes which show a strong correlation between local fluorescence intensity and local (calculated) pressures. The response of the surface to mechanical stimuli was completely reversible and provided a sensitivity under 10 kPa. The combination of very high lateral resolution over large areas, good pressure sensitivity, response times in at least the sub-second range and the ability to measure compression and tension simultaneously makes this sensor an outstanding starting point towards mechanoresponsive surfaces with potential applications in for example robotics or fundamental studies on bioadhesion phenomena.

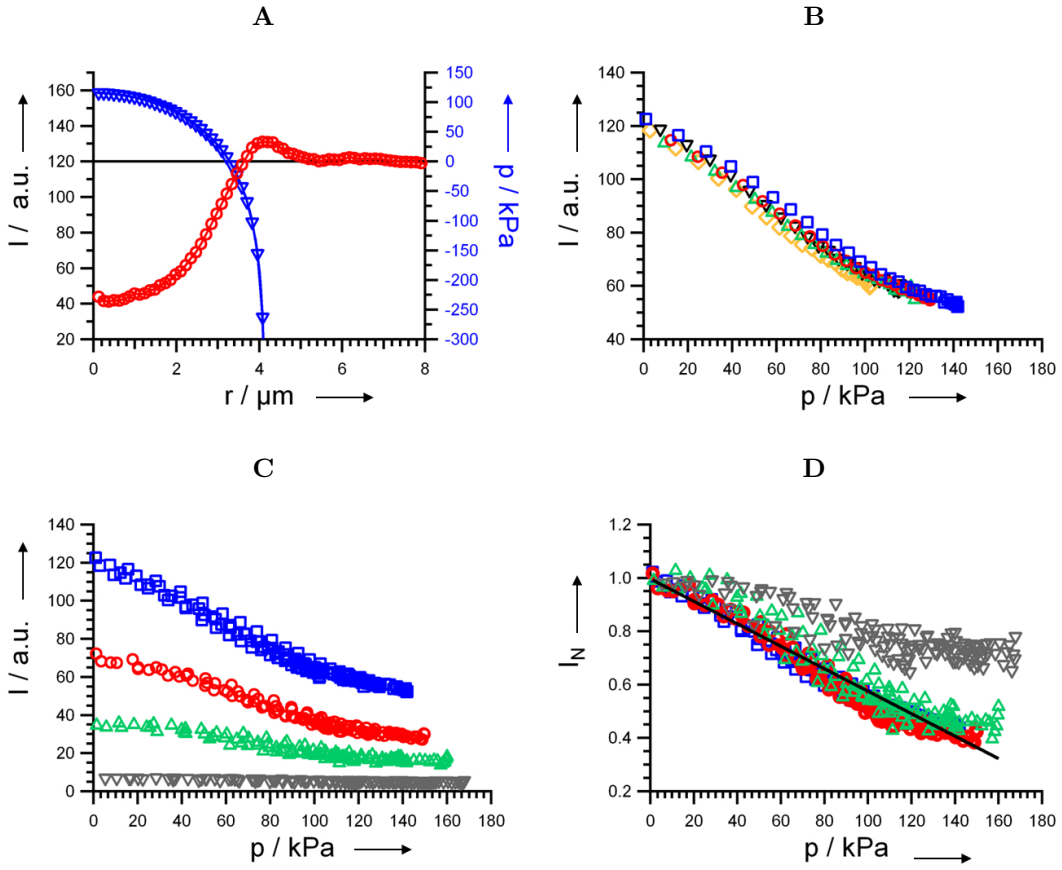

Figure 4.4: 4.4A Extracted intensity profile and calculated pressure profile on applied load (1780 μN) in water while retracting (Young's modulus $E = 0.8$ MPa, adhesion energy per unit area $w = 19\,\mathrm{mJm^{-2}}$): red $\circ$, intensity profile; blue $\bigtriangledown$, pressure profile. 4.4B Response functions $I(p)$ correlating fluorescence intensity vs. calculated pressures under spherical bead at five different loads: blue $\square$, $4.5 \pm 0.9\,\mu$N; red $\circ$, $3.6 \pm 0.7\,\mu$N; green $\bigtriangleup$, $2.7 \pm 0.5\,\mu$N; gray $\bigtriangledown$, $1.8 \pm 0.4\,\mu$N, yellow $\diamondsuit$ $0.9 \pm 0.2\,\mu$N. 4.4C Response functions acquired in Millipore H_2O (blue $\square$), 0.1 M NaCl (red $\circ$), 1.0 M NaCl (green $\bigtriangleup$), 0.1 M $NaClO_4$ (black $\bigtriangledown$). Each dataset contains five different forces while retracting. 4.4D Data of 4.4C normalized by the background intensity. Data for H_2O, 0.1 M NaCl, and 1.0 M NaCl fall on a common mastercurve, shown by the linear fit (black line). (Further details in SI 4.A)

Acknowledgements

W.T.S.H. gratefully acknowledges funding from the Friedrich Wilhelm Bessel Award of the Humboldt Foundation. J.B. thanks the German Research Foundation (Deutsche Forschungsgemeinschaft, DFG) for funding. J.E. and A.F. gratefully acknowledge financial support from the Deutsche Forschungsgemeinschaft (Forschergruppe 608: TP: Fe 600/10-1). We thank Petra Zippelius for helpful assistance in carrying out some of the experiments.

4.5 References

[1] M. A. Cohen Stuart et al. "Emerging applications of stimuli-responsive polymer materials". In: *Nature Materials* 9.2 (2010), pp. 101–113.

[2] J. Buensow, T. S. Kelby, and W. T. S. Huck. "Polymer Brushes: Routes toward Mechanosensitive Surfaces". In: *Accounts of Chemical Research* 43.3 (2010), pp. 466–474.

[3] M. M. Caruso et al. "Mechanically-Induced Chemical Changes in Polymeric Materials". In: *Chemical Reviews* 109.11 (2009), pp. 5755–5798.

[4] J. M. Lenhardt et al. "Trapping a Diradical Transition State by Mechanochemical Polymer Extension". In: *Science* 329.5995 (2010), pp. 1057–1060.

[5] K. M. Wiggins et al. "Mechanical Reconfiguration of Stereoisomers". In: *Journal of the American Chemical Society* 132.10 (2010), pp. 3256–+.

[6] V. Maheshwari and R. Saraf. "Tactile devices to sense touch on a par with a human finger". In: *Angewandte Chemie-International Edition* 47.41 (2008), pp. 7808–7826.

[7] O. Azzaroni et al. "Mechanically induced generation of counterions inside surface-grafted charged macromolecular films: Towards enhanced mechanotransduction in artificial systems". In: *Angewandte Chemie-International Edition* 45.44 (2006), pp. 7440–7443.

[8] U. Raviv et al. "Lubrication by charged polymers". In: *Nature* 425.6954 (2003), pp. 163–165.

[9] E. B. Zhulina, O. V. Borisov, and T. M. Birshtein. "Static forces in confined polyelectrolyte layers". In: *Macromolecules* 33.9 (2000), pp. 3488–3491.

[10] M. J. Kryger et al. “Masked Cyanoacrylates Unveiled by Mechanical Force”. In: *Journal of the American Chemical Society* 132.13 (2010), pp. 4558–+.

[11] J. Erath, S. Schmidt, and A. Fery. “Characterization of adhesion phenomena and contact of surfaces by soft colloidal probe AFM”. In: *Soft Matter* 6.7 (2010), pp. 1432–1437.

[12] I. U. Vakarelski et al. “Deformation and adhesion of elastomer microparticles evaluated by AFM”. In: *Langmuir* 17.16 (2001), pp. 4739–4745.

[13] P. Silberzan et al. “Study of the Self-Adhesion Hysteresis of a Siloxane Elastomer Using the Jkr Method”. In: *Langmuir* 10.7 (1994), pp. 2466–2470.

[14] R. F. Chen and J. R. Knutson. “Mechanism of Fluorescence Concentration Quenching of Carboxyfluorescein in Liposomes - Energy-Transfer to Nonfluorescent Dimers”. In: *Analytical Biochemistry* 172.1 (1988), pp. 61–77.

[15] F. Caruso et al. “Fluorescence studies of the binding of anionic derivatives of pyrene and fluorescein to cationic polyelectrolytes in aqueous solution”. In: *Macromolecules* 31.21 (1998), pp. 7365–7377.

[16] P. Attard and J. L. Parker. “Deformation and Adhesion of Elastic Bodies in Contact”. In: *Physical Review A* 46.12 (1992), pp. 7959–7971.

[17] K. L. Johnson, K. Kendall, and A. D. Roberts. “Surface Energy and Contact of Elastic Solids”. In: *Proceedings of the Royal Society of London Series a-Mathematical and Physical Sciences* 324.1558 (1971), pp. 301–.

[18] M. Biesalski, D. Johannsmann, and J. Ruhe. “Electrolyte-induced collapse of a polyelectrolyte brush”. In: *Journal of Chemical Physics* 120.18 (2004), pp. 8807–8814.

[19] T. S. Kelby and W. T. S. Huck. “Controlled Bending of Microscale Au-Polyelectrolyte Brush Bilayers”. In: *Macromolecules* 43.12 (2010), pp. 5382–5386.

[20] O. Azzaroni et al. “Switching the properties of polyelectrolyte brushes via "Hydrophobic collapse"”. In: *Macromolecules* 38.24 (2005), pp. 10192–10199.

[21] M. Husseman et al. “Controlled synthesis of polymer brushes by "Living" free radical polymerization techniques”. In: *Macromolecules* 32.5 (1999), pp. 1424–1431.

[22] A. M. Jonas et al. “Thermo-responsive polymer brushes with tunable collapse temperatures in the physiological range”. In: *Macromolecules* 40.13 (2007), pp. 4403–4405.

4.A Supporting Information

Experimental

Materials

METAC (80 wt.% in water), AEMA, HEMA, CuBr, CuCl, $CuCl_2$, $CuBr_2$, 2,2'-bipyridyl (bipy), triethylamine, 5(6)-carboxyfluorescein N-hydroxysuccinimide ester (CF-NHS) and sodium dodecyl sulfate were purchased from Sigma Aldrich and used as received unless otherwise stated. NaCl and $NaClO_4$ were from Gruessing (Germany). Prior to polymerisation, METAC and HEMA were activated by passing over a neutral alumina column. Triethylamine was distilled from KOH and stored over molecular sieve (4 Å, Sigma Aldrich). CuBr and CuCl were stored under vacuum. High purity water of a resistance of 18.2 MΩcm was obtained from a Millipore Synergy system. The ATRP initiator 2-bromo-2-methylpropionic acid 3-trichlorosilanlypropyl ester was synthesised according to Ref. [21, 22]. Round cover slips (ø= 24 mm) were purchased from VWR and cleaned by 10 min sonication in ethanol. 5(6)-carboxyfluorescein N-hydroxysuccinimide ester was stored at −20 °C. The PDMS precursor kit Sylgard 184 was obtained from Dow Corning (USA).

Initiator Immobilisation on Glass

Glass cover slips were cleaned in air plasma (Emitech, model K1050X) for 10 min at a power of 100 W. 50.4 µL triethylamine were mixed with 30 mL dry toluene and 10 µL of the ATRP initiator were added under shaking. The mixture was transferred to the petri dish containing the glass slides and initiator immobilisation proceeded under gentle shaking (50 rpm) over night. The modified glass slides were rinsed with toluene, ethanol and water, dried with nitrogen and baked in an oven at 150°C for 3 to 4 hours.

Synthesis of Polymer Brushes

METAC (7 g, 30 mmol), AEMA (0.5 g, 3 mmol), bipy (214 mg, 1.4 mmol) and $CuCl_2$ (3.6 mg, 0.03 mmol) were dissolved in a mixture of water (2.4 mL) and isopropanol (9 mL). The solution was degassed with N_2 for 30 min. CuBr (80 mg, 0.56 mmol) and initiatormodified glass cover slips were placed in separate Schlenk tubes and degassed by evacuating and flushing with N_2 in at least three subsequent cycles. CuBr was dissolved in the monomer solution by sonication. The reactant mixture was added to the cover slips and kept at room temperature under N2 for 5 hours. Samples were

rinsed with ethanol, water, and acetone; and sonicated in water for 10 mins to remove non-covalently attached polymer. Samples were dried with N_2 and kept under N_2 until further use.

Attachment of Carboxyfluorescein

CF-NHS was dissolved in dimethylsulfoxide at a concentration of 1 mg/mL. Brushes on glass slides were immersed in 2 mL 0.1 M aqueous $NaHCO_3$ and 200 μl of the dye stock solution were added under shaking. Dye immobilisation was allowed to proceed in the dark over night under shaking (100 rpm). Samples were rinsed with water and sonicated for 10 min in 1 M NaCl and water, respectively, to remove non-covalently attached dye.

Synthesis of neutral P(HEMA-co-AEMA) brushes

Hydroxyethylmethacrylate (HEMA) was purchased from Sigma Aldrich and activated by passing over neutral alumina. P(HEMA-co-AEMA) brushes were prepared from a solution of HEMA (6 mL, 50 mmol), AEMA (0.9 g, 5 mmol), bipy (163 mg, 2 mmol) and CuBr2 (24 mg, 0.1 mmol) in water (6.5 mL). After degassing with nitrogen for 30 min, the monomer solution was added to degassed CuCl (37 mg, 0.35 mmol) in a Schlenk tube. The reactant mixture was added to the cover slips and kept at room temperature under N2 for 5 hours. Samples were rinsed with ethanol, water, and acetone; and sonicated in water for 10 mins to remove noncovalently attached polymer. Samples were dried with N_2 and kept under N_2 until further use.

Compression Experiments

Compression experiments were carried out with a combination of an AFM (MFP 3D I,Asylum Research, USA) and a CLSM (LSM710, Zeiss, Germany). Using the SCP technique, we compressed the polyelectrolyte brushes in the direction normal to the surface and recorded the optical response via CLSM. Measurements were performed in a 0.1 ml liquid droplet. Samples were stored in water to guarantee full hydration of the brushes. After measurements in 0.1 M $NaClO_4$ solution, samples were regenerated by extensive rinsing in 1 M NaCl and water.

AFM

PDMS beads with diameters of 20 to 40 μm were prepared according to Ref. [11], transferred to a polystyrene dish by dip-coating, and glued with an epoxy resin (UHU

schnellfest, Germany) to pre-calibrated cantilevers (728 N/m, NSC 12, tipless, noAl, Micromash, Estonia) using a micromanipulator (MP-285, Shutter Instrument, USA) and an inverted optical microscope (Axiovert 200, Zeiss, Germany). Force constants of the cantilevers were determined by the thermal noise method. Using AFM forcedistance measurements and Hertz analysis (neglecting adhesion and deformation of the brush), the YoungâĂŹs Modulus of the bead was determined to be in the order of 1 MPa. The SCP was washed with water, dried in a stream of nitrogen and mounted into the AFM holder. Prior to every measurement, the optical lever sensitivity (INVOLS) was determined via a noncontact approach with an error for the applied load of about 15 %. The SCP was pressed against the substrate with a defined force using the AFM feedback loop. Data were collected at discrete load-force intervals of 500 nN with a maximum force of 8 μN. All data are averaged values of measurements on at least three different lateral positions on the substrate.

CLSM
The CLSM was equipped with an EC "Plan-Neofluar" 20x/0.50 M27 objective. Images were acquired with a resolution of $(0.104X0.104)\,\mu m^2$ at a pinhole size of 1 airy unit (= 4.4 μm). Fluorescence was excited at a wavelength of 488 nm and emission was detected from 492 to 625 nm. The focus plane was set to the plane of maximum fluorescence intensity. For P(METAC-co-AEMA) brushes, the master gain (a measure of the power applied to the photodetector) was set to 650 at a laser power of 5%. Neutral brushes showed a higher fluorescence intensity and strong bleaching which made it necessary to reduce the laser power to 0.5%. Images were processed with an ImageJ macro. The radial intensity distribution from the center of the compression zone to the undisturbed background was extracted by averaging the grey value of the images over an angle phi (see below).

Characterization of cationic and neutral brushes

Growth kinetics of cationic homo-and copolymer brushes

Growth kinetics of cationic homo-and copolymer brushes: Figure 4.5

Film thickness and fluorescence intensity of cationic and neutral brushes

Correlation of film thickness as a function of salt concentration and fluorescence intensity of cationic and neutral brushes see Figure 4.6.

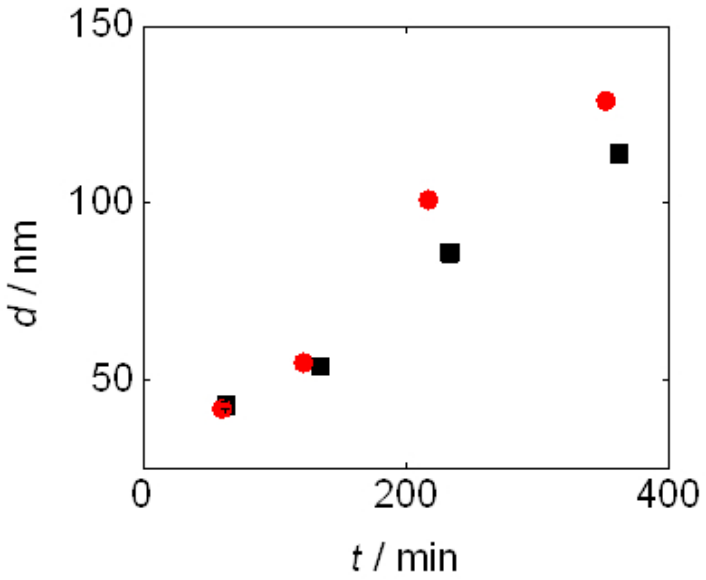

Figure 4.5: Growth kinetics of PMETAC (black □) and P(METAC-co-AEMA) (red ◯) with an AEMA concentration of 10 mol − % in the feed. The dry film thickness d increases linearly with polymerisation time. Growth kinetics of homo- and copolymer brushes are very similar.

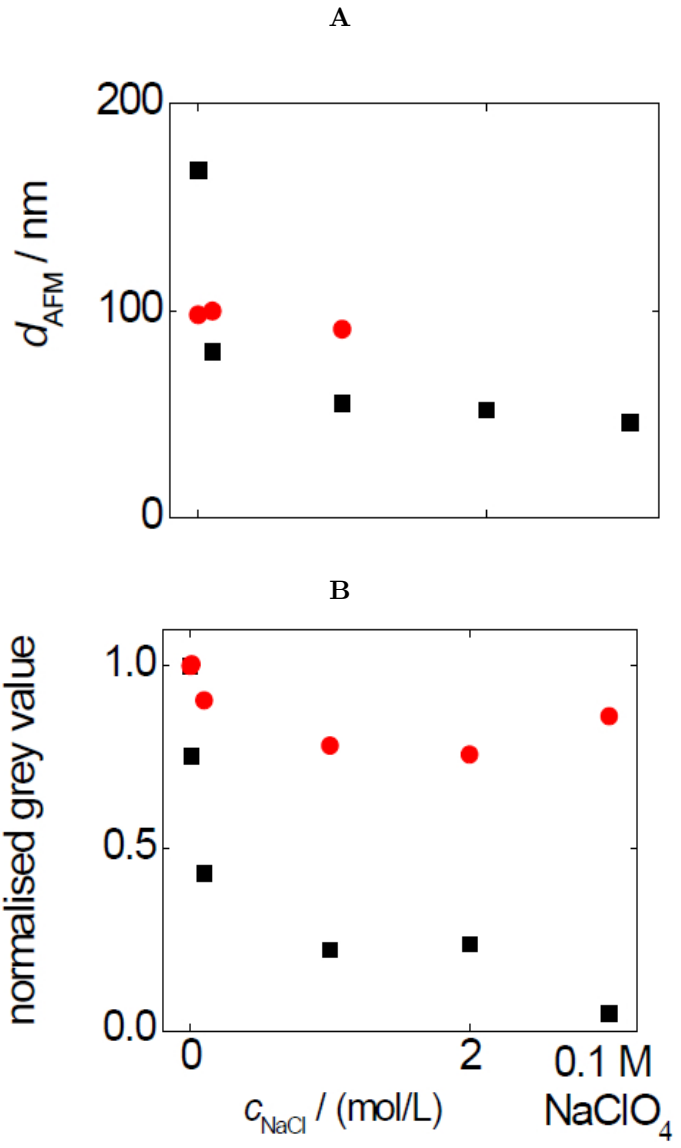

Figure 4.6: 4.6A Film thickness measured by AFM in liquid of P(METAC-co-AEMA) (black □) and P(HEMA-co-AEMA) (red ○) brushes in water, NaCl solutions and 0.1 M $NaClO_4$ solution after the covalent attachment of carboxyfluorescein. Values on the left side refer to water and NaCl solutions of various concentrations; the value on the right side was measured in 0.1 mol/L aqueous $NaClO_4$. The thickness of cationic brushes depends strongly on the salt concentration whereas neutral brushes show little response to the addition of salt. 4.6B Fluorescence intensity of uncompressed brushes immersed in water and salt solutions. Cationic brushes show a strong decrease of fluorescence intensity with increasing salt concentration; the fluorescence intensity of neutral brushes is much less affected by the addition of salt.

Apparent dye concentration

The apparent dye concentration in the brushes was measured by UV-vis spectroscopy using the following procedure. Calibration was realized by dissolving 0.002−0.08 mmol/L carboxyfluorescein in water. Spectra were acquired in a wavelength regime from 400 − 600 nm. The peak height at 480 nm was plotted versus the bulk concentration and the slope of a linear fit to the data was determined to be 8.2. With Beer's law 4.3

$$E_\lambda = -\lg \frac{I_1}{I_0} = \epsilon_\lambda c d, \tag{4.3}$$

where E_λ is the extinction, I_1 and I_0 are the intensities of transmitted and irradiated light, respectively, ϵ_λ is the molar absorbtivity, c is the dye concentration, and d is the path length (here: thickness of cuvette, 0.1 dm) it follows that $\epsilon_\lambda = 82\,\mathrm{dm}^2/\mathrm{mmpl}$.
A droplet of water was added to the surface of glass cover slips covered with brushes. Samples were sandwiched between two PDMS slides and mounted in a home-built holder with a hole (Ø≈ 1 cm) through which the light beam could pass. The maximum intensity was detected at 480 nm. The dye concentration was calculated from

$$c^{\mathrm{app}} = \frac{E_\lambda}{\epsilon_\lambda d_{\mathrm{brush}}}, \tag{4.4}$$

where c^{app} is the apparent dye concentration in the brush and d_{brush} is the thickness of the brush in water.

pKa of carboxyfluorescein attached to charged and neutral brushes

The pKa of carboxyfluorescein covalently attached to brushes was measured with the CLSM by detecting the fluorescence intensity of brushes in contact with diluted HCl and NaOH solutions whose total salt concentration was adjusted to 10 mmol/L by addition of NaCl. Titration curves were fitted with a sigmoidal fit using Microcal Origin 6.0. The inflection point of the fit is the pKa of the dye bound to the brush. (see Figure 4.7)

Film thickness and fluorescence intensity of cationic and neutral brushes

Correlation of film thickness as a function of salt concentration and fluorescence intensity of cationic and neutral brushes see Figure 4.6.

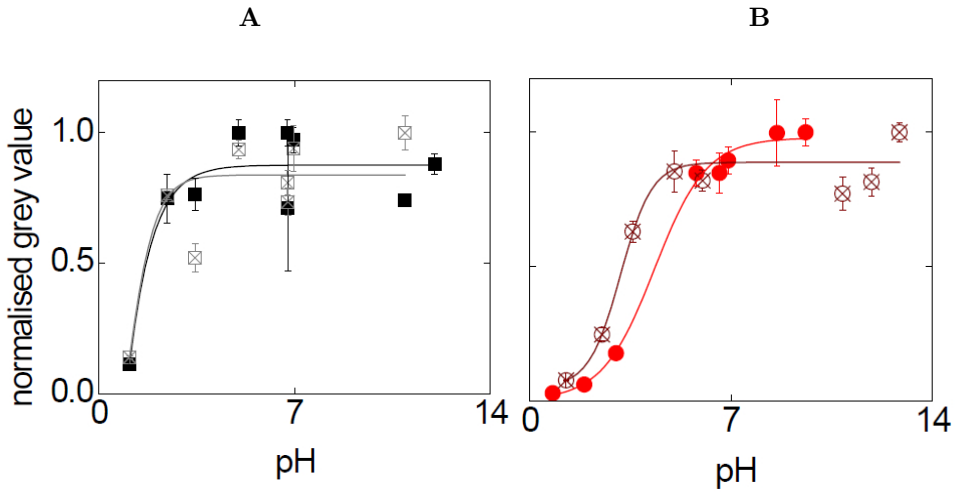

Figure 4.7: Fluorescence intensity, normalized to maximum value, of two titration experiments on 4.7A cationic P(METAC-co-AEMA) (squares) and 4.7B neutral P(HEMA-co-AEMA) (circles)) brushes as a function of pH. Straight lines represent sigmoidal fits to the curves. The inflection point of the fit curve corresponds to the pKa of the dye in the brush. The average pKa was 1 and 3.8 in charged and neutral brushes, respectively.

Bulk Experiments of CF-solutions

Variation of NaCl concentration

The fluorescence of 0.03 mM CF-solution is not affected by the salt concentration.

Dependence of fluorescence on pH

The pKa of carboxyfluorescein in bulk solution was determined by fluorescence spectroscopy of a solution of 0.03 mmol/L dye in diluted HCl and NaOH solutions with an ionic strength 0.01 M NaCl (see Figure 4.8).

Self quenching of CF

Selfquenching of CF, see Figure 4.9.

Quenching of the dye by METAC

Quenching of CF by the monomer of the polymer brush (METAC), see Figure 4.10.

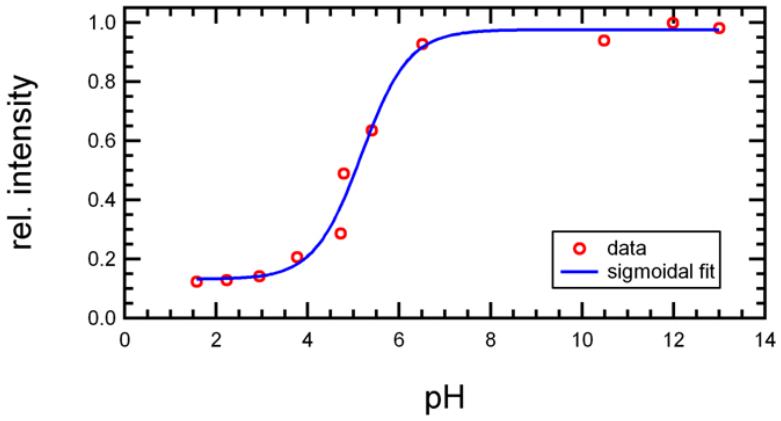

Figure 4.8: Change of pH, CF concentration: 0.03 mM, salt concentration: 0.01 M NaCl; Decrease of fluorescence by decrease of pH, pKa of bulk solution: 5.2. (Lit.: pKa of bulk solution: a: 6.5)

Details on force experiments

Force-distance curves

Exemplary force distance curve of a soft colloidal probe interacting with the brush, see Figure 4.11.

Adhesion in water and NaCl solutions

Interaction engergy between probe and brush, depending on the solution conditions, see Figure 4.12.

Hysteresis

Adhesion hysteresis between probe and brush, see Figure 4.13

Correlation of intensity and pressure profile

Details on JKR theory [17]

The system PDMS bead pressed against a substrate functionalized with a P(METAC-co-AEMA) brush can be described by contact-mechanic theory. H. Hertz presented the first analytic description of two isotropic, homogeneous linear elastic bodies in contact, but without adhesion. If one takes adhesion into account there are several models which apply for certain conditions of contact behavior. The two most common theories were developed by Johnson, Kendall and Roberts (JKR theory) and Derjaguin, Muller and

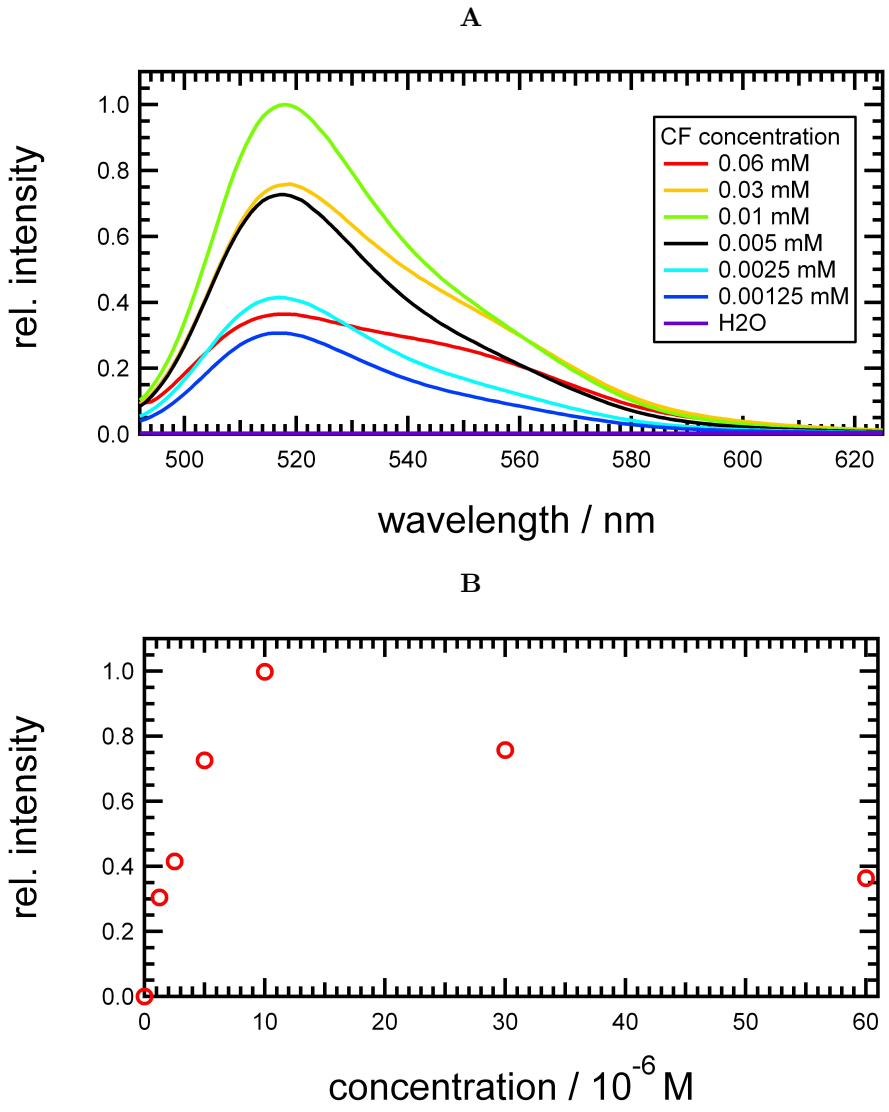

Figure 4.9: 4.9A Emission spectra of CF solutions with different CF concentrations, 4.9B Maxima of the emission spectra as a function of CF concentration

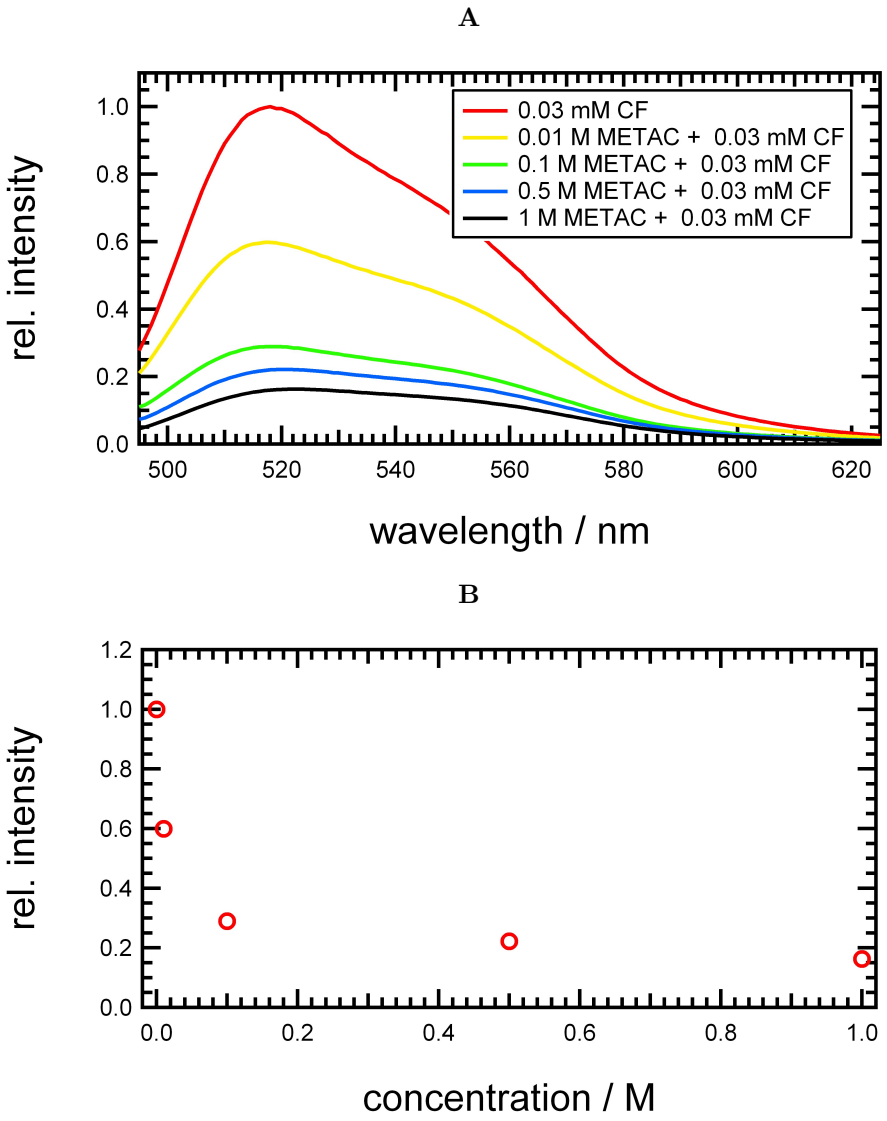

Figure 4.10: Quenching of 0.03 mM CF solution by METAC. 4.10A Emission spectra of CF solutions with different METAC concentrations, 4.10B Maxima of the emission spectra as a function of METAC concentration

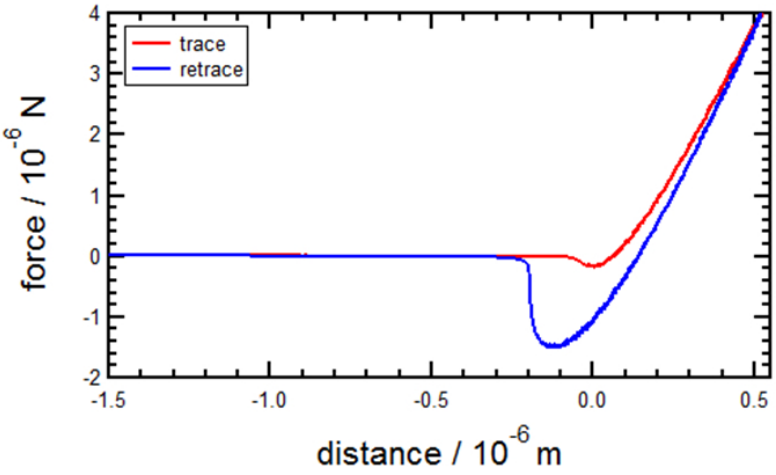

Figure 4.11: Typical force distance curve of a SCP pressed onto a P(METAC-co-AEMA) brush in water. Red line: approach, blue line: retraction. As expected, adhesion is much higher when the PDMS bead is retracted from the surface

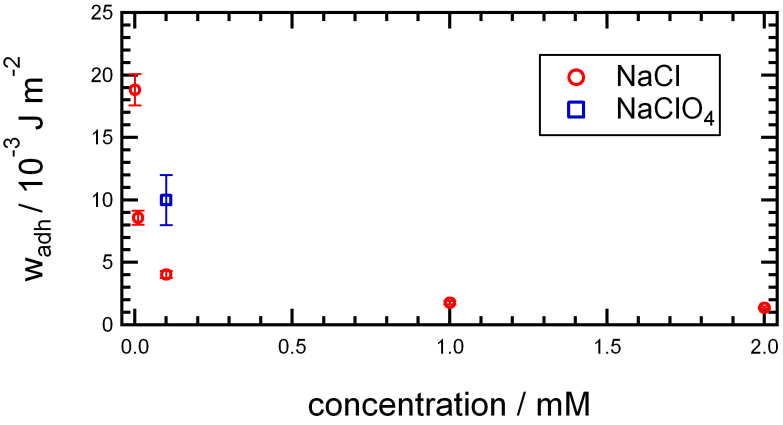

Figure 4.12: Interaction energy per unit area, measured between a PDMS bead and a P(METAC-co-AEMA) brush at various concentrations of sodium chloride. The adhesion force is high in water but drops with increasing salt concentration. The same behavior is observed for the bright rim: Being brightest in water and 0.1 M NaCl, the fluorescence intensity at the rim drops significantly at high salt concentrations. The values result from analysis of force distance curve. The lowest point in the retraction curve is defined as the adhesion force. This force can be accounted to an adhesion energy per unit area by JKR analysis. As well we determine the work of adhesion Wadh (area of the force curve under the baseline). Simultaneously we measure the contact radius a of the adhesion area at maximum load. The adhesion energy per unit area w can than calculated according to dividing Wadh by πa^2. Both procedures lead to a value in the same error range.

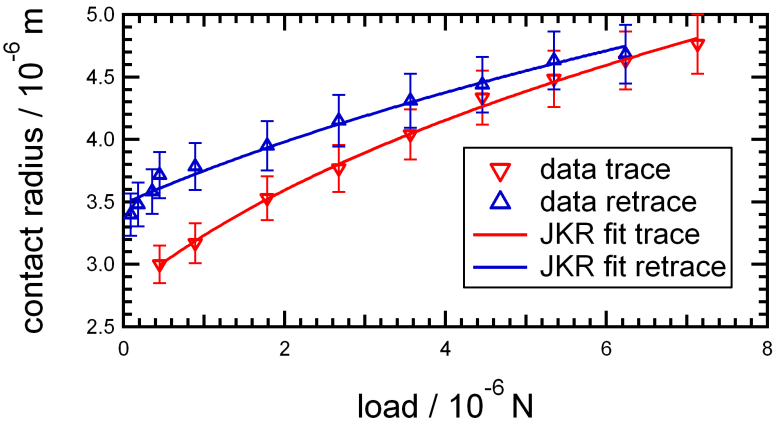

Figure 4.13: With increasing force, the contact area became larger due to elastic deformation of the PDMS bead. When retracting the bead from the brush, the radius of the dark contact area decreased with a significant hysteresis which is a result of adhesion forces acting between the bead and the brush. The data (PDMS bead against a P(METAC-co-AEMA) brush in water) follow the JKR prediction. Fit data are in line with force distance measurements: retrace $w = 28 \pm 1\,\mathrm{mJm^{-2}}$, $E = 0.79 \pm 0.05\,\mathrm{MPa}$ for $R = 15\,\mu\mathrm{m}$ (for trace $w = 12 \pm 1\,\mathrm{mJm^{-2}}$, $E = 0.7 \pm 0.1\,\mathrm{MPa}$ for $R = 15\,\mu\mathrm{m}$)

Toporov (DMT theory). This limits can be quantified with the Taborparameter. For the contact situation of a PDMS bead against a hard substrate the JKR limit is valid. We look on a sphere with a radius R and a reduced modulus $K = 4/3E(1-\nu^2)^{-1}$ (E: Young's modulus of the sphere, ν: Poisson ratio of the sphere) in contact with a flat hard substrate. The contact radius is called a. With assumptions $d, a << R$, where $(R-d)$ is the distance between center of the sphere and the flat substrate, one can make an ansatz for the pressure distribution in the contact area

$$p(r) = p_0 \left(1 - \frac{r^2}{a^2}\right)^{1/2} + p_1 \left(1 - \frac{r^2}{a^2}\right)^{-1/2} \tag{4.5}$$

This equation holds three unknown variables, p_0, p_1, and a. To get these variables we require that the total energy of the system attains a minimum at a constant d. The total energy contains elastic and adhesive parts. One can show that

$$p_0 = \frac{3Ka}{2\pi R} \text{ and } p_1 = -\sqrt{\frac{2Kw}{2\pi a}} \tag{4.6}$$

and

$$a^3 = \frac{R}{K}\left(P + 3\pi Rw + \sqrt{6\pi RwP + (3\pi Rw)^2}\right) \tag{4.7}$$

Table 4.1: Measurement conditions and values for calculating the pressure profiles at various concentrations of sodium chloride and sodium perchlorate: R probe radius, E Young's modulus of the probe detected by Hertz analysis, w adhesion per unit area between a PDMS bead and P(METAC-co-AEMA) brush acquired as described above

solution	$R/\,\mu$m	$E/$ MPa	$w/$ mJm^2
H_2O	15 ± 1	0.8 ± 0.2	19.0 ± 7.0
0.1 M NaCl	15 ± 1	0.8 ± 0.2	4.0 ± 0.5
1.0 M NaCl	15 ± 1	0.8 ± 0.2	2.1 ± 0.3
0.1 M $NaClO_4$	15 ± 1	0.8 ± 0.2	10.0 ± 2.0

As mentioned above the assumption for use of these formulas is that $R >> a$, otherwise finite size effect have to be taken into account. Here we use probes with a radius in the range of 15 μm. The contact radius at 5 μN is around 4 μm. Therefore the ratio of probe radius to contact radius is around 10:2 and finite size effects are negligible and in the order of the error (around 5% of the contact area, around 10 % of pressure). In our case we press the soft PDMS bead onto the polyelectrolyte brush attached to a glass substrate. In a simplified approach, the substrate functionalized with a polyelectrolyte brush is regarded as a hard substrate.

Results from correlation procedure

Values for calculating the pressure profiles, see Tab. 4.1. Correlation of Intensity and pressure at different solution conditions, see Figure 4.14

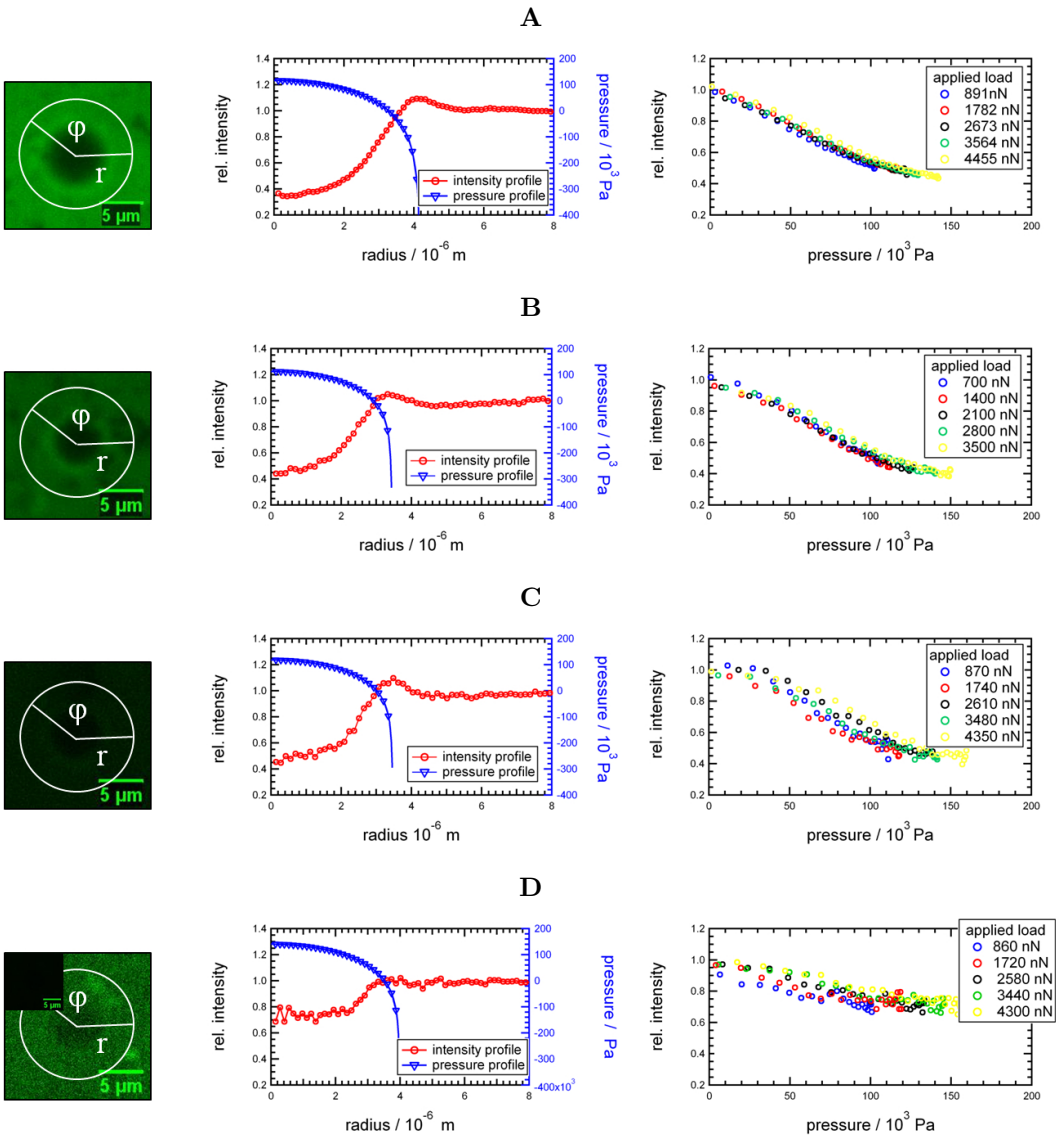

Figure 4.14: Details of the correlation procedure: Left column: detected data for measurements in 4.14A H_2O at 1782 nN, 4.14B 0.1 M NaCl at 1400 nN, 4.14C 1.0 M NaCl at 1740 nN and D) 0.1 M $NaClO_4$ at 1720 nN while retraction. 4.14D shows the data after contrast enhancement, inset original data. Middle column: extracted intensity profiles and calculated pressure profiles of the left column. Right column: Intensity profiles correlated to the pressure for five different applied forces in the order of 1 to 5 μN while retracting.

5

Phototunable Surface Interactions

Erath, J., Cui, J., Schmid, J., Kappl, M., del Campo, A., Fery, A., Phototunable surface interactions. Langmuir, 2013. 29(39): p. 12138-44.

Abstract

Photoresponsive polymer brushes constitute an attractive platform for tuning surface properties and functionality. Since the degree of photoconversion can be controlled by the light dose, functional states with intermediate properties between those of the nonexposed and fully exposed brushes are accessible. Here we investigate the light-modulated interfacial, adhesion, and frictional properties of photosensitive polymer brushes with a methacrylate backbone and ionizable -COOH side groups modified with the photoremovable group 6-nitroveratryloxycarbonyl (NVOC). The original brush (PNVOCMA) gradually changes into a charged poly(methacrylic acid) (PMAA) brush upon exposure to ultraviolet light due to the photoremoval of the chromophore and generation of free COOH groups. We show how the physical properties of the brush can be gradually tuned with the exposure dose using condensation microscopy, atomic force microscopy (AFM), force mapping, and friction force spectroscopy.

5.1 Introduction

Responsive surfaces are able to change their physical properties (wettability, hydrophobicity, lubrication, adhesiveness etc.) in response to external triggers. Application of such systems have been reported in micro/nanofluidics systems, mechanical actuation and chemical sensing, biotribology, controlled drug release, and cell growth and separation, among others [1, 2]. Typical external triggers can be of physical (temperature, electric or magnetic fields, pressure, light), chemical (pH, salt concentration), or biochemical (enzymes) nature [1, 3, 4, 5, 6, 7]. Polymer brushes are attractive systems for generating responsive surfaces because of their robustness and flexibility with respect to their chemical composition, functionalization, and architecture [8, 9, 10]. The property change in responsive polymer brushes is associated with a change in the conformation and swelling of the chains from a extended (hydrated) to a collapsed state or vice versa. Typically this occurs abruptly in response to a change in solvent, temperature, or pH within narrow ranges. Other brush systems combine two or more responses and display adaptive or gated property changes [11, 12]. Modulation of the brush response (and subsequent properties) has been mostly realized by changing the brush length, brush composition via copolymerization, or the packing density using variable grafting densities of the initiator molecules [9, 10, 13]. Combining these methods with lithographic and soft lithographic techniques, gradient surfaces have been realized [14]. Modulated wettability was achieved by such brush substrates and applied to fouling-resistant sur-

faces [15], to sliding surfaces for friction reduction [16], and to microfluidics [17] and lab-on-a-chip devices [18]. Remote modulation of the wettability of brush layers [12, 19, 20, 21, 22] and the permeability of brush-coated membranes [23] using light has also been achieved by incorporating azobenzene or spiropyrane derivatives as chromophores in the brush constituents.

Within the past decade, charged polymer brushes (polyelectrolytes) have been largely studied for (bio)lubrication purposes [24, 25, 26, 27, 28, 29]. The length and grafting density of the brushes and the charge density along the chains are crucial parameters affecting chain mobility and interpenetration and, finally, the friction force. To our knowledge, modulation of the adhesion and frictional properties of brush layers using tunable, lightdriven changes of the charged group density without varying the brush length or grafting density has not been attempted. In this manuscript, we report on the interfacial, adhesion, and frictional properties of tethered photoionizable polymer brushes and investigate their modulation using light exposure. We have recently reported on photoresponsive polymer brushes with light-triggered charge development and swelling changes [30, 31, 32, 33], and we demonstrated their possible application for light-gated ion transport through membranes. These brushes are based on a poly(acrylic acid) backbone where the main-chains have been modified with a 6-nitroveratryloxycarbonyl (NVOC) photocleavable protecting group. In the protected ("caged") state, the brush is neutral. Upon light exposure, the chromophores are removed from the brush structure, and a dose-dependent density of free carboxylic groups is generated. The changes in the molecular structure result in a change of the physical properties, i.e., swelling and permeability [30, 31, 34]. We expected that the light-triggered generation of charged groups would also affect the surface potential and thereby the interfacial surface forces[4, 35, 36, 37, 38, 39, 40, 41, 42]. The light-dependent compositional change should allow us to define intermediate interfacial states between the caged and fully deprotected forms, or a gradual transition between them. We analyze the change of the surface properties of brush covered substrates as a function of the conversion state using wettability measurements [4, 5, 37, 43], atomic force microscopy (AFM), force mapping [44, 45, 46, 47, 48], and friction force spectroscopy [47, 49, 50].

5.2 Experimental

Preparation of Brush Layers

Silicon wafers or quartz slides coated with poly(6-nitroveratryl methacrylate) (PNVOCMA) brushes were prepared via Surface-Initiated Atom Transfer Radical Polymerization (SI-ATRP)[8] as previously reported [30, 31] (Figure 5.1). The obtained brushes had a molecular weight of $Mn = 13300\,\mathrm{g/mol}$ with a Polydispersity Index PDI = 1.48. The average grafting density was $0.56\,\mathrm{chains/nm^2}$, as estimated from AFM and UV spectroscopy data. This analysis was also used as control for the synthesis step. The functionalized Si substrates were glued with epoxy onto glass slides for further investigation.

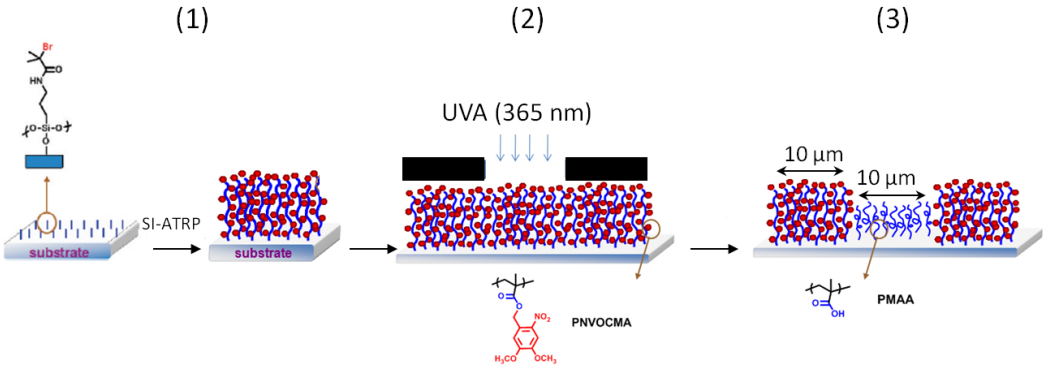

Figure 5.1: Preparation of patterned (PNVOCMA/PMAA) substrates: 1) synthesis of the polymer brush via Surface-Initiated Controlled Radical Polymerization, 2) irradiation of the sample using a LED source and a mask for site-selective photocleavage and generation of surface patterns, 3) exposed and unexposed regions show differences in brush height and chemical composition.

Light Exposure and Photocleavage of the NVOC Groups from the Brush

The brush layers were irradiated using a LED source (LED-UV lamp LTPR 360, OPTO Engineering, Germany) at 365 nm ($4.7\,\mu\mathrm{Wcm^{-2}}$) for photocleavage of the NVOC group. The exposed area was ca. $1\,\mathrm{cm^2}$. After irradiation the substrates were washed with ethanol, buffer of pH 9, and then buffer of pH 4 for removing the photolytic byproducts. The deprotection step was followed by UV spectroscopy analysis of brush layers grafted from quartz substrates after light exposure. The kinetics of photolytic process was extracted from these data (Figure 5.2). The required irradiation doses for 0%, 25%, 50%, 75% and 100% conversion were extrapolated from there (see Results and Discussion section 5.3, Figure 5.2) [30, 31].

Generation of Surface Patterns

The substrates were irradiated through a quartz mask with 10x10 μm^2 chrome squares separated by 10 μm spacings. The mask was placed on the substrate during exposure (5.1). In this way an internal standard (i.e., the brush layer before exposure) was conserved in the experiment and comparison between different substrates was possible [4, 35, 51].

Condensation Microscopy for Qualitative Control of Photoconversion

Condensation microscopy was used to monitor the photoconversion of the PNVOCMA brush to the hydrophilic PMAA brush in response to UV irradiation [4, 52]. The substrate was placed on top of a closed petri dish filled with dry ice (Supporting Information, Figure 5.8). Condensation results in nucleation and growth of water droplets on the substrate surface which were monitored using a KS100 Imaging-system (Zeiss, Jena).

Atomic force microscopy

Imaging: The film thickness of the polymer brush layer grown from a silicon substrate was measured by AFM imaging the topology of a scratch (made with a needle). The AFM (MFP-3D) was operated in contact mode using a silicon cantilever (CSC17) with a spring constant of about 100 mN/m. Height images of the patterned substrates after masked irradiation (contrast between 0%, and 100% conversion) were taken under basic pH condition in salt solution (0.1 mM NaCl, pH 9.5 adjusted with NaOH).
Force Spectroscopy: Interactions between the PNVOCMA brush and an AFM tip before and after gradual light exposure were measured using an AFM (MFP-3D, Asylum Research, Santa Barbara) and cantilevers CSC 17 (noAL) with a spring constant of 100 mN/m. Tips of CSC 17 cantilevers where modified by plasma treatment (O_2 plasma, 0.2 mbar at 0.1 kW, 5 min; flecto10, Plasma Technology, Germany) prior to the measurements. The spring constants and the optic lever sensitivity of the cantilevers were determined by the thermal noise method prior to the measurement [53]. The force-distance curves were recorded using the following parameters (if not mentioned otherwise): the speed of the z- piezo actuator was set to 0.1 μs^{-1}, and the trigger point to $2 - 10$ nN. The force-distance curves were measured on different spots using the force-mapping mode. Measurements were undertaken on at least 100 spots on a 50x50 μm^2 grid on the substrate. The force spectroscopy measurements were performed in a droplet of salt solution (0.1 mM NaCl, pH 9.5 adjusted with NaOH) at

room temperature. The solution was changed at least every 30 min to ensure basic pH conditions during the measurement. After changing the solution, the sample was equilibrated for at least 2 min. The optical lever sensitivity was measured after each exchange.

Quantitative Imaging: In the so-called Quantitative Imaging (QI) mode of the Nanowizard 3 AFM (JPK Instruments, Berlin), a force curve was recorded at each image pixel within 10 ms with an image size of 128x128 pixels. From the stored array of force curves, post-processing of the force curves allows to extract for each pixel information such as height (sample topography), adhesion force, or magnitude of repulsive forces acting on the AFM tip.The cantilevers were plasma treated prior to the experiment to create a SiO_2 surface on the cantilever tip (O_2 plasma, 5 min). For the measurements cantilevers CSC 17 (noAL) with a spring constant of about 100 mN/m were used. The measurements where done in a droplet of salt solution (5 mM NaCl, pH 9.5 adjusted with NaOH) at room temperature. Spring constant and optical lever sensitivity are detected as reported in force spectroscopy. The relative setpoint, i.e. the maximum applied force during force curves, was set to 10 nN.

Friction Force Measurements: The friction contrast of the brush layers before and after light exposure was imaged using an AFM (Nanowizard 3, JPK,Berlin). For the measurements plasma treated cantilevers CSC 17 (noAL) with a normal spring constant of about 100 mN/m were used. The measurements where done in a droplet of salt solution (5 mM NaCl, pH 9.5 adjusted with NaOH) at room temperature. Measurements were undertaken on at least 256x256 Points of a 50x50 μm^2 spot of the substrate respectively 15x15 μm^2 at normal load of 5 nN and 1 Hz scanning rate.

The lateral force coefficient was calibrated following the procedure developed by Anderson et al. [54], prior to the experiment at same conditions.

5.3 Results and Discussion

Photoresponsive PNVOCMA brushes were prepared by surface initiated atom transfer radical polymerization (Si-ATRP) (Figure 5.1) and characterized as described in the Experimental Section. Light exposure of the brush lead to photocleavage of the 6-nitroveratryl units and from the brush backbone and formation of free carboxylic acid ionizable side groups. The density of COOH groups along the chain depends on the exposure dose. Random copolymers of NVOCMA and methacrylic acid (MAA) were obtained at intermediate doses and PMAA homopolymer was obtained after full exposure. We do not expect a gradient in the deprotection degree across the layer thickness

since control experiments show a negligible decay ($< 3\%$) in the light intensity through the substrate. The degree of photoconversion was determined by UV spectroscopy analysis of brushes grafted from quartz substrates and irradiated for different times. The relationship between photoconversion and irradiation time was obtained from the loss in absorbance at $\lambda_{max} = 348\,nm$ after increasing irradiation times and washing, which is associated with the loss of the chromophore from the brush layer (Figure 5.2) [30, 31]. For the present analysis, samples with 0%, 25%, 50%, 75%, and 100% photoconversion were selected.

The light-modulated generation of hydrophilic COOH groups along the brush was analyzed indirectly by the quartzcrystal microbalance (QCM) technique. Light exposure results in a gradually more hydrophilic brush that swells in water, especially when these are ionized at basic pH. QCM allowed in situ monitoring of the hydration of the brush during increasing light exposure (see Refs. [30] and [31] for more details). Figure 5.2 represents Δf values for different photolytic conversions. An increase in mass during exposure, i.e., water uptake, was clearly seen by the decrease of the measured frequency shift. Water uptake did not linearly correlate with the conversion and 80% of the total swelling occurred at conversions between 40 and 80% (Figure 5.2). The light-dependent change in the brush properties, therefore, is expected to be more effective between 40 and 80% conversion values.

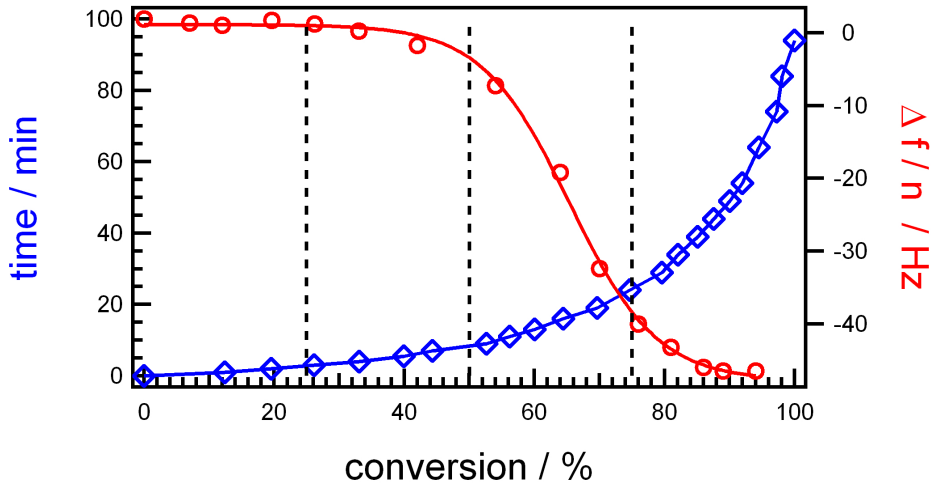

Figure 5.2: Photo-conversion of PNVOCMA brushes: irradiation time vs. conversion (squares) and $\Delta f/n$ vs. conversion (circles) plots. n represents the overtone of frequency and here the third overtone (Data are reproduced from Ref. [31].)

A qualitative control and visualization of the wettability differences between the PNVOCMA and the PMAA brushes was obtained by condensation microscopy on masked

irradiated substrates (Figure 5.3). Water drops preferentially condensed on the exposed regions, i.e., PMAA-rich areas that are more hydrophilic than the unexposed PNVOCMA ones [37] and revealed a clear wettability contrast. The borders between illuminated and nonilluminated areas were sharp within the accuracy of the optical resolution, indicating an explicit wettability contrast between irradiated and nonirradiated areas. These results proof that photocleavage occurs selectively at the irradiated areas. We could not observe differences for the different conversion states.

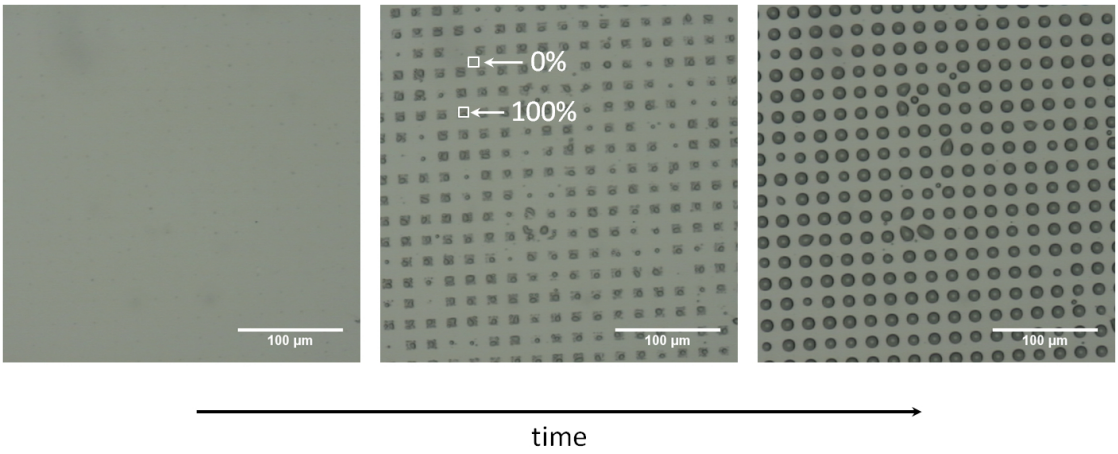

Figure 5.3: Condensation microscopy image of a 100% deprotected brush pattern as a function of time (approx 2 min)

Height changes in the brush layer after irradiation were analyzed using imaging AFM in a scratch assay. The brush height before irradiation was 9 nm and changed to 6 nm after full photoconversion as a consequence of the loss of the bulky chromophore from the brush layer. AFM analysis of the topography on patterned brush layers (100/0% photoconversion) confirmed these results, and the exposed regions appeared as deepened squares in the topography image (see Figure 5.9). The height difference between unexposed and fully exposed brushes at pH 9.5 was $2-4$ nm. This results are in agreement with previous studies on this system [4, 31].

AFM was also used to investigate the light-dependent surface interactions. Force spectroscopy and friction measurements were performed to analyze the interactions between an oxidized Si tip and the brush layer. Force spectroscopy imaging on patterned substrates (100% photocleavage on exposed areas) using an oxidized Si tip revealed a clear contrast between PMAA and PNVOCMA areas at pH 9.5 (Figure 5.4A). Adhesion force at irradiated parts decreased due to repulsive electrostatic double layer interactions between the charged brush and the cantilever tip (labeled with arrows in Figure 5.4B). At the same time, the repulsive part in the force versus distance curves became

more pronounced, which confirmed that irradiated parts are charged. Other forces acting between the AFM tip and the surface grafted with the polymer brush might also contribute to these results, i.e. steric interactions, solvent forces or vdW forces. The contrast was also visible on patterned substrates at 75% photoconversion, but almost not detectable for 50% and 25% photoconversion (see Figure 5.4A). These observations agree with the QCM results (Figure 5.2) that showed low water uptake of the brush film for conversions $< 50\%$. The hydrophobic character of the brush in this case does not allow effective swelling and hinders electrostatic interaction between the partially deprotected brush and the charged tip.

In order to quantify the increase in the repulsive interactions for higher exposure doses, we performed QI imaging (see Experimental Section) of the substrates at pH 9.5. In QI mode 128x128 force distance curves were recorded for each image. To obtain a measure of the repulsive forces between AFM tip and brush, we analyzed the slope within the repulsive parts of each approach force curve. The slope of the repulsive parts of the force distance curves during the approach between PNVOCMA/PMAA brushes and the plasma treated tip will depend on the electrostatic repulsion. For non- or weakly charged and swollen brushes, a steeper slope is expected (upper curve in Figure 5.4B), whereas in the presence of long-range electrostatic repulsion (after photoconversion), a less steep slope is expected (lower curve in Figure 5.4B). The slopes extracted from each force curve are plotted in Figure 5.5 as "slope maps". The slope at irradiated parts (darker areas) is smaller than at nonirradiated parts. Decreasing slopes were observed on substrates with increasing photoconversion (Figure 5.5). This behavior confirms the increase in the brush charge with the photoconversion and, therefore, higher electrostatic repulsion and changes in steric interactions and solvent forces. No contrast could be observed on the substrates with 25% and 50% conversion, in line with results from QCM and force spectroscopy measurements.

We then analyzed the friction behavior of substrates with different photodeprotection degrees by imaging the surface in contact mode. Lateral deflections of the cantilevers were detected and converted into friction force using a previously determined calibration factor (see Experimental Section). Figure 5.6 shows the lateral force (trace minus retrace signal) across the patterned sample. The friction force pattern showed clear contrast between not exposed and exposed areas in the samples with 50%, 75%, and 100% photoconversion at pH 9.5 (Figure 5.6). Interestingly, the threshold value of the photoconversion for friction contrast between exposed/nonexposed brushes was $> 50\%$, significantly lower than for contrast in swelling or adhesion properties. Friction measurements are obviously more sensitive to the photoinduced changes in the molecular

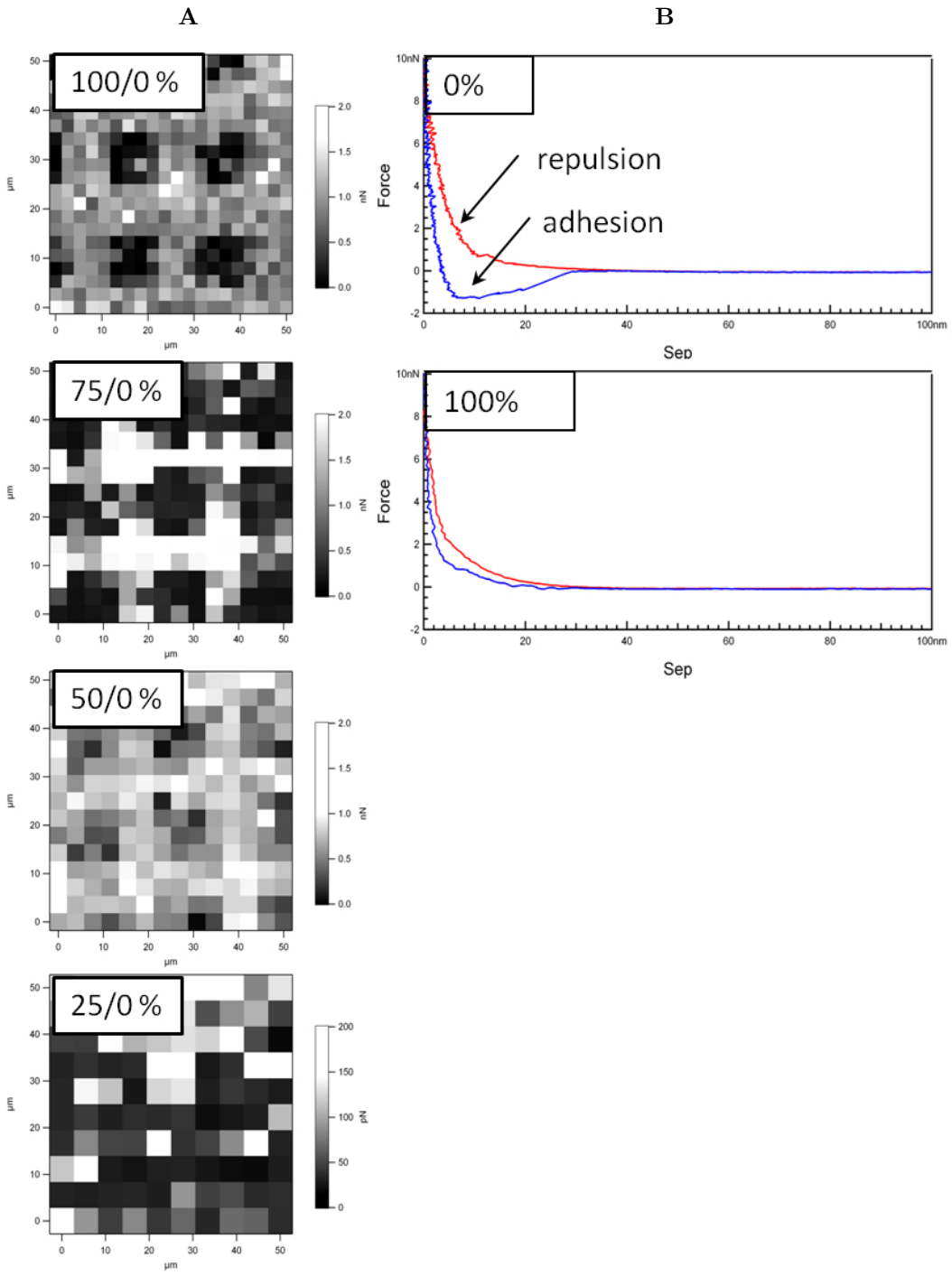

Figure 5.4: Interaction contrast of oxidized Si tip and the patterned substrate of PNVOCMA and PMAA: 5.4A Adhesion force of different conversion states extracted from force mapping data. 5.4B Exemplary force curves for 0% and 100% conversion

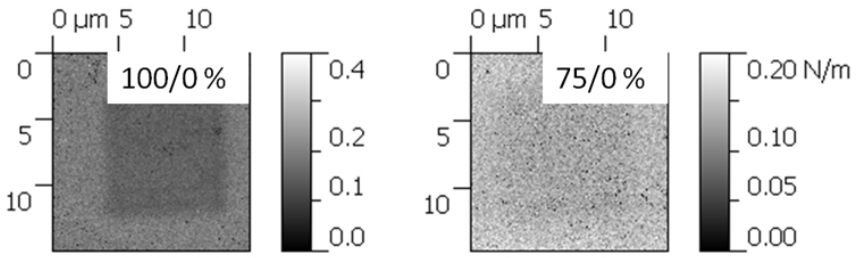

Figure 5.5: Change of repulsive interactions of 100/0% and 75/0% conversion states, detected with the quantitative imaging mode

composition of the brush than the other properties.
Figure 5.7A and 5.7B show histograms of the friction force for different conversion states normalized to the friction of the background (0% conversion). These findings point out a distinct increase of the friction contrast with increasing conversion state (Figure 5.7C). The friction forces of irradiated areas are larger than on nonirradiated areas. This was unexpected, since the repulsive force increase with increasing irradiation dose (respectively the adhesion decreases) as shown above and one might anticipate a lubricating effect of the swollen brush. We believe that this effect is either due to a plowing of the AFM tip through the brush leading to increased dissipation or due to a stronger penetration of the AFM tip through the more swollen and shorter brush layers. Consequently friction with the underlying silicon substrate (with a silica layer) increases.

5.4 Conclusion and Outlook

Photoresponsive brushes containing ionizable -COOH side groups protected with a NVOC photoremovable group allow light-driven tuning of surface interactions. The compositional change in the brush by photocleavage of the NVOC group and generation of ionizable COOH groups along the brush chain results in significant property changes between exposed and nonexposed brushes, which can be modulated by the exposure dose. The exposed areas become more hydrophilic and allow gradual tuning of wettability. Such an approach could be applied to the photomanipulation of the motion of liquids on brush layers [55, 56], or to prepare water harvesting surfaces [57]. More subtle changes in the surface interactions for intermediate chemical states (as a consequence of gradual deprotection degrees controlled by the irradiation dose) were quantified using force spectroscopy and friction measurements in the presence of basic

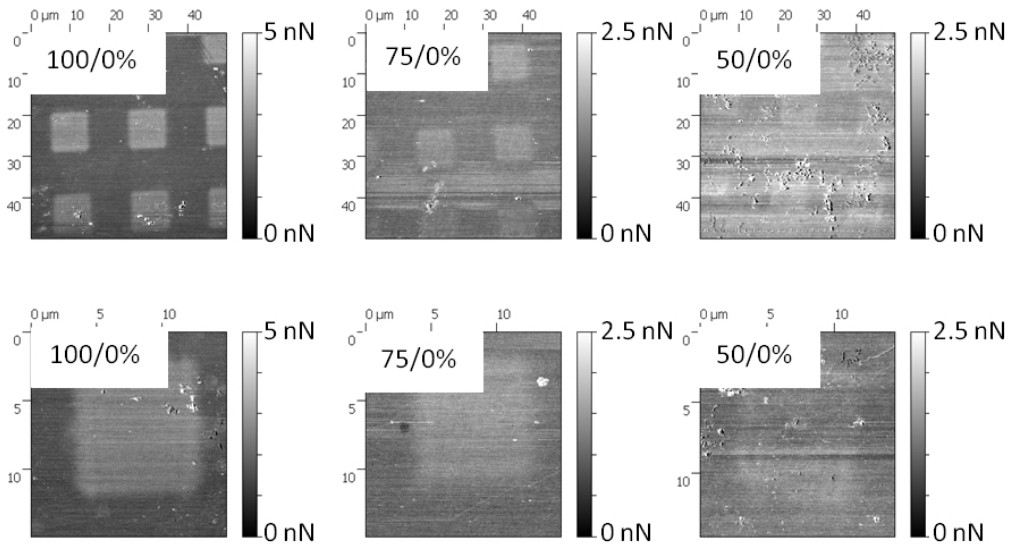

Figure 5.6: Friction forces of different conversion states. Friction contrast increases with increasing conversion

aqueous solution. Force mapping and quantitative imaging showed that adhesion forces decrease with exposure as a consequence of increased electrostatic repulsion between the PNVOCMA/PMAA brush and the negatively charged AFM tip. However, this decrease is only visible for PMAA content $> 75\%$ in the brush. Friction properties seems to be more sensitive than adhesion to the compositional changes. A continuous increase in friction contrast between PNVOCMA and PNVOCMA/PMAA areas was observed already at $> 50\%$ PMAA content in the brush. Our results indicate that PNVOCMA system is a potential platform for investigations of tunable surface interactions. Dose-dependent tuning of the photoconversion allows matching of surface properties for the desired application.

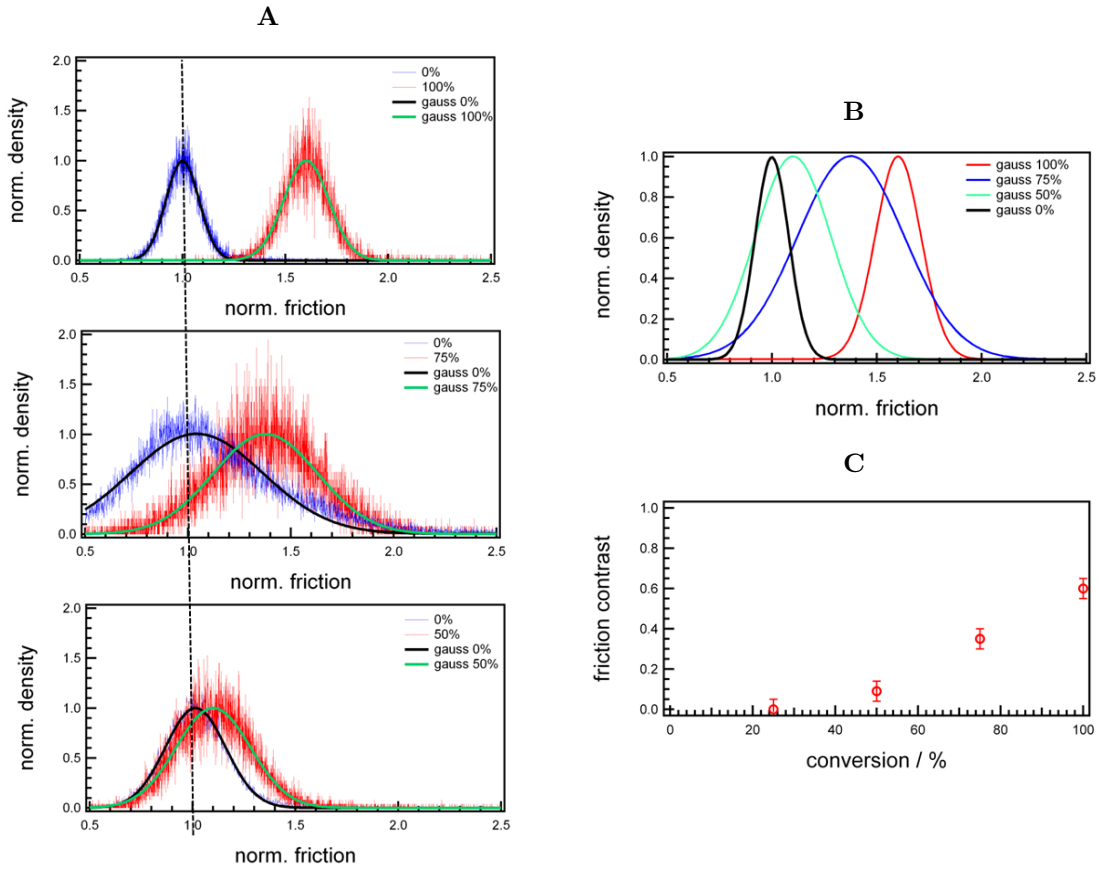

Figure 5.7: Friction contrast for different conversion states. 5.7A Evaluated histograms: friction force is normalized to the background. 5.7B Gauss fits of the different conversion steps. 5.7C Difference in normalized friction force between PNVOCMA and different conversion states to PMAA

5.5 References

[1] M. A. Cohen Stuart et al. "Emerging applications of stimuli-responsive polymer materials". In: *Nature Materials* 9.2 (2010), pp. 101–113.

[2] I. Tokarev, M. Motornov, and S. Minko. "Molecular-engineered stimuli-responsive thin polymer film: a platform for the development of integrated multifunctional intelligent materials". In: *Journal of Materials Chemistry* 19.38 (2009), pp. 6932–6948.

[3] J. Buensow et al. "Direct Correlation between Local Pressure and Fluorescence Output in Mechanoresponsive Polyelectrolyte Brushes". In: *Angewandte Chemie-International Edition* 50.41 (2011), pp. 9629–9632.

[4] A. A. Brown, O. Azzaroni, and W. T. S. Huck. "Photoresponsive Polymer Brushes for Hydrophilic Patterning". In: *Langmuir* 25.3 (2009), pp. 1744–1749.

[5] C. Hanske et al. "Adsorption of Spherical Polyelectrolyte Brushes: from Interactions to Surface Patterning". In: *Zeitschrift Fur Physikalische Chemie-International Journal of Research in Physical Chemistry and Chemical Physics* 226.7-8 (2012), pp. 569–584.

[6] J. Gensel et al. "Reversible swelling transitions in stimuli-responsive layer-by-layer films containing block copolymer micelles". In: *Chemical Science* 4.1 (2013), pp. 325–334.

[7] T. P. Russell. "Surface-responsive materials". In: *Science* 297.5583 (2002), pp. 964–967.

[8] R. Barbey et al. "Polymer Brushes via Surface-Initiated Controlled Radical Polymerization: Synthesis, Characterization, Properties, and Applications". In: *Chemical Reviews* 109.11 (2009), pp. 5437–5527.

[9] J. Buensow, T. S. Kelby, and W. T. S. Huck. "Polymer Brushes: Routes toward Mechanosensitive Surfaces". In: *Accounts of Chemical Research* 43.3 (2010), pp. 466–474.

[10] T. Chen et al. "Stimulus-responsive polymer brushes on surfaces: Transduction mechanisms and applications". In: *Progress in Polymer Science* 35.1-2 (2010), pp. 94–112.

[11] X. Laloyaux et al. "Bidimensional Response Maps of Adaptive Thermo- and pH-Responsive Polymer Brushes". In: *Macromolecules* 43.18 (2010), pp. 7744–7751.

[12] W. F. Yuan et al. "Temperature/light dual-responsive surface with tunable wettability created by modification with an azobenzene-containing copolymer". In: *Macromolecules* 39.3 (2006), pp. 1300–1303.

[13] A. Olivier et al. "Surface-initiated controlled polymerization as a convenient method for designing functional polymer brushes: From self-assembled monolayers to patterned surfaces". In: *Progress in Polymer Science* 37.1 (2012), pp. 157–181.

[14] S. Minko et al. "Gradient stimuli-responsive polymer grafted layers". In: *Stimuli-Responsive Polymeric Films and Coatings*. Vol. 912. ACS Symposium Series. 2005.

[15] Khooi Y. Tan et al. "Nonfouling Capture-Release Substrates Based on Polymer Brushes for Separation of Water-Dispersed Oil Droplets". In: *Acs Applied Materials and Interfaces* 4.12 (2012), pp. 6403–6409.

[16] J. Klein et al. "Reduction of Frictional Forces between Solid-Surfaces Bearing Polymer Brushes". In: *Nature* 370.6491 (1994), pp. 634–636.

[17] X. Liu et al. "Switching Water Droplet Adhesion Using Responsive Polymer Brushes". In: *Langmuir* 26.14 (2010), pp. 12377–12382.

[18] L. Ionov et al. "Smart microfluidic channels". In: *Advanced Functional Materials* 16.9 (2006), pp. 1153–1160.

[19] A. Dirani et al. "Reversible Photomodulation of the Swelling of Poly(oligo(ethylene glycol) methacrylate) Thermoresponsive Polymer Brushes". In: *Macromolecules* 45.23 (2012), pp. 9400–9408.

[20] A. Housni, Y. Zhao, and Y. Zhao. "Using Polymers To Photoswitch the Aggregation State of Gold Nanoparticles in Aqueous Solution". In: *Langmuir* 26.14 (2010), pp. 12366–12370.

[21] M. Piech and N. S. Bell. "Controlled synthesis of photochromic polymer brushes by atom transfer radical polymerization". In: *Macromolecules* 39.3 (2006), pp. 915–922.

[22] S. Samanta and J. Locklin. "Formation of photochromic spiropyran polymer brushes via surface-initiated, ring-opening metathesis polymerization: Reversible photocontrol of wetting behavior and solvent dependent morphology changes". In: *Langmuir* 24.17 (2008), pp. 9558–9565.

[23] Y. S. Park, Y. Ito, and Y. Imanishi. "Photocontrolled gating by polymer brushes grafted on porous glass filter". In: *Macromolecules* 31.8 (1998), pp. 2606–2610.

[24] U. Raviv et al. "Lubrication by charged polymers". In: *Nature* 425.6954 (2003), pp. 163–165.

[25] R. M. Bielecki, M. Crobu, and N. D. Spencer. "Polymer-Brush Lubrication in Oil: Sliding Beyond the Stribeck Curve". In: *Tribology Letters* 49.1 (2013), pp. 263–272.

[26] R. M. Bielecki et al. "Lubrication with Oil-Compatible Polymer Brushes". In: *Tribology Letters* 45.3 (2012), pp. 477–487.

[27] W. Hartung et al. "Aqueous Lubrication of SiC and Si3N4 Ceramics Aided by a Brush-like Copolymer Additive, Poly(llCaps-lysine)-graft-poly(ethylene glycol)". In: *Tribology Letters* 34.3 (2009), pp. 201–210.

[28] R. Heeb et al. "Influence of Salt on the Aqueous Lubrication Properties of End-Grafted, Ethylene Glycol-Based Self-Assembled Monolayers". In: *Acs Applied Materials and Interfaces* 1.5 (2009), pp. 1105–1112.

[29] J. Klein. "Polymers in living systems: from biological lubrication to tissue engineering and biomedical devices". In: *Polymers for Advanced Technologies* 23.4 (2012), pp. 729–735.

[30] J. Cui, O. Azzaroni, and A. del Campo. "Polymer Brushes with Phototriggered and Phototunable Swelling and pH Response". In: *Macromolecular Rapid Communications* 32.21 (2011), pp. 1699–1703.

[31] J. Cui et al. "Phototunable Response in Caged Polymer Brushes". In: *Macromolecules* 45.7 (2012), pp. 3213–3220.

[32] J. Cui, V. San Miguel, and A. del Campo. "Light-Triggered Multifunctionality at Surfaces Mediated by Photolabile Protecting Groups". In: *Macromolecular Rapid Communications* 34.4 (2012), pp. 310–329.

[33] J. Cui et al. "Analysis of Responsive Polymer Films Using Surface Acoustic Waves". In: *Langmuir* (2013).

[34] A. Brunsen et al. "Light-activated gating and permselectivity in interfacial architectures combining "caged" polymer brushes and mesoporous thin films". In: *Chemical Communications* 48.10 (2011), pp. 1422–1424.

[35] J. M. Alonso et al. "Photopatterned surfaces for site-specific and functional immobilization of proteins". In: *Langmuir* 24.2 (2008), pp. 448–457.

[36] J. Auernheimer et al. "Photoswitched cell adhesion on surfaces with RGD peptides". In: *Journal of the American Chemical Society* 127.46 (2005), pp. 16107–16110.

[37] A. A. Brown et al. "Polymer brush resist for responsive wettability". In: *Soft Matter* 5.14 (2009), pp. 2738–2745.

[38] K. Critchley et al. "A mild photoactivated hydrophilic/hydrophobic switch". In: *Langmuir* 21.10 (2005), pp. 4554–4561.

[39] M. Lemieux et al. "Reorganization of binary polymer brushes: Reversible switching of surface microstructures and nanomechanical properties". In: *Macromolecules* 36.19 (2003), pp. 7244–7255.

[40] A. Synytska et al. "Intelligent Materials with Adaptive Adhesion Properties Based on Comb-like Polymer Brushes". In: *Langmuir* 28.47 (2012), pp. 16444–16454.

[41] A. Drechsler et al. "Tuning the Adhesion of Silica Microparticles to a Poly(2-vinyl pyridine) Brush: An AFM Force Measurement Study". In: *Langmuir* 28.44 (2012), pp. 15555–15565.

[42] C. Brieke et al. "Light-Controlled Tools". In: *Angewandte Chemie-International Edition* 51.34 (2012), pp. 8446–8476.

[43] C. Hanske et al. "The Role of Substrate Wettability in Nanoparticle Transfer from Wrinkled Elastomers: Fundamentals and Application toward Hierarchical Patterning". In: *Langmuir* 28.49 (2012), pp. 16745–16750.

[44] C. Kuttner et al. "Photochemical Synthesis of Polymeric Fiber Coatings and Their Embedding in Matrix Material: Morphology and Nanomechanical Properties at the Fiber-Matrix Interface". In: *Acs Applied Materials and Interfaces* 4.7 (2012), pp. 3484–3492.

[45] D. Kluge et al. "Nanomechanical Properties of Supramolecular Self-Assembled Whiskers Determined by AFM Force Mapping". In: *Langmuir* 26.5 (2010), pp. 3020–3023.

[46] S. Schmidt et al. "Adhesion and Mechanical Properties of PNIPAM Microgel Films and Their Potential Use as Switchable Cell Culture Substrates". In: *Advanced Functional Materials* 20.19 (2010), pp. 3235–3243.

[47] H. J. Butt, B. Cappella, and M. Kappl. "Force measurements with the atomic force microscope: Technique, interpretation and applications". In: *Surface Science Reports* 59.1-6 (2005), pp. 1–152.

[48] H. J. Butt et al. "Steric forces measured with the atomic force microscope at various temperatures". In: *Langmuir* 15.7 (1999), pp. 2559–2565.

[49] C. E. McNamee et al. "Surface and friction forces between grafted polysaccharide layers in the absence and presence of surfactant". In: *Journal of Colloid and Interface Science* 364.2 (2011), pp. 351–358.

[50] E. Max et al. "A novel AFM based method for force measurements between individual hair strands". In: *Ultramicroscopy* 110.4 (2010), pp. 320–324.

[51] T. Chen, I. Amin, and R. Jordan. "Patterned polymer brushes". In: *Chemical Society Reviews* 41.8 (2012), pp. 3280–3296.

[52] G. P. Lopez et al. "Imaging of Features on Surfaces by Condensation Figures". In: *Science* 260.5108 (1993), pp. 647–649.

[53] J. L. Hutter and J. Bechhoefer. "Calibration of Atomic-Force Microscope Tips". In: *Review of Scientific Instruments* 64.7 (1993), pp. 1868–1873.

[54] E. V. Anderson et al. "Shape-Independent Lateral Force Calibration". In: *Acs Applied Materials and Interfaces* 3.9 (2011), pp. 3256–3260.

[55] K. Ichimura, S. K. Oh, and M. Nakagawa. "Light-driven motion of liquids on a photoresponsive surface". In: *Science* 288.5471 (2000), pp. 1624–1626.

[56] M. K. Chaudhury and G. M. Whitesides. "How to Make Water Run Uphill". In: *Science* 256.5063 (1992), pp. 1539–1541.

[57] L. Zhai et al. "Patterned superhydrophobic surfaces: Toward a synthetic mimic of the Namib Desert beetle". In: *Nano Letters* 6.6 (2006), pp. 1213–1217.

5.A Supporting Information

Supplementary information contains setup for condensation microscopy and height contrast data. Condensation microscopy was used to monitor the photoconversion of the PNVOCMA brush to the hydrophilic PMAA brush in response to UV irr adiation. Figure 5.8 shows the setup used for condensation microscopy.
Height changes in the brush layer after irradiation were analyzed using imaging AFM. The height difference between unexposed and fully expos ed brushes at pH 9.5 was 2-4 nm (Figure 5.9).

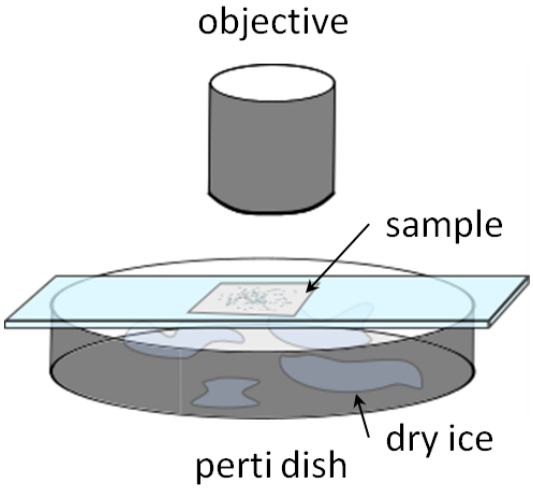

Figure 5.8: Setup for condensation microscopy

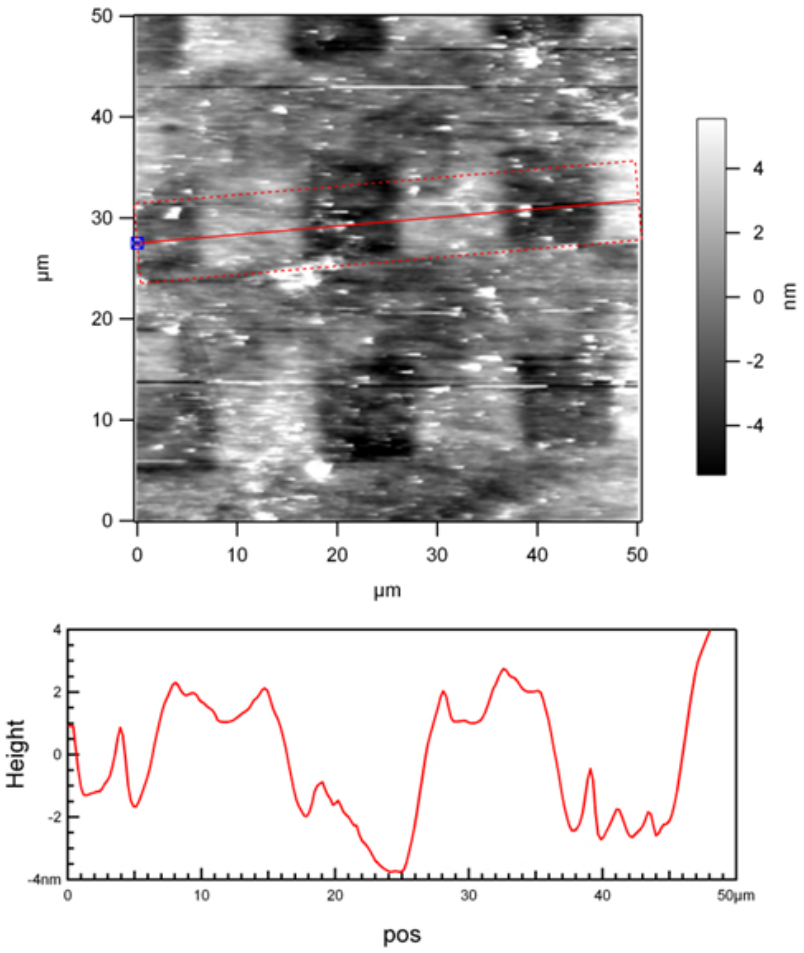

Figure 5.9: Height contrast between protected and 100% deprotected areas, and mean cross-section of the marked part in a indicates height changes of approximately 4 nm.

6

Adsorption of Spherical Polyelectrolyte Brushes: from Interactions to Surface Patterning

Hanske, C., Erath, J., Kuehr, C., Trebbin, M., Schneider, C., Wittemann, A., Fery, A., Adsorption of Spherical Polyelectrolyte Brushes: from Interactions to Surface Patterning. Zeitschrift Fur Physikalische Chemie-International Journal of Research in Physical Chemistry and Chemical Physics, 2012. 226(7-8): p. 569-584.

Abstract

Adsorption of colloidal particles constitutes an attractive route to tailor the properties of surfaces. However, for efficient material design full control over the particle-substrate interactions is required. We investigate the interaction of spherical polyelectrolyte brushes (SPB) with charged substrates based on adsorption studies and atomic force spectroscopy. The brush layer grafted from the colloidal particles allows a precise adjustment of their adsorption behavior by varying the concentration of added salt. We find a pronounced selectivity between oppositely and like-charged surfaces for ionic strengths up to 10 mM. Near the transition from the osmotic to the salted brush regime at approximately 100 mM attractive secondary interactions become dominant. In this regime SPB adsorb even to like-charged surfaces. To determine the adhesion energy of SPB on charged surfaces directly, we synthesize micron-sized SPB. These particles are used in colloidal probe AFM studies. Measurements on oppositely charged surfaces show high forces of adhesion for low ionic strengths that can be attributed to an entropy gain by counterion release. Transferring our observations to charge patterned substrates, we are able to direct the deposition of SPB into two-dimensional arrays. Considering that numerous chemical modifications have been reported for SPB, our studies could open exiting avenues for the production of functional materials with a hierarchical internal organization.

6.1 Introduction

The physisorption of components from solution constitutes a versatile and easily upscalable alternative to surface modifications based on covalent chemical coupling, since coupling by physisorption does not require specific chemical reactions to occur. A prominent example for this approach is the layer-by-layer (LbL) deposition of oppositely charged polyelectrolytes [1, 2, 3, 4]. Multilayers can be applied to large substrates by simple dip or spray coating and the non-covalent nature of the underlying interactions allows for a broad spectrum of molecular components [5, 6, 7, 8]. Other examples are the physisorption of microgel-particles [9] which can be used as temperature-responsive cell substrates [10] or the adsorption of responsive block-copolymer micellar aggregates [11] for controlled release and cellular response. Indeed often colloidal building blocks are integrated in such physisorption-layers [12, 13, 14, 15, 16], since they carry functions (optical, electronic, catalytic, magnetic properties or responsiveness towards various stimuli), but also because the size of colloidal particles increases the

adsorption energy as compared to single (macro-)molecules while still ensuring that interfacial interactions are dominant over inertia or other forces governing the macroscale. The efficiency of these materials depends on both the physical properties of the colloids and their spatial arrangement on the substrate. Modification of the colloidal building blocks by grafting polymer chains prior to physisorption is a promising strategy for optimizing these aspects inasmuch the surface layer moderates the interaction with the substrate independent of the type of particles. Such an approach can be applied to any type of colloids including inorganic and polymer particles. If the packing of the chains is sufficiently dense, i.e. the lengths of the chains tethered with one end to the particle must be considerably larger than the distance between two neighboring chains, a polymer brush results [17]. Moreover, if the brush is made from polyelectrolytes, it adds electrosteric stabilization, stimuli-responsiveness and compatibility as well as adhesiveness or non-adhesiveness to particles that could exhibit special optical, mechanical or magnetic features, thus establishing multi-functional building blocks [18, 19, 20, 21]. Because of the spherical geometry of the colloidal support, such particles are denoted as "spherical polyelectrolyte brushes" (SPB). The core-shell morphology of SPB is schematically depicted in Figure 6.1A. The properties of SPB in solution are widely determined by the confinement of the counterions of the polyelectrolyte chains. Approximately 95% of the counterions of the polyelectrolyte chains are trapped within the brush at low concentrations of added salt [22]. This creates a huge osmotic pressure resulting in a marked stretching of the polyelectrolytes [23, 24]. The responsiveness of the SPB towards external stimuli such as the ionic strength and pH allows precise control over the spatial dimensions of the particles and their mutual interaction [25, 26, 27, 28].

Functionalization of the core-shell colloids can be accomplished by loading the core with hydrophobic substances, including many drugs. Moreover, the surrounding brush layer may serve as a carrier for active nanostructures, namely for metal nanoparticles, enzymes and conductive polymers yielding functional colloids with tailored biological, catalytic or electronic properties [29, 30, 31, 32]. This opens up avenues for multifunctional responsive mesoscopic building units that are stable against coagulation and can be easily handled [33].

Understanding the interaction of SPB with solid substrates is a prerequisite for their technological application in functional coatings. Studies with mica surfaces demonstrated distinct differences in the adsorption behavior of cationic and anionic SPB [34, 35]. While anionic SPB exhibited a high lateral mobility on the negative substrates and formed hexagonally packed arrangements during drying, cationic SPB were strongly af-

fixed to the surface resulting in network-like structures. Recently, we investigated SPB adsorption onto polyelectrolyte multilayers focusing on the kinetics [36]. We found that after an initial diffusion-limited stage SPB adsorption slows down and finally ceases with the formation of a particle monolayer.
In this work we investigate the interaction of anionic SPB and polyelectrolyte multilayers consisting of polystyrene sulfonate (PSS) and poly(diallyldimethylammonium chloride) (PDA). In addition to adsorption studies covering a wide range of ionic strengths [36], we present a direct assessment of the force of adhesion via atomic force microscopy (AFM). We utilize the colloidal probe (CP) technique, in which force-distance curves are recorded with an AFM cantilever bearing a micron-sized spherical particle [37]. This method was developed independently by Butt and Ducker and allows a normalization of the measured forces over the contact area by the Derjaguin approximation [38, 39]. Another advantage of CP-AFM is the possibility to use functionalized particles and measure the interaction between arbitrary surfaces including polyelectrolyte brushes [40, 41, 42, 43]. Building upon the synthetic route to submicron SPB originally developed by Ballauff and co-workers [23, 26], we attach PSS chains to micron-sized polystyrene particles. These SPB microparticles are then used to measure the interaction of SPB with charged surfaces. Finally, we demonstrate that under appropriate deposition conditions SPB can be arranged into well-defined arrays on charge patterned substrates. For this purpose we utilize microcontact printing, which is a prominent technique to facilitate surface patterning and guided adsorption [44, 45, 46].

6.2 Experimental

Materials

Styrene was passed through a catechol inhibitor remover column before use. Irgacure 2959 was kindly supplied by Ciba Specialty Chemicals and transferred into the copolymerizable photoinitiator (HMEM) by a Schotten-Baumann reaction of Irgacure 2959 and methacrylic acid hydrochloride along the lines given in Ref. [23]. Purification was accomplished by column chromatography on silica gel. The purity of the product was verified through NMR spectroscopy (AC 250, Bruker). Deionized water obtained from a reverse osmosis water purification system (Millipore Academic A10) was used throughout the entire studies. All latexes were purified by exhaustive ultrafiltration against deionized water. The other chemicals and solvents were of analytical grade and were used as received.

Nanoparticles synthesis

The synthesis and characterization of submicron SPB following the approach of Ballauff and coworkers are described in Ref. [47]. Briefly, polystyrene cores bearing covalently anchored photoinitiator moieties were produced by soap-free emulsion polymerization in the presence of a UV sensitive comonomer. From the particle surfaces PSS chains were grafted by UV induced polymerization of sodium styrene sulfonate. The PS cores display a narrow size distribution with an average radius of $126 \pm 2\,\mathrm{nm}$ as measured by dynamic light scattering (DLS). The hydrodynamic thickness of the PSS brush is $74 \pm 3\,\mathrm{nm}$ in deionized water. The PSS chains were cleaved from the PS cores and analyzed by size exclusion chromatography. The molecular weight of the longest PSS chains that govern the spatial extension of the brush layer was determined as $67600 \pm 4950\,\mathrm{g/mol}$, which corresponds to a contour length of $82 \pm 6\,\mathrm{nm}$ [47]. The polydispersity of the chains (weight averaged molecular weight by number averaged molecular weight) was calculated as 2.1, which is a common value for polymers prepared by free radical polymerization. The chain grafting density is 0.03 ± 0.01 chains per nm^2 [47].

Microparticles synthesis

PSS brushes were grafted from monodisperse cross-linked PS microparticles with a diameter of $4.8\,\mu\mathrm{m}$ (SX-500 H) which were kindly supplied from Soken Chemical and Engineering Co.

The photoinitiator layer surrounding the microparticles was formed in a seeded growth polymerization. Briefly, 15 g of the microparticle powder was dissolved in 14 g ethanol yielding a homogeneous suspension after sonication for 2 min. 143 g deionized water was added dropwise under continuous stirring followed by further sonication to minimize agglomeration. The PS seeds were swollen with 1.13]g styrene (injection rate 0.02 g/ml) and stirred for a period of 15 h at 130 rpm. The polymerization was performed at 70 °C under a nitrogen atmosphere and continuous stirring (300 rpm). To initiate the reaction, 0.284 g potassium persulfate was added. After 15 min, 2.098 g of a 69.6 wt% solution of the copolymerizable photoinitiator HMEM in acetone was injected into the suspension (rate 0.05 g/min). The reaction was allowed to proceed for 2 h. The microparticles were isolated from the dispersant, redispersed in ethanol and stored in a 1:1 ethanol-water mixture for further use.

Grafting of the polyelectrolyte brushes was carried out in a closed reaction chamber containing a UV emitter with a focusable reflector (Hoenle UV Technology UV-F 400

F). An iron doped metal halogenide lamp with a power of 400 W was used in combination with a blue filter (transmission window: $320 - 450$ nm). 44 mg of sodium styrene sulfonate was added to suspensions of 217 mg photoinitiator-coated microparticles dispersed in 4.8 g of a 1:1 ethanol-water solution. The reaction mixtures were irradiated with UV for 30 minutes at r.t. under permanent stirring. Purification of the suspension was accomplished by exhaustive ultrafiltration against deionized water.

Polyelectrolyte solutions

All polyelectrolytes were used as aqueous solutions containing 1 g/l and varying amounts of NaCl (99.88%, Fisher Scientific). Multilayer coatings were produced with the following polyelectrolytes (Aldrich): PEI (poly(ethylene imine), $M_W = 25,000$ g/mol), PSS (poly(sodium-4-styrene sulfonate), $M_W = 70,000$ g/mol, 50 mM NaCl), PDA (poly(diallyldimethylammonium chloride), $M_W = 100,000 - 200,000$ g/mol, 50 mM NaCl). For microcontact printing we used fluorescently labeled PDA-TRITC (Surflay, $M_W = 70,000$ g/mol, 500 mM NaCl).

Substrate preparation

Glass slides and silicon wafers were cut into pieces of 10 mm$x$25 mm and cleaned by the RCA method using analytical grade chemicals (2-propanol, NH_3, H_2O_2 from VWR) [48]. Functionalization of the wafers with 3-aminopropyldimethylethoxysilane (97%, Sigma Aldrich) was achieved by vapor phase silanization under reduced pressure (10 mbar, 24 h) followed by rinsing with EtOH (VWR) to remove excess molecules. Prior to the multilayer coating the substrates were immersed in PEI solution for 30 min to deposit an adhesion promoting layer. The build-up of $(PSS/PDA)_5$ and $(PSS/PDA)_{5.5}$ multilayers by spray coating followed the procedure reported in Ref. [5]. Multilayers terminated with PSS were charged patterned by microcontact printing of PDA-TRITC following established protocols [49, 50]. For this purpose we used polydimethylsiloxane (PDMS) stamps cast from lithographically patterned silicon masters. On homogeneous substrates SPB were deposited by immersion in suspensions of varying ionic strength (0.1 mM to 1 M, 0.1 wt% particles) for 60 min. Deposition of SPB on charge patterned surfaces was facilitated by drop casting in a humidified desiccator. The suspensions contained 0.1 wt% particles and NaCl concentrations of 1 mM and 100 mM respectively and were left on the substrates for at least 24 h. Before drying, the non-adsorbed particles were removed by thorough washing. In-situ AFM imaging of wet samples showed that the amount of adsorbed particles did not change during

this step.

AFM imaging

Imaging of the SPB assemblies was performed with a Nanowizard I AFM (JPK Instruments) operating in the Intermittent Contact Mode. We used soft cantilevers (0.15 N/m, 12 kHz, CSC-17, MikroMasch Estonia) for in-situ imaging and stiff cantilevers (42 N/m, 300 kHz, OMCL-AC160TS-W2, Olympus) for imaging in air. To estimate the surface coverage in dependence on the ionic strength 100 m^2 scans were recorded on at least three positions per sample using a Dimension IIIa AFM (Bruker). The particle density was determined by the automated counting procedure implemented in ImageJ.

Force spectroscopy

The colloidal particles were attached to calibrated, tipless AFM cantilevers (NSC12, Mikromasch) using a commercial epoxy glue (UHU Endfest 300) and a micromanipulator. The force constants as detected by the thermal noise method [37] ranged from 0.25 N/m to 0.7 N/m. Force-distance curves were recorded in liquid using a Nanowizard I AFM. All solutions were adjusted to pH4 with HCl (Grüssing). Salt concentrations of 1 mM and 100 mM were obtained by addition of NaCl.

Electrophoretic mobility measurements

Double-layer potential measurements of the microparticles were performed with a ZETAVIEW laser scattering video microscope (Particle Metrix GmbH). From the electrophoretic mobilities determined by the implemented image analysis algorithm, zeta potential values were calculated using the Smoluchowski equation [51]. All samples were strongly diluted in 1 mM NaCl solution. Their pH was adjusted by addition of HCl.

Field emission scanning electron microscopy (FESEM)

FESEM specimen were prepared by drying one drop of a highly diluted suspension on a clean silicon wafer (CrysTec) at room temperature and coating with a platinum layer of 2 nm thickness using a sputter coater (Cressington 208HR) to make the specimen conductive. Micrographs were recorded on a LEO Gemini microscope (Zeiss) equipped with a field emission cathode operating at $3 - 5$ kV, which corresponds to a lateral resolution of 2 nm.

Cryogenic transmission electron microscopy (cryo-TEM)

Cryo-TEM sample were contrast enhanced in accordance to Ref.[52] by counterion exchange with CsCl and subsequent adsorption of bovine serum albumin (BSA). The SPB suspension was spread on a hydrophilized lacey carbon TEM grid (mesh size 200, Plano GmbH) and vitrified with liquid ethane. Imaging was performed with a Zeiss EM922 OMEGA EFTEM (Zeiss NTS GmbH) at a temperature of 90 K and an acceleration voltage of 200 kV.

Differential centrifugal sedimentation (DCS)

The average size of the microparticles and their size distribution were measured using an analytical disc centrifuge (CPS Instruments CPS-24000) [53]. Within a hollow disc rotating at 5050 rpm a gradient was prepared by layering eight sucrose solutions of decreasing density (8 to 3 wt%) upon one another. 0.1 ml of a dilute suspension of microparticles was placed on top of the gradient. The distribution of the microparticles was obtained by measuring the time required for the different species to reach a known position within the gradient. The concentration at this position and time was measured by light absorption at 405 nm.

6.3 Results and Discussion

Analysis of the adsorption behavior is an established methodology for investigating the interaction between particles and solid interfaces. Both the adsorption kinetics and the final surface coverage provide insights in this respect. In a recent study we found that SPB adsorption kinetics is diffusion-limited in the low surface coverage regime. After extended adsorption times the process runs into a jamming limit which always results in the formation of a SPB monolayer [36]. The saturation coverage of adsorbed SPB depends on both the surface charge and the ionic strength in solution. Figure 6.1B shows layers formed by the adsorption of particles carrying a PSS brush onto PDA and PSS terminated multilayers. While the SPB adsorb exclusively on the oppositely charged surface at low ionic strength, selectivity vanishes at high concentrations of added salt. The AFM images were recorded in-situ directly after excess particles had been removed by gentle washing. In the absence of attractive capillary forces a liquid-like ordering is preserved, indicating a random sequential adsorption of SPB. Obviously, the characteristic interparticle distance is strongly reduced by the addition of salt, which induces screening of the repulsive electrosteric interaction between the SPB. In Figure 6.1C the

saturation surface coverage on both oppositely and like-charged substrates is plotted as a function of the ionic strength. On PDA the surface coverage increases monotonically with the ionic strength, whereas virtually no adsorption is observed on PSS terminated substrates below 10 mM of added salt. Even higher salt concentrations lead to a gradual loss of the substrate selectivity. Matching surface coverage on both oppositely and like-charged substrates is found at salt concentrations above 100 mM. Interestingly, this value corresponds to the transition from the osmotic brush to the salted brush regime, which is known to have also a pronounced influence on the binding of proteins to SPB [54, 55]. It is reasonable to assume that electrosteric forces dominate the interaction between SPB and charged surfaces in the osmotic brush regime. At low ionic strength SPB attachment to oppositely charged substrates is entropically favored due to counterion release, whereas electrostatic and steric repulsion suppress adsorption onto like-charged surfaces. In the salted brush regime, the polyelectrolyte corona is strongly collapsed due to screening rendering electrosteric interactions insignificant. Instead attractive forces such as van der Waals or hydrophobic interactions become dominant facilitating SPB adsorption independent of the substrate type.

To assess the forces governing the interaction of SPB with charged surfaces directly, we chose the colloidal probe technique, where single colloidal particles are attached to AFM cantilevers. Due to the well-defined geometry a normalization of the measured force data by the Derjaguin approximation is possible. In order to perform such experiments, it was fundamental to modify micron-sized particles of suitable dimensions to be used as colloidal probes by grafting polyelectrolyte brushes. For this purpose, we selected cross-linked polystyrene microparticles, which were supplied from Soken Chemical and Engineering Co.. Measurements of the distribution of the particle diameters by differential centrifugal sedimentation showed that the particles are narrowly dispersed with an average diameter of 4.8 m. Their polydispersity defined as the weight-averaged diameter divided by the number-averaged diameter is as low as 1.001. Moreover, scanning electron micrographs revealed that the particles exhibit a uniform spherical shape with a smooth surface, which was essential to obtain a well-defined core-shell morphology after grafting the polyelectrolyte brush.

As illustrated in Figure 6.2 the surface modification was carried out in two steps, beginning with coating the microparticles with a thin layer of photoinitiator. In the second step, surface-bound radicals, formed upon irradiation with UV light, initiated the polymerization of the water-soluble monomer sodium styrene sulfonate resulting in covalently attached polyelectrolyte brushes. This method is well-established for the synthesis of SPB with submicron dimensions [23, 56], but has to the best of our

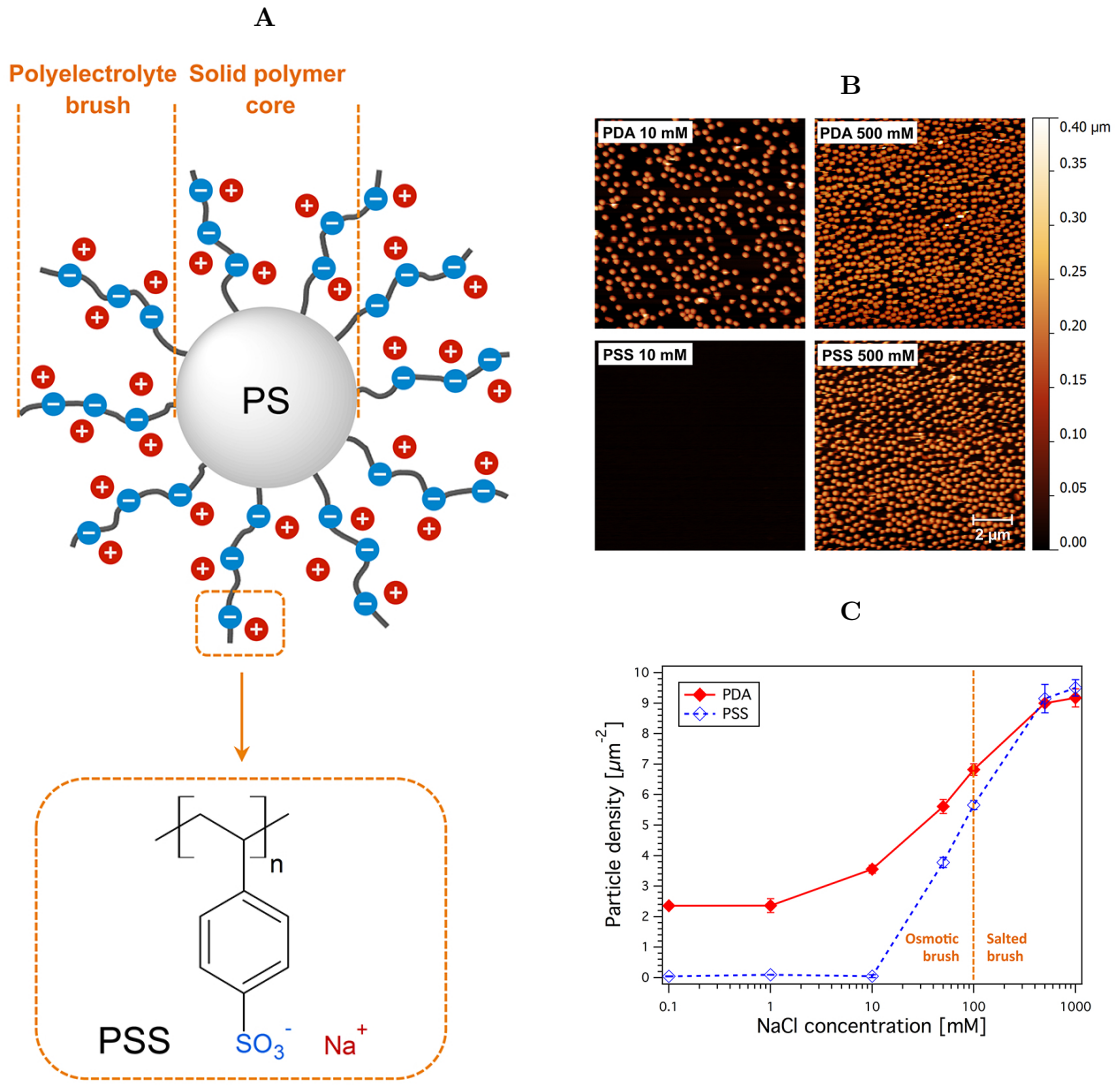

Figure 6.1: Influence of substrate charge and ionic strength on SPB adsorption. For this study anionic SPB consisting of a PS core and attached PSS chains were used 6.1A. Before drying, the films exhibit a liquid-like particle ordering indicating a random adsorption process 6.1B. At 10 mM of added salt the particles bind only to oppositely charged surfaces, whereas particle deposition at 500 mM results in a high surface coverage on both types of substrates. The equilibrium particle density plotted against the ionic strength shows that the loss of substrate selectivity coincides with the transition from the osmotic to the salted brush regime near 100 mM 6.1C.

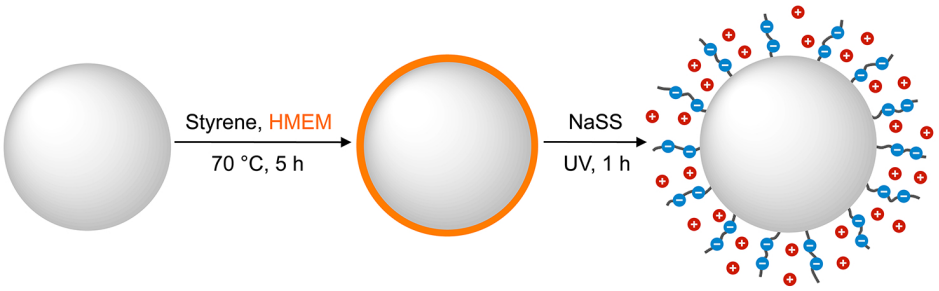

Figure 6.2: Synthesis of micron-sized SPB: Microparticles bearing photocleavable groups at their surface were prepared by seeded growth polymerization of styrene and the polymerizable photoinitiator HMEM onto narrowly dispersed polystyrene seeds. Sodium styrene sulfonate (NaSS) was added and the suspension was irradiated by UV light. Covalently bound surface radicals thus generated initiated the polymerization of the water-soluble monomer resulting in polyelectrolyte brushes attached to the microparticles.

knowledge not been adapted to larger particles. While the general concept is similar to the one developed by Ballauff and co-workers for nanoparticles, special attention had to be paid to prevent aggregation of the micron-sized particles until the brush layer could add electrosteric stabilization. Careful preparation was necessary to obtain homogeneous suspensions of the microparticles. For this purpose, the particles that were supplied as a freeze-dried powder were at first suspended in ethanol before an aliquot of water was added dropwise. Homogenization was accomplished by sonication. The photoinitiator layer was generated by swelling the cross-linked micron-sized seeds with a defined amount of styrene and then initiating the polymerization by addition of potassium persulfate. A water-soluble initiator was chosen to facilitate the polymerization at the surface of the particles. After a time given to form a "fresh" layer of polystyrene, a polymerizable photoiniator was added under starved conditions resulting in a copolymer shell on the seeds. It has to be noted that the microparticles kept their uniform spherical shape during the polymerization as corroborated by electron micrographs (Figure 6.3A). This finding is not trivial, because given appropriate experimental conditions seeded growth polymerization from cross-linked particles can be used to prepare particles that exhibit defined anisotropic shapes, e.g. dumbbell-shaped particles [57, 58]. In the final step, the water soluble monomer sodium styrene sulfonate was added and the suspension of the modified microparticles bearing covalently attached photoinitiator moieties at their surface was irradiated by UV light in a closed reaction chamber. As shown in earlier studies, multiple elastic scattering of the UV light within the turbid suspension enables the decomposition of the surface-

bound photoinitiator. These radicals initiate the polymerization of the water-soluble monomer resulting in polyelectrolyte brushes covalently attached to the particles [23, 56]. The decomposition of the applied photoinitiator results both in surface-bound radicals and free radicals in solution. The free polyelectrolyte chains in solution thus formed were removed by ultrafiltration against water.

Manifold analytical techniques such as small-angle X-ray scattering [59], dynamic light scattering [23], cryogenic transmission electron microscopy [52] and electrophoretic measurements [60] have been used to comprehensively investigate the core-shell character of submicron-sized SPB. While such techniques are well-suited to study submicron-sized particles, they can be hardly applied on microscale objects. In order to estimate the brush thickness, a reference experiment with PS seeds of 169 nm in diameter was carried out in parallel to the photopolymerization onto the microscale seeds in the UV chamber. A brush thickness of 30 nm was obtained by DLS measurements of the hydrodynamic radii before and after the photopolymerization. As a first indication that a brush layer also formed on the microparticles may serve their significantly enhanced stability when dispersed in water. This was already evident from visual inspection. While the unmodified core particles showed rapid sedimentation in water and had thus to be kept in water/ethanol mixtures during surface modification, sedimentation of the brush coated microparticles proceeded much slower. This observation was quantitatively corroborated when measuring the size distribution of the particles by DCS (Figure 6.3B). Considerable amounts of particle dimers, trimers and tetramers were

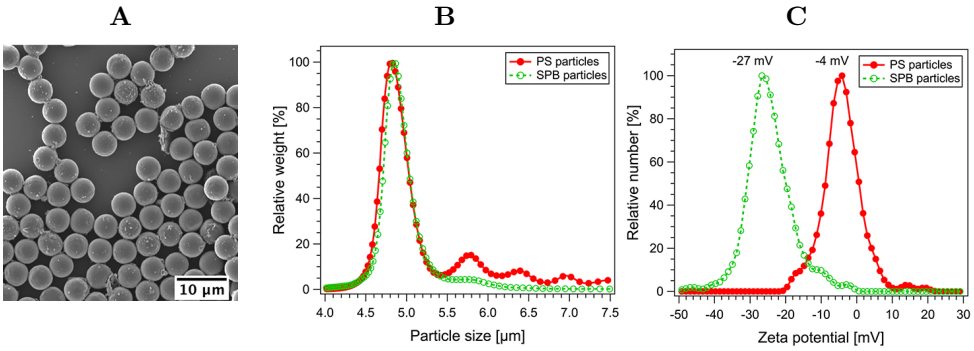

Figure 6.3: Characterization of SPB microparticles. Size and shape of the microparticles are preserved during grafting of the brushes 6.3A. In comparison to the PS seeds the brush decorated SPB microparticles show a significantly reduced amount of aggregates in differential centrifugal sedimentation measurements 6.3B. The zeta potential at pH 4 is clearly shifted to more negative values due to the grafted PSS chains 6.3C.

found in freshly prepared aqueous suspensions of the PS seeds, which is in accord with their high sedimentation rate. Only a small portion of dimer ensembles are found after modification of the microparticles indicating the stabilization effected by the surrounding polyelectrolyte layer. This is further documented by optical measurements of the electrophoretic mobilities of individual microparticles before and after grafting the surface layer. The experiments were carried out at pH 4 to exclude the influence of the carboxylic groups of the PS seeds on the mobility. Calculations of zeta potentials for hairy particles from electrophoretic mobilities are non-trivial [61]. In contrast to submicron-sized SPB, the influence of a 30 nm thick surface layer on the mobility of the 4.8 m SPB microparticles can be widely restricted to the effective charge of the particles. For this reasons, zeta potentials were calculated based on the Smoluchowski equation [51]. The low zeta potential of 4 mV of the PS seeds is in full accord with the modest stability of aqueous suspensions of these particles. There was a significant increase of the absolute value of the zeta potential (-27 mV) after the photopolymerization again indicating the successful formation of the polyelectrolyte layer and the improved stability of the suspensions (Figure 6.3C).

While the standard characterization methods all indicate a successful modification of the PS microparticles, they reflect the averaged properties of a large ensemble of particles. To investigate the single particles by CP-AFM we attached PS core particles and PSS modified particles to tipless cantilevers. In analogy to the zeta potential measurements all AFM experiments were conducted at pH 4 to screen contributions stemming from the carboxyl moieties of the core particles. Figure 6.4A/6.4B displays typical force-distance curves obtained on amino-functionalized Si wafers, which carry a positive net charge under acidic conditions. Independent of the ionic strength the PS core particles show a hard repulsive interaction without noticeable adhesion upon retraction. Retract curves of the modified particles on the other hand display a strongly adhesive interaction most pronounced at low ionic strength. Despite the fact that SPB adsorption is promoted by the addition of salt, electrostatic screening results in significantly decreased binding strengths. Similar trends apply to PDA terminated polyelectrolyte multilayers as substrates with the qualitative difference that we often observe a less rapid, stepwise detachment upon retraction of the cantilever (Figure 6.4C). Measurements in the presence of PSS terminated multilayers (Figure 6.4D) on the other hand displayed small forces of adhesion, which were independent of the ionic strength and can be attributed to secondary interactions and chain entanglements [62]. We have to note that only about half of the probed SPB microparticles showed significant differences from the bare PS cores indicating an incomplete conver-

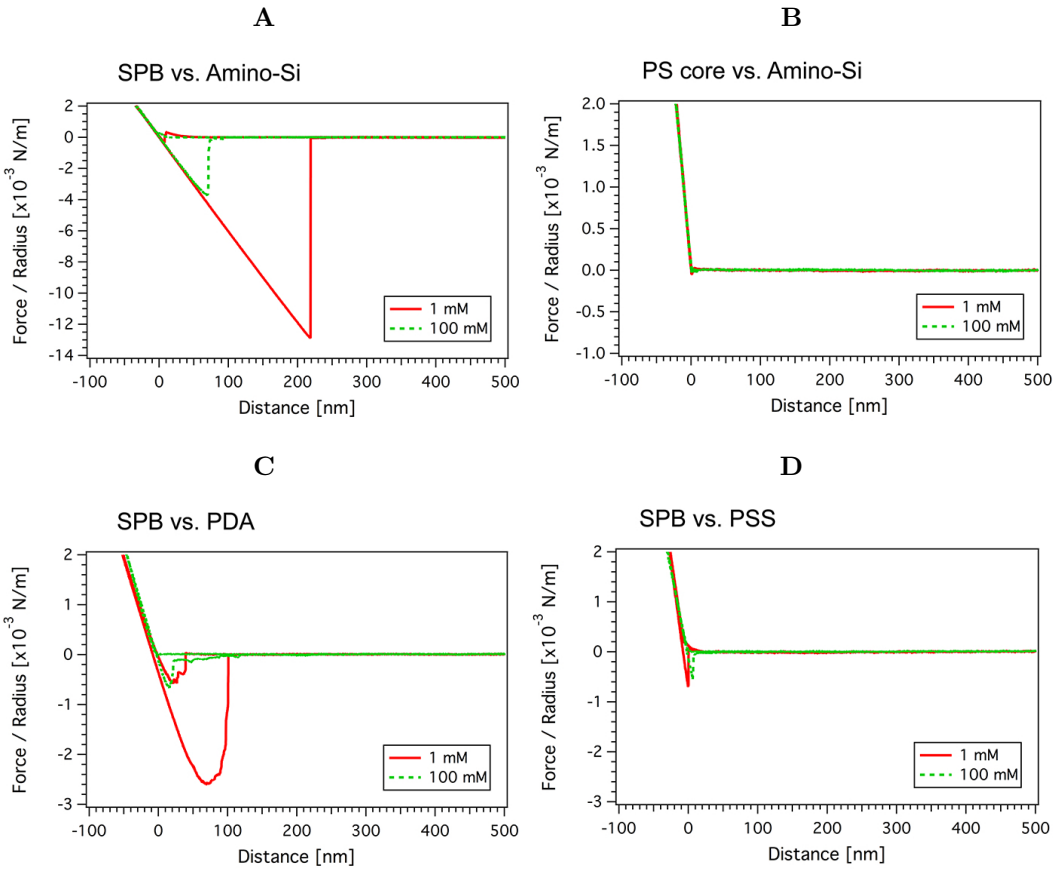

Figure 6.4: Force curves of PS microparticles and SPB microparticles. While the SPB microparticle shows strong adhesion to the oppositely charged, amino-functionalized substrate 6.4A, little adhesion is found for the PS reference particle 6.4B. The strength of the attractive interaction can be controlled by the ionic strength and the charge of the substrate as shown for PDA 6.4C and PSS 6.4D terminated multilayers. All data was obtained at pH4.

sion during photopolymerization. Also with an increasing number of measurements the force of adhesion decreased steadily indicating that PSS chains are partially torn out of the brush. Considering the charged surface as a multivalent counterion very strong binding is expected [35]. In our measurements the retract speeds (500 nm/s) were rather high possibly preventing a stepwise detachment of single charged polymer groups. Whereas more quantitative investigations will have to take these aspects into account, we were primarily interested in a qualitative assessment of the strength of SPB adhesion at high and low ionic strengths.

Both the adsorption study and the single particle study demonstrated the pronounced substrate selectivity of SPB, which is a prerequisite for the construction of SPB surface assemblies on charge patterned substrates. To create substrates with well-defined positive and negative regions we printed labeled PDA-TRITC onto PSS terminated multilayers using hydrophilized PDMS stamps. Successful pattern reproduction was proven by fluorescence microscopy and AFM imaging. A typical microcontact print consisting of negative circles and a surrounding positive matrix is displayed in Figure 6.5A. Onto the patterned region we applied droplets of SPB suspensions containing 1 mM and 100 mM of NaCl. These samples were stored in a humidified desiccator for at least 24 h before washing with water and drying in a nitrogen stream. As shown in Figure 6.5B the SPB adsorbed only onto oppositely charged areas at low ionic strength leading to excellent pattern reproduction. Increasing the ionic strength to 100 mM on the other hand resulted in a complete loss of substrate selectivity (Figure 6.5C). As confirmed by fluorescence microscopy the pattern fidelity was unaffected by the deposition process. The observed non-selectivity can therefore be attributed to attractive secondary interactions, such as van der Waals forces or hydrophobic interaction, dominating the SPB adsorption in the salted brush regime.

As further demonstrated in Figure 6.6, charge patterning is a powerful tool for controlling surface order as well as the patterning of sub-micron SPB on the micron scale and even up to macroscopic dimensions.

6.4 Conclusions and Outlook

We investigated the interaction of spherical polyelectrolyte brushes with charged surfaces. Particle monolayers prepared by SPB adsorption onto positively and negatively charged polyelectrolyte multilayers showed a distinct dependence of the surface coverage on the concentration of added NaCl. The particles adsorbed exclusively onto oppositely charged surfaces at ionic strengths up to 10 mM, whereas higher salt con-

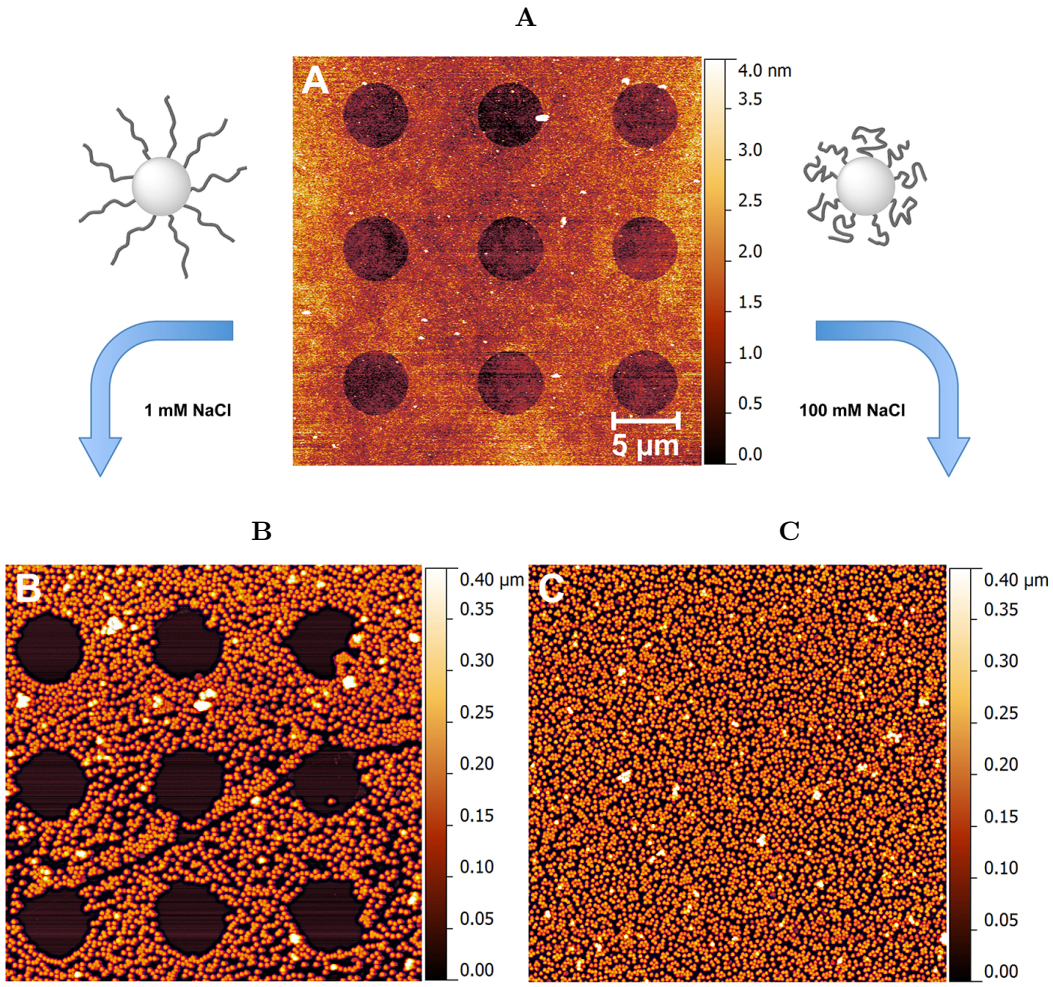

Figure 6.5: SPB adsorption onto charge patterned substrates. The AFM image shows negatively charged areas as dark circles surrounded by a positively charged matrix 6.5A. At low ionic strength the particles adsorb selectively onto the oppositely charged regions 6.5B. Substrate selectivity is completely suppressed at high concentrations of added salt 6.5C.

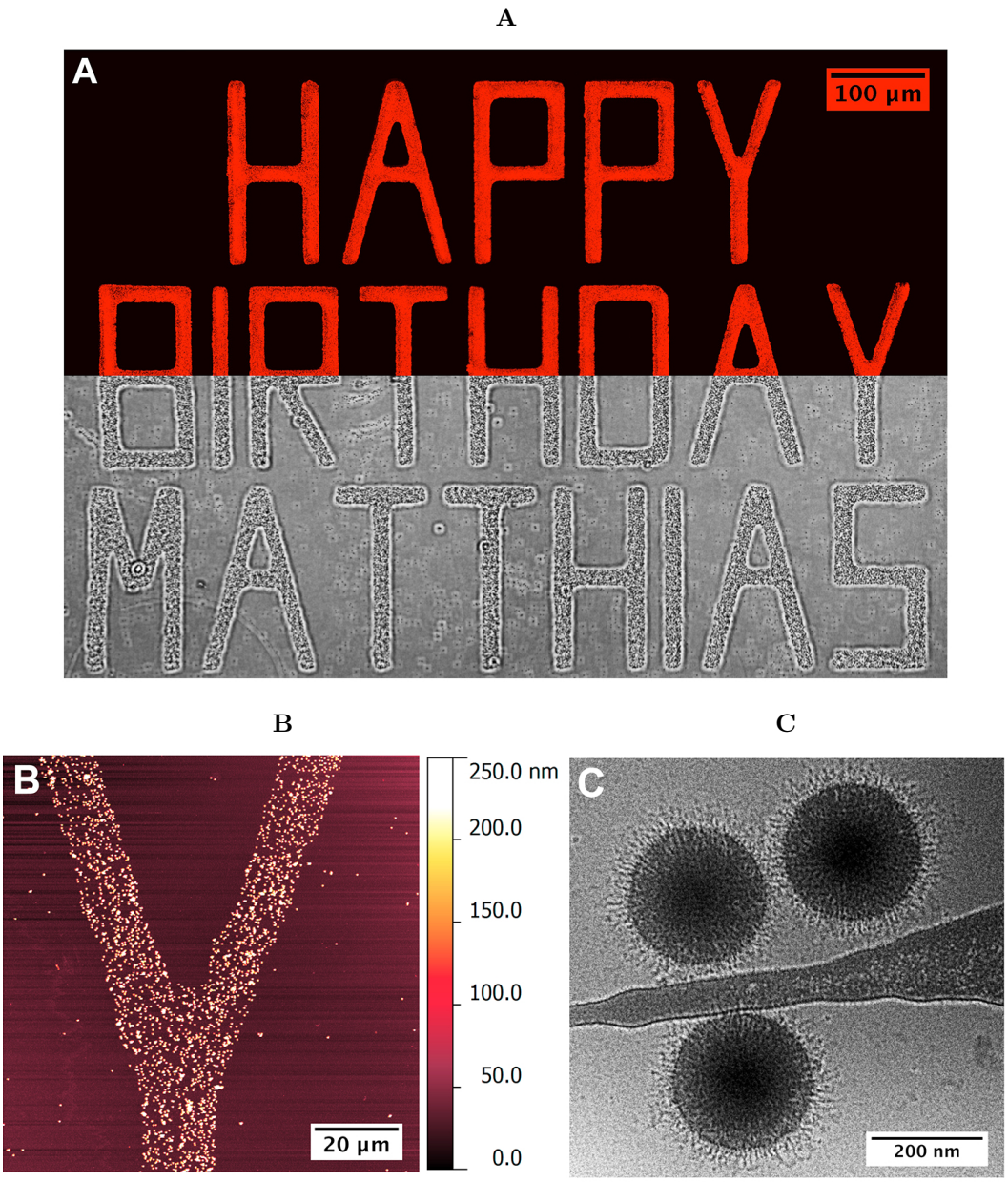

Figure 6.6: Hierarchical structuring by selective SPB adsorption: Millimeter-sized patterned areas were produced by microcontact printing with a custom PDMS stamp (top: fluorescence image, bottom: phase contrast micrograph after SPB deposition) 6.6A. Micron-sized particle arrays are formed upon the adsorption of SPB (AFM) 6.6B. The Cryo-TEM image of individual SPB contrasted by the adsorption of bovine serum albumin demonstrates the core-shell architecture 6.6C.

centrations resulted in a gradual loss of substrate selectivity. While counterion release and electrosteric repulsion govern the interaction between SPB and charged surfaces in the osmotic brush regime, attractive secondary interactions become dominant in the salted brush regime.

The strength of the interaction forces can be assessed on a single particle level by colloidal probe AFM. For this purpose we equipped cross-linked polystyrene microparticles with UV sensitive moieties and grafted chains of polystyrene sulfonate from the particle surfaces. This modification lead to significantly enhanced colloidal stability in water. Further, the PSS grafted microparticles displayed a strongly negative zeta potential even under acidic conditions, where the bare core particles carrying only carboxyl groups are mostly neutral. In analogous single particle AFM measurements the presence of grafted PSS chains resulted in a massively altered interaction with positively charged surfaces. Whereas the bare cores show no attraction towards the substrate under acidic conditions, the modified particles adhere strongly. The force of adhesion can be regulated via the ionic strength in the surrounding medium.

Further, we used charge patterned substrates produced by polymer-on-polymer stamping to arrange SPB into patterned arrays. As expected from the experiments with homogenous surfaces site-selective SPB attachment occurred only at low ionic strength. While this has been demonstrated with hard particles [46], the stimuli-responsive nature of the brush layer avoids an irreversible hit-stick behavior and could therefore allow us to remove structural defects by annealing. Considering the numerous chemical modifications which have been reported for SPB [33, 29, 63], our study opens exiting avenues for the production of stimuli-responsive materials with a hierarchical internal organization.

Figure 6.6 shows a particular example of such a hierarchical structure containing two levels of hierarchy: the internal core-shell character of the particles and their positional order on the printed micropattern. As one can clearly see, completely novel functionalities arise, like the use of nanoparticles for communication, which brings us to the main aim of this manuscript:

Lieber Matthias, wir wünschen Dir alles Gute zu Deinem Geburtstag! Es ist uns eine Freude und ein Privileg mit diesem Manuskript einen wissenschaftlichen Beitrag zu Deiner Geburtstagsfeier leisten zu können! Herzliche Gratulation!

Acknowledgements

This work has been conducted within the special collaborative research project SFB 840 (project B5) and was funded by the German Science Foundation (DFG). The authors would like to acknowledge Carmen Kunert and Dr. Simone Wagner for FESEM imaging as well as Dr. Markus Drechsler for cryo-TEM imaging. We also thank Nicolas Helfricht for his assistance with the colloidal probe preparations.

6.5 References

[1] G. Decher. "Fuzzy nanoassemblies: Toward layered polymeric multicomposites". In: *Science* 277.5330 (1997), pp. 1232–1237.

[2] G. Decher, J. D. Hong, and J. Schmitt. "Buildup of Ultrathin Multilayer Films by a Self-Assembly Process .3. Consecutively Alternating Adsorption of Anionic and Cationic Polyelectrolytes on Charged Surfaces". In: *Thin Solid Films* 210.1-2 (1992), pp. 831–835.

[3] S. T. Dubas and J. B. Schlenoff. "Factors controlling the growth of polyelectrolyte multilayers". In: *Macromolecules* 32.24 (1999), pp. 8153–8160.

[4] D. Yoo, S. S. Shiratori, and M. F. Rubner. "Controlling bilayer composition and surface wettability of sequentially adsorbed multilayers of weak polyelectrolytes". In: *Macromolecules* 31.13 (1998), pp. 4309–4318.

[5] A. Izquierdo et al. "Dipping versus spraying: Exploring the deposition conditions for speeding up layer-by-layer assembly". In: *Langmuir* 21.16 (2005), pp. 7558–7567.

[6] C. H. Porcel et al. "Ultrathin coatings and (poly(glutamic acid)/polyallylamine) films deposited by continuous and simultaneous spraying". In: *Langmuir* 21.2 (2005), pp. 800–802.

[7] J. B. Schlenoff, S. T. Dubas, and T. Farhat. "Sprayed polyelectrolyte multilayers". In: *Langmuir* 16.26 (2000), pp. 9968–9969.

[8] J. E. Wong et al. "Specific Ion versus Electrostatic Effects on the Construction of Polyelectrolyte Multilayers". In: *Langmuir* 25.24 (2009), pp. 14061–14070.

[9] S. Schmidt et al. "Thermoresponsive surfaces by spin-coating of PNIPAM-co-PAA microgels: A combined AFM and ellipsometry study". In: *Polymer* 49.3 (2008), pp. 749–756.

[10] S. Schmidt et al. "Adhesion and Mechanical Properties of PNIPAM Microgel Films and Their Potential Use as Switchable Cell Culture Substrates". In: *Advanced Functional Materials* 20.19 (2010), pp. 3235–3243.

[11] J. Gensel et al. "Cavitation Engineered 3D Sponge Networks and Their Application in Active Surface Construction". In: *Advanced Materials* 24.7 (2012), pp. 985–+.

[12] C. Lu, H. Moehwald, and A. Fery. "A lithography-free method for directed colloidal crystal assembly based on wrinkling". In: *Soft Matter* 3.12 (2007), pp. 1530–1536.

[13] A. Schweikart et al. "Controlling inter-nanoparticle coupling by wrinkle-assisted assembly". In: *Soft Matter* 7.9 (2011), pp. 4093–4100.

[14] W. S. Tan et al. "Effect of Block Copolymer Architecture on the Thermally Induced Swelling of Micelle-Containing Multilayer Thin Films". In: *Macromolecules* 44.19 (2011), pp. 7767–7774.

[15] O. D. Velev and S. Gupta. "Materials Fabricated by Micro- and Nanoparticle Assembly - The Challenging Path from Science to Engineering". In: *Advanced Materials* 21.19 (2009), pp. 1897–1905.

[16] Y. N. Xia et al. "Monodispersed colloidal spheres: Old materials with new applications". In: *Advanced Materials* 12.10 (2000), pp. 693–713.

[17] S. T. Milner. "Polymer Brushes". In: *Science* 251.4996 (1991), pp. 905–914.

[18] M. Ballauff and O. Borisov. "Polyelectrolyte brushes". In: *Current Opinion in Colloid and Interface Science* 11.6 (2006), pp. 316–323.

[19] M. Biesalski, D. Johannsmann, and J. Ruhe. "Synthesis and swelling behavior of a weak polyacid brush". In: *Journal of Chemical Physics* 117.10 (2002), pp. 4988–4994.

[20] T. Chen et al. "Stimulus-responsive polymer brushes on surfaces: Transduction mechanisms and applications". In: *Progress in Polymer Science* 35.1-2 (2010), pp. 94–112.

[21] M. A. Cohen Stuart et al. "Emerging applications of stimuli-responsive polymer materials". In: *Nature Materials* 9.2 (2010), pp. 101–113.

[22] G. (Ed.) Lagaly. *Molecular Organisation on Interfaces*. Springer Berlin. Berlin/Heidelberg, 2002.

[23] X. Guo and M. Ballauff. "Spatial dimensions of colloidal polyelectrolyte brushes as determined by dynamic light scattering". In: *Langmuir* 16.23 (2000), pp. 8719–8726.

[24] A. Jusufi, C. N. Likos, and M. Ballauff. "Counterion distributions and effective interactions of spherical polyelectrolyte brushes". In: *Colloid and Polymer Science* 282.8 (2004), pp. 910–917.

[25] G. Dominguez-Espinosa et al. "Optical tweezers to measure the interaction between poly(acrylic acid) brushes". In: *Polymer* 49.22 (2008), pp. 4802–4807.

[26] X. Guo and M. Ballauff. "Spherical polyelectrolyte brushes: Comparison between annealed and quenched brushes". In: *Physical Review E* 64.5 (2001).

[27] C. Gutsche et al. "Micro-rheology on (polymer-grafted) colloids using optical tweezers". In: *Journal of Physics-Condensed Matter* 23.18 (2011).

[28] Y. Mei et al. "Collapse of spherical polyelectrolyte brushes in the presence of multivalent counterions". In: *Physical Review Letters* 97.15 (2006).

[29] A. N. Korovin et al. "Nanoreactor-Assisted Polymerization Toward Stable Dispersions of Conductive Composite Particles". In: *Macromolecular Rapid Communications* 32.5 (2011), pp. 462–467.

[30] F. Schacher et al. "Interpolyelectrolyte Complexes of Dynamic Multicompartment Micelles". In: *Acs Nano* 3.8 (2009), pp. 2095–2102.

[31] M. Schrinner et al. "Single Nanocrystals of Platinum Prepared by Partial Dissolution of Au-Pt Nanoalloys". In: *Science* 323.5914 (2009), pp. 617–620.

[32] A. Wittemann and M. Ballauff. "Interaction of proteins with linear polyelectrolytes and spherical polyelectrolyte brushes in aqueous solution". In: *Physical Chemistry Chemical Physics* 8.45 (2006), pp. 5269–5275.

[33] Y. Lu, A. Wittemann, and M. Ballauff. "Supramolecular Structures Generated by Spherical Polyelectrolyte Brushes and their Application in Catalysis". In: *Macromolecular Rapid Communications* 30.9-10 (2009), pp. 806–815.

[34] H. Gliemann et al. "Adhesion of spherical polyelectrolyte brushes on mica: An in situ AFM investigation". In: *Langmuir* 22.17 (2006), pp. 7254–7259.

[35] Y. Mei et al. "Engineering the interaction of latex spheres with charged surfaces: AFM investigation of spherical polyelectrolyte brushes on mica". In: *Macromolecules* 36.10 (2003), pp. 3452–3456.

[36] C. Hanske et al. “Adsorption of Spherical Polyelectrolyte Brushes: from Interactions to Surface Patterning”. In: *Zeitschrift Fur Physikalische Chemie-International Journal of Research in Physical Chemistry and Chemical Physics* 226.7-8 (2012), pp. 569–584.

[37] H. J. Butt, B. Cappella, and M. Kappl. “Force measurements with the atomic force microscope: Technique, interpretation and applications”. In: *Surface Science Reports* 59.1-6 (2005), pp. 1–152.

[38] H. J. Butt. “Measuring Electrostatic, Vanderwaals, and Hydration Forces in Electrolyte-Solutions with an Atomic Force Microscope”. In: *Biophysical Journal* 60.6 (1991), pp. 1438–1444.

[39] W. A. Ducker, T. J. Senden, and R. M. Pashley. “Direct Measurement of Colloidal Forces Using an Atomic Force Microscope”. In: *Nature* 353.6341 (1991), pp. 239–241.

[40] S. Block and C. A. Helm. “Single Polyelectrolyte Layers Adsorbed at High Salt Conditions: Polyelectrolyte Brush Domains Coexisting with Flatly Adsorbed Chains”. In: *Macromolecules* 42.17 (2009), pp. 6733–6740.

[41] V. Bosio et al. “Interactions between silica surfaces coated by polyelectrolyte multilayers in aqueous environment: comparison between precursor and multilayer regime”. In: *Colloids and Surfaces a-Physicochemical and Engineering Aspects* 243.1-3 (2004), pp. 147–155.

[42] J. Buensow et al. “Direct Correlation between Local Pressure and Fluorescence Output in Mechanoresponsive Polyelectrolyte Brushes”. In: *Angewandte Chemie-International Edition* 50.41 (2011), pp. 9629–9632.

[43] E. Spruijt et al. “Binodal Compositions of Polyeleetrolyte Complexes”. In: *Macromolecules* 43.15 (2010), pp. 6476–6484.

[44] Q. Chen et al. “Patterns of surface immobilized block copolymer vesicle nanoreactors”. In: *European Polymer Journal* 47.2 (2011), pp. 130–138.

[45] T. Chen, R. Jordan, and S. Zauscher. “Dynamic Microcontact Printing for Patterning Polymer-Brush Microstructures”. In: *Small* 7.15 (2011), pp. 2148–2152.

[46] H. P. Zheng, M. F. Rubner, and P. T. Hammond. “Particle assembly on patterned "plus/minus" polyelectrolyte surfaces via polymer-on-polymer stamping”. In: *Langmuir* 18.11 (2002), pp. 4505–4510.

[47] M. Hoffmann et al. "Surface potential of spherical polyelectrolyte brushes in the presence of trivalent counterions". In: *Journal of Colloid and Interface Science* 338.2 (2009), pp. 566–572.

[48] W. Kern and D. A. Puotinen. "Cleaning Solutions Based on Hydrogen Peroxide for Use in Silicon Semiconductor Technology". In: *Rca Review* 31.2 (1970), pp. 187–.

[49] X. P. Jiang et al. "Polymer-on-polymer stamping: Universal approaches to chemically patterned surfaces". In: *Langmuir* 18.7 (2002), pp. 2607–2615.

[50] M. Pretzl et al. "A Lithography-Free Pathway for Chemical Microstructuring of Macromolecules from Aqueous Solution Based on Wrinkling". In: *Langmuir* 24.22 (2008), pp. 12748–12753.

[51] M. von Smoluchowski. In: *Zeitschrift fuer Physikalische Chemie* 92 (1917), p. 129.

[52] A. Wittemann et al. "High elongation of polyelectrolyte chains in the osmotic limit of spherical polyelectrolyte brushes: A study by cryogenic transmission electron microscopy". In: *Journal of the American Chemical Society* 127.27 (2005), pp. 9688–9689.

[53] D. J. Scott, S. E. Harding, and A. J Rowe. *Analytical Ultracentrifugation - Techniques and Methods*. Cambridge, 2005.

[54] A. Wittemann, B. Haupt, and M. Ballauff. "Adsorption of proteins on spherical polyelectrolyte brushes in aqueous solution". In: *Physical Chemistry Chemical Physics* 5.8 (2003), pp. 1671–1677.

[55] A. Wittemann, B. Haupt, and M. Ballauff. "Controlled release of proteins bound to spherical polyelectrolyte brushes". In: *Zeitschrift Fur Physikalische Chemie-International Journal of Research in Physical Chemistry and Chemical Physics* 221.1 (2007), pp. 113–126.

[56] M. Schrinner, B. Haupt, and A. Wittemann. "A novel photoreactor for the production of electrosterically stabilised colloidal particles at larger scales". In: *Chemical Engineering Journal* 144.1 (2008), pp. 138–145.

[57] J.-W. Kim, R. J. Larsen, and D. A. Weitz. "Uniform nonspherical colloidal particles with tunable shapes". In: *Advanced Materials* 19.15 (2007), pp. 2005–+.

[58] E. B. Mock et al. "Synthesis of anisotropic nanoparticles by seeded emulsion polymerization". In: *Langmuir* 22.9 (2006), pp. 4037–4043.

[59] M. Ballauff. "Spherical polyelectrolyte brushes". In: *Progress in Polymer Science* 32.10 (2007), pp. 1135–1151.

[60] M. L. Jimenez et al. "Giant permittivity and dynamic mobility observed for spherical polyelectrolyte brushes". In: *Soft Matter* 7.8 (2011), pp. 3758–3762.

[61] H. Ohshima and K. Makino. "Electrophoretic mobility of a particle covered with a partially ion-penetrable polyelectrolyte layer". In: *Colloids and Surfaces a-Physicochemical and Engineering Aspects* 109 (1996), pp. 71–75.

[62] R. Pericet-Camara et al. "Interaction forces and molecular adhesion between pre-adsorbed poly(ethylene imine) layers". In: *Journal of Colloid and Interface Science* 296.2 (2006), pp. 496–506.

[63] Y. Lu et al. "'Nano-tree' - type spherical polymer brush particles as templates for metallic nanoparticles". In: *Polymer* 47.14 (2006), pp. 4985–4995.

7

Reversible swelling transitions in stimuli-responsive layer-by-layer films containing block copolymer micelles

Gensel, J., Dewald, I.,Erath, J.,Betthausen, E., Mueller, A. H. E., Fery, A., Reversible swelling transitions in stimuli-responsive layer-by-layer films containing block copolymer micelles. Chemical Science, 2013. 4(1): p. 325-334.

Abstract

We present a new nanoporous multilayer system with a reversible pH-triggered swelling transition. Using the layer-by-layer approach, pH-responsive block copolymer micelles with a hydrophobic core, a weak polyanion shell and a strong polycation corona formed from an ABC triblock terpolymer are included within multilayer films. The approach of complexing the strong polycationic corona with a strong polyanion leads to the creation of novel double-end-tethered polyelectrolyte brush structures confined between the hydrophobic micellar cores and the interpolyelectrolyte complexes. The swelling degree, morphology as well as the mechanical properties of the coatings are reversibly tunable by the solution pH due to the ionization-induced swelling of the pH-sensitive polyelectrolyte-brush-like shell of the incorporated micelles resulting in large-scale volumetric changes of the film. Moreover, controlling the internal film architecture by the number of deposition steps allows tuning the properties of the porous multilayers such as the density of incorporated micelles, the porosity, and the equilibrium swelling degree to more than 1200%.

7.1 Introduction

The design of "smart" coatings, which can reversibly switch their physico-chemical characteristics in reaction to external stimuli is a very attractive research field regarding its diverse applications, e.g. in drug delivery and microfluidic systems, cell tissue engineering, as well as sensing, or actuation (see reviews [1, 2, 3, 4, 5, 6, 7, 8, 9, 10]). The adsorption of stimuli-responsive soft matter systems on a solid support is an effective and simple way to fabricate switchable surfaces. Coatings which respond to changes in pH or ionic strength can be obtained by chemical grafting of polymer or polyelectrolyte brushes onto planar [11, 12, 13, 14] or curved [15] surfaces. Alternatively, thin films of polymer networks can be used as smart coatings. In most of these cases hydrogel-like films can uptake large amounts of water, whereby their swelling degree (the ratio of swollen to dry volume), which can be controlled by external physical or chemical signals, determines their mechanical and optical properties, permeability, adhesion etc. Such a modulation of the mechanical properties of coatings can be used for example to control cell adhesion [16].

Another elegant approach to design smart surfaces is the adsorption of block copolymer micelles. Several research groups have studied the stimuli-responsive behavior of an adsorbed monolayer of micelles [17, 18, 19, 20, 21]. Recently, we reported on the

immobilization of micelles of a linear ABC triblock terpolymer consisting of polybutadiene (B), poly(methacrylic acid) (MAA), and quaternized poly(2-(dimethylamino)ethyl methacrylate) (Dq), BMAADq on silica [22]. We have found that by controlling the solution pH at the solid-liquid interface of the adsorbed micelles, it is possible to reversibly switch the micellar morphology and charge density of the corona. This pH-responsive behavior can be controlled by the ionization degree of the weak polyelectrolyte middle block (MAA) and is completely reversible on a short time scale. More recently, we have successfully used these switchable coatings as active surfaces for bio-applications, in particular for controlled self-regulated bacteria release [23]. However, the long-term treatment at $pH < pK_{\mathrm{a,apparent}}$ of MAA causes irreversible changes in themorphology of the immobilized BMAADq micelles [22]. In general, the instability of a monolayer of stimuli-responsive micelles is a challenging aspect [22, 24, 19, 21, 25] which is critical for many applications. One way to improve the resilience of such structures is the chemical crosslinking of the hydrophobic cores. [22] Sukhishvili and co-workers reported another facile method for stabilization against environmental influences for otherwise instable surface-attached micelles via self-assembly of the micelles with a polyelectrolyte layer using physical cross-linking [25]. They observed irreversible morphological changes and desorption of a significant fraction of temperature-responsive micelles of poly(N-vinylpyrrolidone)-bpoly(N-isopropylacryl-amide) into the solution, while the same surface-adsorbed micelles covered with a top layer of poly- (methacrylic acid) maintained their original structural integrity. Besides the improved stability, this strategy allows coverage of any type of substrate and fine-tuning the thickness and nanostructure of the stimuli-responsive film via layer-by-layer (LbL) assembly of oppositely charged polymers [26, 27, 28]. In particular, Tan et al. reported that temperature-sensitive core-shell micelles of ABA triblock copolymers can be incorporated within the LbL films while retaining their stimuli-responsive properties [29, 30]. The obtained films are generally very thin ($10 - 100\,\mathrm{nm}$) enabling a rapid response to environmental changes as compared to bulk materials. The incorporation of charged nanoparticles [31, 32] as well as diblock copolymer micelles into multilayers with integrated stimuli-responsive properties has been previously reported for one-type-micellar [33, 34, 35, 36, 37] or micelle-micelle-systems [38, 39, 40]. These types of systems are particularly suitable for the fabrication of hydrogel-like films [34] for drug delivery [33, 35, 25], coatings with tunable optical properties [40, 36], or antibacterial coatings [41]. Furthermore, LbL assembly of micelles offers the advantage of fabricating porous thin films [40] without any of the additional post-treatment steps usually required for their preparation [42] A special class of stimuli-responsive porous hydrogel-like thin films

combines fast response and precise control over the pore closing/opening by an external signal. [7, 9].
Here, we study a new LbL system, consisting of ABC block terpolymer micelles with a hydrophobic polybutadiene (B) core, a pH-sensitive poly(methacrylic acid) (MAA) shell, and a cationic corona of quaternized poly(2-(dimethylamino)ethyl methacrylate) (Dq) (BMAADq) and linear strong polyanion poly(sodium 4- styrene sulfonate) (PSS). Due to the pH-sensitive character of the incorporated micelles, the system allows the ionization degree of the weak polyelectrolyte block (MAA) to be varied by changing the pH. One remarkable feature of the system is that the pHsensitive block is not a component of the multilayer complexes, but is covalently bound to the micellar core on the one side and to the multilayer-forming corona on the other side. This approach leads to the formation of a double-end-tethered weak polyelectrolyte brush-like shell. Hence, we investigated the effect of solution pH on the swelling behavior as well as on the mechanical properties of the hydrogel film. In addition, the influence of the swelling on the film porosity was studied.

7.2 Experimental

Materials

The triblock terpolymer consisting of polybutadiene (B), poly-(methacrylic acid) (MAA), and quaternized poly(2-(dimethylamino) ethyl methacrylate) (Dq), $B_{800}MAA_{200}Dq_{285}$ (subscripts denoting the degrees of polymerization of the respective blocks) with an M_n of $\approx 110000\,\mathrm{gmol}^{-1}$ and a PDI of 1.10 was synthesized *via* sequential living anionic polymerization followed by polymer-analogous modifications as described elsewhere. [43] In particular, the poly(2-(dimethylamino)ethyl methacrylate) block was exhaustively quaternized with dimethyl sulfate. After quaternization in a dioxane-water mixture (1:1, v/v), the BMAADq terpolymer was dialyzed against pH 10 buffer solution to obtain a micellar stock solution with a concentration of $0.5\,\mathrm{gL}^{-1}$. From this stock solution changes in pH were performed by dialyzing against the corresponding buffer solutions (pH 4, VWR, AVS Titrinorm). [43] The obtained micelles have a spherical shape as confirmed by cryogenic TEM and DLS experiments [43]. The hydrodynamic radius R_h of the micelles in pH 4 buffer was determined by DLS to 107 nm. According to the core radius obtained via cryo-TEM, the aggregation number, N_{agg}, of the BMAADq

micelles can be calculated with Eq. 7.1:

$$N_{\text{agg}} = \frac{m_{\text{core}}}{m_{\text{PB}}^{\text{chain}}} = \frac{4\pi N_A \rho_{\text{PB}} R_{\text{core}}^3}{3M_{\text{PB}}^{\text{chain}}} \tag{7.1}$$

where m_{core} is the mass of the micellar core; $m_{\text{PB}}^{\text{chain}}$ is the mass of an individual PB chain; N_A is the Avogadro constant; ρ_{PB} is the density of polybutadiene; R_{core} is the radius of the micellar core according to cryo-TEM and $M_{\text{PB}}^{\text{chain}}$ is the molecular weight of an individual PB chain. At pH 4 the core radius is 32 nm, which yields an aggregation number of approximately 1800. Please note that this method is just a rough estimate and strongly depends on the quality of the cryo-TEM micrographs for the determination of the core interface. Poly(sodium 4-styrene sulfonate) (PSS, $M_w = 70000\,\text{gmol}^{-1}$) was purchased from Sigma-Aldrich. HCl and NaOH solution ($0.1\,\text{molL}^{-1}$, Grüssing) were used to adjust the pH of water.

Multilayer deposition

The LbL films were assembled on silicon wafers (CrysTec) from $0.45\,\text{gL}^{-1}$ polymer solutions via dip coating. The substrates were cleaned using the RCA technique [44] (sonication in a 1 : 1 mixture of water and 2-propanol for 15 min, followed by heating at 70° C in a 5 : 1 : 1 mixture of water, 25% ammonia solution, and 30% hydrogen peroxide solution for 10 min). The freshly cleaned substrates were then dipped into a solution of BMAADq micelles in pH 4 buffer solution (VWR, AVS Titrinorm, ionic strength ≈ 0.05 M) for 15 min before rinsing with water. Next, the substrates were dipped into an aqueous solution of PSS (adjusted to pH 4 with 0.1 M HCl) for 15 min. The films were dried in a stream of nitrogen before characterization.

Methods

Ellipsometry measurements in air were performed with a Sentech SE 850 spectroscopic ellipsometer at a constant incidence angle of 70°. A home-built liquid cell [45] was used for *in situ* ellipsometry in water of a different pH at a constant incidence angle of 65°. Measurements were performed after a minimum equilibration time of 20 min. Atomic force microscopy (AFM) images were taken with a commercial AFM (Dimension^{TM} 3100 equipped with a Nano-Scope V controller, both from Bruker AXS Inc., USA) operating in TappingMode^{TM} using Si_3N_4 cantilevers from Olympus with a typical spring constant of $\approx 42\,\text{Nm}^{-1}$ and a typical resonance frequency of 300 kHz (OMCL-AC160TS).

Scanning in fluid was performed with a direct driven TappingMode^{TM} probe holder (DTFML-DD-HE, Bruker, AXS Inc., USA) using cantilevers with a spring constant of $\approx 0.06\,\mathrm{Nm}^{-1}$ and a resonance frequency of $12 - 24\,\mathrm{kHz}$ (Bruker, SNL-10).
Scanning electron microscopy (SEM) measurements were obtained on a Gemini Leo 1550 instrument operating at 3 keV. Samples were sputtered with a 1.3 nm thin platinum layer.
The colloidal probe atomic force microscopy (CP AFM) measurements were performed on an Asylum MFP 3D AFM (Mannheim, Germany) in a water droplet at the corresponding pH. Glass particles (Polysciences, Germany) were used as force sensors. The CPs, made of SiO_2, were glued with an epoxy resin (UHU schnellfest, Germany) to pre-calibrated cantilevers (force constant $\approx 0.1\,\mathrm{Nm}^{-1}$, NSC 12, tipless, noAl, Micromash, Estonia) using a micromanipulator (MP-285, Shutter Instrument, USA) and an inverted optical microscope (Axiovert 200, Zeiss, Germany). Force constants of the cantilevers were determined by the thermal noise method introduced by Hutter and Bechhoefer. [46] For all the presented data, a cantilever with a force constant of $0.125\,\mathrm{Nm}^{-1}$ and a CP with a radius of $R = 23\,\mathrm{mm}$ was used. The optical lever sensitivity was always detected prior to recording the data by reference measurements on a hard glass substrate.

7.3 Results and Discussion

Layer-by-layer assembly

To develop pH-responsive layer-by-layer hydrogel coatings, we used a linear ABC triblock terpolymer consisting of polybutadiene (B), poly(methacrylic acid) (MAA), and quaternized poly(2-(dimethylamino)ethyl methacrylate) (Dq), BMAADq. The molecular structure is given in Figure 7.1A. Details regarding the synthesis and characterization of the polymer can be found elsewhere. [43] In aqueous solution, BMAADq self-assembles into core-shell-corona micelles with a hydrophobic B core, a pHsensitive MAA shell and a strong cationic Dq corona.
At low pH ($pH < pK_{\mathrm{a,app}}$ of MAA ≈ 5.5 (Ref. [47])), the pH-sensitive MAA block is uncharged and does not form an IPEC, but rather phase separates from the corona as shown in Figure 7.1B. At high pH, this block is negatively charged through the deprotonation of the carboxylic acid groups leading to intramicellar interpolyelectrolyte complex (im-IPEC) formation with the cationic corona of Dq. Hence, the composition of the micellar shell as well as the charge density of the corona can be controlled by

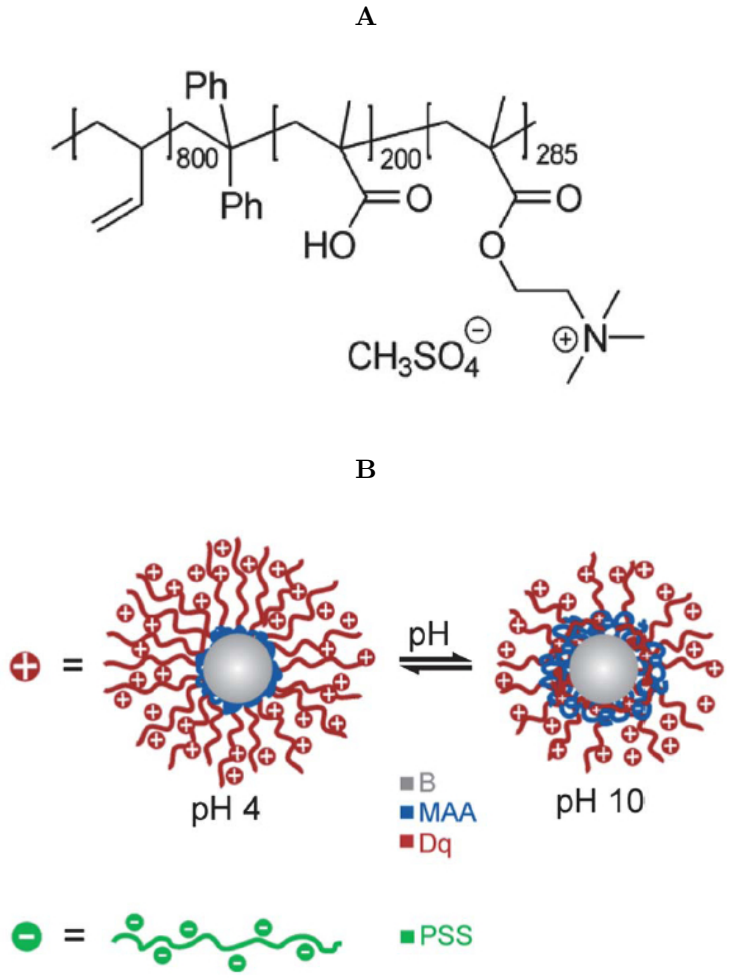

Figure 7.1: Chemical structure of the BMAADq triblock terpolymer 7.1A, schematic representation of the solution structure of positively charged BMAADq micelles at pH 4 and pH 10, and negatively charged PSS 7.1B.

the solution pH (Figure 7.1B.

Due to the cationic character of the micelles, we chose anionic poly(sodium 4-styrene sulfonate) (PSS) as the counterpart for the layer-by-layer assembly. PSS is known to form stable complexes/multilayers with strongly charged polycations (like Dq) because of its permanently high charge density [48].

We prepared LbL films at pH 4. At this pH, the MAA shell is protonated and does not form an im-IPEC with the Dq corona. Therefore, all of the coronal chains are expected to form stable complexes with PSS. Consequently, the MAA block should form an uncharged shell around the B core at this pH. Figure 7.2A displays the ellipsometric dry film thickness plotted versus the number of triblock terpolymer/polyanion deposition steps, x. The film growth follows a square root dependency (Figure 7.2B). This behavior indicates a diffusion-limited assembly process, which may originate from the diffusion of the micelles into the pores of the film: further deposited micelles do not adsorb on top of the film, but diffuse through the pores to fill them and thus increase the micelle density in the multilayers.

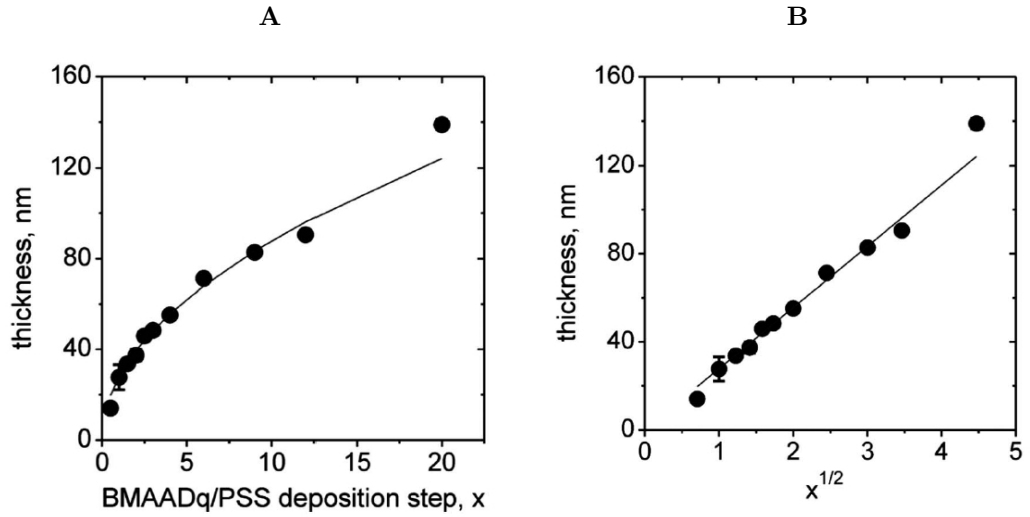

Figure 7.2: Ellipsometric dry thickness vs. the number of BMAADq/PSS deposition steps, x 7.2A and vs. the square root of x 7.2B. The lines are a square root fit and a linear fit to the data, respectively.

To obtain detailed structural information about the LbL multilayers, atomic force microscopy (AFM) and scanning electron microscopy (SEM) measurements were performed on dried samples. From the AFM height image of one bilayer of BMAADq/PSS (denoted as $(\text{BMAADq/PSS})_1$) (Figure 7.3 a), the average diameter and the height of

the spherical-cap-like structures (based on the average of at least 30 features) were estimated to be (125 ± 8) nm and (49 ± 5) nm, respectively. The dimensions obtained by AFM correspond to the topography image including the core, the shell, and the IPEC between the Dq corona and the extrinsic homopolymer PSS. In contrast, the SEM image of one bilayer in the dry state (Figure 7.3 c) shows the hydrophobic cores (bright) surrounded by a dark shell and the Dq/PSS IPEC indicating the retained core-shell-IPEC-structure upon incorporation of the micelles into multilayers. The diameter of the hydrophobic core is (71 ± 8) nm (based on the average of at least 30 micelles), which is comparable with the diameter of the cores in pH 4 buffer solution (≈ 64 nm) [43]. In our previous work, we have shown that the adsorption of BMAADq micelles onto a silica surface follows the random sequential adsorption (RSA) model with a maximum surface coverage of 0.54 [22]. Therefore, micelles can only be randomly dispersed on the substrate for the first layer leading to a porous structure of the resulting LbL films (Figure 7.3). The adsorption of the same micelles on the substrates covered with a layer of negatively charged PSS resulted in similar adsorption kinetics as well as the saturation value of ≈ 0.5 (Supporting Information, Figure 7.9). A further example is the random adsorption of the micelles studied on ultrasonically formed mesoporous aluminum [22]. These examples confirm that the system studied here can be used to cover different substrates in a controlled and reproducible manner. Note that since this hit-stick RSA adsorption behavior is associated with the immobilization of micelles, rearrangements inside the film should not be possible. This is consistent with the work of Kabanov and co-workers: the high affinity of PSS to polycations imposes kinetic restrictions on the exchange reactions of PSS/Dq IPECs [49]. Therefore, to the best of our knowledge, the nonlinear buildup and the reduction of porosity do not occur as a result of the rearrangement of micelles during the deposition.

The assumption of micelles filling the void space in the film instead of attaching on the top (resulting in a non-linear buildup behavior (Figure 7.2)) is supported by a detailed study of the nanostructure (Figure 7.3). The AFM height and SEM images in Figure 7.3 demonstrate a significant increase in the micelle density in the film and therefore a decreased porosity with increasing number of deposition steps.

The porosity (P) of the films was evaluated from refractive index measurements applying the mixing rule to the Lorentz-Lorenz equation [50]

$$\frac{n_x^2 - 1}{n_x^2 + 2} = P\frac{n_{\text{air}}^2 - 1}{n_{\text{air}}^2 + 2} + (1 - P)\frac{n_f^2 - 1}{n_f^2 + 2} \tag{7.2}$$

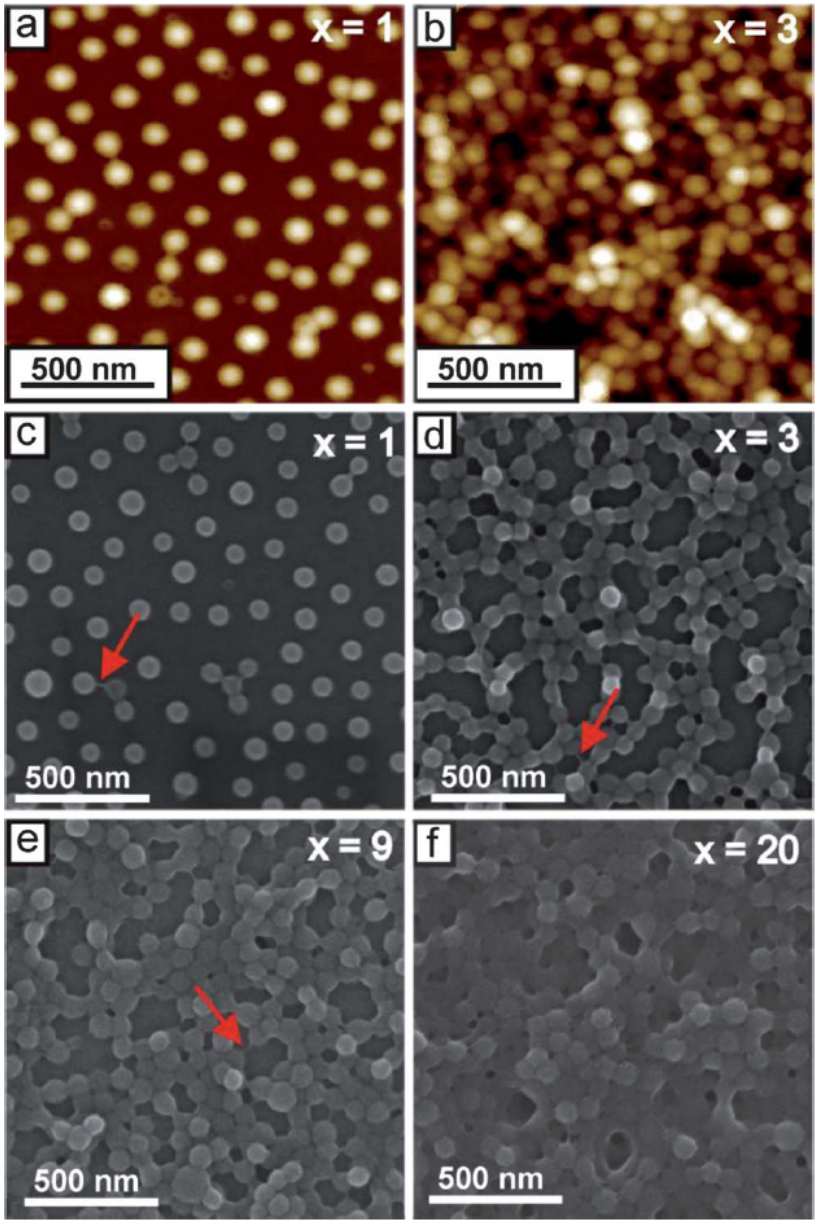

Figure 7.3: $1.5\,\mu\mathrm{m}X1.5\,\mu\mathrm{m}$ AFM height images (a and b) (color equates to $z = 0 - 100\,\mathrm{nm}$) and SEM images (c-f) of $(\mathrm{BMAADq/PSS})_x$ porous films. x is the number of build-up steps. Arrows indicate the formation of hydrophobic bridges

where n_x, n_{air}, and n_f are the refractive indices of the porous film, air, and the dense film and P and $(1-P)$ are the volume fraction of the pores and of the dense film, respectively. With $n_{\text{air}} = 1$, the Eq. 7.2 can be simplified to

$$P = 1 - \frac{n_x^2 - 1}{n_f^2 - 1} \cdot \frac{n_f^2 + 2}{n_x^2 + 2} \tag{7.3}$$

Figure 7.4 shows the refractive indices n_x of porous films measured by ellipsometry and the resulting porosity values obtained from (7.3), assuming that the refractive index of the dense film $n_f = 1.51$ (estimated by ellipsometry of drop-coated PSS (n = 1.51) and BMAADq (n = 1.51) films).

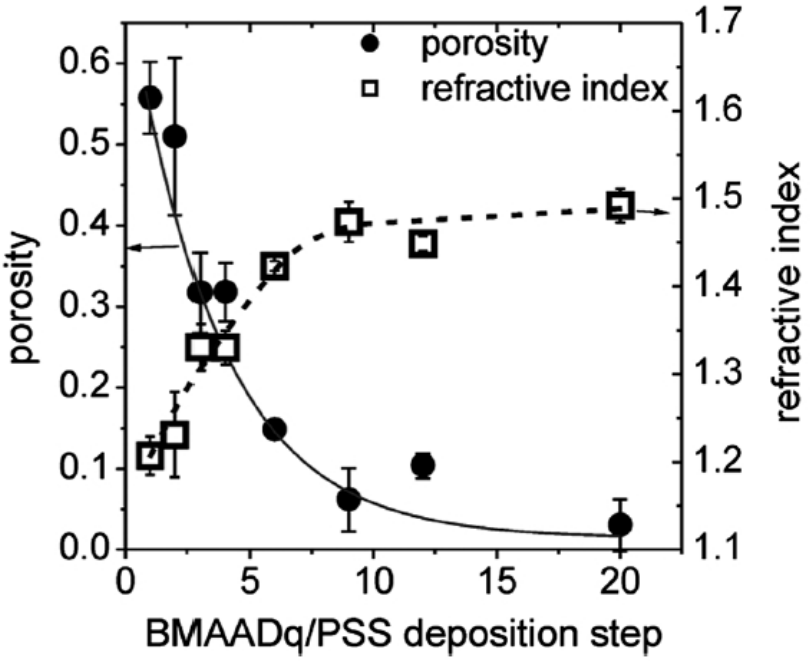

Figure 7.4: Porosity (∘) and refractive index (□) vs. the number of BMAADq/PSS deposition steps. The lines are guides to the eye.

The porosity of the multilayers can be easily tuned between ≈ 50% and 0% by the number of deposition steps. Such interconnected micellar network formation can be explained by the generation of hydrophobic bridges during the assembly process as indicated by the arrows in the SEM-images (Figure 7.3 c-e). Hydrophobic bridges were also found in aqueous solutions of the same micelles [43] as well as those of other block terpolymer micelles with a low glass transition temperature of the coreforming block.[51, 52] Still, mainly spherical particles are found in the multilayers indicating that the core-shell structure remains intact upon integration into multilayers.

Stimulus response

On the basis of the retained core-shell structure of the LbLincorporated micelles and due to the pH-responsive character of the polyelectrolyte brush-like MAA shell, we investigated the swelling behavior of these films by in situ ellipsometry. To confirm data obtained from ellipsometry, we additionally measured the height difference at the edge of a scratch by AFM in a liquid cell. Exemplarily, results for a three-bilayer-film $(BMAADq/PSS)_3$ at different pH between pH 4 and 12 are shown in Figure 7.5. Films with differing number of bilayers follow the same trend with varying pH.

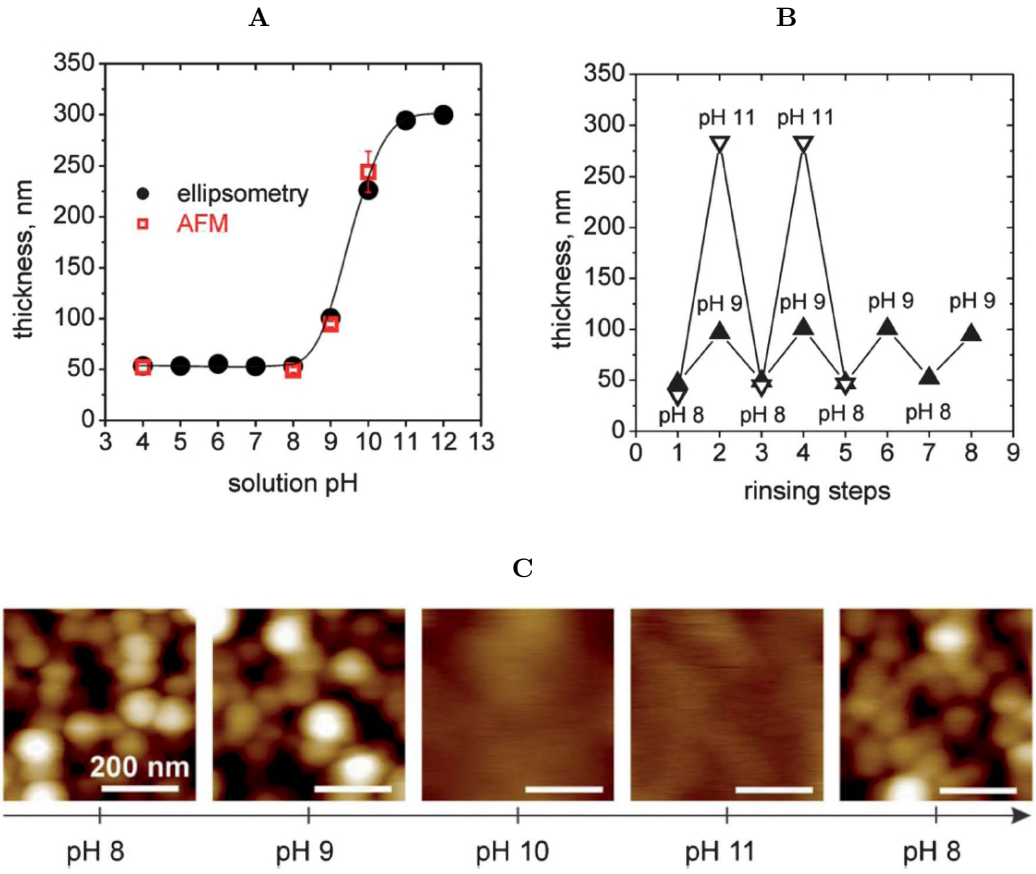

Figure 7.5: In situ measurements of the ellipsometric thickness (∘) and liquid cell AFM height difference at a scratch (red *box*) of $(BMAADq/PSS)_3$ vs. the solution pH 7.2A, *in situ* ellipsometry measurements of reversible pH-triggered swelling and contraction of $(BMAADq/PSS)_3$ film 7.2B and corresponding $500\,nm X 500\,nm$ AFM height images (color equates to $z = 0 - 100\,nm$) in water at different pH values 7.5C.

Swelling of the film is observed when the pH is increased to alkaline values with a transition at pH $\approx$ 9.5. The increase in thickness corresponds to the deprotonation of the carboxylic groups of the MAA shell and can be tuned by the degree of dissociation a. In acidic solutions at $\alpha \approx 0$, the film is in a contracted state. With increasing pH, a increases leading to a higher charge density and therefore increased repulsive interactions between the COO^- groups. This results in a higher osmotic pressure of trapped counter ions, a stretching of the MAA chains and a swelling of the film.
The transition region at $pH \approx 9.5$ (corresponding to the pH at which $\alpha \approx 0.5$) is significantly higher than the apparent pK_{a} ,value of PMAA reported in the literature ($pK_{\mathrm{a,app}} \approx 5.5$ (Ref. [47])) indicating that when confined into the micellar multilayer film, MAA becomes a weaker polyacid in comparison to its behavior in dilute solution. The shift in the apparent pK_a values of weak polyelectrolytes upon incorporation into multilayered films is also known from other work.[53, 54, 55, 56, 57] In contrast to our results, in the latter cases, the apparent pK_a values of incorporated weak polyacids and polybases were shifted by $\approx$ 1 to 4 pH units to the acidic or alkaline values, respectively. The above cited results indicate that the polyacid becomes a stronger acid if it is the component of a polyelectrolyte multilayer film.
However, we observed an opposite effect, which originates from the fact that the MAA block is not a component of the multilayer complexes. In our system, the MAA block, which is covalently bound to the core-forming B block on the one side and to the Dq block (forming stable IPECs with PSS) on the other side, can be described as a spherical polyelectrolyte brush (around the micellar core), confined between electrostatically assembled layers. In fact, the shift to higher pH values agrees with experiments on polyelectrolyte brushes. The swelling transition of grafted PMAA brush layers with a high grafting density was found to be shifted to pH 9 as a result of the Coulombic repulsion of neighboring charges. [58] Currie et al. reported similar pKa shifts of poly(acrylic acid) brushes that became more pronounced with increasing grafting density. [59] In potentiometric titrations of multi-arm star-shaped poly(acrylic acid) we also observed an increase in the $pK_{\mathrm{a,app}}$ with increasing arm number [60]. These findings are additionally supported by theoretical predictions. [61]
The pH switch is fully reversible after several pH 8/pH 9 and pH 8/pH 11 cycling steps (Figure 7.5B). The MAA domains respond to pH switching by changing between high and low ionized states resulting in the swelling and shrinking of the multilayers.
Although a single layer of micelles studied here shows irreversible morphological changes at pH 4 or lower [22], micelles that are covered with a layer of PSS are very robust and stable after long-term treatment (in the order of several hours) at pH values between

pH 4 and pH 12. This is due to the formation of a stable IPEC of PSS and the cationic corona of the micelles. A similar method for the stabilization against environmental influences for otherwise instable surface-attached micelles was reported by Sukhishvili and Zhu [25]. They observed that surface-adsorbed micelles covered with a top layer of poly(methacrylic acid) remained stable and maintained their original structural integrity, while the same uncovered micelles showed irreversible morphological changes and desorption into the solution. The corresponding AFM images in water at different pH values are shown in Figure 7.5C. At slightly alkaline pH (pH 8), the film maintains its porous micellar morphology with an average pore diameter of $\approx$ 70 nm ranging from 30 to 160 nm. At higher pH (pH 9), the micellar diameter increases while the pore diameter decreases to a mean value of $\approx$ 50 nm. Here, the pores range in diameter from 20 to 120 nm. At even higher pH (pH 10 and pH 11), the volume filling factor $V = V_{\text{micelle}}/V_{\text{total, film}}$ is changed significantly upon swelling. After decreasing the pH to 8, the film regained its original porous structure indicating the reversible morphology changes triggered by pH. On the basis of the ellipsometric and AFM studies, we propose a schematic illustration of the reversible pH-triggered swelling and contraction of BMAADq/PSS multilayers (Figure 7.6).

As IPECs have an important and characteristic feature of competition (polyion exchange) and replacement (polyion substitution) reactions, the ionized MAA brush at pH 11 might compete with PSS in participating complexation with quaternized amine groups of the coronal chains. However, the rate and position of the equilibrium of these reactions is strongly dependent on the nature of the polyelectrolyte pair within a polyelectrolyte complex or multilayer (e.g. reviews [49],[62]). A comparable polyion interchange reaction in polyelectrolyte multilayers (PSS or PMAA and a polycation containing quaternized amine groups) was studied by Jomaa and Schlenoff [63]. They demonstrated that PSS irreversibly replaced all PMAA chains that were already part of the multilayer film at alkaline pH, when PMAA groups are completely ionized. Exposure of the PSS-containing multilayers to an alkaline solution of PMAA yielded no incorporation of PMAA as this would result in the formation of the energetically less favorable complex. This is as well in line with earlier findings of Kabanov and coworkers that in mixtures of polyanions, a polycation preferentially binds with sulfonate-containing polyanions [49, 64, 62]. PSS is one of the strongest competitors for associating with polycations, whereas PMAA is known to form weakly bound complexes. [65, 63, 62] Dubas and Schlenoff reported the difference in free energy of complexation of a quaternized amine group with an acrylic acid group and a sulfonate group to be 14.9 kJmol^{-1}. [65] As a consequence of this strong binding of sulfonate-containing

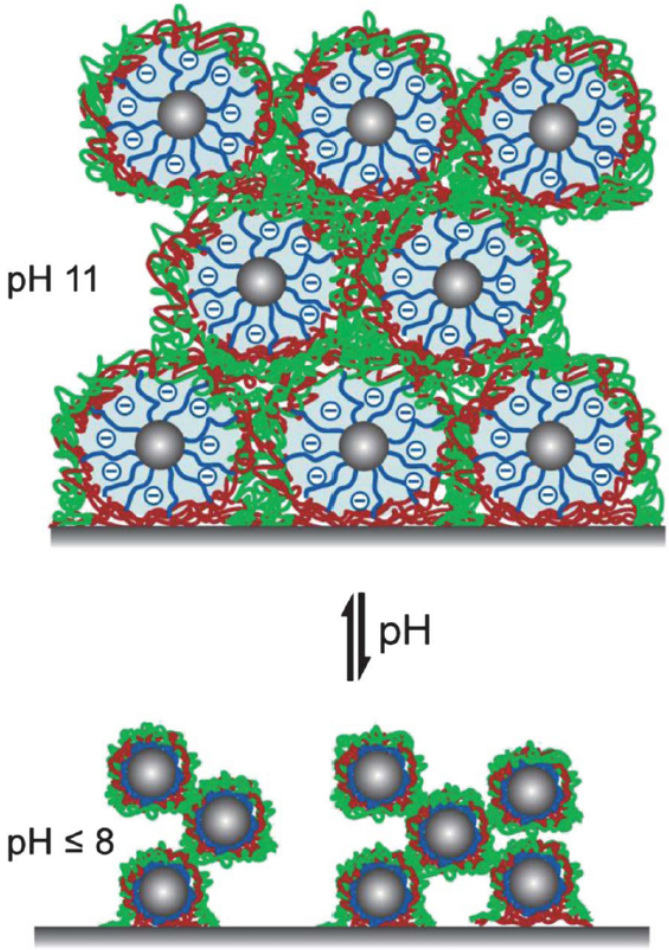

Figure 7.6: Proposed schematic illustration of reversible pH-triggered swelling and contraction of BMAADq/PSS multilayers.

polyanions with polycations, the interpolyelectrolyte chain exchange is inhibited. Thus, for our system, the positively charged Dq corona will preferentially associate with PSS rather than PMAA, even at pH 11.

Mechanical characterization

As the BMAADq/PSS multilayers swell upon increasing the pH of the solution, we expect that the mechanical properties change with the degree of swelling. To study these changes we used the colloidal probe technique introduced by Butt [66] and Ducker [67]. Data were recorded by force-mapping measurements with an AFM. The detected force-distance curves were transformed into force-indentation curves of the coatings by subtracting the effect of the cantilever deflection. Figure 7.7A shows the recorded force-indentation data for different swelling states of a $(BMAADq/PSS)_3$ multilayer. As upper force threshold we defined 20 nN which corresponds to deformations of around 80% of the film thickness. Measurements on the same spot of the sample show that the film is not plastically deformed (see Supporting Information Ch. 7.A Figure7.10). Since the adhesion in liquid is low and the films are not plastically deformed during the measurement, we used the linear elasticity theory to evaluate the mechanical properties of the system. The indentation of a sphere into a linear elastic infinite half space can be described by the Hertz model [68]

$$F = \frac{4}{3}\frac{E}{1-\nu^2}R^{1/2}\delta^{3/2}, \tag{7.4}$$

where F is the force applied by a spherical indenter (CP) with radius R, ν is the Poisson ratio, E the Young's modulus, and δ the indentation of the film. To avoid substrate effects, only data below 30% of indentation were used for the Hertz analysis. However, the values should be treated only as a rough estimation because the Hertz model is not exactly suited for inhomogeneous systems as in our case. Still, our data is well represented by the Hertz model as shown by the comparison of force curves plotted in log-log scale together with the power function $F \propto \delta^{3/2}$, confirming the Hertzian power law (supporting information Ch. 7.A, Figure 7.11). The Young's modulus was estimated using Eq. 7.4. Figure 7.7B summarizes the obtained data of the Young's modulus and the swelling degree as a function of the solution pH. Each value for the Young's modulus contains at least 300 data points.

The swelling degree was estimated from the ellipsometric measurements as $d_{\mathrm{sw}}/d_{\mathrm{dry}}$, where d_{sw} and d_{dry} are the film thicknesses in the swollen and dry state, respectively. As can be clearly seen, the Young's modulus is inversely proportional to the degree of

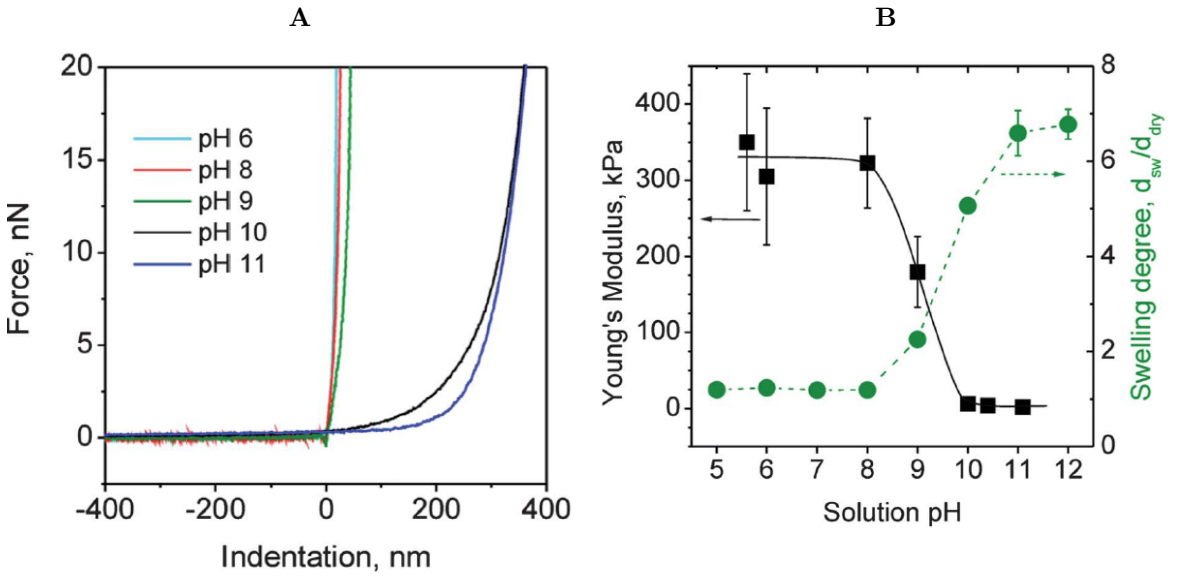

Figure 7.7: Force-indentation data for different swelling states 7.7A and Young's modulus (□) and swelling degree (○) (determined by ellipsometric measurements) as a function of the solution pH for a $(BMAADq/PSS)_3$ film 7.7B.

swelling. The modulus decreases with increasing pH (6 to 11) by at least 2 orders of magnitude from around 100 to 1 kPa. Surface force spectroscopy studies performed by Tsukruk and co-workers have also shown a softening of pHsensitive LbL capsules by 2 orders of magnitude (in the range of $0.1 - 1$ MPa in the contracted and 10 kPa in the swollen state) within a narrow pH range [69, 70, 71]]. Their results are comparable to our system: for the quenched state ($pH \leq 8$), the modulus is nearly constant at around 300 kPa, which is typical for partially swollen hydrogel films [16] or LbL capsules [70]. The transition between the contracted and swollen states occurs at $pH \approx 9$ corresponding to the estimated apparent pK_a value of the MAA brush. At $pH \geq 10$ (highly swollen state), the modulus converges to the low kPa range. This low kPa range of the Young's modulus is characteristic for highly swollen hydrogel materials [69, 70, 72, 71].

Effect of film thickness on swelling behavior

Due to significant differences in the density of the incorporated micelles and the porosity of the $(BMAADq/PSS)_x$ layers (Figure 7.3), we studied the effect of film microstructure on the macroscopic swelling behavior. The swelling degree (the ratio of swollen to dry volume) of surface-attached films equals the linear degree of swelling [73] and can

be calculated using ellipsometric thickness measurements. The equilibrium swelling degrees of the hydrogel-like films as a function of the dry thickness are summarized in Figure 7.8A. Ellipsometric measurements show that the swelling degree is strongly dependent on the LbL film thickness and therefore on the porosity of the multilayers, which can be tuned by the number of LbL deposition steps. The maximum swelling degree of ≈ 12 is obtained for the thinnest films made by one deposition step. With increasing thickness (decreased porosity), the swelling degree drops to a value of 2 for the thickest film studied.

Taking the differences in the microstructure into account, the observed trend of decreased swelling degree with increasing dry thickness is reasonable. The equilibrium swelling degree is a balance between two opposing forces: on the one hand the electrostatic self-repulsion and osmotic pressure of the trapped counter ions, which favor swelling, and on the other hand the elastic free energy, which opposes swelling. Thus, with increasing dry thickness the decreasing void fraction confines the particle volume change to one dimension perpendicular to the substrate. Consequently, steric effects may lead to a dominating contribution of the stretching entropy resulting in decreased swelling.

Additionally, the solvent gradient induced by the accumulation of solvent at the outmost layers may impact the swelling behavior. A similar trend of decreased swelling degree with increasing thickness was found for block copolymer films [74] and for polyelectrolyte multilayers in saturated solvent vapor [75] and solvents. [76]

Recalculation of the data to the water content in a swollen film ($1 - d_{\mathrm{dry}}/d_{\mathrm{sw}}$) results in a linear decrease with increasing dry thickness for all films with more than one bilayer (ch. 7.A, Figure 7.12). The highly swollen films exhibit a maximum water content of $\approx 90\%$. Interestingly, the plot of the swelling degree versus the porosity of the films yields a linear dependence (Figure 7.8B), reconfirming the dominating elastic energy contribution with decreasing porosity. The non-zero intercept means that a closepacked film with a porosity of 0 would still swell by a factor of 2 due to the contribution of the PSS/Dq IPEC and the swelling of the MAA brush. Note that in the case of zero porosity, only 1D swelling perpendicular to the substrate is possible.

7.4 Conclusion and Outlook

Using the layer-by-layer technique, ABC block terpolymer micelles with a hydrophobic B core, a pH-sensitive MAA shell and a charged Dq corona were included within multilayer films with tailored porous nanostructure and integrated pH-responsive proper-

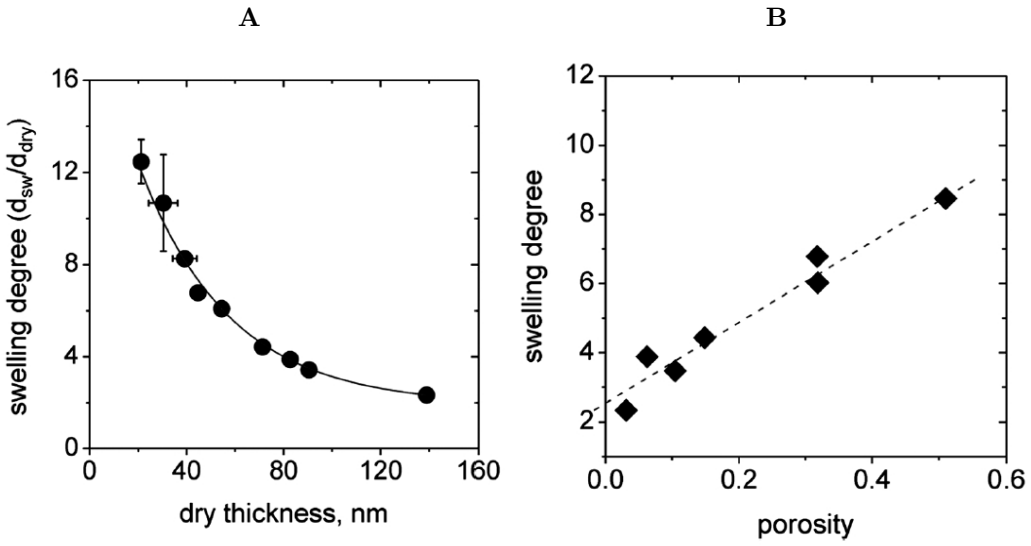

Figure 7.8: Swelling degree vs. dry thickness determined by ellipsometric measurements 7.8A and swelling degree vs. porosity showing a linear dependency 7.8B.

ties. The approach of ionic cross-linking of the cationic corona with a strong polyanion leads to the creation of a novel polyelectrolyte brush-like structure, which is doubleend-tethered between the hydrophobic cores and the flexible IPECs of the Dq corona and PSS. The purpose of the latter is to prevent the dissolution of incorporated micelles providing the stability of the multilayers on the one hand. On the other hand, IPECs are penetrable for water and electrolytes enabling high pH-induced volumetric changes. The medium surrounding the $(BMAADq/PSS)_x$ multilayers strongly influences the ionization degree of the double-end-tethered MAA brush and therefore its degree of swelling and mechanical properties.

The film swelling degree and morphology, as well as the mechanical properties of the coatings, are reversibly tunable by the solution pH. Furthermore, the swelling behavior and the water content in the hydrogel-like films can be tuned by the porosity of the multilayers, which can be adjusted by the number of micelles/PSS deposition steps to more than 1200% swelling degree and 90% water content in the swollen films. With increasing thickness (decreased porosity), the swelling degree drops since the contribution of the elastic energy dominates the osmotic pressure. Surface-attached pH-responsive hydrogel-like LbL films can be assembled from weak polyelectrolytes. [77] Although these films are highly swellable, they are often unstable with respect to pH variations. [78] Other LbL-derived stimuli-responsive hydrogel-like systems, whose structure is stabilized by covalent cross-links often show considerably lower swelling degrees. [79] In

our case, the stabilization results from the formation of IPECs, which are covalently bound to the pH-sensitive component. Thus, no stabilization by covalent bonding is needed to trap the PMAA chains and significantly higher swelling degrees are observed. High swelling due to the separation of the binding and responsive components within the LbL films is also known for multilayers with other incorporated core-shell ABA triblock copolymer micelles with temperature-sensitive cores.[29, 30] In this particular case, Tan et al. reported on the temperature-driven swelling behavior of LbL films with swelling degrees ranging from 4 to 10. Our results demonstrate that significant (2-12 fold), reversible, and controllable (by pH and bilayer number) swelling can be realized via the incorporation of core-shell-corona micelles into the LbL films. Here we take advantage of the separation of the functional components and the retained internal structure consisting of hydrophobic core, a pH-sensitive double-endtethered polyelectrolyte brush shell and a binding corona.

Acknowledgements

This research was supported by SFB840, COST D43, and COST Action CM1101. The authors thank S. Sukhishvili (University of New Jersey) and F. Boulmedais (University of Strasbourg) for fruitful discussions. They are also thankful to C. Kunert (University of Bayreuth) for conducting the SEM experiments.

7.5 References

[1] K. Glinel et al. “Responsive polyelectrolyte multilayers”. In: *Colloids and Surfaces a-Physicochemical and Engineering Aspects* 303.1-2 (2007), pp. 3–13.

[2] V. Kozlovskaya et al. “Multilayer-derived, ultrathin, stimuli-responsive hydrogels”. In: *Soft Matter* 5.21 (2009), pp. 4077–4087.

[3] Y. Liu et al. “Controlled switchable surface”. In: *Chemistry-a European Journal* 11.9 (2005), pp. 2622–2631.

[4] J. F. Mano. “Stimuli-responsive polymeric systems for biomedical applications”. In: *Advanced Engineering Materials* 10.6 (2008), pp. 515–527.

[5] P. M. Mendes. “Stimuli-responsive surfaces for bio-applications”. In: *Chemical Society Reviews* 37.11 (2008), pp. 2512–2529.

[6] M. A. Cohen Stuart et al. "Emerging applications of stimuli-responsive polymer materials". In: *Nature Materials* 9.2 (2010), pp. 101–113.

[7] I. Tokarev and S. Minko. "Multiresponsive, Hierarchically Structured Membranes: New, Challenging, Biomimetic Materials for Biosensors, Controlled Release, Biochemical Gates, and Nanoreactors". In: *Advanced Materials* 21.2 (2009), pp. 241–247.

[8] I. Tokarev, M. Motornov, and S. Minko. "Molecular-engineered stimuli-responsive thin polymer film: a platform for the development of integrated multifunctional intelligent materials". In: *Journal of Materials Chemistry* 19.38 (2009), pp. 6932–6948.

[9] I. Tokarev and S. Minko. "Stimuli-Responsive Porous Hydrogels at Interfaces for Molecular Filtration, Separation, Controlled Release, and Gating in Capsules and Membranes". In: *Advanced Materials* 22.31 (2010), pp. 3446–3462.

[10] I. Tokarev, M. Motornov, and S. Minko. "Molecular-engineered stimuli-responsive thin polymer film: a platform for the development of integrated multifunctional intelligent materials". In: *Journal of Materials Chemistry* 19.38 (2009), pp. 6932–6948.

[11] S. Minko. "Responsive polymer brushes". In: *Polymer Reviews* 46.4 (2006), pp. 397–420.

[12] A. Synytska et al. "Simple and fast method for the fabrication of switchable bicomponent micropatterned polymer surfaces". In: *Langmuir* 23.9 (2007), pp. 5205–5209.

[13] P. Uhlmann et al. "Polymer Brushes for Surface Tuning". In: *Macromolecular Rapid Communications* 30.9-10 (2009), pp. 732–740.

[14] E. B. Zhulina, O. V. Borisov, and T. M. Birshtein. "Structure of Grafted Polyelectrolyte Layer". In: *Journal De Physique Ii* 2.1 (1992), pp. 63–74.

[15] M. Ballauff. "Spherical polyelectrolyte brushes". In: *Progress in Polymer Science* 32.10 (2007), pp. 1135–1151.

[16] S. Schmidt et al. "Adhesion and Mechanical Properties of PNIPAM Microgel Films and Their Potential Use as Switchable Cell Culture Substrates". In: *Advanced Functional Materials* 20.19 (2010), pp. 3235–3243.

[17] K. Sakai et al. "pH-responsive behavior of selectively quaternized diblock copolymers adsorbed at the silica/aqueous solution interface". In: *Journal of Colloid and Interface Science* 314.2 (2007), pp. 381–388.

[18] K. Sakai et al. "Characterizing the pH-responsive behavior of thin films of diblock copolymer micelles at the silica/aqueous solution interface". In: *Langmuir* 22.20 (2006), pp. 8435–8442.

[19] G. B. Webber et al. "Tunable diblock copolymer micelles-adapting behaviour via subtle chemical modifications". In: *Faraday Discussions* 128 (2005), pp. 193–209.

[20] G. B. Webber et al. "Nano-anemones: Stimulus-responsive copolymer-micelle surfaces". In: *Advanced Materials* 16.20 (2004), pp. 1794–+.

[21] G. B. Webber et al. "Self-organized monolayer films of stimulus-responsive micelles". In: *Nano Letters* 2.11 (2002), pp. 1307–1313.

[22] J. Gensel et al. "Surface immobilized block copolymer micelles with switchable accessibility of hydrophobic pockets". In: *Soft Matter* 7.23 (2011), pp. 11144–11153.

[23] J. Gensel et al. "Cavitation Engineered 3D Sponge Networks and Their Application in Active Surface Construction". In: *Advanced Materials* 24.7 (2011), pp. 985–+.

[24] B. Mahltig et al. "Highly regular polyampholytic structures adsorbed directly from solution". In: *Journal of Colloid and Interface Science* 242.1 (2001), pp. 36–43.

[25] Z. Zhu and S. A. Sukhishvili. "Temperature-Induced Swelling and Small Molecule Release with Hydrogen-Bonded Multilayers of Block Copolymer Micelles". In: *Acs Nano* 3.11 (2009), pp. 3595–3605.

[26] G. Decher. "Fuzzy nanoassemblies: Toward layered polymeric multicomposites". In: *Science* 277.5330 (1997), pp. 1232–1237.

[27] G. Decher and J. D. Hong. "Buildup of Ultrathin Multilayer Films by a Self-Assembly Process .2. Consecutive Adsorption of Anionic and Cationic Bipolar Amphiphiles and Polyelectrolytes on Charged Surfaces". In: *Berichte Der Bunsen-Gesellschaft-Physical Chemistry Chemical Physics* 95.11 (1991), pp. 1430–1434.

[28] G. Decher, J. D. Hong, and J. Schmitt. "Buildup of Ultrathin Multilayer Films by a Self-Assembly Process .3. Consecutively Alternating Adsorption of Anionic and Cationic Polyelectrolytes on Charged Surfaces". In: *Thin Solid Films* 210.1-2 (1992), pp. 831–835.

[29] W. S. Tan et al. "Temperature-Induced, Reversible Swelling Transitions in Multilayers of a Cationic Triblock Copolymer and a Polyacid". In: *Macromolecules* 43.4 (2010), pp. 1950–1957.

[30] W. S. Tan et al. "Effect of Block Copolymer Architecture on the Thermally Induced Swelling of Micelle-Containing Multilayer Thin Films". In: *Macromolecules* 44.19 (2011), pp. 7767–7774.

[31] F. G. Aliev et al. "Layer-by-layer assembly of core-shell magnetite nanoparticles: Effect of silica coating on interparticle interactions and magnetic properties". In: *Advanced Materials* 11.12 (1999), pp. 1006–1010.

[32] N. A. Kotov, I. Dekany, and J. H. Fendler. "Layer-by-Layer Self-Assembly of Polyelectrolyte-Semiconductor Nanoparticle Composite Films". In: *Journal of Physical Chemistry* 99.35 (1995), pp. 13065–13069.

[33] T. Addison et al. "Incorporation of Block Copolymer Micelles into Multilayer Films for Use as Nanodelivery Systems". In: *Langmuir* 24.23 (2008), pp. 13328–13333.

[34] K. Emoto et al. "Functionality of polymeric micelle hydrogels with organized three-dimensional architecture on surfaces". In: *Journal of the American Chemical Society* 122.11 (2000), pp. 2653–2654.

[35] B.-S. Kim, S. W. Park, and P. T. Hammond. "Hydrogen-bonding layer-by-layer assembled biodegradable polymeric micelles as drug delivery vehicles from surfaces". In: *Acs Nano* 2.2 (2008), pp. 386–392.

[36] N. Ma et al. "Polymer micelles as building blocks for the incorporation of azobenzene: Enhancing the photochromic properties in layer-by-layer films". In: *Langmuir* 22.8 (2006), pp. 3906–3909.

[37] Z. Zhu and S. A. Sukhishvili. "Layer-by-layer films of stimuli-responsive block copolymer micelles". In: *Journal of Materials Chemistry* 22.16 (2012), pp. 7667–7671.

[38] T. Addison et al. "Polymeric Microcapsules Assembled from a Cationic/Zwitterionic Pair of Responsive Block Copolymer Micelles". In: *Langmuir* 26.9 (2010), pp. 6281–6286.

[39] S. Biggs et al. "Layer-by-layer formation of smart particle coatings using oppositely charged block copolymer micelles". In: *Advanced Materials* 19.2 (2007), pp. 247–+.

[40] J. Cho et al. "Nanoporous block copolymer micelle/micelle multilayer films with dual optical properties". In: *Journal of the American Chemical Society* 128.30 (2006), pp. 9935–9942.

[41] P. M. Nguyen et al. "Extended release antibacterial layer-by-layer films incorporating linear-dendritic block copolymer micelles". In: *Chemistry of Materials* 19.23 (2007), pp. 5524–5530.

[42] D. A. Bernards and T. A. Desai. "Nanoscale porosity in polymer films: fabrication and therapeutic applications". In: *Soft Matter* 6.8 (2010), pp. 1621–1631.

[43] E. Betthausen et al. "Dual stimuli-responsive multicompartment micelles from triblock terpolymers with tunable hydrophilicity". In: *Soft Matter* 7.19 (2011), pp. 8880–8891.

[44] W. Kern and D. A. Puotinen. "Cleaning Solutions Based on Hydrogen Peroxide for Use in Silicon Semiconductor Technology". In: *Rca Review* 31.2 (1970), pp. 187–.

[45] H. Elbs and G. Krausch. "Ellipsometric determination of Flory-Huggins interaction parameters in solution". In: *Polymer* 45.23 (2004), pp. 7935–7942.

[46] J. L. Hutter and J. Bechhoefer. "Calibration of Atomic-Force Microscope Tips". In: *Review of Scientific Instruments* 64.7 (1993), pp. 1868–1873.

[47] H. Dautzenberg. *Polyelectrolyts*. Hanser. Munich, Germany, 1994.

[48] N. G. Hoogeveen et al. "Formation and stability of multilayers of polyelectrolytes". In: *Langmuir* 12.15 (1996), pp. 3675–3681.

[49] V. A. Kabanov. "Polyelectrolyte complexes in solution and in the condensed phase". In: *Uspekhi Khimii* 74.1 (2005), pp. 5–23.

[50] M. Born and E. Wolf. *Principles of Optics*. Cambridge University Press. Cambridge, 1999.

[51] C. V. Synatschke et al. "Double-layered micellar interpolyelectrolyte complexes-how many shells to a core?" In: *Soft Matter* 7.5 (2011), pp. 1714–1725.

[52] A. Walther and A. H. E. Mueller. "Formation of hydrophobic bridges between multicompartment micelles of miktoarm star terpolymers in water". In: *Chemical Communications* 9 (2009), pp. 1127–1129.

[53] T. Mauser, C. Dejugnat, and G. B. Sukhorukov. “Reversible pH-dependent properties of multilayer microcapsules made of weak polyelectrolytes”. In: *Macromolecular Rapid Communications* 25.20 (2004), pp. 1781–1785.

[54] J. D. Mendelsohn et al. “Fabrication of microporous thin films from polyelectrolyte multilayers”. In: *Langmuir* 16.11 (2000), pp. 5017–5023.

[55] H. H. Rmaile and J. B. Schlenoff. “"Internal pK(a)'s" in polyelectrolyte multilayers: Coupling protons and”. In: *Langmuir* 18.22 (2002), pp. 8263–8265.

[56] S. S. Shiratori and M. F. Rubner. “pH-dependent thickness behavior of sequentially adsorbed layers of weak polyelectrolytes”. In: *Macromolecules* 33.11 (2000), pp. 4213–4219.

[57] Z. J. Sui and J. B. Schlenoff. “Phase separations in pH-responsive polyelectrolyte multilayers: Charge extrusion versus charge expulsion”. In: *Langmuir* 20.14 (2004), pp. 6026–6031.

[58] A. J. Parnell et al. “Synthesis, characterization and swelling behaviour of poly(methacrylic acid) brushes synthesized using atom transfer radical polymerization”. In: *Polymer* 50.4 (2009), pp. 1005–1014.

[59] E. P. K. Currie et al. “Polyacrylic acid brushes: Surface pressure and salt-induced swelling”. In: *Langmuir* 16.22 (2000), pp. 8324–8333.

[60] F. A. Plamper et al. “Synthesis, characterization and behavior in aqueous solution of star-shaped poly(acrylic acid)”. In: *Macromolecular Chemistry and Physics* 206.18 (2005), pp. 1813–1825.

[61] E. B. Zhulina, T. M. Birshtein, and O. V. Borisov. “Theory of Ionizable Polymer Brushes”. In: *Macromolecules* 28.5 (1995), pp. 1491–1499.

[62] S. A. Sukhishvili, E. Kharlampieva, and V. Izumrudov. “Where polyelectrolyte multilayers and polyelectrolyte complexes meet”. In: *Macromolecules* 39.26 (2006), pp. 8873–8881.

[63] H. W. Jomaa and J. B. Schlenoff. “Accelerated exchange in polyelectrolyte multilayers by "catalytic" polyvalent ion pairing”. In: *Langmuir* 21.18 (2005), pp. 8081–8084.

[64] V. A. Kabanov et al. “Cooperative Interpolyelectrolyte Reactions”. In: *Makromolekulare Chemie-Macromolecular Chemistry and Physics* (1985), pp. 137–155.

[65] S. T. Dubas and J. B. Schlenoff. "Swelling and smoothing of polyelectrolyte multilayers by salt". In: *Langmuir* 17.25 (2001), pp. 7725–7727.

[66] H. J. Butt. "Measuring Electrostatic, Vanderwaals, and Hydration Forces in Electrolyte-Solutions with an Atomic Force Microscope". In: *Biophysical Journal* 60.6 (1991), pp. 1438–1444.

[67] W. A. Ducker, T. J. Senden, and R. M. Pashley. "Direct Measurement of Colloidal Forces Using an Atomic Force Microscope". In: *Nature* 353.6341 (1991), pp. 239–241.

[68] H. Hertz. "Ueber die Beruehrung fester elastischer Koerper". In: *Journal fuer die reine und angewandte Mathematik* 92 (1881).

[69] I. Drachuk et al. "pH-Responsive Layer-by-Layer Nanoshells for Direct Regulation of Cell Activity". In: *Acs Nano* 6.5 (2012), pp. 4266–4278.

[70] M. O. Lisunova et al. "Direct Probing of Micromechanical Properties of Hydrogen-Bonded Layer-by-Layer Microcapsule Shells with Different Chemical Compositions". In: *Langmuir* 27.17 (2011), pp. 11157–11165.

[71] O. Shchepelina et al. "Morphology and Properties of Microcapsules with Different Core Releases". In: *Chemistry of Materials* 24.7 (2012), pp. 1245–1254.

[72] C. Picart et al. "Measuring mechanical properties of polyelectrolyte multilayer thin films: Novel methods based on AFM and optical techniques". In: *Colloids and Surfaces a-Physicochemical and Engineering Aspects* 303.1-2 (2007), pp. 30–36.

[73] R. Toomey, D. Freidank, and J. Ruhe. "Swelling behavior of thin, surface-attached polymer networks". In: *Macromolecules* 37.3 (2004), pp. 882–887.

[74] J. Gensel et al. ""Micro-structure-macro-response" relationship in swollen block copolymer films". In: *Soft Matter* 5.13 (2009), pp. 2534–2537.

[75] J. E. Wong et al. "Swelling behavior of polyelectrolyte multilayers in saturated water vapor". In: *Macromolecules* 37.19 (2004), pp. 7285–7289.

[76] S. E. Burke and C. J. Barrett. "Swelling behavior of hyaluronic acid/polyallylamine hydrochloride multilayer films". In: *Biomacromolecules* 6.3 (2005), pp. 1419–1428.

[77] J. Hiller and M. F. Rubner. "Reversible molecular memory and pH-switchable swelling transitions in polyelectrolyte multilayers". In: *Macromolecules* 36.11 (2003), pp. 4078–4083.

[78] S. T. Dubas and J. B. Schlenoff. "Polyelectrolyte multilayers containing a weak polyacid: Construction and deconstruction". In: *Macromolecules* 34.11 (2001), pp. 3736–3740.

[79] E. Kharlampieva, I. Erel-Unal, and S. A. Sukhishvili. "Amphoteric surface hydrogels derived from hydrogen-bonded multilayers: Reversible loading of dyes and macromolecules". In: *Langmuir* 23.1 (2007), pp. 175–181.

7.A Supporting Information

Adsorption kinetics of BMAADq micelles

Adsorption kinetics of BMAADq micelles, see fig 7.9.

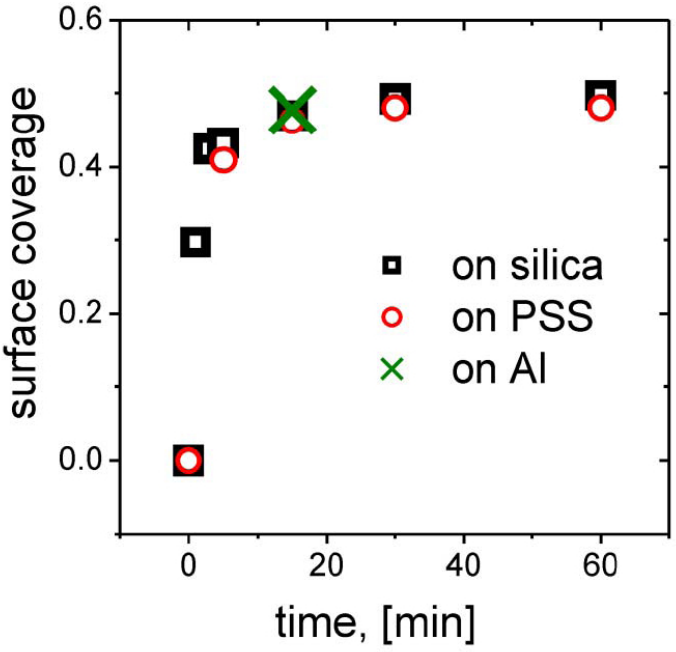

Figure 7.9: Adsorption kinetics of BMAADq micelles onto different substrates studied by AFM

Linear elasticity

Measurements on the same spot of the sample show that the film is not plastically deformed, see fig 7.10.

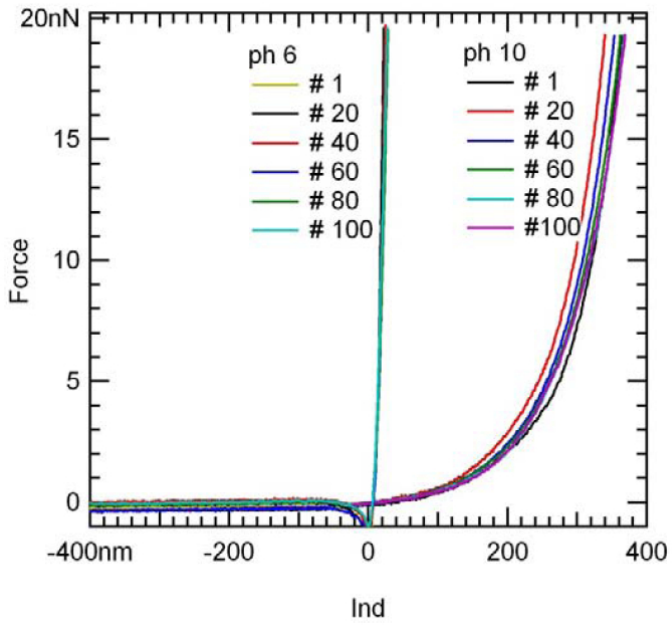

Figure 7.10: Force-indentation measurements on the same spot of the sample show that the film is not plastically deformed. Legend indicates the number of measurements

Availability of the Hertz model

Our data is well represented by the Hertz model as shown by the comparison of force curves plotted in log-log scale together with the power function $F \propto \delta^{3/2}$, confirming the Hertzian power law, see Figure 7.11.

Water content of swollen LBL films containing block copolymer micelles

Recalculation of the data to the water content in a swollen film $(1 - d_{\mathrm{dry}}/d_{\mathrm{sw}})$ results in a linear decrease with increasing dry thickness for all films with more than one bilayer, see Figure 7.12.

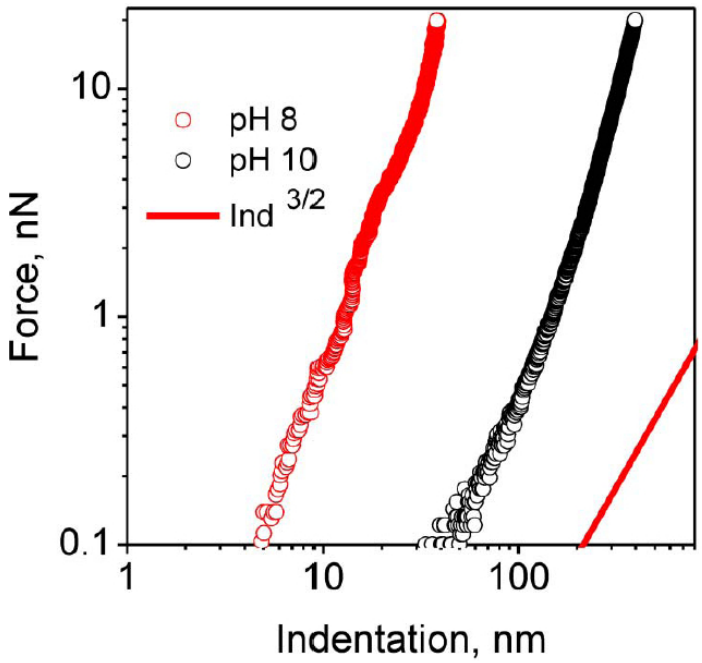

Figure 7.11: log-log plot of the force-indentation data for different swelling states of a $(BMAADq/PSS)_3$ film. The force is proportional to the 3/2 power of the indentation confirming the validity of the Hertzian model. For comparison, a line corresponding to the 3/2 power law relationship is plotted (solid line).

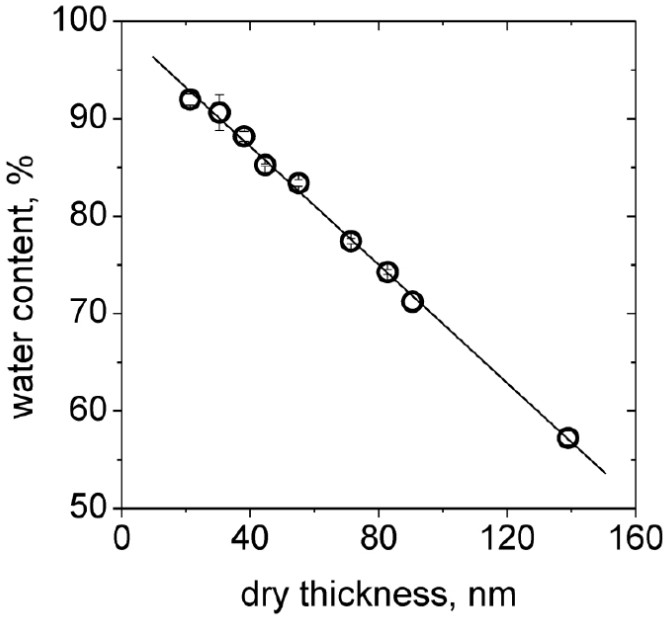

Figure 7.12: Water content vs. the dry thickness of $(BMAADq/PSS)_x$ films.

8

Further Perspectives

8.1 Direct Measurements of Contact Stresses of Soft Materials

Understanding the nature and the distribution of stresses at the contact of deformable solids is fundamental to the fields of soft mechanics and adhesion. While the results of mechanoresponsive systems based on cationic polymer brushes are very promising (Ch.4) [1], several fundamental aspects have to be addressed to fully unlock the potential of this detection scheme.

In particular, only the response to brush compression could be quantitatively assessed so far. The polymer brushes do show response to tensile stresses but these effects could only be described qualitatively. Since tensile stresses are of particular interest for the contact adhesion problems, a quantitative description of response to tensile stresses is of prime interest.

In addition, pressure response was quantitatively analyzed for one particular probe geometry only: A spherical probe with a fixed Young's modulus (ca 1 MPa). The method needs validation using other probe geometries with systematically variable elastic constants. These results should be compared to contact mechanics models. Also, the influence of mechanical modulus, as well as the influence of interaction potential of the contacting bodies on the sress distribution should be investigated in the future.

Examples for possible geometries are spheres, paraboloids, cones, and flat stamps of crosslinked ideal networks of polydimethyl siloxane (PDMS). The elastic modulus of those networks can be varied in a range from 100 kPa to 10 MPa.

To understand how chemistry affects the contact stress profile, the impact of chemical interactions on stress distributions can be studied by chemical functionalization or by changing the environment. The chemical composition of the PDMS surface might be controlled using procedures described in Ref. [2]. Chemisorption of alkyltrichlorosilanes onto an oxidized PDMS surface (generated by oxygen plasma) produces a monolayer of the corresponding alkylsiloxanes. By varying the head-group functionalities of the silanes, the chemical composition and thus the interaction potential of the PDMS surface can be controlled. The SAMs can further be functionalized with moieties that allow for specific interactions. Another route to control the surface potentials might be HCl treatment, alteration of the environment i.e. ionic strength and pH. The impact of changes in chemical interactions on the stress distribution can be visualized using the same method (mechanoresponsive surfaces) as described in chapter 4.

Also, fundamental for the understanding of reversible adhesion is to quantify both contact formation and detachment process such as peeling events [3, 4]. For this reason,

extension of the methods is required to capture the dynamic effects.
In addition theoretical analysis of the experimental results could be carried out when needed. Possible realizations are existing analytical models based on linear elasticity as well as numerical methods as finite element modeling. By combining the characterization of stress profile in the contact zone and modelling of contact mechanics it will be able to examine the validity and limitations of the existing models of contact mechanics. This will be a fundamental contribution to tackle numerous problems of soft matter physics.
Another object is the enhancement of the sensitivity of the system under traction forces. For this purpose Förster resonance energy transfer (FRET) could be a possible approach. Suitable donator and acceptor molecules could be spaced along a polymer brush or an alternative system. A similar approach has been recently used for measuring traction forces on myosin proteins in-vitro and pN resolution has been reported in Ref. [5]. In the unloaded state, donor and acceptor molecules will be close to each other ($2<$ distances <10 nm) and the intramolecular resonance energy transfer between the fluorophores will occur depending on the selected donor-acceptor pair. Upon traction loading, the brush is stretched and the distance between donator and acceptor molecules increases. In consequence, the intensity of the acceptor emission will decrease.
Mechanoresponsive surfaces and the theoretical understanding of their response will allow tackling problems in many different fields. Such surfaces are of particular interest for the understanding of bioinspired reversible adhesives. This aspect will be discussed in the following chapter (Ch. 8.2). Further possible enhancement of the sensitivity and resolution of the mechanoresponse by rational design of brush layers is discussed in chapter Ch. 8.3. Also, polymer brushes designed for this research can be adapted to study chemical interaction (e.g. swelling, conformational changes) related to stress in terms of a readable optical output. An example for the turn off (quenching) of fluorescence as a response to ionic strength is already shown in Ch. 4 (Figure 4.6). The fluorescence intensity decreases with decreasing brush thickness.
Another payoff of mechanoresponsive materials is that the in-situ stress sensor may have the potential to visualize and quantify the traction forces during cell adhesion cell migration, and the effect of forces on stem cell differentiation with a far greater sensitivity than what has been achieved so far [5]. For this purpose, the detection scheme and polymer brush architecture may need to be changed.

8.2 Contact and Adhesion of Biomimetic Patterned Adhesives

Abstract

Microstructured surfaces have demonstrated the high relevance of the contact geometry for adhesion enhancement. Theoretical considerations indicate that the stress distribution in the contact zone is a fundamental parameter but experimental evidence is missing so far. In this work, we propose a method that allows the detection of local contact stresses of biomimetic adhesives. For this purpose, we use a commercial machine (PVM-A) combined with a confocal microscope. The PVM-A allows controlled contact formation of microstructured surfaces with a flat substrate. The resulting spatial stress distribution was observed by fluorescence microscopy with high lateral ($< 1\,\mu$m) and pressure ($< 10\,$kPa) resolution using mechanoresponsive fluorescent surfaces. We apply this method to study the enhanced adhesive performance of mushroom- vs. flat-terminated adhesive microstructures. The measured stress profiles are compared to finite elemente (FE) simulations. These simulations indicate significant differences in the stress distribution between mushroom- and flat-terminated pillars, which finally result in different adhesive properties.

Introduction

The understanding of the nature and the distribution of stresses at the contacts of deformable solids is essential to the understanding of reversible adhesive systems in biological and non-biological settings [6, 7, 8]. Structures mimicking topographic features of different animal pads have been studied with respect to their adhesive properties. In particular, the characteristics of gecko pads were analyzed due to the superior adhesive strength of gecko feet. It has been found that the contact shape is crucial for this feature, i.e. the role of the "spatular" found in the fibrillar adhesive structures of gecko pads [9, 8, 10, 11]. Recently, micro- and nanofabrication technologies have been applied to mimic the adhesive structures of geckos and other animals [9, 12, 8]. Patterned areas up to some cm^2 could be obtained and adhesion measurements were realized on the micro-, meso- and macroscopical scale. Microstructured surfaces obtained by soft lithography methods with micropillars terminated in flat or mushroom-shaped tip have demonstrated the relevance of the contact geometry for adhesion enhancement. The

mushroom- (T-shaped) and spatula-shaped tips show a remarkably improved performance compared to the flat punch (I-shaped) and other shapes (spherical or concave) [8]. These findings indicate that the contact geometry plays a major role in adhesion performance [12, 13, 14, 15, 16, 17]. Additional theoretical analysis have shown that T- and spatula-shaped tips have so far the highest potentials for adhesion enhancement [18, 19, 20, 21, 22]. There are many indications that contact shape is the determing factor on adhesion. Also, theoretical analysis proposes that the originating stress distribution in the contact zone determines adhesion strength. However, experimental evidence for a relation between stress distribution and adhesion strength is missing so far.

We have recently demonstrated that modification of polymer brushes with suitable fluorophores is one approach for monitoring contact stresses with high resolution [1, 23]. For certain dyes, i.e. carboxyfluorescein, that are covalently immobilized on the brush, local brush compression causes an increase in the quenching of fluorescence. In contrast local brush stretching causes a decrease in quenching. Thus, laterally varying brush compression or stretching results in local variation of fluorescence intensity and can be translated into stress distributions with a lateral resolution limited by optical read-out ($< 1\,\mu$m) and a pressure sensitivity of at least 10 kPa.

In this study, we use this approach to study pressure distributions of biomimetic adhesive patterns in order to clarify the origin of enhanced adhesion of T-shaped structures compared to I-shaped ones. For that purpose, we prepared micropatterned surfaces by soft molding using polydimethysiloxane (PDMS). For surface analysis we combined a commercially avilabe setup and confocal microscopy to follow pressure distributions of I- and T-shaped adhesive structures at controlled contact formation. The stress distribution in the contact area was observed using mechanoresponsive surfaces. These findings were compared to numerical finite element simulations.

Preparation of Biomimetic Structures

Masters for flat punch (I-shaped) pillars and mushroom (T-shaped) pillars (simple flat punch pillars with a thin annular plate at the top of the central pillar) are prepared via an optical lithography approach, as explained elsewhere [10]. Little modifications of the protocol were conducted in order to obtain masters for T-shaped pillars. Therefore the development time was slightly increased to hollow out the photoresist around the cavity base and thus from an inverse T-shape.

For the preperation of the biomimetic stamps, PDMS (Sylgard 184 kit) was purchased

from Dow Corning, USA. The prepolymer was mixed with the curing agent using a 10:1 ratio and was stored at low pressure in a desiccator for degassing for 15 min. The blank of the stamp was treated with an adhesion promoter (Wacker Grundig G 790, Wacker Chemie AG, München) to achieve air impermeability of the stamp. After evaporation of the adhesion promoter, the blank on top of the master, separated by a teflon ring was mounted into the preparation holder (Figure 8.1A). Then PDMS was injected up to complete filling of the chamber (Figure 8.1B). The thickness of the PDMS membrane was controlled using a glass stopper. After curing for 6 hours at 65 °C, the holder, the teflon ring, and the master were removed gently (Figure 8.1C). The resulting PDMS structures are shown in Figure 8.2A.

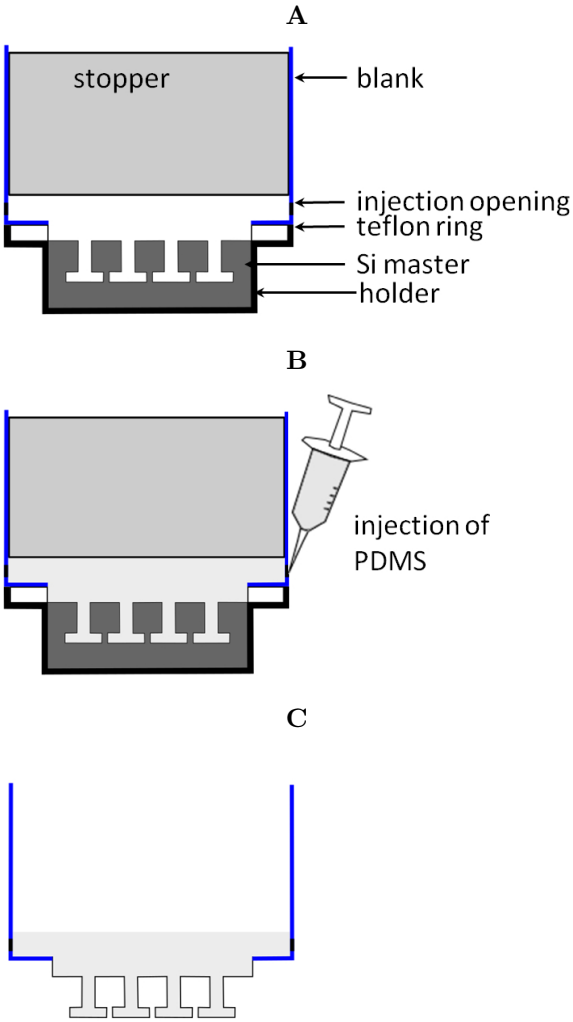

Figure 8.1: Preparation of biomimetic stamps: 8.1A Assembly of the preperation station, 8.1B Injection of PDMS, 8.1C Seperation of the master

Adhesion of flat and T-terminated micropatterns

To confirm the enhanced adhesive properties of T-shaped pillars compared to I-shaped ones we performed force spectroscopic measurements. Force profiles on structured PDMS surfaces were recorded using custom-built adhesion measurement equipment. It consists of a ruby sphere mounted at the end of a cantilever with a thin film force sensor. The sphere was pressed against the structured PDMS substrates. After reaching an adjusted pre-load the sphere was retracted. The cantilever deflection was recorded as a function of the moving distance. The retracting curve showed higher pull-off force for mushroom shaped structures than for flat punches, what can be determined from distance between the baseline (where no forces acting to the cantilever) and the minimum of the retrace curve (see Figure 8.2). It should be noted that the adhesion force for I-shaped pillars increase up to a pre-load of 2.5 mN. Further increase of the pre-load showed no effect. For T-shaped pillars the adhesion force inreased up to a pre-load of 19 mN. These results are in agreement with reported data in the literature [7, 8]. Details on the experimental setup can be found in Ref. [10]).

Contact Formation of Bioinspired surfaces

In order to study the lateral pressure distribution in a flat-flat contact configuration (in contrast to the self-aligning sphere-flat situation) a well-defined contact between the two surfaces needs to be achieved. For this purpose we used an automatised microcontact printing setup (Manual Microcontact Printing System μ-CP PVM-A, GeSiM GmbH, Germany) in combination with a confocal microscope (CLSM: LSM 710, Zeiss). The principle is shown in Figure 8.3. The structured PDMS stamp is prepared onto a blank (Figure 8.3) and gets inflated by an external air pressure. Then the stamp is brought into the pre-position by adjusting the Z-level of the print head. The pre-position is defined as the position where the stamp enters the confocal observation volume of the CLSM at 100 kPa overpressure in the stamp. By inflation of the stamp with additional air, an overpressure in the stamp is produced. Due to this pressure the PDMS matrix bends and creates a contact with the mechanoresponsive substrate. The response of the mechanoresponsive polyelectrolyte brush can be observed by the confocal microscope. By changing the overpressure in the stamp, an approach and a retraction cycle can be driven (possible range $90 - 190$ kPa).
The deformation behaviour as response to inflation of an elastic membrane and its adhesive properties are described by Shull et al. [24, 25].

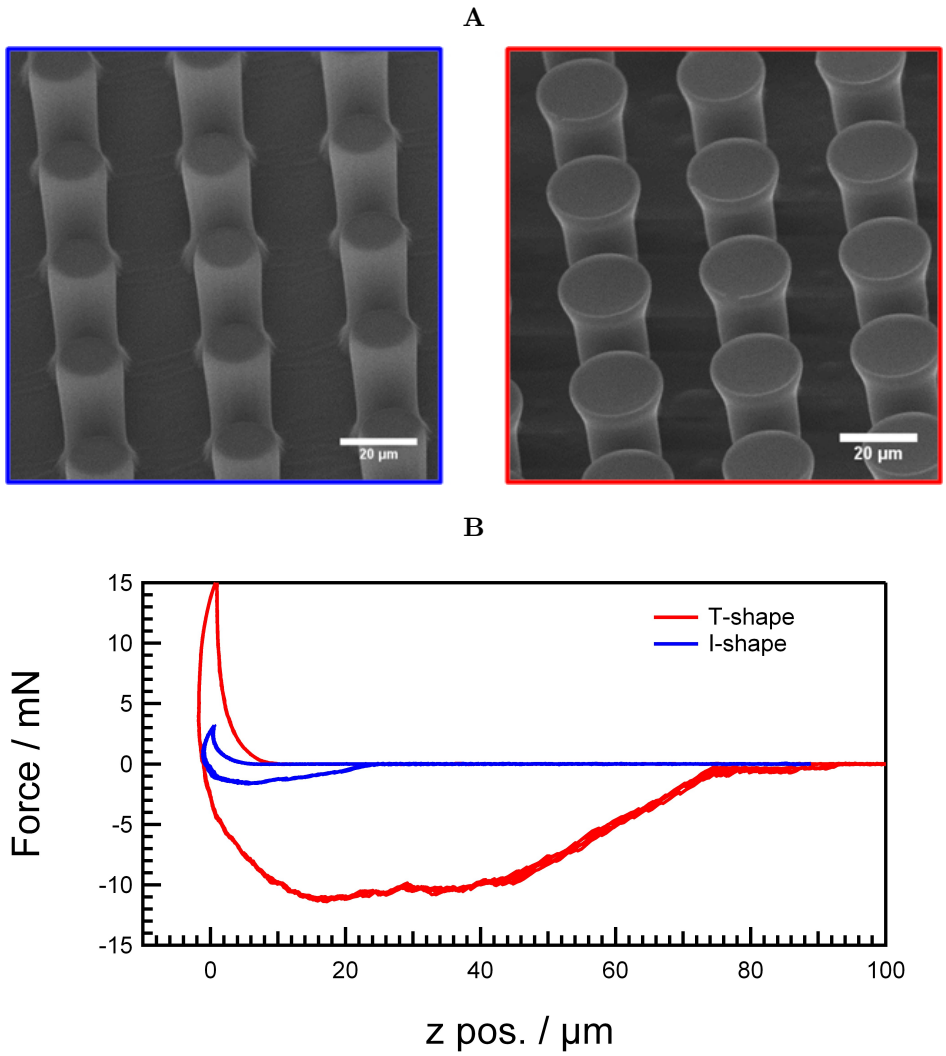

Figure 8.2: Adhesive properties of different contact terminals: 8.2A SEM pictures for the different contact terminals: flat punch and mushroom shaped. 8.2B Force profiles of different microfibrillar arrays: I and T shaped. Arrays of T-shaped fibrils show the highest adhesion performance.

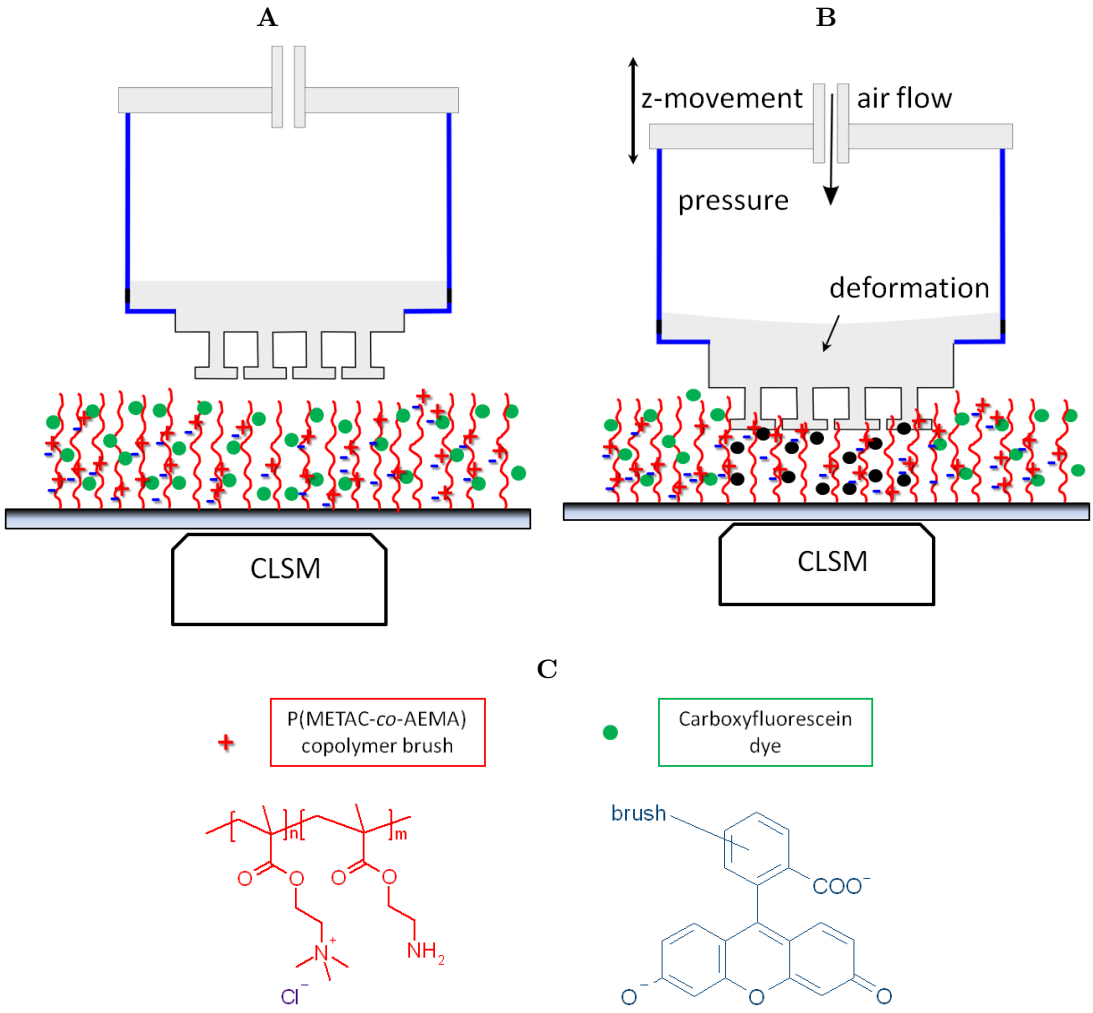

Figure 8.3: Experimental setup to establish and to characterize a biomimetic contact: Sketch of the experimental setup: combination of Manual Microcontact Printing System (PVM-A) and confocal microscope (CLSM) 8.3A, 8.3B moving into preposition, and increasing overpressure result in contact formation and deformation of the brush 8.3C chemical details of the mechanoresponsive system

Stress distribution under the patterned surfaces

Preparation of the mechanoresponsive surfaces is adapted from our recent paper [1]. Briefly cationic PMETAC copolymer brushes are grafted from glass slides using SI-ATRP. In a second step carboxy-fluorescein is covalently attached to the brush. The resulting brush substrates are calibrated following the procedure described in Ref. [1]. For this purpose the soft colloidal probe technique was used [26]. Thus, we could determine a response function that correlates local pressure (p) with local fluorescence intensity (I).

After calibration, the bioinspired patterns are brought in defined contact using the PVM-A approach introduced before. Figure 8.4A shows a typical experiment of a T-shape structured stamp on fluorescently labeled PMETAC copolymer brushes in water. Upon contact of the stamp with the surface, dark spots occur surrounded by a bright rim. The dark areas indicate compressive stress resulting from fluorescence quenching between the quaternary ammonia groups of PMETAC and the dye. At the rim of the contact areas, tensile forces cause the reverse effect. An increase of the overpressure in the stamp leads to an increase of both the contact area (due to elastic deformation of the pillars) and the pressure acting onto the brush. As a result of increased pressure, the fluorescence intensity in the contact area decreases further. When retracting the stamp by decreasing the external overpressure, the fluorescence intensity increases. The rim is more pronounced as the stamp is retracted, indicating stronger tensile forces and a larger area of tensile stress. These results point out that the method is sensitive enough to study adhesion of bioinspired stamps. Especially, the hysteresis of adhesion during the loading-unloading cycles can be visualized. With adequate calibration (using sphere-flat measurements as a reference, like discussed above), it is now possible to transform the intensity maps (Figure 8.4B) to local pressure profiles (Figure 8.4C).

Origin of the adhesive performance of mushroom-shaped pillars

The adhesive performance of pillars can attributed to its debonding mechanism. Three different types of failure modes for pillar detachment are possible. The pillar can detach due to cohesive failure, due to crack nucleation at defects, or due to crack nucleation at the edge. Which type of failure is energetically favorable depends on the pillar geometry and on the interfacial forces, which influence the stress distribution in the contact area of a pillar and the underlaying substrate. Calculations based on analytical linear elastic models predict that the stress at the edge of the contact is very large

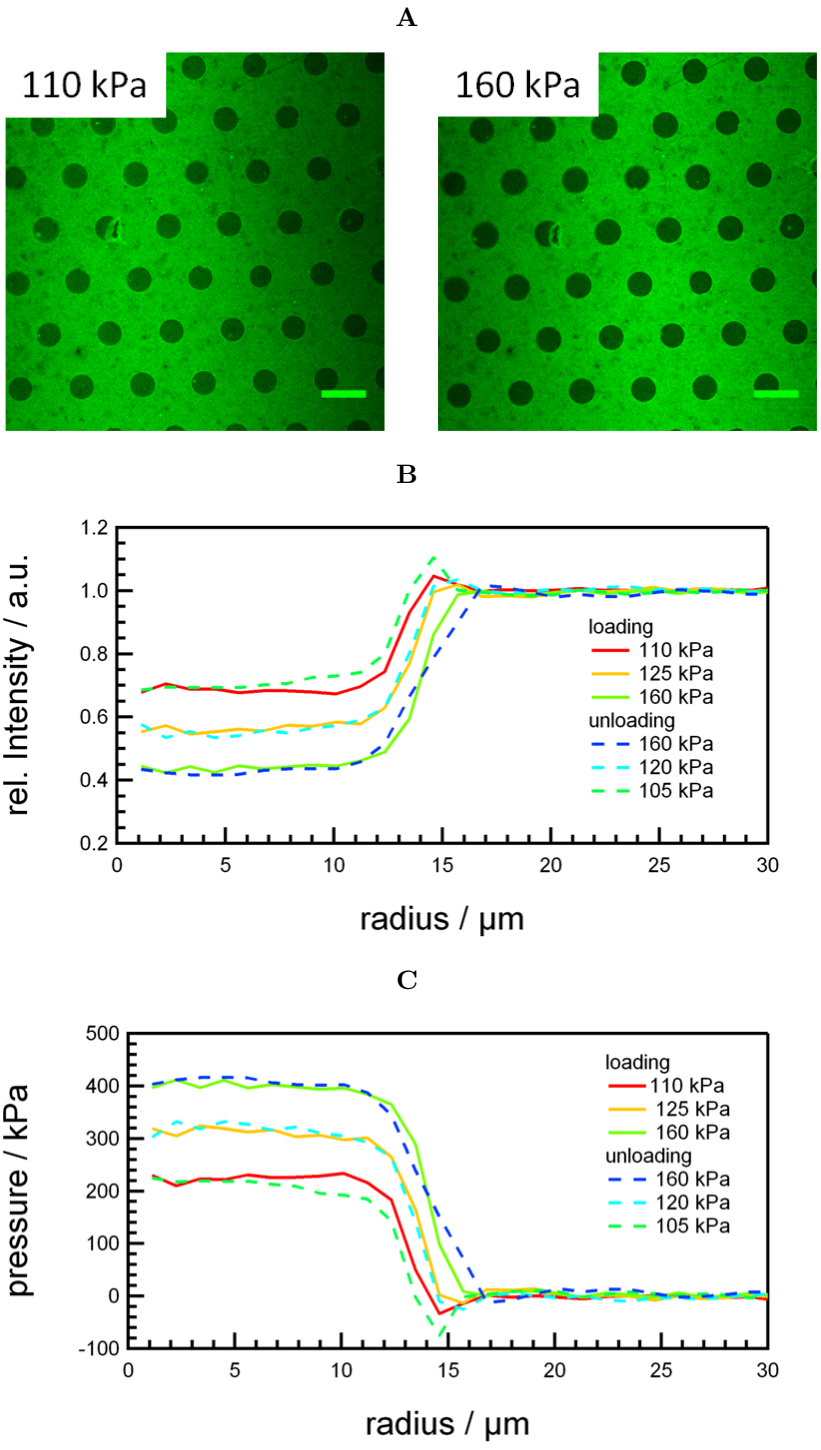

Figure 8.4: Pressure profile of biomimetic contacts: 8.4A optical response (scale bar 50 μm), 8.4B intensity distribution of different loading and unloading steps adjusted by changing the overpressure in the stamp, 8.4C calculated stress distribution

(converge to infinite) for a I-shaped pillar. It has been suggested [18, 19] that the cap of a T-shaped pillar changes the stress distribution in a way that the singularities of the stress distributions at the edges of a flat punch contact vanish for a proper thickness of the cap. This causes that crack propagation cannot occur from the edges and nucleation of cracks is favored from defects in the contact zone [18, 19], which needs higher seperation forces [19, 27].

To confirm these predictions, we made finite element (FE) simulations with simple model systems for the different pillar geometries used in the experiments. The interactions with the substrate are modeled by a spring potential $U = 0.5kD^2$, where k is the spring constant, and D the separation distance. The geometries are modeled as sketched in Figure 8.5A.

From FE simulations we extracted the von Mises stress in the contact area (Von Mises stresses are not directly correlated to the stress profile. Anyway it is possible to compare the experimental with the simulated data qualitatively.). FE simulations show that the stress peak for flat punch geometries vanishes, when the thickness of the cap increases, up to a critical thickness where the stress peak disappears completely (Figure 8.5B). Further increase of the thickness causes the profile to converge to the one which could be observed for a flat punch. This results are in agreement to findings reported in Ref. [19, 28].

We have to mention that in our case it was hard to control the exact pillar geometry. From SEM measurements (Figure 8.2A), we know that the real picture of the T-shaped pillar differs (edges of the cap are rounded). Also, the approximated interaction potential is a strong simplification. However, the results are qualitative in agreement to Ref. [19, 18]. moreover, already small caplike structures enhance the adhesion drastically as shown in previous studies by A. del Campo et al.

As an experimental confirmation of these findings, the calculated stress distribution must be compared to measured stress profiles. First measurements pointed out that the stress depends on the radial position in the contact area (Figure 8.6). For this purpose, we focused on the intensity profile created by the stress distribution of a single T-pillar, using the combination of PVM-A and CLSM. Beside quenching of the fluorescence in the contact area and the bright rim at the edge one can observe a slight increase of fluorescence intensity in the center of the contact zone. This might be assigned to an intermediated state of the cap thickness.

Having established the setup further experiments are necessary to confirm these hypotheses. Also, the comparison between flat punch and mushroom shaped pillars is missing.

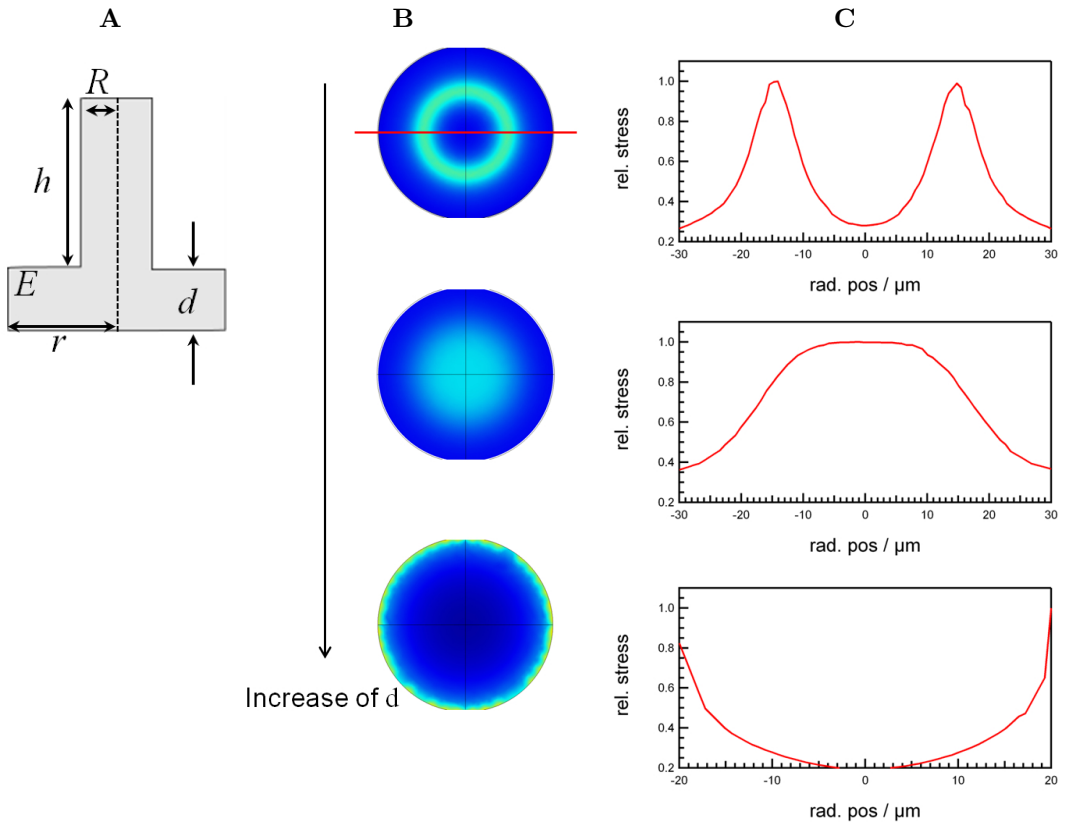

Figure 8.5: FEM simulations of the pressure profile for different pillar geometries: 8.5A sketch of the pillar geometry, thickness of the cap d increases from $5 - 20\,\mu$m. 8.5B Calculated von Mises stresses in the contact area. 8.5C Relative stress profiles (along the red line shown in 8.5B). Finite Element simulations were performed using commercial software (Comsol Multiphysics Version 4.2). The Pillars were modeld by the flowing parameters: for I-shaped pillars $h = 40\,\mu$m, $R = 20\,\mu$m, Young's modulus $E = 1\,$MPa, load $1\,$N and $k = 1\,$N/m and for T shaped pillars the cap radius was set to $r = 30\,\mu$m and the cap thickness was varied between $d = 5 - 20\,\mu$m.

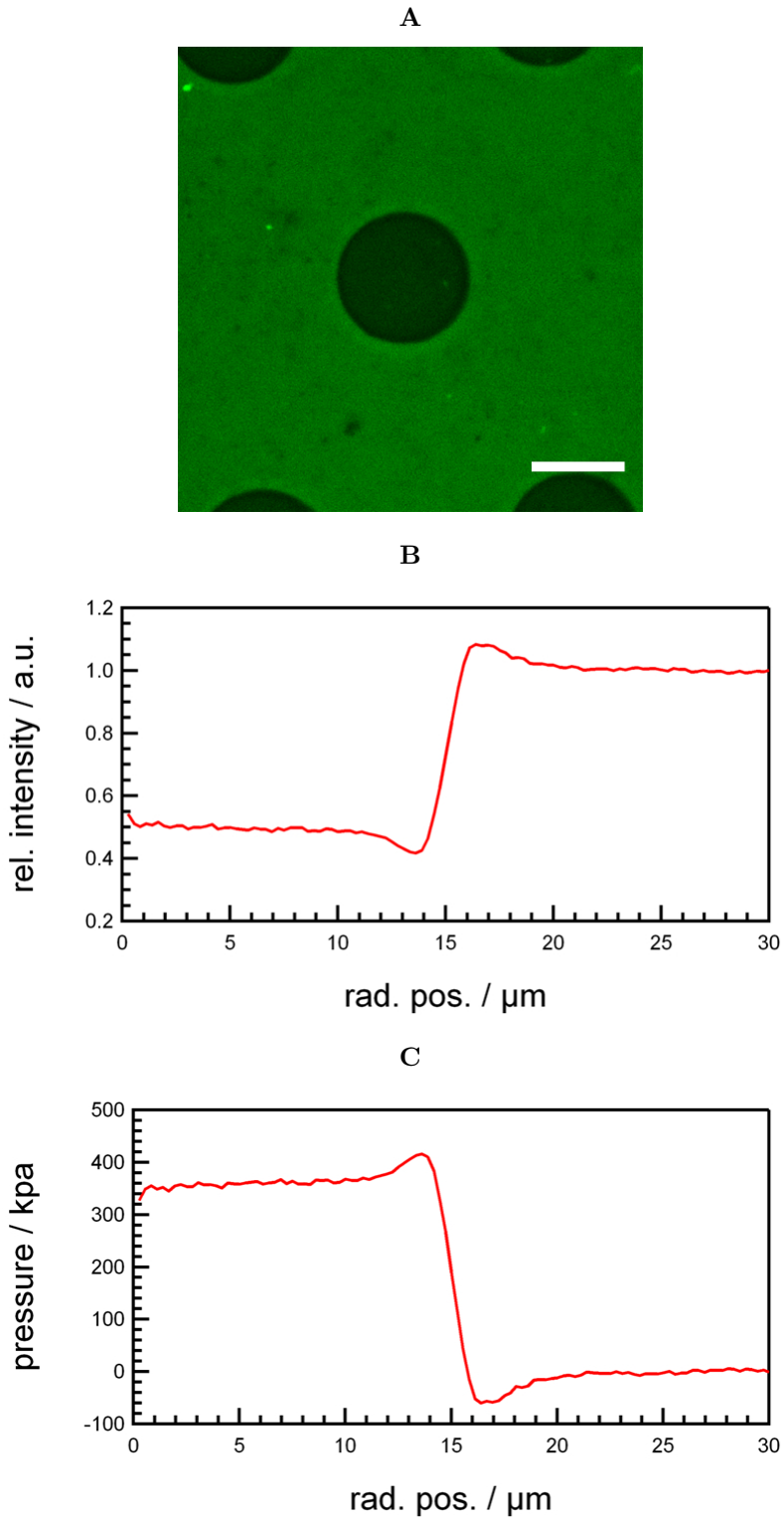

Figure 8.6: Stress distribution of a mushroomshaped pillar: 8.6A Optical response of the mechanoresponsive surface (scale bar 20 μm. 8.6B Extracted intensity distribution, 8.6C Calculated stress distribution

Conclusion and Outlook

In summary, we established a setup to generate a defined contact situation between soft biomimetic stamps (punches) with rigid flat substrates using stamps that can be air filled. The contact situation was studied by detecting the spatial fluorescence distribution on mechanoresponsive surfaces. First results indicate that we are able to measure stress profiles of bioinspired stamps. These findings could be confirmed by FE simulations at simplified model systems.

Measurements, like those presented in this section, will help to generate a detailed understanding of the effect of geometrical structure on contact mechanics and adhesion. So far measurements are missing on flat punch pillars to compare the local stresses of flat and mushroom shaped pillars. Also, the contact areas should be assign the stress to the local position in the contact zone. This can be done with micro interferometry for example. Further failure mechanisms between the pillars and a flat surface shall be investigated as a function of geometric properties of the biomimetic structured stamps using microinterferometry. These findings will be correlated to stress distributions measured during the detachment and contact formation processes. For this purpose, it is also necessary to determine the limits of time resolution of the sensor material and the detection setup.

An important feature for the reversibility of adhesion of topographically structured surfaces is the mechanical instability of the pillars. Using confocal microscopy (or other common microscopy techniques) and incorporating dye molecules directly into the PDMS stamps, it may be possible to follow deformation modes of the pillars. In particular, the buckling force of the pillars can be measured in that way. Beyond topographic changes, stress fields in the contact area between the buckled pillars and the substrate are detectable with the mechanoresponsive surfaces.

New types of structured membranes can be designed that allow the study of peeling events using the introduced Manual Microcontact Printing System μ-CP PVM-A. Membranes that are not homogeneous in thickness or elastic modulus are possibly the approach to achieve this. While loading (unloading) the membrane, an inhomogeneous deformation will take place which results in an inhomogeneous spread and can mimic spatula movement.

8.3 Tuning the Response of Mechanoresponsive Brushes

Abstract

In chapter 4 we developed a system for local pressure detection based on fluorescent labeled cationic polymer brushes [1]. However, this approach has some limitations. In particular: 1) measurements are just possible in solution, 2) fluorescence quenching is not specific and difficult to relate directly to the compressibility of PE polymer brushes (as a function of the brush parameter), and 3) just one potential system was characterized. Improvements could be changes of the mechanophores, the structure of the polymer brush (e.g. grafting density and height) or alternative brush compositions. For a rational design of surface layers with optimized mechanochemical response, the molecular mechanism behind fluorescence quenching in response to pressure needs to be understood. Therefore, one has to understand how the conversion of mechanical energy into changes of the chemical environment inside the brush happens. Here we show work in progress to characterize the compressibility of PE brushes as a function of the brush parameter using force spectroscopy and fluorescence measurements. This will help to understand the relation between compressibility, response and polymer brush parameters.
Also, other types of response mechanism can be established in polymer brushes which do not rely on quenching but for instance on changes of the emission spectrum of the mechanophore. Using such a type of mechanophore that is more specific as quenching allows to gain information from the interior of charged brushes. We discuss a possible response by using seminaphtharhodafluor (SNARF) that shows a shift in the emission spectrum in response to changes in the chemical environment.
With the knowledge about compressibility and potential responses the build-up of various sensors that detect chemical interaction related stresses will be possible.

Introduction

The response of mechanoresponsive systems based on polymer brushes depends on the nature of the polymer, grafting density, brush length, and the nature of the dye and dye density. Thus, the effect of these parameters needs to be studied. By systematic variation of the length and surface density of the brush, as well as fluorescein ratios in PMETAC brushes, the effect of these factors in quenching the fluorescence signal and the final mechano response can be investigated. Achieving this understanding can help to improve mechano responsive systems with regard to ultimate pressure sensitivity.

The sensitivity of the response and the force range can possibly be extended by combining other mechanophores with alternative brush compositions and architectures [23]. For instance annealed polyelectrolyte brushes allow externall triggering of the mechanochemical response by pH or ionic strength, or vice versa. That means that vertical compression of the brush could lead to a shift of the dissociation equilibrium. This variation could be measured using pH-sensitive indicators for example.
An alternative could be to use polyelectrolyte gel films rather than polymer brushes. Polymer gels systems could allow alternative routes for surface functionalization and the usage of other mechanophores. They are flexible in handling and steric hindrance for the mechanophore could be overcome. Also, measurements in air could be possible.
For the understanding of the processes in strongly compressed PMETAC brushes, we combined AFM force spectroscopy with polymer brush theory. First experiments are underway to study the effect of brush parameters on the compressibility. These experiments are evaluated on basis of AdG theory (developed by Alexander and de Gennes [29, 30]). Also, the relation between response and compressibility, i.e. the state of quenching as a function of applied force is investigated.
Further other types of response will be addressed. A more specific response than quenching is possible by using dyes, which show a shift in the emission spectrum (rather than a shift in intensity) in response to changes in the chemical environment. For instance seminaphtharhodafluor (SNARF), which responds to changes of the dissociation equilibrium. For this purpose, we have established a synthesis protocol for the attachment of SNARF dye to PMETAC polymer brushes. In order to quantify the response of SNARF dye, the detection scheme was changed from fluorescence intensity mapping to mapping of spectroscopic properties.

8.3.1 Understanding of the Mechanoresponse

For the design of mechanoresponsive systems based on polymer brushes we have to understand how the brush is affected by the environment and the applied force, and how the response is related to the compression state of the brush.

Brush Compresssion

We performed (first) force spectroscopic experiments to gain information about the compressibility of cationic PMETAC polymer brushes with a covalently attached 5(6)carboxyfluorescein (CF) [1] dependent on the ionic strength. We used the colloidal probe

(CP) technique, where a CP was attached to an AFM cantilever using micromanipulation. In a further step the CP was functionalized with a 3-Aminopropyl di isopropyl ethoxysilane (97%) to avoid electrostatic attraction between the CP and the cationic brush. After silanization force distance data were recorded in a droplet of aqueous NaCl solution.

As expected, we could observe that the repulsive forces increase (strength and range) as the ionic strength I is decreased. This can be attributed to multiple origins. On the one hand the electrostatic interactions are screened. In addition the brush swells and steric interactions are more dominant.

In a first approximation, we analyzed the measurements in terms of the AdG theory for an asymmetric situation (brush/ no brush; electro static interactions are neglected).

$$\frac{F(D)}{2\pi R} = \frac{2k_BTH}{35\sigma^{3/2}}\left[7\left(\frac{D}{H}\right)^{-5/4} + \left(\frac{D}{H}\right)^{7/4} - 12\right] \quad \text{for } D < H, \tag{8.1}$$

As it can be seen in Figure 8.7 the AdG model fits well to the recorded data (For the

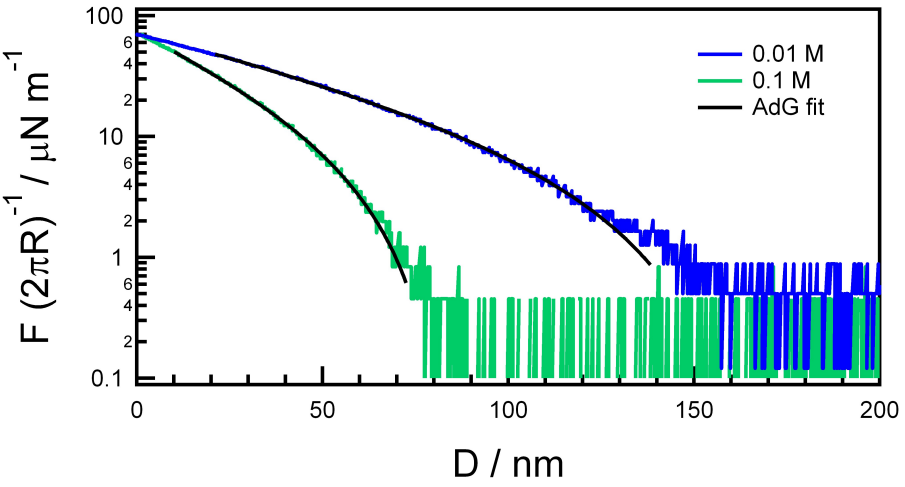

Figure 8.7: Force measurements at PMETAC brushes: Force profiles for NaCl salt concentrations of 0.1 M and 0.01 M Measured data are firtted with the AdG model.

fitting procedure we included a displacement parameter δ because we could not reach the constant compliance regime: $D = D' - \delta$). The resulting brush parameters are physically in the right order. The brush height was 150 ± 30 nm, and the separation distance of grafting points $\sigma^{1/2} = 15 \pm 3$ nm for a salt concentration of 0.1 M. For a concentration of 0.01 M the brush height was 300 ± 50 nm, and a separation distance of grafting points $\sigma^{1/2} = 19 \pm 4$ nm. The obtained values for the brush height are slightly to large compared to values detected using ellipsometry [1]. However this can

attributed to the electrostatic repulsion of the sample and the probe.
To analyze the effect of swelling, we normalized the force profiles as suggested by S. Block [31]. The AdG model predicts that the steric interactions scale linear with the brush height. The brush height again scales with the salt concentration as $H \propto I^{-1/3}$. Obviously, the force profiles should show the same behavior if they are plotted over $DI^{1/3}$, where D is the separation distance of the probe and the brush. Normalization of the resulting force profiles by $I^{1/3}$ should lead to a collapse of the curves for different salt concentrations onto a master curve. Following this procedure the effect of swelling and the resulting steric interactions could be confirmed as pointed out in Figure 8.8 (The same procedure can be applied for mean field (MF) theories (and others). For the MF approach the force profiles must be normalized by $I^{2/3}$. However, rescaling is just sucessful if the force profiles are shifted).

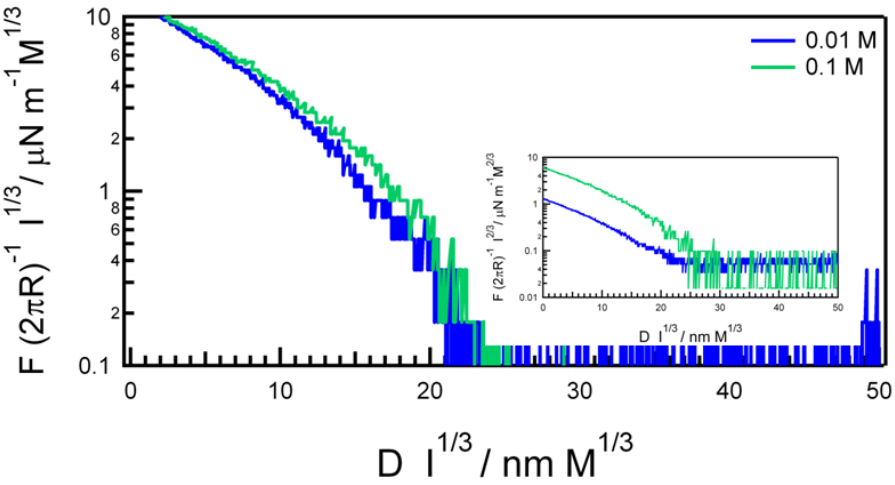

Figure 8.8: Normalization of the force profiles using the AdG model: Force profiles collapse onto a master curve if they are normalized as predicted by the AdG model. Inset shows rescaling using a mean field model. Rescaling in that case is just sucessfull if the force profiles are shifted

Interpretation of the Response Function

In our previous study on mechanoresponsive polymer brushes we analyzed the mechanoresponse in the contact zone of a soft colloidal probe that is pressed against the PMETAC polymer brush layer. In our case, we could observe fluorescence quenching as response to pressure. From these measurements we could determine a response function $I(p)$, which correlates local fluorescence intensity (I) to local pressure (p). The pressure is calculated with use of the JKR theory. To relate the mechanoresponse, i.e. state

of quenching to the applied force and the compressibility of the polymer brush, we can assume that the applied pressure p in the contact zone of the colloidal probe is proportional to the osmotic pressure inside the polymer brush

$$p(D) = p_{\text{osm}} = \frac{k_B T}{\sigma^{3/2}} \left[\left(\frac{D}{L} \right)^{-9/4} - \left(\frac{D}{L} \right)^{3/4} \right]. \tag{8.2}$$

Intermolecular deactivation processes, such as quenching, can be described using the Stern-Volmer equation [32].

$$\frac{I_0}{I_Q} = 1 + K c_Q, \tag{8.3}$$

where I_0 is the intensity of fluorescence without quenching, I_Q is the intensity with the quencher of the concentration c_Q and K is the quencher rate. We could show in our previous study [1] that the fluorescence intensity of 5(6)carboxyfluorescein (CF) is mainly quenched by METAC molecules ($K c_{\text{METAC}} >> 1$). Thus the intensity of fluorescein with METAC can be expressed by

$$I_{\text{Metac}} = \frac{I_0}{1 + K c_{\text{Metac}}} \approx \frac{I_0}{K c_{\text{Metac}}} = \frac{I_0 \sigma}{K N_{\text{Metac}}} D \Rightarrow I \propto D. \tag{8.4}$$

This assumption allows to interpret the detected "inverse" response function $p(I)$ directly as force-distance profiles. For a confirmation of this hypothesis we fitted the recorded response functions with Eq.8.2 where D is replaced by I. The shown curves

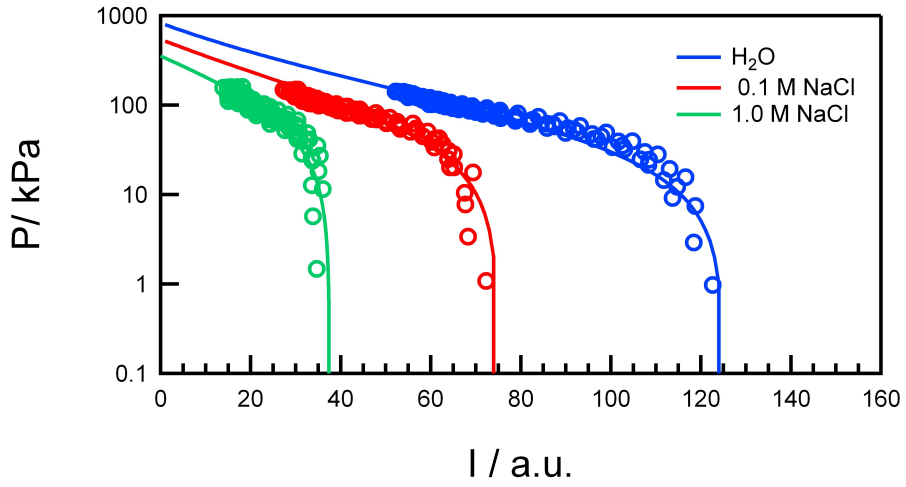

Figure 8.9: Interpretation of the Response Function: Response functions for H_2O, 0.1 M NaCl and 1 M NaCl solution: datapoints (reproduced from Ref. [1]) fitted with AdG profiles (solid lines).

(Figure 8.9) demonstrate that the measured data points are located on the falling edge of the AdG profiles. However, according to the fit the grafting density decreases with decreasing salt concentration. Further experimnts are necessary to varify these presumptions.

Conclusion and Outlook

In summary, we investigated the steric interactions of mechanoresponsive polymer brush systems. We could show that the AdG model can describe the steric interactions in the brush layers. Further experiments are necessary to confirm the observed behavior. In future, we will perform force spectroscopic measurements on patterned substrate (areas with and areas without brush) to achieve an internal reference of the brush height. Also, this will help to separate long and short range interactions. The effect of brush parameters on force profiles should be studied as well. For this purpose the brush height can be varied by a change of the polymerization time. The grafting density can be varied using different silanes as initiators or blocking the initiator (grafting sites) using suitable blocking molecules (Also other variations of the synthesis protocol are possible, e.g. type ligand, solvent). This will help to understand the influence of the brush parameters on compressibility and the mechanoresponse. Further force experiments and rescaling evaluation can help to prove experimentally, the validity and limitation of the existing theories on polymer brushes.

8.3.2 Change of the Detection Scheme

A more specific detection scheme than fluorescence quenching will help to understand how mechanical energy converts into changes of the chemical environment inside the brush. Here we introduce an alternative to fluorescence quenching using a pH sensitive fluorophore, i.e. seminaphtharhodafluor (SNARF). The physical properties of this type of dye are triggered by the dissociation equilibrium inside the brush. Variation of this equilibrium results in changes of the emission spectra.

Dye Attachment

The target was to bind SNARF molecules to the primary amine of the polymer PMETAC brushes, like shown in Figure 8.10. For this purpose, we used NHS-SNARF so that the succinimidyl ester reacts with the primary amine forming a peptide bond. After synthesis of the copolymer PMETAC brush (on glass slides) as established in Ref. [1], a functionalized glass slide was sonicated for 10 min in 1 M aqueous NaCl solution,

washed with water and dried in a N_2 stream. The NHS-SNARF (Invitrogen # S22801) was treated with 10 μl dimethylsulfoxid (DMSO) and incubated at room temperature for ca. 5 min. The dye solution was mixed with water to get a final dye concentration of 0.281 mM, and was filled on the bottom of a centrifuge cap. A glass slide (with the copolymer PMETAC polymer brush) was placed in the cap, with the polymer film towards the dye solution. After reaction time over night at room temperature the glass slide was rinsed with water and sonicated 2 times, each ca. 5 min, in 1 M aqueous NaCl solution. Finally, the slide was washed with water and dried in a N_2-stream.

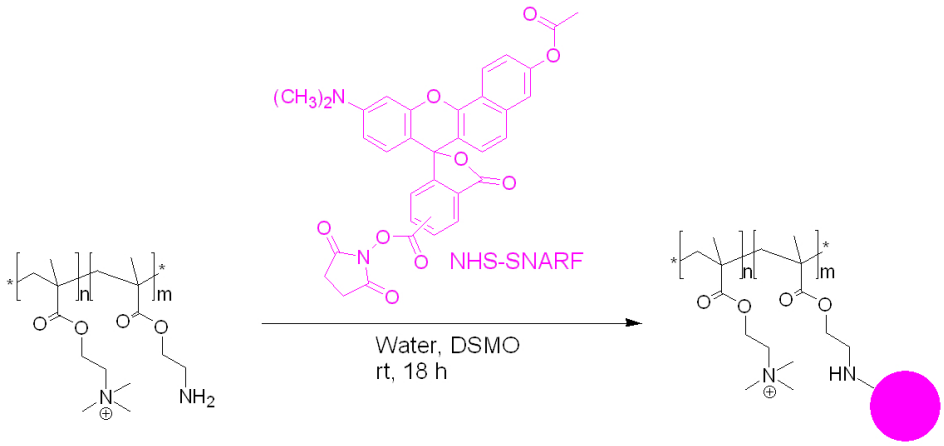

Figure 8.10: Attachement of SNARF to polymer brushes

Characterization

For the characterization of the dye attachment and of the response of the polymer brushes with covalent attached SNARF dye we performed fluorescence microscopy and fluorescence spectroscopy. The functionalized glass slides were placed on a fluorescence microscope and images were take in a range of pH 4 to pH 9 (pH solutions with different buffers listed in Tab. 8.1). A color change is clearly visible (Figure 8.11). This can be related to a shift in the emission spectra of the substrates. To quantify this alteration we analyzed the ratio of the intensity from the red channel I_r (red fluorescent emission) of the fluorescent microscope and I_y the intensity of the yellow channel, following Ref. [33, 34] (Figure 8.12). From these calibration curves we could determine pKa of the covalently attached SNARF [33, 34]. The mean value of three slides could be determined to $pKa = 9 \pm 1$.

Furthermore, we performed fluorescence spectroscopy. For this purpose the functionalized glass slides were analyzed using a confocal microscope in spectroscopy mode. Here, for each wavelength interval (3 nm) an intensity image was detected to create

Table 8.1: Buffers that were used to study the response of PMETAC-SNARF brushes on pH.

pH	composition
4	citric acid / NaCl / NaOH
5	citric acid / NaOH
6	citric acid / NaOH
7	KH_2PO_4 / Na_2HPO_4
8	$Na_2B_4O_7$ / HCl
9	$Na_2B_4O_7$ / KCl
10	$Na_2B_4O_7$ / NaOH
11	$Na_2B_4O_7$ / NaOH / KCl
12	Na_2HPO_4 / NaOH

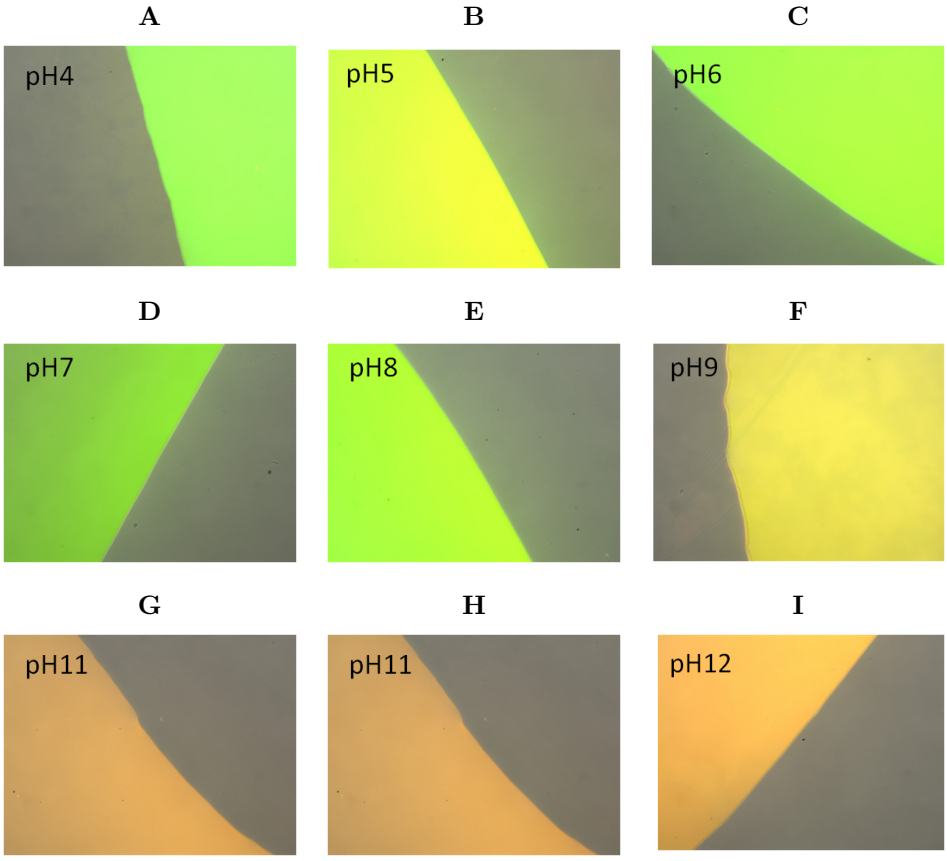

Figure 8.11: Fluorescence Microscope Images of SNARF functionalized brushes: pH4 (8.11A) - pH12 (8.11I)

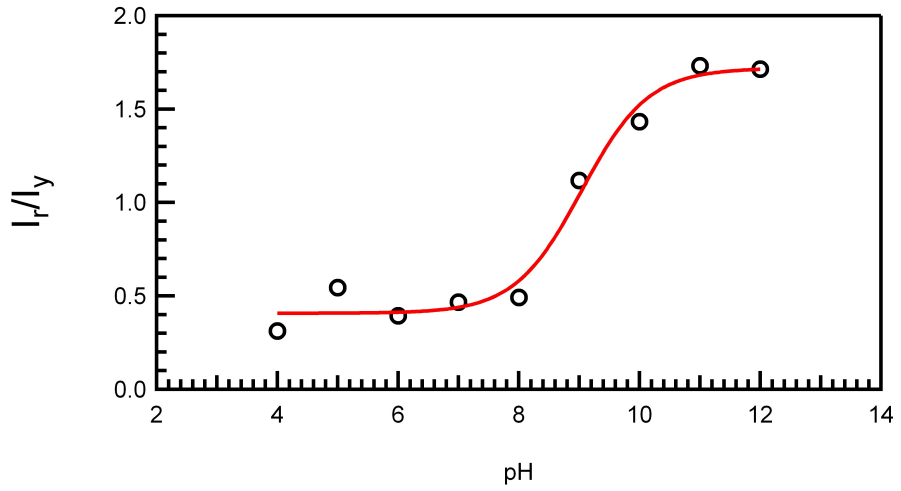

Figure 8.12: Calibration curve of the SNARF functionalized brushes

spectral profiles of the dye. For two pH values a clear change of the emission spectra could be identified (Figure 8.13).

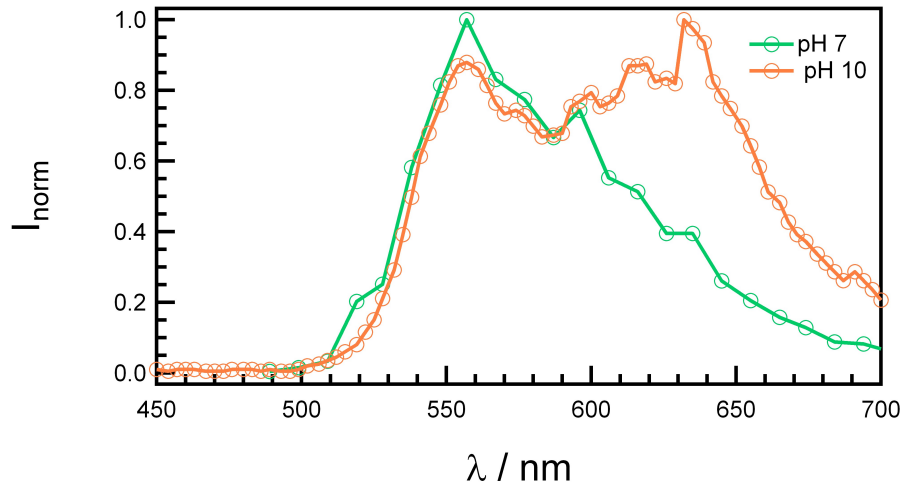

Figure 8.13: Emission spectra of SNARF functionalized brushes at pH7 and pH10

Conclusion and Outlook

In summary, we have established a protocol to attach the pH-sensitive dye seminaphtharhodafluor covalently to PMETAC polymer brushes. The obtained substrates were characterized with respect to functionalization and the resulting fluorescence properties as a function of pH. Further studies will verify these results. Follow up projects are planned to study the chemical environment inside polyelectrolyte brushes, with and

without compression, by analysis of fluorescence properties of the brush depending on the conformation of the polymer brush. A quantitative evaluation on the effect of these chemical modifications on response, in particular pressure sensitivity could be carried out in these experiments. In that context, annealed PE polymer brushes and polyelectrolyte gels could be tested as well.
Beside the question about compressibility and potential responses such an approach can help to "look" inside a brush and, thereby, allows proving the existing theories on polymer brushes.

8.4 References

[1] J. Buensow et al. "Direct Correlation between Local Pressure and Fluorescence Output in Mechanoresponsive Polyelectrolyte Brushes". In: *Angewandte Chemie-International Edition* 50.41 (2011), pp. 9629–9632.

[2] M. K. Chaudhury and G. M. Whitesides. "How to Make Water Run Uphill". In: *Science* 256.5063 (1992), pp. 1539–1541.

[3] M. K. Chaudhury and P. S. Goohpattader. "Noise-activated dissociation of soft elastic contacts". In: *European Physical Journal E* 35.12 (2012).

[4] A. Ghatak et al. "Peeling from a biomimetically patterned thin elastic film". In: *Proceedings of the Royal Society of London Series a-Mathematical Physical and Engineering Sciences* 460.2049 (2004), pp. 2725–2735.

[5] B. D. Grashoff C.and Hoffman et al. "Measuring mechanical tension across vinculin reveals regulation of focal adhesion dynamics". In: *Nature* 466.7303 (2010), 263–U143.

[6] E. Arzt, S. Gorb, and R. Spolenak. "From micro to nano contacts in biological attachment devices". In: *Proceedings of the National Academy of Sciences of the United States of America* 100.19 (2003), pp. 10603–10606.

[7] A. del Campo et al. "Patterned surfaces with pillars with controlled 3D tip geometry mimicking bioattachment devices". In: *Advanced Materials* 19.15 (2007), pp. 1973–+.

[8] A. del Campo, C. Greiner, and E. Arzt. "Contact shape controls adhesion of bioinspired fibrillar surfaces". In: *Langmuir* 23.20 (2007), pp. 10235–10243.

[9] L. F. Boesel et al. “Gecko-Inspired Surfaces: A Path to Strong and Reversible Dry Adhesives”. In: *Advanced Materials* 22.19 (2010), pp. 2125–2137.

[10] D.-M. Drotlef et al. “Insights into the Adhesive Mechanisms of Tree Frogs using Artifi cial Mimics”. In: *Advanced Functional Materials* (2012).

[11] C. Greiner, A. del Campo, and E. Arzt. “Adhesion of bioinspired micropatterned surfaces: Effects of pillar radius, aspect ratio, and preload”. In: *Langmuir* 23.7 (2007), pp. 3495–3502.

[12] J. Cui, V. San Miguel, and A. del Campo. “Light-Triggered Multifunctionality at Surfaces Mediated by Photolabile Protecting Groups”. In: *Macromolecular Rapid Communications* 34.4 (2012), pp. 310–329.

[13] C. Y. Hui et al. “Design of biomimetic fibrillar interfaces: 2. Mechanics of enhanced adhesion”. In: *Journal of the Royal Society Interface* 1.1 (2004), pp. 35–48.

[14] Y. Menguec et al. “Gecko-Inspired Controllable Adhesive Structures Applied to Micromanipulation”. In: *Advanced Functional Materials* 22.6 (2012), pp. 1246–1254.

[15] M. P. Murphy, B. Aksak, and M. Sitti. “Gecko-inspired Directional and Controllable Adhesion”. In: *Small* 5.2 (2009), pp. 170–175.

[16] D. Paretkar et al. “Bioinspired pressure actuated adhesive system”. In: *Materials Science andja Engineering C-Materials for Biological Applications* 31.6 (2011), pp. 1152–1159.

[17] J. Yu et al. “Gecko-Inspired Dry Adhesive for Robotic Applications”. In: *Advanced Functional Materials* 21.16 (2011), pp. 3010–3018.

[18] G. Carbone and E. Pierro. “Sticky Bio-inspired Micropillars: Finding the Best Shape”. In: *Small* 8.9 (2012), pp. 1449–1454.

[19] G. Carbone, E. Pierro, and S. N. Gorb. “Origin of the superior adhesive performance of mushroom-shaped microstructured surfaces”. In: *Soft Matter* 7.12 (2011), pp. 5545–5552.

[20] M. Schargott, V. L. Popov, and S. Gorb. “Spring model of biological attachment pads”. In: *Journal of Theoretical Biology* 243.1 (2006), pp. 48–53.

[21] R. Spolenak, S. Gorb, and E. Arzt. “Adhesion design maps for bio-inspired attachment systems”. In: *Acta Biomaterialia* 1.1 (2005), pp. 5–13.

[22] R. Spolenak et al. "Effects of contact shape on the scaling of biological attachments". In: *Proceedings of the Royal Society of London Series a-Mathematical Physical and Engineering Sciences* 461.2054 (2005), pp. 305–319.

[23] J. Buensow, T. S. Kelby, and W. T. S. Huck. "Polymer Brushes: Routes toward Mechanosensitive Surfaces". In: *Accounts of Chemical Research* 43.3 (2010), pp. 466–474.

[24] E. J. Laprade et al. "Large Deformation and Adhesive Contact Studies of Axisymmetric Membranes". In: *Langmuir* 29.5 (2013), pp. 1407–1419.

[25] R. Long and C.-Y. Hui. "Axisymmetric membrane in adhesive contact with rigid substrates: Analytical solutions under large deformation". In: *International Journal of Solids and Structures* 49.3-4 (2012), pp. 672–683.

[26] J. Erath, S. Schmidt, and A. Fery. "Characterization of adhesion phenomena and contact of surfaces by soft colloidal probe AFM". In: *Soft Matter* 6.7 (2010), pp. 1432–1437.

[27] G. Carbone and E. Pierro. "Effect of interfacial air entrapment on the adhesion of bio-inspired mushroom-shaped micro-pillars". In: *Soft Matter* 8.30 (2012), pp. 7904–7908.

[28] G. Castellanos, E. Arzt, and M. Kamperman. "Effect of Viscoelasticity on Adhesion of Bioinspired Micropatterned Epoxy Surfaces". In: *Langmuir* 27.12 (2011), pp. 7752–7759.

[29] P. G. de Gennes. "Conformations of Polymers Attached to an Interface". In: *Macromolecules* 13.5 (1980), pp. 1069–1075.

[30] P.G. de Gennes. *Scaling Concepts in Polymer Physics*. Vol. 1. Cornell University Press. NY, USA, 1979.

[31] S. Block. *On surface forces and morphology of linear polyelectrolytes physisorbed onto oppositely charged surfaces*. Greifswald, Germany, 2010.

[32] J. R. Lakowicz. *Principles of Fluorescence Spectroscopy*. Vol. 3. Berlin, Germany: Springer, 2006.

[33] L. L. del Mercato et al. "LbL multilayer capsules: recent progress and future outlook for their use in life sciences". In: *Nanoscale* 2.4 (2010), pp. 458–467.

[34] G. Pasparakis and M. Vamvakaki. "Multiresponsive polymers: nano-sized assemblies, stimuli-sensitive gels and smart surfaces". In: *Polymer Chemistry* 2.6 (2011), pp. 1234–1248.

9

Summary

In this thesis, so-called ”polyelectrolyte brushes” are addressed. The focus is on the investigation and understanding of the response properties of these polymer surfaces. For that purpose new methods are developed which combine force spectroscopy and optical microscopy, as well established physico-chemical techniques are used.

Polymer brushes form when many polymer chains are grafted at a minimum distance to a substrate surface so that their interaction potentials overlap. Thus, the polymers align and can form a responsive film, in particular if polyelectrolytes are used. In this thesis the ”grafting-from” method has been used for the treatment of the polymer chains. In this approach polymerization is carried out directly from the surface. The synthesis of the polymer brushes is very flexible in terms of their molecular architecture because any type of polymerization can be used, as long as the required initiator can be attached to the surface. Furthermore, the conformation and thus the physical properties of the polymer brushes are highly dependent on the surrounding environment, in particular for polyelectrolyte brushes. Moreover, it is possible to bring functional groups to the polymer chains that can be addressed by external stimuli. Thus, polyelectrolyte brushes provide an excellent building block for responsive surfaces. Surface properties that can be triggered are for example adhesion, charge, friction, stiffness, optical properties, porosity, or biocompatibility. This can be obtained by changing the environment, such as ionic strength, pH, or temperature or by external stimuli such as electric or magnetic fields, or light and pressure. For this reason, such systems are ideal for the rational design of sensors that can detect environmental conditions or external stimuli. Also, they can realize the build up of actuators. These can be used for example in stem cell research to stimulate cells and to control their growth and properties.
For the design of such applications, a fundamental understanding of the polymer brushes, the properties of their response and the associated surface properties is required.

The first part of this thesis covers new measuring techniques for the investigation of responsive systems. Furthermore, polyelectrolyte brushes are used for the design of sensors and for selective adjustment of surface properties.

The soft colloidal probe (SCP) force spectroscopy method has been developed. This method combines the advantages of a JKR-apparatus (large contact area) and the AFM force spectroscopy (high force resolution). For this purpose, a soft colloidal particle made from Polydimethylsiloxane (PDMS) is mounted at the tip of an AFM cantilever

and a defined microscopic contact can be produced. This allows in-situ determination of the contact area as a function of applied load and elastic properties of the system. Contact parameters such as thermodynamic work of adhesion and stress distributions can then be accessed by using the JKR approach. The method has been tested in ambient conditions as well as in aqueous media on well-known surface chemistries, where the contributions of capillary in air, hydration forces and hydrophobic interactions in water are characterized. This technique makes a broad range of systems and scientific issues accessible due to its enhanced sensitivity.

Knowledge of the stress distribution within a contact is fundamental for the understanding for all kind of contact phenomena. For this purpose a sensor has been developed, on the basis of mechanoresponsive polymer brushes, that change their optical properties as a function of applied pressure (cationic poly [2-(methacryloyloxy)ethyl]trimethyl ammoniumchloride (PMETAC) brushes with a covalently attached fluorescent dye, 5(6)carboxyfluorescein (CF)). The polymer brush changes its fluorescence properties dependent on its state of compression. This allows to detect pressure distributions with high spatial ($<1\,\mu$m) and high pressure resolution (<10 kPa).
The system has been investigated and calibrated with the SCP method. Therefore the soft particle is brought into contact with the polymer brush and a contact area is formed. The fluorescence changes within the contact area are detected with a confocal microscope with high resolution. A local dependence of the fluorescence intensity distribution can be observed. To understand the nature of this distribution, the contact zone is described with a contact mechanics model, developed by Johnson, Kendall and Roberts. The decrease in fluorescence intensity (as compared to the background intensity) can be related to areas of compression and increase of fluorescence to areas of tension. Physically / chemically these fluorescence changes can be associated with a quenching mechanism. Also, the response is stabilized well before acquisition times, is constant over several minutes and is completely reversible. All these features make such a mechanoresponsive system a unique starting point for the development of stress sensors. Furthermore, three perspectives of the mechanoresponsive polymer brushes are discussed: 1) Analytical description of the relationship between compression and response in the fluorescence signal; 2) Alternative detection mechanisms such as changes of the emission spectrum as a function of brush compression, which can be realized by modifying the mechanophore and 3) Applications to study of biomimetic systems to understand e.g. the superior adhesive strength of gecko feet.

Light can not only be used as response, but also as trigger. A system of polymer brushes has been established that changes its chemical structure under irradiation with light. These brushes (PNVOCMA) are composed of a methacrylate backbone and ionizable -COOH side groups modified (caged) with a photo-removable group, 6-nitroveratryloxy carbonyl (NVOC). Irradiation results in a conversion of the polymer brush from neutral to a negative charged poly(metacrylic acid) (PMAA) brush and makes it hydrophilic. Adjusting the exposure time and intensity allows, determining defined intermediate interfacial states between the caged and the charged (fully de-protected) forms, or a gradual transition between them. This allows matching of surface properties for the desired application.
This thesis shows how the exposure time affects the conversion state of the polymer brush and what is the resulting impact on wettability, adhesion and friction. With increasing exposure time, the water absorption of the brush increases. Also, the surface forces between the polymer brush and a cantilever tip of silica change due to an increase in charge with photconversion, or the adhesive properties decrease, respectively. On the other hand, the friction between the probe and the substrate increases with exposure time, which can be related to substrate effects. These photoresponsive brushes can be used for example to manipulate water condensation and motion of liquids on brush layers by realizing surface gradients, which can utilize for the design of water harvesting surfaces or micro fluidic systems. Other potential applications are controlled attachment or detachment of chemical compounds or biological objects, which can used for the design of ”Lab-on-Chip” devices.

An alternative to polymer brush systems for responsive layers as discussed in the first part are colloidal building blocks. The second part of the thesis deals with the development of responsive systems composed of such colloidal building blocks. These posses several advantages: The handling of colloidal building blocks is usually simple and their arrangement can be easily controlled by targeted self-organization. In addition, the colloidal building blocks may have various functionalities and new properties can be generated due to the colloidal character. Examples are the localization of light or collective optical processes. Requirements for such applications are an understanding of the interactions of the colloidal objects with the substrate and the responsive character of such systems triggered by the environment.

In this thesis, the adsorption of anionic spherical polymer brushes (SPBs) composed of a polystyrene (PS) core and attached polystyrene sulfonate (PSS) chains on charged

surfaces has been investigated. The observations are correlated to force-spectroscopic measurements. For this purpose micron sized model particles were prepared which could be used as probes in a colloidal probe AFM setup. These probes were used to measure the interactions between these "micro SPBs" and positively or negatively charged surfaces. We showed that the adhesive properties of the SPBs can be controlled by the ionic strength of the surrounding solution and the substrate charge. At low ionic strength, the negatively charged SPBs preferably adsorb onto the positively charged substrates. Above a critical ionic strength, this selectivity is lost. Due to secondary interactions the particles adsorb in these condition on both systems equally. The observations have been used to build up hierarchical structures from SPBs, which are adsorbed from a suspension. The hierarchy can be controlled by the micro-contact printing technique. Such systems can be exemplarily used for optical applications, if a metal core is employed.

Furthermore, highly active surfaces have been prepared on basis of polyelectrolyte-copolymer micelles. For this, a triblock terpolymer is used (BMAADq: polybutadiene (B), poly(methacrylic acid) (MAA), and quaternized poly(2-(dimethylamino)ethyl methacrylate) (Dq)) which forms micelles in solution composed of a hydrophobic core, a middle block of an annealed polymer brush, and a positively charged corona. These micelles have been disposed in multilayers using the layer-by-layer method with a negative polymer. The advantage of the micelles used in this approach is that the central block is shielded by the other two blocks from complexation with the multilayer. Because of the central block, the micelles and thus the multilayers are strongly dependent on the pH of the environment. At a low pH, the middle block contracts, whereas it is highly swollen at high pH. In this thesis we investigate the swelling behavior of the multilayer-system on the number of deposition steps and as a function of the pH value. Further, we correlate the swelling behavior with porosity and mechanical properties of the multilayers. Due to their high sensitivity, these responsive layers are suitable for the design of actuators.

In summary, this work bridges from fundamental polymer chemistry (chemistry of polymer brushes) over physics (contact mechanics, adhesion, and polymer physics) to potential applications (sensors and actuators). Scientific input has been provided for the research on polymer brushes, mechanoresponsive systems, force sensing, and active materials, as well as contact mechanics, colloidal arrangement, and (bio) adhesion.

10

Zusammenfassung

In dieser Arbeit werden sogenannte "geladene Polymer Bürsten" untersucht. Dabei liegt der Fokus auf der Untersuchung und dem Verständnis der schaltbaren Eigenschaften dieser Polymer Oberflächen. Dazu werden sowohl neue Methoden aus Kombination von Kraft Spektroskopie und optischer Mikroskopie eingeführt, sowie bereits etablierte physikalisch-chemische Techniken verwendet.

Polymer Bürsten bilden sich aus, wenn viele Polymerketten in einem Mindestabstand an einer Substrat Oberfläche angebunden werden, so dass deren Wechselwirkungspotentiale überlappen. Dadurch richten sich die Polymere aus und bilden einen responsiven Film. Das Anbinden der Polymerketten erfolgt in dieser Arbeit mit der sogenannten "Grafting from" Methode, bei der eine Polymerisation direkt von der Oberfläche ausgeführt wird.
Die Synthese der Polymer Bürsten ist sehr flexibel im Hinblick auf ihre molekulare Architektur, da jede Art von Polymerisation anwendbar ist, solange der benötigte Initiator an die Oberfläche gebunden werden kann. Des Weiteren hängt die Konformation und damit die physikalischen Eigenschaften der Polymer Bürsten, stark von deren Umgebung ab, insbesondere bei geladenen Polymer Bürsten. Außerdem ist es möglich funktionelle Gruppen an die Polymere anzubinden, so dass diese durch externe Stimuli geschaltet werden können. Damit erweisen sich geladene Polymer Bürsten als exzellente Bausteine für schaltbare Oberflächen. Schalten lassen sich Oberflächeneigenschaften, wie zum Beispiel Adhäsion, Ladung, Reibung, Mechanik, optische Eigenschaften, Porosität oder Biokompatibilität. Dieses Schalten kann durch Veränderung der Umgebung wie Ionenstärke, pH-Wert oder Temperatur und durch externe Stimuli wie elektrische oder magnetische Felder, Druck oder Licht ausgelöst werden. Damit eignen sich solche Systeme ideal, um Sensoren auf Umgebungseigenschaften oder externe Stimuli bzw. Aktuatoren aufzubauen.
Diese lassen sich zum Beispiel in der Stammzellenforschung einsetzen um Zellen zu stimulieren und deren Wachstum und Eigenschaften zu kontrollieren.
Für solche Anwendungen ist ein fundamentales Verständnis der Polymer Bürsten, deren Schalteigenschaften und den damit verbundenen Oberflächeneigenschaften notwendig.

Im ersten Teil dieser Arbeit werden neue Messmethoden für die Untersuchung von schaltbaren Systemen vorgestellt. Desweiteren werden geladene Polymer Bürsten für den Aufbau von Sensoren und für die gezielte Einstellung von Oberflächeneigenschaften verwendet.

Es ist die kolloidale Kraft-Spektroskopie mit weichen Partikeln (engl. Soft colloidal probe: SCP) entwickelt worden. Diese Methode kombiniert die Vorteile eines JKR-Messgeräts (große Kontaktfläche) und der AFM Kraftspektroskopie (hohe Kraftauflösung). Durch ein am vorderen Ende einer AFM-Blattfeder (Cantilever) angebrachtes weiches Partikel aus Polydimethylsiloxan (PDMS) wird ein definierter mikroskopischer Kontakt erzeugt. Dazu wird das Partikel mit kontrollierter Kraft gegen eine Oberfläche gefahren, wodurch sich eine Kontaktfläche ausbildet. Diese kann mittels Mikrointerferometrie beobachtet werden. Mit Hilfe von Kontakt-Mechanik Modellen lassen sich so aus den gemessenen Größen verschiedene Parameter wie etwa die Adhäsionsenergie pro Einheitsfläche und Spannungsverteilung in der Kontaktzone bestimmen.
Diese Methode ist an verschiedenen Modellsystemen mit bekannter Oberflächenchemie zur Bestimmung der Adhäsionsenergie pro Einheitsfläche getestet worden. Dabei kann klar zwischen kapillaren, hydrophilen und hydrophoben Wechselwirkungen unterschieden werden. Des Weiteren ermöglicht die SCP Methode durch ihre hohe Sensitivität die Untersuchung eines breiten Spektrums an Systemen und die Aufklärung wissenschaftlicher Fragen.

Kenntnisse über die Spannungsverteilung innerhalb eines Kontakts sind fundamental für das Verständnis von Kontaktphänomenen, insbesondere auf der kolloidalen Skala. Auf der Basis von mechanoresponsiven Bürstensystemen ist ein Sensoren entwickelt worden, der seine optischen Eigenschaften als Funktion der angelegten Kraft ändert. Dies ermöglicht Spannungsverteilungen mit hoher lateraler Auflösung ($< 1\,\mu$m) und hoher Druckempfindlichkeit ($< 10\,$kPa) zu detektieren.
Dieser Sensor besteht aus kationischen, fluoreszenzmarkierten Polyelektrolyt Bürsten (Poly [2 - (Methacryloyloxy) ethyl] trimethyl-ammoniumchlorid (PMETAC) Bürsten, markiert mit einem kovalent angebundenen Fluoreszenzfarbstoff, 5 (6) Carboxyfluorescein (CF)). Die Polymer Bürsten ändern ihre Fluoreszenzeigenschaften abhängig von ihrem Kompressionszustand. Dieses System ist mit der SCP Methode untersucht und kalibriert worden. Dazu wir das weiche Partikel mit der Polymer Bürste in Kontakt gebracht. Unter Kompression bildet sich eine Kontaktfläche aus. Die optischen Signale aus der Kontaktfläche, Fluoreszenzänderungen, können mit einem Konfokalen Mikroskop mit hoher Auflösung detektiert werden. Dabei kann in der Kontaktfläche eine lokal vom Ort abhängige Fluoreszenzintensitäts-Verteilung beobachtet werden. Um den Verlauf dieser Verteilung zu verstehen, ist die Kontaktzone mit einem Kontaktmechanik Modell, entwickelt von Johnson, Kendall und Roberts, beschrieben worden. Dabei zeigt sich, dass unter Kompression die Fluoreszenzintensität kleiner wird. An-

dererseits nimmt die Fluoreszenzintensität zu, wenn man an den Bürsten zieht. Mit diesen Überlegungen ist es möglich eine Antwortfunktion zu bestimmen, die der lokalen Fluoreszenzintensität einen lokalen Druck zuordnet. Physikalisch/Chemisch kann die Fluoreszenzänderungen einem "Quenching Mechanismus" zugeordnet werden. Außerdem ist das Signal reversibel und stabil. All diese Eigenschaften machen ein solches mechanoresponsives System zu einer einzigartigen Basis für den Aufbau von Druck Sensoren.
Darüber hinaus werden drei Perspektiven der mechanoresponsiven Polymer Bürsten diskutiert: 1) Analytische Beschreibung des Zusammenhangs von Kompression und Änderung des Fluoreszenzsignals; 2) Alternative Detektionsmechanismen wie Änderung des Emissionsspektrums als Funktion der Bürstenkompression durch Modifikation des Mechanophors und 3) Anwendungsmöglichkeiten auf die Untersuchung von biomimetischen Systemen, wie zur Aufklärung der bemerkenswerten Hafteigenschaften von Geckofüßen.

Licht kann nicht nur als Antwortfunktion verwendet werden, sondern auch als Trigger. Es ist ein System von Polymer Bürsten etabliert worden, das aufgrund der Einstrahlung von Licht seine chemische Struktur ändert. Diese Polymer Bürsten (PNVOCMA) bestehen aus einem Methacrylat Rückgrat mit ionisierbarem -COOH Seitengruppen, die durch Bestrahlung des photosensitiven 6-nitroveratryloxy Carbonyl (NVOC) frei werden und eine Poly (Methacrylsäure) (PMAA) Bürste ausbilden. Dadurch ändert sich die Oberfläche von neutral zu negativ geladen und wird hydrophil. Mit diesen photoresponsiven Systemen ist es möglich Oberflächeneigenschaften nicht nur zwischen ihren Extremwerten hin und her zu schalten, sondern diese durch Anpassung der Belichtungszeit und Intensität definiert einzustellen und damit für die gewünschte Anwendung zu optimieren.
In dieser Arbeit wird gezeigt, wie sich die Belichtungszeit auf den Umwandlungszustand der Polymer Bürste auswirkt und wiederum was für einen Einfluss das auf Benetzbarkeit, Adhäsion und Reibung hat. Mit Zunahme der Belichtungszeit wird die Wasseraufnahme der Bürste größer. Außerdem verändern sich mit der Photokonversion auch die Oberflächenkräfte. Mit Zunahme der Bestrahlungsdauer werden Reichweite und Stärke von repulsiven Wechselwirkungen zwischen der Polymer Bürste und einer Cantileverspitze aus Siliziumdioxid größer und die Hafteigenschaften nehmen ab. Andererseits wird die Reibung zwischen der Sonde und dem Substrat mit Zunahme der Belichtungszeit größer, was durch Substrateffekte erklärt werden kann. Diese photoresponsiven Systeme können zum Beispiel dazu verwendet werden, um Wasserkondensa-

tion und die Bewegung von Flüssigkeiten zu manipulieren. Dies kann in "Wasserernte-" oder Mikrofluidik-Systemen eingesetzt werden. Eine weitere Anwendung ist das gezielte Ankoppeln oder Abtrennen von chemischen Verbindungen oder biologischen Objekten. Dies kann beispielsweise in "Lab-on-Chip"-Geräten verwendet werden.

Alternativ zu den gezeigten Ansätzen von Polymer Bürsten auf flachen Substraten lassen sich responsive Systeme auch aus kolloidalen Bausteinen aufbauen. Der zweite Teil dieser Arbeit befasst sich mit dem Aufbau von Schaltbaren Systemen aus solchen Bausteinen. Dies bringt einige Vorteile mit sich: Die Handhabung von kolloidalen Bausteinen ist in der Regel einfach, bzw. lässt sich die Anordnung dieser durch gezielte Selbstorganisation gut kontrollieren. Außerdem können die kolloidalen Bausteine diverse Funktionalitäten besitzen und durch den kolloidalen Charakter ganz neue Eigenschaften generieren, beispielsweise die Lokalisierung von Licht oder kollektive optische Prozesse.
Voraussetzung für solche Anwendungen ist das Verständnis der Wechselwirkungseigenschaften mit dem Substrat und des Verhaltens solcher Bausteine abhängig von ihrer Umgebung.

In dieser Arbeit ist das Adsorptionsverhalten von geladenen sphärische Polymer Bürsten (SPBs) bestehend aus einem Polystyrene (PS) Kern und angebundenen Polystyrene Sulfonate (PSS) Ketten) auf geladenen Oberflächen untersucht und dieses mit kraftspektroskopischen Messungen korreliert worden. Dazu sind Modell-Partikel hergestellt worden, die als kolloidale Sonden an einem AFM-Cantilever verwendet werden können. Mit diesen Sonden und Messung der Wechselwirkungen zwischen diesen "Mikro-SPBs" und positiv bzw. negativ geladenen Oberflächen wird gezeigt, dass die Hafteigenschaften der SPBs durch Ionenstärke und Ladung des Substrats gesteuert werden können. Bei geringer Ionenstärke adsorbieren die negativ geladenen SPBs vorzugsweise auf den positiv geladenen Substraten. Ab einer kritischen Ionenstärke geht diese Selektivität aber verloren und die Partikel adsorbieren aufgrund sekundärer Wechselwirkungen auf beiden Systemen gleich gut. Dieses Verständnis wird weiter dazu genutzt, um hierarchische Strukturen aus SPBs aufzubauen, die aus einer Suspension adsorbiert werden. Die Strukturierung kann hierbei durch die Mikrokontaktdruck-Technik gesteuert werden. Verwendet man metallische Kerne (anstatt der bei unserem Modellsystem verwendeten PS Kerne) lassen sich für optische Anwendungen interessante Strukturen aufbauen.

Weiterhin sind aktive Oberflächen durch Polyelektrolyt Copolymer- Mizellen hergestellt worden. Dazu werden Triblockterpolymere verwendet (BMAADq: Polybutadienblock (B), einem pH-sensitiven Polymethacrylsäure-Mittelblock (MAA) und einem permanent geladenen Block aus quarternisiertem Poly(2-dimethylamino)ethylmethacrylat) (Dq)), welche in Lösung Mizellen mit einem hydrophobischen Kern, einen Mittel-Block aus einer schwachen Polymer Bürste und einer positiv geladenen Korona ausbilden. Diese Mizellen werden mit der "Layer-by-Layer-Methode" mit einem negativ geladenem Partner-Polymer in Multilagen angeordnet. Durch den Mittelblock sind die Mizellen, und damit auch die Multilagen stark von dem pH Wert der Umgebung abhängig. Bei einem niedrigen pH Wert zieht sich der Mittelblock zusammen, wogegen er bei einem hohen pH Wert stark gequollen ist. Der Vorteil der hier verwendeten Mizellen ist, dass der Mittelblock durch die anderen beiden Blöcke von der Komplexierung in der Multilage abgeschirmt ist. In dieser Arbeit haben wir das Quellverhalten dieser Systeme in den Multilagen untersucht und dieses abhängig von Anzahl der Multilagen und pH-Wert quantifiziert. In einem weiteren Schritt haben wir dieses Verhalten mit Porosität und mechanischen Eigenschaften der Multilagen korreliert. Durch ihre hohe Sensitivität eignen sich diese responsiven Lagen sehr gut als Aktuator-Materialien.

Zusammenfassend wurde in dieser Arbeit eine Brücke von Polymer Chemie (Chemie der Polymerbürsten) über die Physik (Kontaktmechanik, Adhäsion und Polymerphysik) zur potentiellen Anwendung (Sensoren und Aktuatoren) geschlagen. Dabei wurden wissenschaftliche Beiträge zur Forschung an Polymer Bürsten, mechanoresponsiven und aktiven Materialien, Krafterkennung und Kontaktmechanik, kolloidaler Anordnung und (Bio-) Haftung geleistet.

A

Theory of Polymer Brushes

Polyelectrolyte Brushes

Local Neutrality Approximation

The local neutrality LEA makes the approximation that the charge and the force is locally balanced in the polymer brush system. This section is oriented on Ref. [1].
The brush is immersed in an infinte reservoir of solution that contains besides H^+ and OH^- a concentration of (e.g. monovalent) ions of different chemical nature (e.g. Na^+ and CL^-).

charge balance

For charge balance, two electroneutral subsytems are assumed: the polymer brush and the bulk solution seperated by a semipermeable membrane. In the brush, mobile ions $c_{+/-}$ are balanced by the immobilized charge αc_p.

$$\alpha c_p + c_- = c_+ \text{ brush} \tag{A.1}$$

$$C_- = C_+ \text{ bulk} \tag{A.2}$$

where c_p is the concentration of polymer units (charged and uncharged), $c_{+/-}$ is the total molar concentration of positive or negative mobile ions in the brush and $C_{+/-}$ are the total molar concentrations of positively and negatively charged ions in the bulk solution. Due to the electrostatic potential u, the mobile ions are redistributed, showing a Boltzmann like behavior.

$$c_{i+/-} = C_{i+/-} \exp(eu/K_bT) \tag{A.3}$$

Donnans Rule declare that the ratios of concentrations of different positively charged ions inside and outside the brush are not equal to each other and are inverse to that for negatively charged ions:

$$c_{i+}/C_{i+} = C_{j-}/c_{j-} \tag{A.4}$$

With Eq. A.1 and A.4 the total concentration of mobile ions inside the brush is

$$(c_+ + c_-)^2 = \alpha 2c_p^2 + 4C_+C_+. \tag{A.5}$$

To show what one can learn from the charge balance discussed above, we treat on a system with an external characteristic given by:

$$\begin{aligned} C_{H^+} = C_{OH^-} = \quad & C_{H^*} \quad && = 10^{-7}\,\text{mol/l for pH} = 7 \\ C_{S^+} = C_{S^-} = \quad & C_S \quad && \text{eg.: } Na^+ \text{ and } Cl^- \\ \Rightarrow C_+ = C_- = \quad & (C_{H^*} + C_S) \end{aligned}$$

Using of Eq. A.4, one can deviate the dependence of the degree of ionization α on polymerbrush and external characteristic represented by the dissociation constant K_D, c_p and $(C_{H^*} + C_S)$.

$$\frac{\alpha c_p}{C_{H^*} + C_S} = \frac{K_D}{C_{H^*}} \frac{\alpha}{1-\alpha} - \frac{C_{H^*}}{K_D} \frac{\alpha}{1-\alpha} \tag{A.6}$$

because, the the dissociation constant is related to the degree of ionization of the brush $(HA = H^+ + A^-)$ by mass law:

$$K_D = \frac{c_{H^+}\alpha}{1-\alpha} \tag{A.7}$$

With eq. A.6, the dependence of c_+ and c_- on the system parameters follows as

$$(c_+ + c_-)^2 = \alpha 2c_p^2 + 4(C_{H^*} + C_S)^2. \tag{A.8}$$

Force Balance

The conformation of the brush is determined by the balance between electrostatic forces (F_{ion}), steric (volume) interactions (F_{conc}), and elastic repulsion of the chains (F_{conf}).

$$F_{conf} = F_{conc} + F_{ion} \tag{A.9}$$

The free energy of one polymer chain is defined as

$$f(\vec{R}, N) = U(\vec{R}, N) - TS(\vec{R}, N). \tag{A.10}$$

whith $U(\vec{R}, N)$ the inner energy and S the entropy defined by

$$S(\vec{R}, N) = K_b T \ln \psi(\vec{R}, N). \tag{A.11}$$

In Eq. A.11 ψ is the number of conformations of the chain with N monomers and end to end vector $\vec{R}$.

The volume or steric interactions can be approximated by a viraial expansion:

$$\begin{aligned} \frac{f_{conc}}{K_bT} &= \int d\vec{r}\left(\frac{1}{2}v_2c(\vec{r})^2+\frac{1}{6}v_3c(\vec{r})^3+O(c(\vec{r})^4)\right) \\ &\approx v_2\left(\frac{N}{\sigma H}\right)^2 \end{aligned} \tag{A.12}$$

The elastic repulsion of a polymer chain can be modeled by entropic springs connecting the monomers. The spring constant holding the chain in conformation is

$$k_G = 3K_bT/Na^2 \tag{A.13}$$

and thus

$$\frac{f_{conf}}{K_bT} \propto \frac{1/\sigma \cdot H^2}{Na^2}$$

The partial pressures P of f_{conc} and f_{conf} are given by $P = -(\partial f/\partial h)_{T,N}$:

$$\begin{aligned} P_{conc} &= -v^2\left(\frac{1/\sigma N}{H}\right)^2 \\ P_{conf} &= -\frac{H}{Na^2} \end{aligned} \tag{A.14}$$

The electrostatic force can be estimated by the difference of the osmotic pressure of mobile ions inside and outside the brush $\Delta\pi$

$$\frac{f_{ion}}{K_bT} \propto \sigma P_{ion} = \sigma(c_+ + c_- - (C_+ + C_-)) \tag{A.15}$$

Using Eq. A.8 this results in

$$P_{ion} \propto \sigma\left[\sqrt{\left(\frac{\alpha\phi}{a^3}\right)+4(C_{H^*}+C_S)^2}-2(C_{H^*}+C_S)\right]. \tag{A.16}$$

With these expressions follows:
In case of neutral polymer brushes:

$$P_{conf} = P_{conc} \Rightarrow \frac{1/\sigma H}{Na^2} = v^2\left(\frac{1/\sigma N}{H}\right)^2 \Rightarrow H \propto \sigma N\sigma^{-1/3} \tag{A.17}$$

For PE brushes: short range interactions are in general weak compared to electrostatic forces.

$$P_{conf} = P_{ion}. \tag{A.18}$$

Convertion leads to

$$H \propto Na\alpha^{1/2} \quad , \quad \text{for } C_{H^*} + C_S << \frac{\alpha\phi}{a^3} \tag{A.19}$$

$$H \propto N(a^2\alpha^2\sigma^{-1}C_S^{-1})^{1/3} \quad , \quad \text{for } C_S >> \frac{\alpha\phi}{a^3}, C_{H^*}. \tag{A.20}$$

PE brushes which can be described by Eq. A.19 are called Osmotic brush (OsB). This is the case if the concentration of salt in solution is small and the concentration of counterions inside the brush equal to that of immobilized charge. If the salt ion charges dominate compared to the immobilized charges inside the brush (Rq. A.20) the PE brush is named salted brush (SB). Here, the brush height decreases weakly with increasing in salt concentration and grafting density.

A.1 References

[1] E. B. Zhulina, T. M. Birshtein, and O. V. Borisov. "Theory of Ionizable Polymer Brushes". In: *Macromolecules* 28.5 (1995), pp. 1491–1499.

B

A Little Coding with Igor

In the following the main evaluation procedures used for the evaluation of the experimental data written for IgorPro are listed. The full code is availabe from CD stored at University Bayreuth, Physical Chemistry II.

1. Evaluation of force map data (JPK Nanowizard I): EvalJPKFD.ipf
2. Evaluation of force map data (MFP 3D): EvalMFPFD.ipf
3. Communication of MFP and LSM 710: CommAFMCLSM.ipf
4. Reconstruction of object topographies from RICM-measurements: ReconstructRICM.ipf
5. Response function of mechanoresponsive surface: Responsemechano.ipf

Danke!

Wie sagt man nach so vielen Jahren am besten allen Danke, die zum Gelingen eines Projekts, wie der vorliegenden Arbeit beigetragen haben? Um nicht den ein oder anderen zu vergessen möchte ich mich erst einmal grundsätzlich bei **ALLEN** bedanken mit denen ich zusammen arbeiten durfte. So nun der Reihe nach:

Andreas Fery, Danke für die super Betreuung, die vielen interessanten Diskussionen, die Freiheit mich entfalten zu können und auch dafür, das ein oder andere Projekt mit anstoßen zu dürfen. Es hat mir ehrlich immer viel Spaß gemacht mit Dir zu arbeiten. Meistens hat es sich daher gar nicht wie Arbeit angefühlt. Außerdem Danke, dass ich so viele Konferenzen besuchen und dadurch die Welt besser kennenlernen durfte.

Sybille Zimmermann, du weißt, ohne Dich wäre der Lehrstuhl nicht so wie er ist. Du hältst deine "Familie" echt super zusammen. Danke für alles was du für mich erledigt hast.

Johanna Bünsow, dir möchte ich Danke sagen für Deine Einführung in die Welt der Polymer-Bürsten, Deine Geduld, wenn ich mal etwas nicht gleich verstanden habe und natürlich das Korrekturlesen dieser Arbeit. Ich freue mich einfach, dass wir auf dem Weg der Wissenschaft Freunde geworden sind, juhu!
An dieser Stelle möchte ich auch **Wilhelm** Huck danken, der viel zu meinem Polymer-Bürsten Verständnis beigetragen hat und für die gute Kooperation.

Arancha del Campo, Danke dass ich bei Euch am MPI für Polymer-Forschung in Mainz immer willkommen war, die nette Atmosphäre und die vielen interessanten Diskussionen. Außerdem natürlich für die gute Zusammenarbeit an unseren Projekten. Hier auch Danke an Dirk, Michael und Jiaxi für die tolle Zusammenarbeit.

Danke an **Stephan** Block, für tolle Disussionen und den regen E-Mail Kontakt.

Ein besonderer Dank gilt all meinen Kollegen aus der **Physikalische Chemie II**. Ich hab hier bei euch immer eine super Arbeitsatmosphäre und Hilfsbereitschaft vorgefunden und fand es immer toll, mein Wissen so gut wie möglich mit Euch zu teilen. Ich denke, die Kombination Chemie/ Physik war nicht schlecht, und jeder hatte etwas davon. Ich hab jedenfalls viel von Euch gelernt!
Besonders möchte ich mich bei Daniel bedanken, für die vielen Momente, die wir zusammen hatten, Melani für die vielen interessanten Diskussionen und Hilfestellungen bei verschiedensten Fragen, Ben dafür, dass Du so bist, wie Du bist und für das Korrekturlesen von Abschnitten dieser Arbeit, Chris dafür, dass Du immer positiv warst und vor Ideen sprühst, Christoph für die tolle Zusammenarbeit und die Unternehmungen die wir zusammen hatten, Bernhard für die Einführung in die Kletterei, Martin für Deine Gesellschaft, Inna für interessante Diskussionen und für das Korrekturlesen von Abschnitten dieser Arbeit, Max, Moriz und Jens für die Zusammenarbeit und die tollen Sprüche. Georg Papastavrou danke ich für die vielen interessanten Diskussionen. Außerdem möchte ich Alex und Stephan dafür danken, dass Ihr mich in die PC II eingeführt habt, Julia und Katja für die lustigen und interessanten Gespräche und Öznur für die Freundschaft. Danke Euch allen für Eure Motivation, die interessanten Diskussionen und den Spaß, den wir zusammen hatten.

Arbeiten geht bei mir aber nicht ohne Freunde und Unternehmungen außerhalb der Uni. Bei allen meinen **Freunden aus der Physik, Sport und den Anderen** (Ihr wisst schon, wen ich so meine...) möchte ich mich für all die Jahre voller Spaß, Sport und natürlich gute Zusammenarbeit bedanken und dafür, dass ich durch Euch den Blick für die wesentlichen Dinge behalten habe.

So, jetzt kommen wir zu den wichtigsten Menschen in meinem Leben.
Erst einmal ein riesengroßer Dank, den man gar nicht in Worte fassen kann, an meine neu dazugewonnene **Familie** (Wagner, Schulte), dafür, dass ich mich bei Euch geborgen fühle.
Der größte Dank zum Schluss gilt Euch, meiner Familie daheim und Dir, Susanne, meiner kleinen Fee. Danke Susanne für die unglaublichen Jahre und Momente, die wir zusammen hatten, und dass Du mich so nimmst, wie ich bin! Danke, Mama, Papa, T, und Regina für Eure moralische Unterstützung in allen Lebenslagen, durch die ich der werden konnte, der ich jetzt bin. Ich bin ganz zufrieden damit!

Erklärung

Die vorliegende Arbeit wurde von mir selbstständig verfasst und ich habe dabei keine anderen als die angegebenen Hilfsmittel und Quellen benutzt.
Ferner habe ich nicht versucht, anderweitig mit oder ohne Erfolg eine Dissertation einzureichen oder mich der Doktorprüfung zu unterziehen.

Johann Erath